Geology of Mount Pirongia and the Alexandra Volcanic Group, New Zealand

Oliver Emerson McLeod

A thesis submitted in partial fulfilment of the requirements for the degree of

Doctor of Philosophy in Earth Sciences

University of Waikato

School of Science, Earth Sciences

Hamilton, New Zealand

2020

Abstract

The geological mapping of ancient stratovolcanoes reveals a portrait of their stratigraphy, structural architecture and chemical cyclicity formed in response to magmatism over periods typically spanning 100 to 1000 kyr.

In back-arc settings, detailed stratigraphic studies are especially pertinent because these volcanic fields are characterised by long-lived, chemically diverse volcanism that is sensitive to changes in tectonic conditions (e.g. back-arc extension) associated with the down going slab.

The Alexandra Volcanic Group (AVG) of western North Island, New Zealand is a prime example of a back-arc, basaltic volcanic field that preserves a record of chemically complex, arc to intraplate volcanism from the Late Pliocene to Early Pleistocene (2.7–1.6 Ma). The aim of this research is to reconstruct the volcanic history of Mt Pirongia, and its underlying arc to intraplate magmatic system in the context of the broader AVG.

Detailed mapping on Pirongia has yielded the first 1:30,000 geological map of the volcano. Unit correlations are based on field and geomorphic observations, radiometric dates (with two new $^{40}Ar/^{39}Ar$ ages) and detailed petrography. The Pirongia Volcanic Formation is now subdivided into six new stratigraphic members and 36 new lithostratigraphic units, which collectively form the largest basaltic volcano (~30 km^3) in North Island. The edifice has formed from at least 18 vents that define an ankaramite shield structure surmounted by three steep sided cones. Major cone-building stages are separated by sector collapse events. The largest collapse deposit is the 3.3 km^3 Oparau breccia debris avalanche, which was channelised into its namesake graben and extends 20 km southwest of Pirongia. Collapse was likely triggered by normal fault reactivation and followed by resurgent volcanism at Pirongia Summit (1.6 Ma).

A comprehensive set of 200 rock samples from Pirongia, Karioi, Te Kawa and Kakepuku were analysed for major oxide, trace element and (selected) Sr-Nd isotope compositions. The dataset shows that arc-type (IAB) basalt is volumetrically dominant in the stratovolcanoes, which are interspersed with monogenetic intraplate (OIB) basalts of the Okete Volcanics. Minor intercalation of IAB-OIB occurs at Pirongia and Kakepuku, whereas OIB lavas comprise almost half of Karioi. Elemental and isotopic data indicate that all arc lavas have compositions falling on a spectrum between IAB and OIB endmembers.

Cross-arc geochemical variation indicates a northwestward enrichment of Nd-isotope ratios from Te Kawa to Karioi that corresponds to an increase in the OIB signature with increasing slab depth.

Stratigraphically, Karioi is defined by sharp alternations of OIB-IAB volcanism, while Pirongia displays progressive and cyclical enrichment from IAB to transitional compositions. At Pirongia, sustained injection of OIBs into the IAB magma reservoirs has led to cyclical contamination and more OIB-like compositions through time.

The juxtaposition of IAB and OIB is explained in terms of slab rollback, which induces vertical and lateral upwelling of asthenosphere, via slab tear and along the slab edge, into the metasomatized mantle wedge. Initial decompression melting forms OIB, which triggers secondary conductive melting of the wedge to form IAB magmas.

This study demonstrates the importance of robust stratigraphy for unravelling complex chemical cyclicity in stratovolcanic systems.

Acknowledgements

In its original form, I was warned this project would take 20 years to complete. Thanks to the following people and organisations, it only took four.

Funding came from the University of Waikato Doctoral Scholarship, along with small grants from the Faculty of Science and Engineering Student Research Trust Grant, Broad Memorial Fund and the Royal Society Te Aparangi Hutton Fund.

Access to the sacred mountains of Pirongia, Karioi and Kakepuku was granted by the Department of Conservation under sample collection permit 52176-GEO, in consultation and agreement with Tainui stakeholders.

To Adrian Pittari, in your role as chief supervisor I express my utmost gratitude to you for taking a risk on this project when I first proposed it in early 2016. Through our many hundreds of conversations, the scope, clarity and impact of this work was greatly improved. You allowed me to develop this project according to my own vision, and thus gave me great freedom as a young geologist. Thank you for your tireless advocacy of my work, especially your support of the production and distribution of the Pirongia geological map book.

To Marco Brenna, your acumen in the areas of petrology and field geology has substantially influenced the final results of this thesis. Thank you for guiding me through the complex and changing landscape that is geochemistry, and for your patience as I learned the ins and outs of data collection, analysis and interpretation. You generously provided funding for Ar-Ar age dating on Pirongia. Your insights into the nature of arc and intraplate volcanism were fundamental in unravelling the petrogenesis of the Alexandra Volcanic Group.

To Shaun Barker, you were instrumental in the early stages of the research proposal, and establishing the XRF dataset that formed the foundation of my geochemical work.

To Roger Briggs, I thank you immensely for your mentorship from the earliest stages of project development to the last days of hand in. I was profoundly touched and influenced by your papers on Pirongia and the Alexandra Volcanic Group, which capture the essence of these landscapes most perfectly. Your wisdom on fieldwork strategy and geochemistry were invaluable. Your encouragement has had a profound impact on my development as a young geologist. I have the utmost respect for you as a scientist, an educator, a mentor and a family man. Your humility and life balance between academia and all other things is truly an example to follow. I am honoured to have had your guidance in this project. Pirongia remains your mountain.

To David Lowe, I express my greatest thanks for your sustained interest in my work. Your enthusiasm for my mapping has renewed and reinvigorated its sense of purpose many a time. You have gone to considerable effort in reviewing the map bulletin and have put in the good word for me on numerous occasions. I admire you as a role model of what a professor should be. It is an honour to have crossed paths in the last four years.

To Peter Kamp, I have enjoyed our many long discussions on the volcanic and sedimentary stratigraphy of North Island. It has been inspiring to work alongside you, Sophie and Dan in the last years as you have prepared your regional map of the Whanganui Basin.

To Tom Roa of Maori and Indigenous studies, thank you for connecting my work to the Maori people of the Pirongia area, introduction to the Purekireki marae, and for providing the original place names of peaks on Pirongia. I look forward to future collaboration.

To my colleagues in the world of F block, Ben Andrews, John Mering, Rosie Hughes, Alex Harpur, Marlena Prentice, Xu Ganqing, George McQuillan, Francesca Spinardi and Jackson White – thanks for all the laughs and friendship. You all truly made it worth it.

To my contemporaries Leo Pure (VUW) and Callum Rees (Massey), I have greatly enjoyed our conversations on the art and relevance of geological mapping in the context of our own projects.

I am most grateful for field assistance from Chris Morcom, Selwyn June, Matt House, George McQuillan and Szabolcs Kósik.

Outstanding technical support and analyses were provided by Annette Rodgers, Kirsty Vincent and Renat Radosinsky (XRF and thin section making, WU), Steve Cameron and Amanda French (LA-ICPMS, WU), Bruce Charlier (Sr-Nd isotopes, VUW), Ian Schipper (EPMA, VUW) and Dan Miggins (Ar-Ar dating, Oregon State University).

To the people of the Waikato region, I express my thanks for your interest and support of this project. In particular, members of the Pirongia Restoration Society; Selwyn and Diane June, Steve McClunie and Tom Davies are thanked for their support and encouragement, along with Alan Hall of the Pirongia Heritage Centre, who wrote the foreword to the map bulletin.

To my family in New Zealand and Mexico, you have provided unconditional love and patience during these four years that cannot be underestimated. You have made great sacrifices so that I could do this project unimpeded by the other demands of life. You believed in me and during the toughest moments of uncertainty I drew on that for strength.

Finally, to my darling wife – Julieta, you have been beside me from the very first day. We are a team and you deserve this PhD as much as I do. We got married during the PhD! Every field trip, late night of writing, conference, public lecture and dinner discussion, you have selflessly nurtured my success. Above all else, you are the ultimate inspiration for this work, and I love you with all my heart!

Table of contents

Chapter 1

Introduction

'Thus appears the Staedt Landt in the Southern Latitude of 38 degrees 30 minutes'

Abel Tasman, 1642

1.1 Mapping of New Zealand volcanoes

Stratovolcanoes, calderas and volcanic shields are the pre-eminent foundation of the New Zealand volcanic landscape. During the last 66 million years, about one hundred volcanoes and volcanic fields have erupted throughout New Zealand, which are preserved as remnants or active centres across the North and South islands. Onshore volcanism represents only a fraction of the volcanic record in the Zealandia continent, which is mostly submerged and contains over 500 individual volcanoes and volcanic fields active over the last 105 million years (Mortimer and Scott, 2020).

Volcanic mapping is the necessary foundation for all detailed geological studies of active or extinct volcanoes (Martí et al. 2018). In particular, mapping provides a crucial framework for large scale petrogenetic studies, which require well-established stratigraphy to provide temporal and spatial constraints on petrogenetic processes (e.g. Holm, 1988; Hildreth and Fierstein, 1995; Bacon, 2008; Santacroce et al. 2003, Branca et al. 2011). No common approach to volcanic mapping has yet been established, with correlation of formations, members and units according to various petrographic, geochemical, radiometric, volcanological and stratigraphic criteria.

In New Zealand, volcanic mapping has a strong tradition dating back to the mid-19th century (Hochstetter, 1864), and in the 20th century yielded a number of substantial geologic maps for Dunedin Volcano (Benson, 1968), Waitakere (Hayward, 1975), Ruapehu (Hackett, 1985), Banks Peninsula (Sewell 1985), Okataina (Nairn, 2002) and Taranaki (Neall and Alloway, 2004).

In the 21st century, new geological mapping campaigns have emerged for the Taupo Volcanic Zone, led by Dougal Townsend and Graham Leonard, including detailed geochronological-glaciological studies of Ruapehu and Tongariro (Conway, 2016; Cole, 2019; Pure, 2020). These studies have been incorporated into the current (and forthcoming) edition of Geology of the Tongariro National Park Area 1:60,000 (Townsend et al. 2017), which forms part of a larger project by GNS to map the entire Taupo Volcanic Zone at 1:120,000 scale. Another detailed mapping study of the Taranaki volcanic ring plain was completed by Zernack (2008).

The summation of all but the most recent New Zealand volcanic mapping is presented in the national 1:250,000 scale QMap series of GNS, compiled from 21 map sheets published between 1996 and 2010.

1.2 Rationale for this project

The study of ancient, extinct stratovolcanoes provides crucial information on the growth and destructive processes involved in arc accretion and petrogenesis. In contrast to geologically young (Late Pleistocene and Holocene), active stratovolcanoes, the stratigraphy of their ancient

counterparts preserves a 'frozen picture' of the *complete* evolution of a volcanic system, from inception to cessation, which may take place over hundreds of thousands to millions of years (e.g. Holm, 1988). While studies of young volcanoes can reveal intricate details of eruption styles, ash deposition, lava flows, ice-lava interactions, sector collapse, lahars and ring plain accumulation, these deposits generally represent the youngest material that covers and obscures the underlying, older volcanic stratigraphy. This presents limitations for volcanic mapping, especially where substantial portions of the edifice are composed of transient pyroclastic material and draped by extensive ring plain deposits (e.g. Taranaki, New Zealand; Neall and Alloway, 2004). In contrast, ancient stratovolcanoes are characterised by extensive erosional denudation, with deep radial valleys, post-volcanic collapse scarps (e.g. Holm, 1988), and substantial erosion of their summits. Erosion removes surficial material from the edifice and exposes the inner volcanic succession, thus enabling the investigation of complete, or more comprehensive, stratigraphy than is present at active volcanoes. These eroded structures are thus very important proxies for understanding modern volcanic settings, and can provide insights into the nature of volcanic vent distribution, the sub-surface magma plumbing system (i.e. dykes), flank structure, ring plain development, compositional variation with time, and tectonic-magmatic interrelationships.

The Late Pliocene-Early Pleistocene basaltic Pirongia Volcano, and associated volcanoes of the Alexandra Volcanic Group of the western North Island, New Zealand are old enough to be significantly eroded, yet young enough to have retained their basic volcanic geomorphology. Hence, they are an ideal case study for investigating the inner parts of a volcanic succession.

1.3 Aim and objectives

1.3.1 Aim

The aim of this research is to reconstruct the volcanic growth and collapse history of Mount Pirongia and its underlying arc to intraplate magmatic system in context of the broader Alexandra Volcanic Group.

1.3.2 Objectives

1. The first objective of this research is to establish the volcanic stratigraphy of Mount Pirongia, in order to identify the key magmatic and tectonic events involved in its formation. A fundamental aspect of this objective will be the production of a 1:30,000 scale geological map of Mount Pirongia and its ring plain, the most detailed geological map of the mountain

to date, with subdivision of the Pirongia Volcanic Formation into new volcanic-stratigraphic members and units.

2. The second objective is to characterise the geochemical systematics of arc to intraplate volcanism within the Alexandra Volcanic Group. This objective involves the collection and presentation of a comprehensive suite of geochemical data for the Alexandra Volcanic Group, with emphasis on the largest volcanoes of Pirongia and Karioi. The dataset includes whole-rock major and trace element data, Sr-Nd radiogenic isotope data and mineral chemistry.

   This geochemical data will be applied to the stratigraphy established in objective 1 to construct temporal-chemical and spatio-chemical models of the volcanic system in terms of arc and intraplate magmas.

3. The third objective is to constrain the origin and timing of emplacement of the Oparau breccia debris avalanche deposit in southwestern Pirongia as a case study for collapse events on Pirongia.

1.4 General methodology

The foundation of this study is a large-scale field survey to map and sample the virgin volcanic stratigraphy of Mount Pirongia and its ring plain. This work is coupled with additional sampling of volcanic rocks from the other Alexandra Volcanic Group centres of Mount Karioi, Kakepuku, Te Kawa and the Okete Volcanics.

Correlation of map units on Pirongia was based on field observations, geomorphological interpretation, radiometric (K-Ar and new $^{40}Ar/^{39}Ar$) dating and detailed petrographic characterisation using thin sections.

Selected rock samples from Pirongia, Karioi, Kakepuku and Te Kawa were analysed for major and trace elements using XRF and LA-ICP-MS on whole-rock powders. Sr-Nd isotopes were measured on a subset of Pirongia samples using TIMS. Additional whole-rock data for Karioi (major and trace elements, and Sr-Nd) was compiled from Briggs (unpublished data).

Major and trace element mineral chemistry data were collected for Pirongia rocks by Electron Microprobe and LA-ICPMS on thin sections.

1.5 State of knowledge

Geological investigations of the Alexandra Volcanic Group have occurred sporadically over the last one and a half centuries (see Table 1.1). The field has received considerably less attention from geologists compared to the actives centres of North Island in the Taupo Volcanic Zone, Mount Taranaki and the Auckland Volcanic Field. This is mainly because of the isolated, back-arc position of the volcanic field, extreme terrain and thick forest cover which hinder access to outcrops for geological investigation.

The first European-trained geologist to explore the region was Ferdinand von Hochstetter, who in 1859 produced reconnaissance maps of the western Waikato on his pioneering geological expedition of New Zealand (Hochstetter, 1864; Hochstetter and Peterman, 1864). The first dedicated mapping and sampling campaign took place 67 years later, when the Geological Survey Branch employed John Henderson and Leslie Grange to map the volcanic terrain between Kawhia and the Alexandra survey district in a series of 1-inch to 1-mile geological maps (Henderson and Grange, 1926).

In the second half of the twentieth century, the geological maps of the volcanic field and western Waikato were refined by David Kear (Kear, 1960; Kear and Schofield, 1978). Kear (1960) defined the Alexandra Volcanic Group and its stratigraphic members. Research from 1980 onwards was associated with Roger Briggs, who was the first geologist to describe in detail the Alexandra Volcanic Group from a volcanological and petrological perspective. His early work covered the general morphology and formation-level stratigraphy of the volcanic field (Briggs, 1983). This was later followed by a substantial publication on the volcanic geochronology (Briggs et al. 1989) which contributed twenty-one new K-Ar radiometric dates on lava flows, bringing the total for the field to 47. Significantly this work indicated that the volcanic chain is non-age progressive, in contrast to the Taranaki volcanics south of the Alexandra Volcanic Group.

Geochemical work was published in Briggs and Goles (1984), Briggs (1986) and a major publication by Briggs and McDonough (1990). The latter included the first mineral chemistry, rock geochemical classification, whole-rock major and trace element data for Pirongia, Kakepuku and Te Kawa. Related studies by masters students of Roger Briggs yielded valuable information on the stratigraphy of Mount Karioi (Matheson, 1981), the Okete Volcanics (Keane, 1985) and the mafic-ultramafic xenolith suite contained in the latter field (Sanders, 1994). The last publication on the field was a detailed stratigraphic and paleomagnetic study of Mount Karioi by Goles et al. (1996).

To date, no published or unpublished geological maps exist for Mount Pirongia beyond the formation level at 1:63,360 scale (Kear, 1960) and 1:50,000 scale for part of the

(undifferentiated) southwestern ring plain (Waterhouse and White, 1994). Only eight whole-rock geochemical analyses have been published for Karioi, with six of these dating back to 1926.

Table 1.1. Summary of all published and unpublished geological studies on the Alexandra Volcanic Group.

Study	Description
Hochstetter (1864); Hochstetter and Peterman (1864)	Sketched Pirongia during his survey of the North Island (1864). Hochstetter was the first to mention Karioi, describing it as an old basalt volcano. Hochstetter and Peterman (1864) denoted Karioi as a trachydolerite volcano in their geological and topographical Atlas of New Zealand.
Hutton (1867) Cox (1876) Park (1885)	The first detailed geological study of the Waikato Region was by Hutton (1867) who mapped Karioi as an extinct volcano surrounded by basaltic boulders. Further mapping by Cox (1876, 1877) and Park (1885) mostly characterised sedimentary stratigraphy of the Waikato area, but large areas of undifferentiated lavas were also mapped between Raglan and Kawhia as 'boulder formation'.
Park (1892)	Made a few comments about Pirongia on p.356 as 'trachyte tuffs and lavas that go into the sea at Kawhia'.
Marshall (1907)	Made observations and took samples from Karioi and Pirongia. Comments on p.88: 'the rocks differ markedly from all other volcanic material of the North Island'. Comments p.96: the basalts 'resemble the dolerites of Dunedin'.
Henderson and Grange (1926)	The first detailed geological study, which produced a 1:63,360 scale geological map of the Alexandra-Pirongia-Kawhia areas. First published geochemical analyses of Alexandra rocks.
Cotton (1944)	Pirongia and Karioi mentioned p.92 as examples of eroded volcanoes, and a few interesting comments postulate on their original landform. A sketch of Pirongia is given, based on the earlier sketch of Hochstetter (1864).
Player (1958)	Concerned with geology of northern Kawhia. Player's map negated the idea of Henderson and Grange (1926) that a surface fault existed parallel to the AVL.
Kear (1957, 1959, 1960, 1964)	Defined the erosional stages, stratigraphy and volcanic alignment of Alexandra Volcanic Group centres. Produced a 1:250,000 map (1960) of the Waikato region that followed on from and updated the map of Henderson and Grange (1926).
Schofield (1967)	Geological map of Auckland-Waikato at 1:250,000 scale.
Stipp et al (1967), Stipp (1968)	K-Ar ages of Alexandra Volcanic Group rocks from Karioi and the Okete Volcanics.
Hatherton (1968, 1969). Hatherton and Dickinson (1968)	Studies on the geophysical significance of calc-alkaline magmas in relation to the depth to the Benioff zone.
Sameshima (1975)	Karioi included as part of a regional geochemical study to develop a silica index.
Robertson (1976)	K-Ar ages of Karioi, Okete Volcanics, Pirongia and Te Kawa.
Kear and Schofield (1978)	*Geology of the Ngaruawahia Subdivision;* 1 inch to 1 mile map Hamilton sheet covers most of Pirongia.
Matheson (1981)	First detailed study of Mt Karioi coastal stratigraphy. *Volcanic Geology of the Karioi Region* (Master's thesis).

Briggs (1981)	Field guide on the volcanic geology of the field.
Briggs (1983)	Foundational paper on the volcanic geology of the field.
Briggs and Goles (1984)	Detailed geochemical study of the Okete Volcanics.
Keane (1985)	*Physical volcanology and stratigraphy of the Okete Volcanics*. Master's thesis.
Briggs (1986)	Provided a suite of new major and trace element data for the Alexandra Volcanic Group and discussed the subduction setting of the field.
Briggs et al (1989)	Presented 21 new K-Ar age dates for the Alexandra Volcanic Group
Briggs and McDonough (1990)	Major geochemical study of Pirongia, Kakepuku and Te Kawa.
Sanders (1994)	*Ultramafic and mafic xenoliths from the Okete, Ngatutura and South Auckland volcanics*. (Master's thesis).
Waterhouse and White (1994)	*Geology of the Raglan–Kawhia Area*. 1:50,000 scale map that covers the southwestern Pirongia ring plain.
Lowe (1994)	Raglan geology field guide
Goles et al (1996)	Stratigraphy of Karioi Volcano
Briggs et al (1997)	Geology of Gannet Island
Ritchie and Brideau (2012)	Slope stability study on the Te Toto Amphitheatre.
Briggs and Pittari (2012)	Field guide on the stratigraphy and geochemistry of the field, with new geochemical and isotope data.
Briggs et al (2013)	*Karioi Volcano, western North Island, New Zealand: a behind arc polygenetic intraplate-convergent margin volcanic complex*. Poster at IACEI 2013 Scientific Assembly, Japan.

1.6 Thesis structure

This thesis presents the first geological map of the entire Pirongia volcanic edifice, which defines new stratigraphy for the volcano. The map is coupled with new petrographic, mineral, whole-rock geochemical and isotope data that has been collected, presented and interpreted in the context of the new stratigraphy. Chapters 2–4 are self-contained journal-style manuscripts with their own introductions, methods, results, discussions and references.

The new 1:30,000 geological map and associated explanation are presented in Chapter 2. This work is published as a map bulletin in the Miscellaneous Publication Series of the Geoscience

Society of New Zealand, which includes the 1:30,000 geological map of Pirongia. The map explanation includes introductory information on the geological setting, and an explanation of the geological chronology of Pirongia, followed by detailed descriptions of the new volcanic-stratigraphic units presented on the geological map.

Chapter 3 is a manuscript that has been prepared for publication and will be submitted for review in an international specialist volcanology and petrology journal. The manuscript presents the petrography and all geochemical data collected during this study of Pirongia and the Alexandra Volcanic Group: whole-rock major and trace element compositions, mineral major and trace element chemistry, and whole-rock Sr-Nd isotopes. The data is complemented by a set of unpublished geochemical data provided with permission of Roger Briggs. These data are used to examine temporal and spatial trends in eruption composition, with a focus on arc and intraplate basaltic volcanism.

Chapter 4 is a manuscript that has been invited to be submitted as a book chapter in a forthcoming Geological Society of London special publication and is focused on the Oparau breccia, a newly discovered 3.3 km^3 sector collapse deposit from Pirongia. The manuscript presents detailed field observations and stratigraphy that expand on the 1:30,000 geological map presented in Chapter 1. Archive drill core data is used to reconstruct the emplacement surface of the debris avalanche, and thickness variation in the deposit. Field observations and stratigraphy related to the geological map are examined in the context of debris avalanche processes to determine the emplacement age and triggering mechanism for collapse.

Chapter 5 summarises the main findings presented in chapters 2–4 and addresses the objectives of the study. Then the wider implications of the study are addressed, relating the geological work on Pirongia to broader issues and applications associated with back-arc basaltic volcanism globally.

Chapter 2

Geology of the Pirongia Volcano, Waikato: 1:30,000 Geological Map

'Here I beheld for the first time an extensive low-land spreading into distant mountain cones and remote mountain-chains'

Hochstetter, 1867

O.E. McLeod

A. Pittari

M.B. Brenna

R.M. Briggs

Please find accompanying geological map in the supplementary file

GEOLOGY OF THE PIRONGIA VOLCANO, WAIKATO

1:30,000 Geological Map

O.E. McLEOD

with

A. PITTARI

M. BRENNA

R.M. BRIGGS

Geoscience Society of New Zealand

GEOLOGY OF THE PIRONGIA VOLCANO, WAIKATO

1:30,000 Geological Map

Authors
O.E. McLeod
A. Pittari
M. Brenna
R.M. Briggs

Geoscience Society of New Zealand Miscellaneous Publication 156

Geoscience Society of New Zealand

2020

BIBLIOGRAPHIC REFERENCE

McLeod, O. E., Pittari, A., Brenna, M., and Briggs, R. M., 2020, Geology of the Pirongia Volcano, Waikato: 1:30,000 Geological Map. Wellington, New Zealand, Geoscience Society of New Zealand, Miscellaneous Publication, v. 156, 60p.

Printed by Graphic Press & Packaging Ltd, Levin
Geological map printed by Boxkraft Ltd, Auckland

Published with the assistance of generous sponsorship from:
Waipa District Council Pirongia Ward Committee
Waipa Distict Council Te Awamutu Ward Committee

Author affiliations
O.E. McLeod, A. Pittari, R.M. Briggs: University of Waikato, Hamilton
M. Brenna: University of Otago, Dunedin

ISBN (print): 978-0-473-52832-4
ISSN (print): 2230-4487

FRONT COVER

Mount Pirongia, viewed from the rolling lowland hills of the Hamilton Basin. The northern slopes of Pirongia are marked by a series of planezes forming remnants of the original volcanic flanks. The volcano is now deeply incised by radial valleys, many kilometres in length, such as the Mangakara stream (centre) which has entrenched over three hundred metres into the volcanic stratigraphy.

Photo: Oliver McLeod

CONTENTS

FOREWORD

Geology of the Pirongia Volcano, Waikato and the accompanying text is particularly welcome because it provides, at last, a comprehensive and up-to-date specialist map showing the geological features, rock units and strata, together with a coherent account of the volcanic and geological history of this, the largest basaltic volcano in the North Island. Over a period of one million years, Pirongia grew from numerous vents to become what must have been an impressive stratovolcano standing at least 1200 metres above sea level.

The period of volcanic activity in the area was followed by more than a million years of erosion. Sector collapses, lahars, mass movement and fluvial action resulted in a substantial loss of vertical height to its present 959 metres. Previously sub-surface volcanic rock structures were exposed on the ridgelines to produce the present jagged set of summit peaks such as Mahaukura, with streams flowing in radial valleys separated by thin ridges of volcanic rock. Soils developed, supplemented by later ash shower material from central North Island eruptions, to sustain the growth of vegetation in a mild climate with high rainfall, clothing the mountain over time in a richly varied forest of podocarp and ferns, with sub-alpine plants on its summit peaks, and rich birdlife.

Thus, Mount Pirongia became an imposing geological remnant of the original stratovolcano. However, what we see today has since been heavily influenced by human occupation.

The first occupants were people of the Tainui canoe who settled on the coast more than 700 years ago. During the following 500 years, sub-tribal groups of Tainui, such as Ngāti Mahanga, Ngāti Apakura, Ngāti Horotakere and Ngāti Hikairo, established territories around the forest-clad mountain where berries and plant products were collected and birdlife was hunted as a food source. However, the mountain was regarded as having its own mana and was treated as tapu. It was believed to be occupied by a spirit people, Patupaiarehe, who came out at night and were effectively its guardians. In turn, the hapū had obligations of kaitiakitanga (guardianship) to respect the mountain's mana and conserve its resources. Initially, they knew it as Paewhenua (The Land Barrier), a name used when their earliest explorers, travelling up the Waipā river, first saw its jagged summit peaks. Several generations later, Paewhenua became known as Pirongia Te Aroaro o Kahu (The Scented Presence of Kahu) in honour of Kahu-peka who is said to have travelled through the area on a later journey of exploration. Other features on the geological map also have traditional Māori names, many of them associated with a rich legacy of traditional stories.

A dramatic change in the ownership and use of the land resulted from government-imposed surveys between 1864 and 1890 which defined specific land blocks and identified their legal owners. Land confiscated from Māori ownership was surveyed following the Waikato War, including that part of Mount Pirongia east of the confiscation line from the mouth of the Puniu Stream to the peaks of Mahaukura and Tahuanui. The bush-covered land was divided into farm blocks for private ownership by mainly soldier settlers. This facilitated the clearing of land and the establishment of farms on the lower volcanic slopes and ring-plain to the east of the mountain. Twenty years later, following King Tawhiao's declaration of peace in 1881, further government surveys were made of the remainder of the mountain as a part of the survey of the King Country. Large blocks of land on and around Mount Pirongia, initially in Māori tribal ownership, were then purchased by the government, allowing land on the lower slopes and ring plain in the King Country to be subdivided, sold and cleared for farming. Thus, by the early 20th Century, the mountain was surrounded by cleared, privately-owned farmland. The state owned most of the more mountainous and forested upper sections not in private ownership, encircled by a fringe of privately-owned sections of forest, yet to be cleared on the upper slopes.

Today, the greater part of Mount Pirongia lies within the 12,919 hectare, Pirongia Forest Park area, surrounded by developed farmland. However, the forest park, as we know it, was not constituted until 1971. Sawmilling, which was under way on privately-owned blocks of forest in 1914, continued in different locations until 1959, and after World War 1, some forested blocks in the north of the park were allocated to be cleared by returned servicemen who later walked off properties around Wilson's and Taylor's Clearings, leaving them to revert to forest.

At the same time, concerns were being expressed by councils, chambers of commerce, farmers and others dwelling within view of the landmark, about the possible loss of its grandeur and scenic beauty if forest clearance continued. Others warned of the loss of water catchments for town supplies and the possibility that rainfall patterns might be affected. The government response was to make a number of its surveyed blocks state forest reserves, managed by the State Forest Service, and others became scenic reserves, managed by the Department of Lands & Surveys. From time to time, other small blocks were added before they were all combined in 1948 on condition that no further milling or logging would be permitted in the state forest.

The Pirongia Forest Park was formally constituted in May 1971, under new legislation granting public access to forest parks for recreational use. Since that time, the NZ Forest Service, and since 1987 the new Department of Conservation, focussed on catering for a wide range of recreational users. This is reflected in the development and maintenance of today's extensive system of walks, tracks, and routes, together with the gradual development of other facilities for visitors such as camping and picnic areas, viewing platforms and the 20 bunk Pahautea Hut near the summit. The development of a section of the New Zealand Te Araroa Trail via the Tahuanui and Hihikiwi tracks in 2009, included eight kilometres of boardwalk constructed to improve travel over higher-level swampy sections of track and protect threatened vegetation. Local councils, trusts, landowners and eight Waikato secondary schools provided tangible support for the development; it is estimated that half the $400,000 cost of the Te Araroa trail cost was contributed locally.

A continuing focus on conservation of the forest resource has been reflected in initiatives to control goats, possums and other species that threaten both the flora and fauna. Since 2001, these initiatives have been supplemented by a continuing, intensive pest control programme over 1000 hectares by the voluntary Pirongia Te Aroaro o Kahu Restoration Society. Its success led to the more recent re-introduction of two native bird species, pitoitoi and kōkako. The Te Pahu Landcare Group also continues to be involved in planting and maintaining native vegetation along the Nikau walkway. These initiatives are supported by Māori who remind us that the maunga continues to have a life of its own, noting that the rivers and streams are its arteries, feeding the mountain's essence and purifying it. But it is humans who provide the being's consciousness, the centre of feeling and responsibility.

Today, the forest park which encompasses the single largest area of native forest in the Waikato, attracts up to 40,000 visitors a year.

Geology of the Pirongia Volcano, Waikato and its accompanying text is a seminal publication, useful to students of geology and volcanology, which will also provide a basis for further research to extend its findings. It will be of interest to those who live around the mountain, particularly for the descriptions of the map units which are accompanied by photographs and useful interpretive diagrams. For visitors to the forest park it will add depth to their appreciation of the mountain's interesting geological history, particularly if they visit the upper reaches or follow the Te Araroa Trail.

The Earth Sciences group at the University of Waikato is to be congratulated for its promotion, over many years, of the research which culminates in this publication.

Alan Hall
Pirongia Heritage & Information Centre

INTRODUCTION

Mount Pirongia (37°59'S/175°5'E) is the remnant of the largest basaltic volcano in North Island, New Zealand. Formation of the Pirongia Volcano began around 2.5 million years ago during a period of profound tectonic change in Zealandia. The subducted Pacific Plate underlying northern New Zealand began to steepen and retreat eastwards, resulting in the gradual pulling apart of the crust in western North Island. In the subsequent disruption to the regional volcanic system, eruptive activity in the Coromandel Volcanic Zone ceased and was replaced by a series of isolated and unusual basaltic eruptions in the distal back arc, which now form Mount Pirongia and the Alexandra Volcanic Group (AVG). The final eruptions of Pirongia foreshadowed the first super eruptions of the modern Taupo Volcanic Zone, which occurred 1.6 million years ago in the Mangakino area.

Pirongia Volcano is one of the last unmapped stratovolcanoes in New Zealand. The mountain stands out as a significant geological site because Pirongia, along with its sister volcano Karioi, have erupted (by volume) almost half of all the basaltic lavas in North Island since Miocene times. This significance is compounded because most of Pirongia and the AVG's lavas are extremely crystal-rich basalts called ankaramites, a distinct rock-type with no close comparison in Zealandia but that is characteristic of some South Pacific volcanic islands such as Tahiti and Samoa. In this respect, the AVG represents not only the best-preserved chain of basaltic stratovolcanoes in Zealandia, but also provides a direct window into the submarine basaltic landscapes of the South Pacific, including the >2000 km long Tonga-Kermadec arc system, north of New Zealand.

This study presents the first geological map of Pirongia Volcano at the scale of 1:30,000. The new map illustrates, in fine detail, the complex inner stratigraphy of a stratovolcano now exposed by two million years of intense erosion. In a philosophical sense, the Pirongia Volcano is a perfect map subject because it allows us to envisage the fate of other

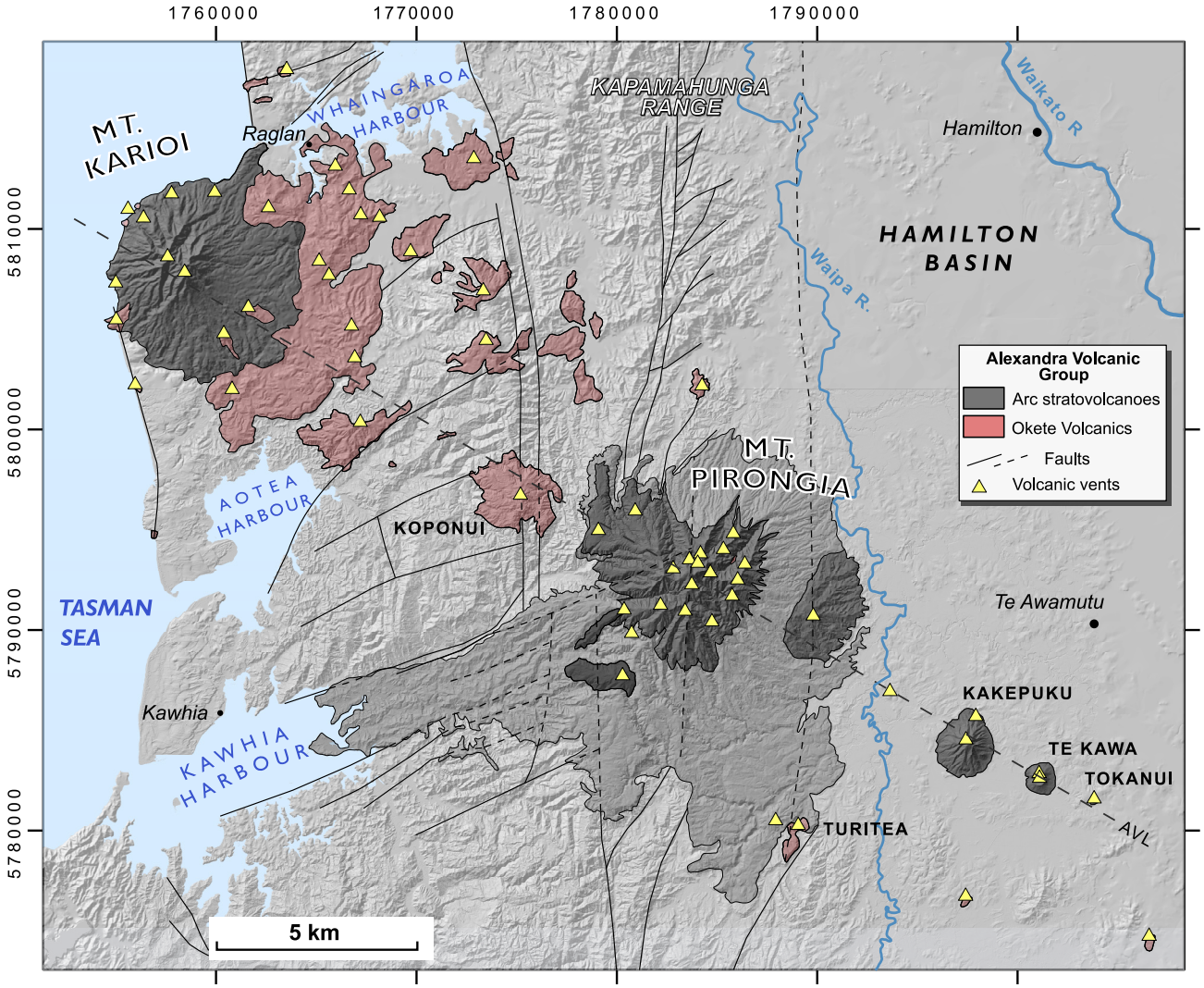

Figure 1: Hillshaded map of the Alexandra Volcanic Group and the surrounding terrain of western Waikato, New Zealand. The field consists of a chain of stratovolcanoes, domes and cones (black) that span a 60 km distance from the southern Hamilton Basin to the Tasman coast. An intraplate basaltic volcanic field, the Okete Volcanic Formation (red), is interspersed with the volcanic chain and most prominent between Aotea and Whaingaroa harbours. Most of the Alexandra volcanoes overlie mountainous terrain uplifted along the regional fault network; other vents in the east of the field occur within the lowlands of the Hamilton Basin graben. Pirongia Volcano occurs in the middle of the field, mantling the major tectonic boundary between mountain and basin.

active volcanoes in North Island (e.g. Ruapehu and Taranaki), many millions of years from now, as they enter extinction and the deep erosional state.

EARLY EXPLORATION

Oral tradition states that the Tainui people sailed from Hawaiiki, the ancestral home of Maori, with a vision of a new homeland that would be marked by a 'quiet harbour of water, overshadowed by a volcanic mountain peak'. Thus, around 1280 AD (Wilmshurst et al., 2008), the seafaring ancestors of Tainui made landfall at the Kawhia Harbour, a shallow and tranquil mooring framed by the dark, forested silhouette of Pirongia Mountain. In the centuries thereafter, numerous communities were established around the Kawhia, Aotea and Whaingaroa Harbours, and eventually also inland towards the other local volcanic peaks and Waipa River.

Paewhenua (horizontal ridge or barrier over the land) was the name given by Rakataura of the Tainui people as he crossed over the Pirongia range. An earlier name, apparently given by the 'patupaiarehe, the fairy people of the mountain', was Pūawhe, for the strong winds that blew over the mountain. Pukehoua (the hill of entry) was another early name. That now belongs to a small flank cone, on the east side of the mountain range. The mountain was renamed 'Pirongia te aroaro o Kahu' (The Scented Presence of Kahu) by Kahu, a descendant of Rakataura. She journeyed east from Kawhia over the range in search of solace and medicinal plants to help her heal following the death of her husband Ue, and the miscarriage of their unborn child (T. Roa, pers. comm, 2020).

It was not until over 400 years later that Abel Tasman and his crew on *Heemskerck* and *Zeehaen* (1642) sighted Kawhia, Mount Karioi, and probably also Pirongia on their circumnavigation of the Pacific (Sharp, 1968). Documentation of this discovery is preserved in navigational sketches of the coastline of western Waikato, including a long-shore sketch of Karioi, with Pirongia just visble behind, by Isaack Gilsemans, a cartographer with Tasman (Anderson, 2001, p. 101).

The first European geological observations of the Alexandra Group were made by Hochstetter in 1859 during his formative geological tours of New Zealand. Hochstetter produced two important geological maps, of the North Island (1:700,000) and the Kawhia-Aotea area (1:120,000; von Hochstetter and Petermann, 1864), that identify Pirongia as a (trachytic) volcanic cone '*trachytische kegelberge*'. Intricate watercolour sketches of Mt Pirongia, Karioi and Kakepuku are preserved from this time (von Hochstetter and Sauter, 1867), several of Pirongia being reproduced by Johnstone and Nolden (2011). The geology of the mountain is known mainly from the detailed physiographical and geochemical work of Briggs (1983; 1986), Briggs et al. (1989) and Briggs and McDonough (1990), and older geological surveys by Henderson & Grange (1926), Kear (1960) and Kear & Schofield (1978). In these studies, notes on the volcanic succession were primarily descriptive and focused on the main landmark peaks and distal stream sections. To date, no geological map of the edifice exists beyond the regional scale delimitation of Pirongia Volcanic Formation in the 1 inch to 1 mile (1:63,360) geological map of Hamilton (sheet 4; Kear, 1960).

PHYSIOGRAPHY

Mount Pirongia (Fig. 2) is the most prominent landmark in the Waikato region. The 959 m (a.s.l.) peak lies east of the Kawhia Harbour, where it mantles the Kapamahunga Range and resides over the Hamilton Basin (Fig. 1). The mountain is a strong presence on the skyline of Hamilton city (30 km northeast) and Te Awamutu (20 km east). Pirongia forms a broad cone, 13 km wide and covering 175 km^2, that rises through its piedmont into a series of jagged mountain peaks. The summit itself is an inconspicuous saddle ridge surmounting other lower peaks. Pirongia Summit is framed

Figure 2. The forested peaks of Mount Pirongia, as viewed from the lowland farms of Hamilton Basin near to Pirongia township (view looking southwest).

to the west by the nearby pinnacle of The Cone (953 m a.s.l.), which in its original name was called Pūawhe. The Waipa River, which is the largest tributary of the Waikato River, flows around the eastern slopes of Pirongia and passes through its namesake village.

The majority of Mt Pirongia is contained within the Pirongia Forest Park (est. 1975), a 168 km^2 reserve managed by the Department of Conservation (Fisher, 2014). Livestock farming occurs on most of the lower slopes of the ring plain. The mountain's climate is relatively mild and wet, receiving high orographic rainfall (2400 mm) year-round on its western side. Light winter snow fall occurs approximately every three years. The mountain is of considerable ecological significance, being covered almost entirely by native podocarp, ferns and sub-alpine plants on its summit peaks (Clarkson et al. 2002). Species of interest include the tallest kahikatea tree in New Zealand, and the parasitic wood rose *Dactylanthus taylorii* which is foraged by the endemic short tailed bat. Among the native bird life are kereru, tui, pirairaka (fantail), miromiro (Tomtit) and kokakō, the latter reintroduced to Pirongia in 2018 by the Mount Pirongia Restoration Society.

Access to the mountain ridgetops is by five public walking tracks: the Tahuanui, Bell, Tirohanga-Ruapane, Wharauroa-Mahaukura and Hihikiwi routes. A combination of these routes bridge the Te Araroa national trail, which passes over the mountain. The many valleys of Pirongia are generally accessible along their stream beds, where wide stretches of gravel are covered only by shallow streams in the summer months.

OBJECTIVES

Overview and approach

The primary goal of mapping was to establish a volcanic stratigraphy for Pirongia Volcano that could be used as a reference point for interpreting the sub-edifice structure of other (primarily basaltic) stratovolcanoes. Aspects of mapping that achieve this goal include the recognition of volcanic facies, identification of vent zones and their plumbing systems, and development of a framework for future spatio-temporal studies of edifice growth and magmatic petrogenesis. The secondary goal was to document a method for geological mapping in heavily forested volcanic terrain that is normally considered untenable for stratigraphic work because of a lack of outcrops.

Additional goals have been to enhance the geoheritage value of Pirongia with the New Zealand public, local and international scientific community. The production of a detailed geological map showcases the unique geology of the volcano and supports its conservation as a landform and site of significant biodiversity. The geological map and text will provide a useful, informative resource for visitors to the Pirongia Forest Park and can be used as part of public outreach programmes in the future.

METHODS

Geologic mapping (between the years of 2016–2020) involved traverses of the mountain where systematic, georeferenced observations of morphology, volcanic facies and lithology were made. Sample locations were recorded with a Garmin eTrex® handheld GPS (accurate to ± 3 m). Rock outcrops in the densely forested terrain are restricted to exposures along peaks and ridges, within cliff successions, and the beds of streams. The mapping strategy thus targeted these locations specifically. Initial reconnaissance involved examination of orthophotographs to identify the most well exposed outcrops that were later visited during fieldwork. All other outcrops (beneath the forest cover) were identified incidentally during traverses.

The mapping process involved subdivision of Pirongia Volcanic Formation into three main volcanic facies, defined as the central vent facies, flank facies and ring plain facies (following Davidson and de Silva, 2000; see Appendix A for details). The central edifice was further subdivided into stratigraphic members, with each member representing a package of lavas and vent-related deposits (dykes, domes and pyroclastics) separated by an unconformity. Members are subdivided into informal lithostratigraphic units based on stratigraphic continuity and lithological characteristics (i.e. rock texture and mineralogy). Names for lithostratigraphic units are based on nearby topographic features, e.g. *andesite dykes of Pirongia Summit*.

Geological units were drafted onto a series of base map tiles created with ESRI ArcMap 10.5. The base map consisted of (1) mosaic orthophotographs (0.5 m resolution, horizontal accuracy ± 3 m) from the Waikato Regional Aerial Photography Service (WRAPS, 2012) referenced to NZTM2000 and datum NZGD2000; (2) a photogrammetry-based digital terrain model (DTM) with approximately 5 m spatial resolution using the same projection as the orthophotographs; and (3) the New Zealand 1:50,000 topographic contours with 20 m interval. The published map utilises the NZ Topo50 map grid with relevant topographic information overlaid (e.g. streams, roads, tracks).

Map boundaries

The boundaries of the geological map were delimited by the extent of Pirongia Volcanic Formation that could be presented at 1:30,000 scale. The northern and eastern extents were defined by the onlap of Quaternary deposits of the Hamilton Basin. The western and southwestern extents occur where Pirongia Volcanic Formation onlaps the Kapamahunga Range, and where debris avalanche deposits extend to the Kawhia Harbour. The southern extent of the map truncates the southern ring plain which is expansive, yet poorly exposed and does not contain enough mappable information to justify its inclusion in the map.

The boundary of Pirongia Volcanic Formation was adapted from the 1:250,000 scale QMAP Waikato (Edbrooke, 2005).

The QMAP integrated previous larger scale geological maps (e.g. Fergusson, 1986; Waterhouse & White, 1994) for the Pirongia area (see Appendix B for complete summary of previous local mapping).

Analogue for mapping

The well-exposed coastal sections of Karioi Volcano (Matheson, 1981) were used throughout this study as an analogue for the buried Pirongia succession. Direct field observations of flank lava geometries, cross cutting dykes and ring plain deposits at Karioi (as described by Goles et al., 1996) were fundamental for the identification and interpretation of the volcanic landforms in the less well-exposed stratigraphy of Pirongia.

DEFINITION OF VOLCANIC STRATIGRAPHY NOMENCLATURE

In their original definition (Kear, 1960), *Alexandra Volcanics* designates volcanic rocks or deposits belonging to Karioi, Pirongia, Kakepuku, Te Kawa and Tokanui. All of these rocks or deposits were given formal stratigraphic recognition as the *Alexandra Volcanic Group* by Kear and Schofield (1978) (refer therein to Fig. 3). These authors considered the products of each volcanic centre to define a separate stratigraphic formation – thus *Karioi Formation, Pirongia Formation, Kakepuku Formation, Te Kawa Formation* and *Tokanui Formation*. Briggs (1983) proposed the *Okete Volcanic Formation* to subdivide fine-grained alkaline basalts that were petrographically distinct from those in the larger volcanic centres. He also merged Tokanui Formation into Te Kawa Formation.

Goles et al. (1996) defined stratigraphic members of Karioi Formation as *Te Toto Member, Whaanga Member* and *Wairake Member*. These members define packages of edifice-forming lavas, each demarcated by erosional unconformities, which are exposed in coastal outcrops. Goles et al. (1996) also subdivided Okete Volcanic Formation into the Pauaeke and Marumaruaitu Members, based on lavas that pre- and post-date Karioi Formation. None of the Karioi stratigraphic members were adopted for the Waikato QMAP (Edbrooke, 2005) because no definitive lateral field boundaries have yet been established.

In this study, we propose subdivision of Pirongia Formation into six new stratigraphic members: Paewhenua Member, Tirohanga Member, Hihikiwi Member, Te Akeohikopiro Member, Oparau Member, and Pirongia Summit Member. Detailed information on these members is given in the 'Description of map units' section.

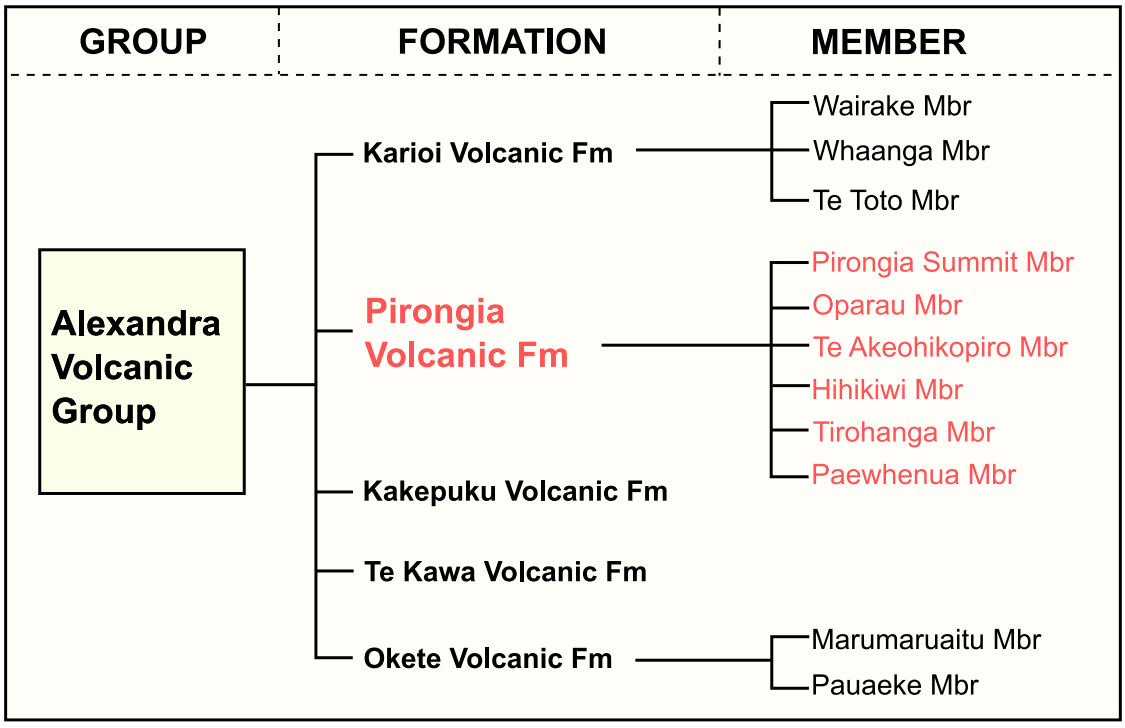

Figure 3: Summary of lithostratigraphic rank for the Alexandra Volcanic Group, with rocks of Pirongia Volcano highlighted in red.

GEOLOGIC SETTING

Alexandra Volcanic Group

The Alexandra Volcanic Group (AVG) is an extinct, Quaternary volcanic field in western North Island that produced ~55 km^3 of mainly basaltic eruptive material over a total area of 1100 km^2. The field consists of two moderate sized stratovolcanoes (Pirongia and Karioi), and two smaller cones (Kakepuku and Te Kawa), that were active between 2.74 and 1.60 Ma (Briggs et al, 1989). Interspersed with these centres is the Okete volcanic field (2.69 and 1.80 Ma), a scattered group of scoria cones, lava flows and tuff rings of alkaline basaltic composition (Briggs, 1983; Briggs and Goles, 1984) that is particularly prominent in the Raglan area.

Tonga-Kermadec arc system

The AVG forms a volcanic chain oriented perpendicular to the arc front of North Island, the Taupo Volcanic Zone (TVZ), located 70–120 km to its east. The TVZ is the onshore extension of the intra-oceanic Tonga-Kermadec volcanic arc system that stretches 2500 km from New Zealand to Tonga and Samoa (e.g. Mortimer et al. 2020). The Tonga-Kermadec arc is the manifestation of westward subduction of the Pacific Plate beneath the Australian Plate in the southwest Pacific. West of the Tonga-Kermadec system another parallel chain of volcanoes, the Colville Ridge, extends southward into the North Island where it manifests as the Coromandel Volcanic Zone (CVZ; e.g. Timm et al., 2019). The AVG, situated ~100 km southwest of the CVZ, may delineate the southernmost volcanic expression of the Colville Ridge.

The North Island arc

North Island subduction-related volcanism has migrated eastward from the NNW-oriented CVZ (Miocene-Pliocene) to the NE-oriented, active TVZ (Adams et al., 1994; Wilson et al., 1995; 2009; Briggs et al., 2005; Pittari et al., 2016). The transition was marked by a progressive increase in magma output rates and shift towards almost exclusively silicic (~95%) volcanism in the TVZ. The increased generation of silicic magma was probably associated with intensified subduction and crustal extension (Briggs et al., 2005). Extensional processes in the back-arc zone during this period are evident from the graben structures of Hamilton Basin and the Hauraki Rift.

Arc-related basaltic volcanism

Basaltic volcanism is widespread across continental Zealandia and occurs in both the convergent margin and intraplate settings (e.g. Mortimer and Scott, 2020). Although basaltic magmas are widely acknowledged as the source of all TVZ arc volcanism (e.g. Gamble et al., 1990; 1993; Wilson et al., 2006), they represent only a small fraction (<1 %) of the total erupted volume of the CVZ-TVZ arc system (Wilson et al., 1994). Localised basaltic deposits occur within the CVZ (Mercury basalts, Adams et al., 1994 and Matakana basalts, Briggs et al., 1996) and throughout the TVZ (e.g. K-Trig Basalt; Brown et al., 1994; Waimarino basalt; Gamble et al., 1993; and Tarawera 1886 eruptives). The relative proportion of arc-basalt is higher in the offshore portion of the Tonga-Kermadec arc (Timm et al., 2019), where the mantle wedge is overlain by thinner oceanic crust.

Intraplate basaltic volcanism

Intraplate basalts in the 'behind-arc' region of western North Island have produced ~7 km^3 of lava and volcaniclastics since 2.7 Ma. The associated volcanic fields young northward from Okete (2.69–1.8 Ma; Briggs et al., 1989) to Ngatutura (1.83–1.54 Ma; Utting, 1986; Briggs et al., 1989), South Auckland (1.59–0.51 Ma; Briggs et al., 1994b) and Auckland (193–0.50 ka; Leonard et al., 2017). Another ~30 km^3 of basalt was erupted in Northland from two monogenetic volcanic fields at Kaikohe-Bay of Islands (9.7 Ma–0.26 Ma) and Whangarei (2.24 Ma–36 ka) (Smith et al., 1993). These fields have an unclear tectono-magmatic relationship to those further south and appear to be unrelated to the active subduction setting. Arc basalts of Miocene age also occur in Northland at Waipoua stratovolcano (Hayward, 1975) active between 19 and 18 Ma (Hayward et al., 2001). The youngest intraplate basaltic vent near to the Alexandra Group is Gannet Island (0.51 ± 0.05 Ma; Briggs et al., 1997), a small nephelinitic tuff ring 19 km northwest of Kawhia Harbour. The island represents an isolated rift-related volcano with geochemical affinity to the South Auckland Volcanic Field.

Geological setting of the AVG

Eruptive activity of the AVG was associated temporally (2.7–1.6 Ma), tectonically (extensional back-arc environment) and spatially (western North Island) with the transitioning CVZ to TVZ arc front. The earliest AVG eruptions overlap with the last volcanism of the CVZ (2.69–1.95 Ma rhyolites and dacites at Tauranga; Briggs et al., 2005) and beginning of major caldera forming eruptions within the TVZ (~1.6 Ma). Some of these eruptions were centred east along strike of the AVG lineament at Mangakino caldera (1.68–1.53 Ma; Houghton et al., 1995). The AVG also marks the beginning of *back-arc associated* intraplate basaltic volcanism (Okete Volcanics). Relatively small-volume andesitic stratovolcanoes at Maungatautari (1.8 Ma; Robertson, 1983); Pureora and Titiraupenga (1.6 and 1.9 Ma, respectively; Graham et al., 1995) populated the early Pleistocene arc front to the east of AVG. The AVG thus represents an arc-perpendicular chain of basaltic stratovolcanoes situated within the back-arc zone of the CVZ-TVZ transitional arc. The Alexandra volcanic lineament (NW-SE, 300º, Fig. 1) is concordant in orientation to other arc-perpendicular chains along both the Colville and Kermadec Ridges, including the prominent Rumble V ridge (Fig. 4) (Gamble et al., 1995).

Pre-volcanic stratigraphy

The stratigraphy beneath Pirongia Volcano consists of Paleogene marine sedimentary rocks and uplifted Mesozoic metasediments (refer to Fig. 5 therein). Most of the edifice overlies the Te Kuiti Group, a mixed carbonate-siliciclastic

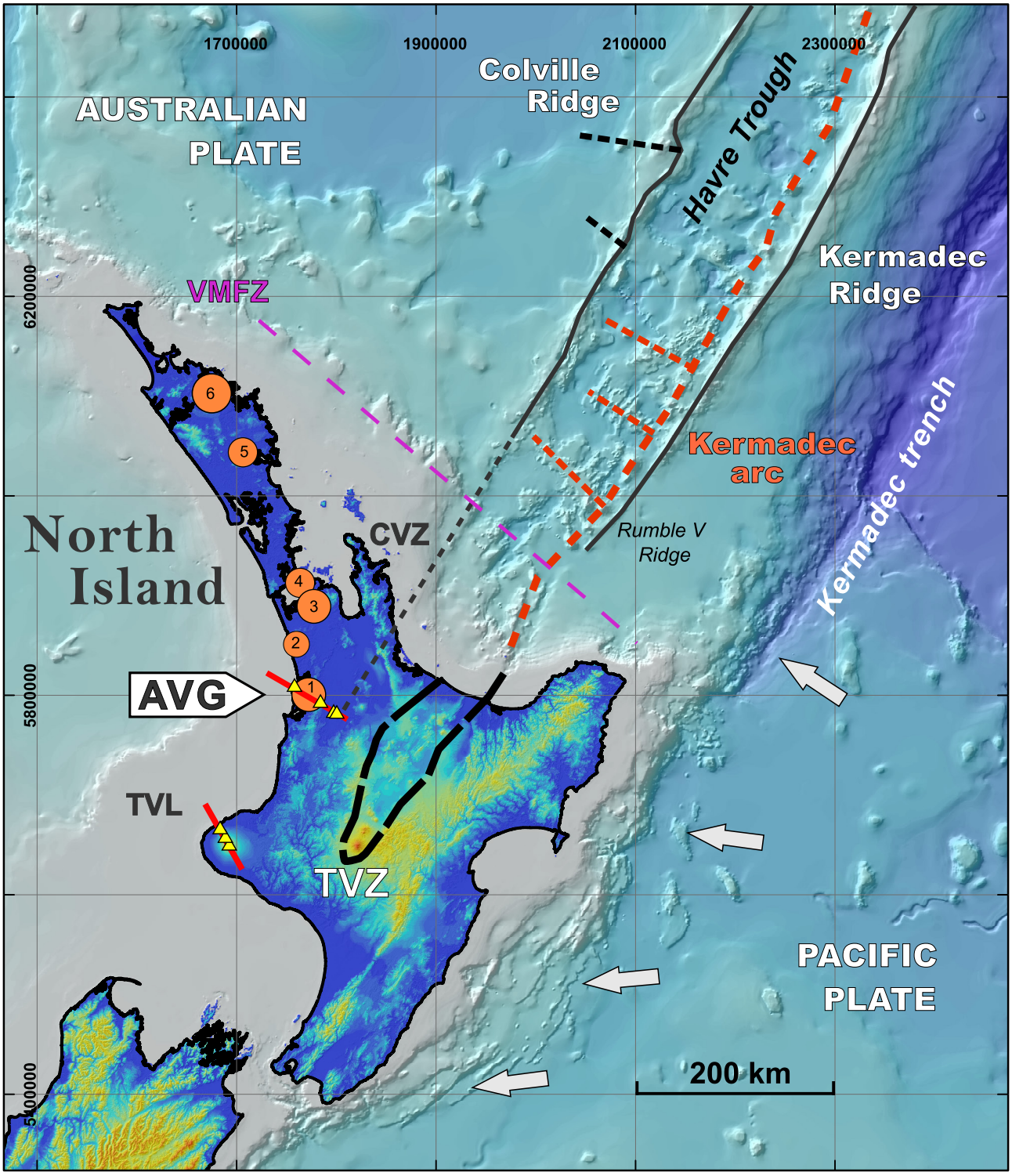

Figure 4: Regional geologic setting of the Alexandra Volcanic Group (AVG) in relation to the active Kermadec arc (orange dashed line), Taupo Volcano Zone (TVZ, black dashed line), Taranaki Volcanic Lineament (TVL) and older rifted Kermadec-Colville ridges separated by the Havre Trough. The volcanic system is the manifestation of westward subduction of the Pacific Plate beneath the Australian Plate (shown by arrows). Cross-arc volcanic chains parallel to the Alexandra Volcanic Lineament occur along the Kermadec arc (the largest being Rumble V Ridge) and Colville Ridge. Also shown are terrestrial basaltic volcanic fields (orange circles), which are (1) Okete, (2) Ngatutura, (3) South Auckland, (4) Auckland, (5) Whangarei and (6) Bay of Islands. The boundary of continental and oceanic crust is marked by the Vening Meinesz Fracture Zone (VMFZ, purple dashed line). Map data sources: bathmetry is from NIWA New Zealand Regional Bathymetry (2016) dataset; onshore topography is NZ 8 m Digital Elevation Model from Geographx; onshore volcanic geology is from 1:1M GMNZ (Edbrooke, 2017); and offshore volcanic geology and lineaments interpreted from the bathmetry data of Timm et al. (2019).

succession that forms the Late Eocene–Oligocene cover sequence over much of western Waikato (Nelson, 1978; Tripathi et al., 2008). The group is up to several hundred metres thick. South of Mt Karioi and east of Kawhia Harbour, the Te Kuiti Group consists of widespread siltstones, sandstones and limestones. The oldest deposits of Te Kuiti Group, Waikato Coal Measures (Late Eocene–early Oligocene), form thick beds (>200 m) south of Mt Pirongia at the Tihiroa coal field (Henderson and Grange, 1926; Kear and Schofield, 1959).

The Paleogene marine succession unconformably overlies indurated Triassic and Jurassic basement rocks of (from west to east) the Murihuku, Dun Mountain and Waipapa terranes. In the Waikato area, the western boundary of Murihiku Terrane is the offshore Taranaki Fault, and the eastern boundary is the Waipa Fault Zone (Edbrooke, 2005). The Murihiku Terrane forms prominent mountain ranges north and south of Kawhia Harbour and is continuous up to the Hakarimata Range anticline at Ngaruawahia (Edbrooke et al., 1994). The majority of the steep, forested terrain west of Mt Pirongia is composed of uplifted Murihiku greywacke.

Highly magnetic serpentinites associated with the Dun Mountain Ophiolite Belt (Coombs et al., 1976; Spörli et al., 1989) are present in the sub-surface below most of western North Island (e.g. Eccles et al., 2005). Projection of the Junction Magnetic Anomaly in the field area indicates that the Dun Mountain Terrain directly underlies the summit of Mt Pirongia (Fig. 5). Based on observation of the only North Island outcrop, 60 km south of Pirongia (*Wairere serpentinite*, O'Brien and Rodgers, 1973), the substratum of Pirongia Summit thus likely consists of dunitic to harzburgitic serpentinite with intense fracturing and shearing near the boundary to neighbouring terranes.

Metasediments of the Waipapa Composite Terrane are volumetrically significant basement components of the central, western and northern North Island. The terrane is sub-divided into Permian-Triassic Hunua and Jurassic Morrinsville facies – equivalent to the Manaia Hill Group (Edbrooke, 2001). In the Waikato region, the Manaia Hill Group crops out east of the Waipa Fault Zone, where prominent exposures of folded Morrinsville facies occur along the Rangitoto Range (east of Te Kuiti). In the field area, Waipapa Terrane outcrops on the northern flank of Kakepuku, and as a low range of hills 5 km further south. The terrane probably underlies the eastern flanks of Mt Pirongia and all Alexandra vents further east (Kakepuku, Te Kawa, Tokanui and Waikeria).

Paleogeography

Paleogeographic reconstructions of the Early Pleistocene North Island shoreline at 2.4 Ma indicate that Pirongia Volcano erupted through the edge of the terrestrial land mass (Trewick and Bland, 2012). The volcano was thus never an island or partially submerged. By contrast, early eruptions of Karioi Volcano began from shallow submarine vents, as indicated by pillow lavas that are preserved at Te Toto Gorge (Goles et al., 1996). The present coastal position of Mount Karioi is much the same as when it formed in early Pleistocene times. Interactions between Pirongia Volcano and the ocean are restricted to its debris avalanche fields, which extend southwest into the Kawhia Harbour.

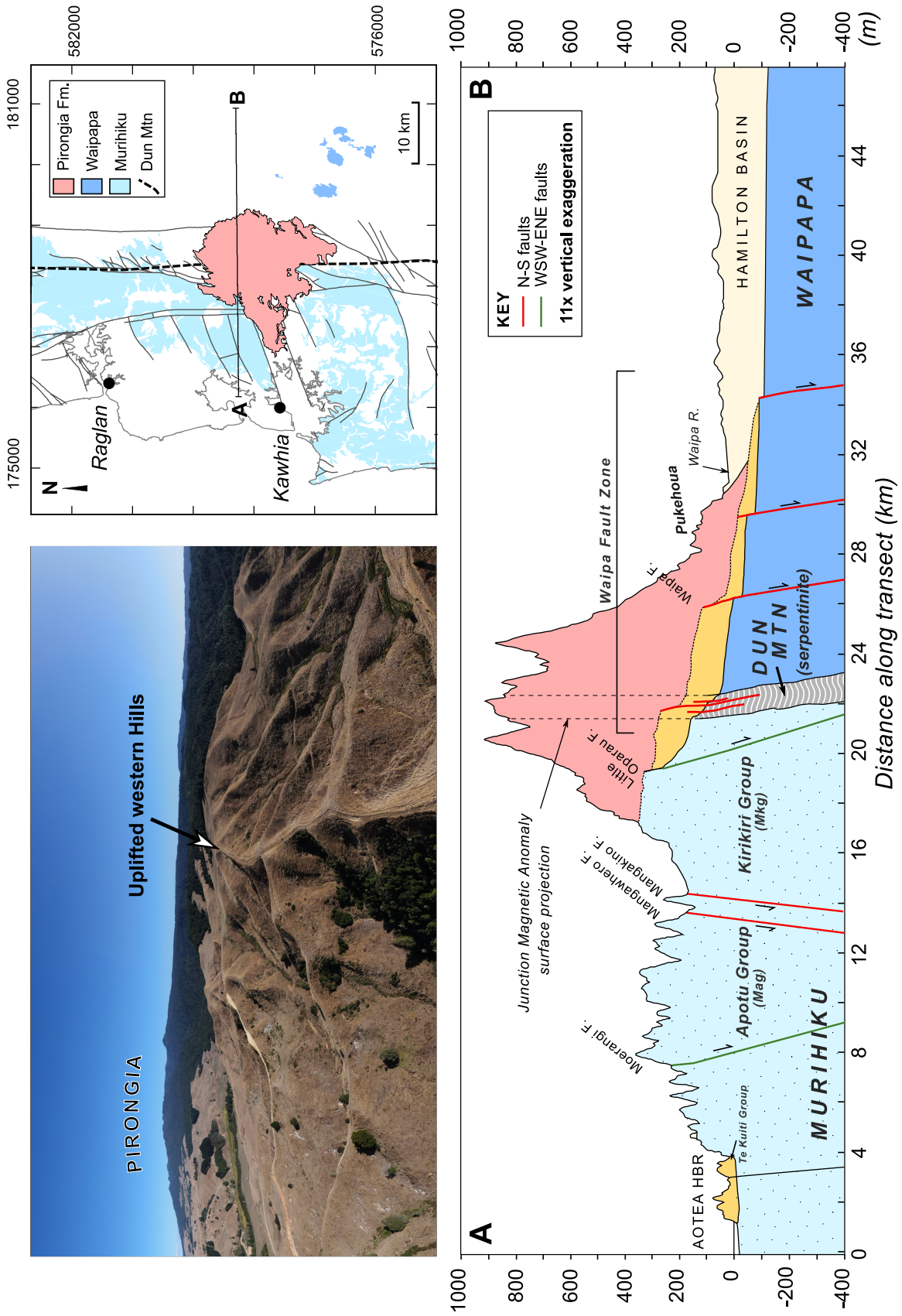

Figure 5: Cross section (see inset map for location) showing the regional structural relationship between the Pirongia Volcano and underlying substratum. The volcano is situated at a major horst-graben interface bounded by normal faults of the Waipa Fault Zone. The uplifted western block consists of Murihiku Terrane rocks (Apotu and Kirikiri Groups) overlain by a veneer of Te Kuiti Group sedimentary rocks (see photograph, top left). The eastern block consists of Waipapa Terrane that is dissected by a series of stepping normal faults that form the Hamilton Basin. The Waipa Fault Zone is focused within the Junction Magnetic Anomaly (JMA), which marks the position of the Dun Mountain serpentinite belt. The Pirongia edifice is situated above the JMA and its summit directly overlies it (dotted lines).

Faults

Numerous faults dissect the basement and Oligocene-Miocene strata of western Waikato. The regional fault pattern consists of two groups trending N-S and ENE-WSW (Pilaar and Wakefield, 1978). The longest on-land faults belong to the Waipa Fault Zone, which trends NNE from Waitaanga (North Taranaki) to Ngaruawahia and has sub-vertical inclination at Wairere (O'Brien and Rodgers, 1973). In the Hamilton Basin, normal faulting along the Waipa Fault Zone has occurred parallel to a belt of serpentinites (Dun Mountain Terrane; see Fig. 5). Total vertical displacement amounts to approximately two kilometres in the mid basin and 200–300 m in the southern areas (Kear and Schofield, 1978).

The Whaingaroa (Raglan), Aotea and Kawhia Harbours all represent depressional features bounded by normal faults (Fig. 1) (Henderson and Grange, 1926). In the Kawhia area, the meridional fault pattern is connected by a series of stepping, ENE-WSW transfer faults which form the harbour and its onshore extension, the Oparau Graben. The largest vertical displacement occurs on the Oparau Fault, where greywackes are uplifted to the north by ~200 m (Waterhouse and White, 1994). Five new faults striking parallel to the Oparau Fault were identified in this study through field mapping and drill core data from the New Zealand Geological Survey. The Little Oparau Fault, which runs adjacent to the Oparau Fault, truncates the meridional fault system and projects under Mount Pirongia. North of Kawhia, the Karioi block is detached from the Kapamahunga Range by meridional faults on the inland and coastal margins, and another major fault aligned with the axis of Aotea Harbour (Waterhouse and White, 1994; Goles et al., 1996).

ALEXANDRA VOLCANIC LINEAMENT

The near perfect alignment of Tokanui, Te Kawa, Kakepuku, Pirongia and Karioi along a NW-SE (300º) axis defines the Alexandra Volcanic Lineament (AVL; see Fig. 1). This remarkable volcanic-tectonic feature was first identified by Henderson and Grange (1926) and later described as the single largest (60 km), continuous volcanic lineament within the North Island volcanic fields (Kear, 1964; Briggs 1983). Early mapping suggested that the AVL was parallel to a partially buried fault trending NW-SE from Raglan (Henderson and Grange, 1926). However, no further evidence for such a fault was found in the detailed mapping of Player (1958), Kear (1960), Briggs (1983) or the more recent QMAP compilation (Edbrooke, 2005). Instead, these maps indicate that the lineament is discordant to the regional fault pattern of western North Island, which shows meridional and ENE-WSW orientation (see Fig. 1).

The presence of a deep-seated crustal fault, with no surface expression, was postulated by Kear (1964) and Briggs (1983) as a possible control on development of the AVL. A fracture in the mid to lower crust may have conceivably formed under an extensional stress regime, perpendicular to the subduction margin, and channelled magmas along a linear zone into the upper crust where they erupted along the surficial fault system. However, an unresolved problem with this model is that all major normal faults in western North Island propagate deeply into the crust, in many cases to its base (~25 km deep; Stern, 1985), and it thus appears unlikely that a major crustal fracture could exist without any surface expression. An alternative explanation is that the AVL is controlled by a NW-SE striking tear on the subducted Pacific slab that underlies western North Island. Slab tearing may explain not only the linear distribution of volcanoes, but also the geochemical diversity of lavas erupted in the volcanic field, which originate from several discrete zones in the mantle that ultimately relate to the transient subducted slab (Briggs and McDonough, 1990).

Formation of Hamilton Basin

The extensional depression of the Hamilton Basin is the largest tectonic feature of western Waikato (McCraw, 2011; Fig. 1). The basin lies within the back-arc zone of western North Island and is parallel to another major graben structure, the Hauraki Rift. The landscape consists of an expansive lowland (25 km wide, 80 km long) elongated from north to south, bordered by parallel highland blocks (up to 400 m high) to the west (Hakarimata and Kapamahunga Ranges) and east (central hills). The western blocks were uplifted along normal faults of the Waipa Fault Zone. The basin is cut along its northern edge by the NE–SW oriented Taupiri Range. South of Mt Pirongia, the basin gradually shallows and merges with the Waipa basin and King Country plateau. The Waikato and Waipa Rivers flow through central and southern parts of the basin (Fig. 1).

The age of normal faulting and thus geomorphic development of the Hamilton Basin is poorly constrained. Principal fault displacements probably occurred between the Pliocene and Early Pleistocene (Selby and Lowe, 1992), followed by infill of the basin by Quaternary pyroclastic deposits and sediments. The spatio-temporal relationship between volcanoes and underlying faults in the basin provides a useful constraint on late-stage fault activity. Extension-related volcanoes of the area include arc-type stratovolcanoes (Alexandra and Maungatautari groups) and intraplate volcanics of Late Pliocene to Early Pleistocene age. The spatial relationship between these volcanoes and the highland blocks suggests that their distribution is normal fault controlled and may have a temporal association with periods of more active faulting in the basin. The Waipa Fault Zone, which is overlain by non-displaced flank deposits (age correlated to ~2.4 Ma) of Pirongia Volcano, has been inactive since at least the early Pleistocene. The earliest vent flare-up of the Alexandra Volcanic Group at ~2.7 Ma (at Kakepuku, Te Kawa and Turitea), and the later development of Pirongia Volcano (~2.5 Ma), probably coincides with the last major movements along stepping faults of the Waipa Fault Zone.

Throughout the Quaternary, the Hamilton Basin was infilled by large volumes of ignimbrites, sediment and tephra-fall

deposits from distant volcanic centres and local reworking. Accretion of tephra fallout gradually buried the flanks and ring plain of Pirongia Volcano, as well as the cones of Te Kawa and Kakepuku farther east.

Pirongia vent distribution

The broad mountainous landscape of Pirongia reflects the growth of the volcano from many distinct volcanic vents over a period of about one million years. The location of individual vents within the edifice is the product of a complex interplay between the deep-seated Alexandra Volcanic Lineament and normal faults linked to the Hamilton Basin graben and surrounding horst blocks. It is possible, if not probable, that extension on the faults underlying Pirongia prohibited the development of a stable, long-lived vent system. Instead, the magmatic 'plumbing system' of the volcano periodically established new vents in response to changes (i.e. faulting) in the local tectonic environment. An excellent modern analogue of this process is Tongariro Volcano (see Gómez-Vasconcelos et al., 2017), situated within an actively extending graben, which continues to expand as new vents develop across the mountain (e.g. Ngauruhoe, Te Maari, Pukekaikiore).

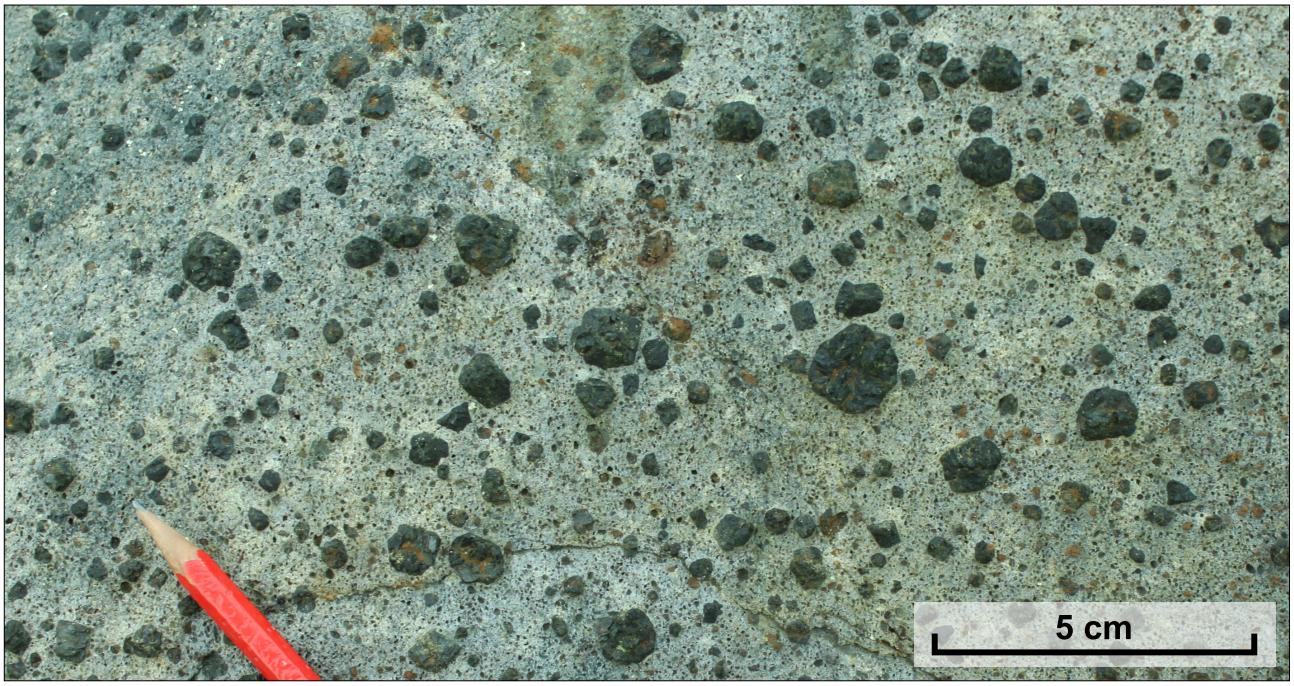

Figure 6: Ankaramite basalt from Pirongia Volcano. The rock contains megacrysts of clinopyroxene (black) set within a finer grained groundmass of plagioclase, clinopyroxene, olivine and magnetite.

BASALT

Basalt is a dark grey, fine-grained rock formed by the solidification of lava flows. This rock comprises most of the ocean floor within the Pacific region, and locally forms volcanic islands (e.g. Hawaii) and continental volcanic fields, such as those found across Zealandia. Basaltic lava flows typically erupt from fluidal fire fountains or from over-spilling lava lakes that construct either volcanic shields (e.g. Rangitoto Island, Auckland) or scoria mounds (e.g. Mt Eden, Auckland) depending on the effusion rate and dissolved gas content of the magma. The appearance of basalt varies widely in terms of colour (dark grey when fresh to red when oxidised), vesicularity (from escaped gas bubbles) and crystal content, but its composition is always low in silica and abundant in iron and magnesium. The key minerals in basalt, which are pyroxene (dull black), olivine (greenish-yellow), plagioclase (white) and magnetite (black), crystallise within the host magma as it ascends from the mantle to the Earth's surface. The largest crystals, termed phenocrysts, are generally <2 mm in size but visible to the naked eye. In rare cases, basalts may contain actual fragments of the mantle ('ultramafic xenoliths') comprised of striking-green olivine and other minerals, that are ripped up by the host magma at depths exceeding 30 km. Spectacular examples of such xenoliths occur in the Okete Volcanics near Raglan.

The distinctly crystal-rich basaltic rocks (called 'ankaramites') that dominate the Alexandra Volcanic Group are unique within New Zealand, rare across Zealandia and sporadic throughout the south Pacific (occurring in Tahiti, Rarotonga, Tonga, Fiji and Vanuatu). Ankaramites are a highly porphyritic variant of basalt abundant in clinopyroxene and lesser amounts of olivine (mega-) phenocrysts, first identified in Ankaramy, Madagascar (La Croix, 1916). The ankaramites of Kakepuku were first described by Hochstetter as '*trachydolerite containing numerous pyroxene crystals*' (p. 317, von Hochstetter and Sauter) and later remarked on by (influential Otago Professor) Patrick Marshall, who, in 1907, noted that *'the rocks differ markedly from all other volcanic material of the North Island*' (Marshall, 1907, p.96). The Alexandra ankaramites were described in some detail by Briggs and McDonough (1990), and in earlier works by Henderson and Grange (1926), Kear and Schofield (1978), Matheson (1981), Briggs (1983), Briggs & Goles (1984), and later by Goles et al. (1996). In outcrop, the ankaramites contain large blackish-green clinopyroxene phenocrysts that protrude from weathered surfaces (Fig. 6). Olivine phenocrysts are honey-brown coloured when fresh, and weather to orange-coloured, low-relief crystals. The phenocrysts are set within a groundmass that ranges from dark purple and very fine-grained to paler grey with abundant, tabular prisms of plagioclase. Rarely, the phenocryst content is so high that almost no groundmass is present and the rocks essentially appear doleritic. Most ankaramites are weakly to non-vesicular, except for those of pyroclastic origin, which form scoria with glassy groundmass, or lavas located very near to vents. Accesible outcrops of ankaramite occur at Ruapane Peak (see Table 1).

Basalts with textures finer than the ankaramites, but with an equivalent mineral assemblage, are common throughout the volcanic field. Rarely, basalts containing olivine as their only or dominant phenocryst phase occur on flank vents. Fine-grained, alkali basalts with textures equivalent to the basanites and hawaiites of the Okete Volcanics are intercalated in the successions of both Pirongia and Karioi volcanoes.

Basaltic andesites

Medium grey-coloured basaltic andesites occur as single lava flows and thick lava successions on Pirongia. In outcrop, they are notably finer-grained than the basalts, containing sparse phenocrysts or glomerocrysts of black clinopyroxene and abundant plagioclase. Hornblende is relatively abundant as vitreous, needle-like black laths that are often skeletal and sometimes replaced by phlogopite. Olivine is sparse or absent either as phenocrysts or groundmass. The groundmass is fine-grained and commonly has a distinctive dark-purple to grey tone with abundant laths of plagioclase throughout.

Andesites

The Alexandra andesites are leucocratic rocks, rich in plagioclase, that commonly outcrop along the tops of ridges and in dyke walls. Accessible outcrops of andesite occur at Tirohanga, Wharauroa, Mahaukura and Pūawhe peaks (Table 1). The phenocryst assemblage is dominated by pale-white plagioclase laths, commonly seriate textured, and hornblende in variable abundance. The latter occurs as prominent, vitreous laths (with megacrysts exceeding 1 cm in length) and smaller acicular microphenocrysts. Clinopyroxene content is generally subordinate to hornblende. The phenocrysts are set within a fine-grained, pale-grey holocrystalline to dull, darkish-grey glassy groundmass.

OVERVIEW OF EDIFICE CONSTRUCTION

The Pirongia Volcano is a stratigraphically complex, long-lived compound volcanic system that produced the single largest basaltic landform in the North Island. The geological map illustrates the spatial and temporal association of its main volcanic units. The mapped deposits imply that the Pirongia edifice was formed through multiple stages of cone-building and collapse within a dispersed area of its present summit zone. Each central vent produced a thick, volcanic shield of basaltic lavas that evolved gradually in magmatic composition and eruption style towards more explosive, andesitic volcanism. The overall edifice was broadened progressively through time by Hawaiian-type fissure eruptions on the mid to lower flanks, and the continual aggradation of debris to its ring plain.

In addition to phases of growth, edifice morphology has been strongly influenced by repeated, large-scale sector collapses throughout its history. The largest of these events, the Oparau debris avalanche, excavated an area of 2×4 km on the southwest flank down to the underlying basement and produced a run-out deposit of at least 20 km. Large volumes of undifferentiated, polymict volcaniclastic breccias similar to the Oparau deposit are also dispersed within the ring plain to the south of the volcano. These deposits attest to the occurrence of numerous other large collapse events within the history of Pirongia. The distribution of ring plain deposits suggests that many more debris avalanches also flowed northwestward into the Hamilton Basin and have subsequently been buried by younger basin-filling deposits. Many of the collapse deposits cannot be traced back to an obvious scarp, which probably reflects the important role of edifice 'healing' through emplacement of younger lavas into the scarps. Occupation of sector collapse scarps by younger vent deposits is apparent in the youthful ridge morphology of lavas from Pūawhe/The Cone and Te Akeohikopiro (see Fig. 7), which lie juxtaposed between morphologically older flanks.

Ankaramite volcanic landforms

The Pirongia edifice has been described as a low-angle shield volcano or stratovolcano (Briggs, 1983; Briggs, 1986; Briggs and McDonough, 1990) that has reached the end of the planeze stage of erosion (Kear and Schofield, 1978). This view was based, in part, on the relatively subdued lower slopes of the mountain that were interpreted as gently dipping (5–10°) flank lavas. While both Pirongia and Karioi are characterised by phases of *sensu stricto* shield-building with shallowly dipping lavas, their overall volcanic structures are complicated by the presence of overlying stratovolcanic cones. New mapping indicates that, with a few exceptions, most of the lower flanks on Pirongia are composed of ring plain rather than lavas, and therefore do not represent the core structure of a simplistic volcanic shield. Instead, where lavas are mapped on the mid-flanks, they are steeply inclined at 15–20° and reach a maximum of 28° on the upper ridges. This is consistent with the natural inclination of ankaramite cones at Kakepuku (13–18°) and Te Kawa (18–23°), and the dip of basaltic strata in cliff sections of Mt Karioi (18–23°). Ankaramites throughout the Alexandra Volcanic Group thus show a rheological preference to form steeply-dipping cone structures. The rheology of such coarse-grained basalts contrasts with that of finer-grained basaltic lavas, as demonstrated at Rangitoto Island (Auckland Volcanic Field), which although of similar volume to Kakepuku (~0.7 km^3), forms a pancake-like shield structure with flank inclinations of 4–6°.

Table 1: Summary of important geographic locations on Pirongia and their corresponding geological structure and lithology.

Peak name	NZ Topo 50 GR	Elevation (m a.s.l.)	Volcanic structure
Basaltic peaks			
Tiwarawara	BE33 849 903	710	Ankaramite dome
Ruapane	BE33 858 948	723	Ankaramite dyke swarm
Tahuanui	BE33 844 943	850	Ridge of basaltic lavas
Te Akeohikopiro	BE33 836 908	869	Basaltic scoria and lavas
Tireni	BE33 847 927	868	Lava lake
Andesitic peaks			
Tirohanga	BE33 853 941	770	Andesite dyke
Kohatupiko	BE33 838 904	785	Andesite dyke
Tihitoetoe	BE33 859 921	845	Andesite dyke
Wharauroa	BE33 864 931	850	Andesite dome
Mahaukura	BE33 862 927	902	Andesite dyke
Hihikiwi	BE33 838 922	905	Basaltic andesite dyke
Pūawhe/The Cone	BE33 824 927	953	Andesite dyke
Pirongia Summit	BE33 843 929	959	Andesite dyke and basaltic deposits

ERUPTIVE HISTORY

ALEXANDRA VOLCANIC GROUP

Earliest activity

Volcanism began around 2.7 Ma in the far eastern edge of the field, where Strombolian eruptions formed the early cone of Kakepuku and a lava field at Te Kawa. Both vents were aligned along the Alexandra Volcanic Lineament and may represent a single fissure system that rose along crustal faults. Another vent at Turitea (see Fig. 1), 10 km southwest of Kakepuku, produced a small lava field of more silicic composition than the other centres. The first eruptions of alkaline basalt (of the Okete Volcanic Formation) occurred around 2.6 Ma in the Aotea-Whaingaroa area at Taranaki Point (2.6 Ma), Bridal Veil Falls (2.57 Ma), Okete Quarry (2.69 Ma) and Haroto Bay (2.58 Ma) (Briggs et al. 1989).

MOUNT PIRONGIA

The Pirongia Volcano has grown from numerous overlapping vent structures and accumulated deposits over a period of one million years. Accretion of the edifice was sporadic and characterised by flare ups in volcanism separated by repose periods of 20, 50, 30 and ~100–350 kyr respectively. The overall tempo of volcanic activity was probably controlled to a first order by the regional tectonic setting, where heightened vent activity corresponded to periods of crustal extension in western North Island.

Six main stages of growth and collapse are recognised in the history of Pirongia. Each stage is separated temporally from other stages by an erosional unconformity or sector collapse related disconformity. In the following sections, the edifice building stages are described in stratigraphic order from oldest to most recent. Stages are indicated by different colours in Fig. 7 and on the geological map. Unit symbols in text refer to units on the geological map. Radiometric age dates referred to in text are summarised in Table 2.

Stage I – The Paewhenua edifice (~2.5–2.42 Ma)

A focused site of magmatism was established in the area of Mount Pirongia around 2.5 Ma. Basaltic magmas upwelled along the Alexandra Volcanic Lineament were intersected at crustal levels by normal faults of the Waipa Fault Zone hosted within weak, serpentinitic host rocks (Dun Mountain Terrane).

The oldest edifice of Pirongia, called Paewhenua, likely began its formation from fissure vents aligned north-south along the fault zone. Fissure lavas initially flowed eastwards from the Kapamahunga Range into the Hamilton Basin, where a broad lava field developed. Following stabilisation of the vent, continual accretion of lavas formed a volcanic shield (the Ppe unit) with prominent shield-building around 2.49 ± 0.09 Ma (Briggs et al., 1989). Lavas and ring plain deposits accumulated against the Kapamahunga Range, forming a plateau. The overall effect on volcanic morphology was a highly asymmetrical edifice, with shallowly dipping western flanks and smoothly arcuate, ring-plain (Pru) mantled slopes on the northern and southern flanks.

Lava compositions of the Paewhenua edifice span the typical range for Pirongia Volcano with abundant ankaramite and subordinate basaltic andesite. Andesitic dykes are relatively rare compared to younger vent centres on Pirongia. Lavas with alkalic compositions were erupted contemporaneously with Pirongia ankaramites in the lower succession of the main Paewhenua shield. Another flank vent on the Paewhenua ridgeline produced an extremely porphyritic lava flow field (Ap) with mineralogy typical of an alkali basalt (titanaugite and olivine) and texture similar to a coarse-grained ankaramite.

The Paewhenua shield built to a height of at least 870 m (a.s.l.) with its central vent(s) dispersed in the area of Pirongia Summit. The basaltic surface at Tireni Peak (Ptr) is the eroded remnant of a lava lake that grew within one of the vents of the early shield. The lava lake surmounts vent proximal lavas along the adjacent ridgeline that include basaltic andesites of marked textural diversity from porphyritic to strongly trachytic. One of the last known deposits of the Paewhenua shield is a basaltic andesite lava flow (Ptpb), dated at 2.418 ± 0.05 Ma (new age). The lava flowed NNW for three kilometres from a vent north of Tireni Peak (now partially buried by later eruptives).

Stage 1 eruptions were coincident with emergent alkaline volcanism at Karioi Volcano (2.58–2.48 Ma; Goles et al. 1996), which produced a tuff ring and lava flow (Pauaeke member). The main Karioi edifice building phases overlapped with Stage I and Stage II (2.48–2.28 Ma) of Pirongia Volcano.

Stage II – Tirohanga Volcano (2.4–2.35 Ma)

Vent activity migrated north-eastward from the summit zone by 2.4 Ma to form the Tirohanga Volcano, which surmounts older lavas of the Paewhenua shield. Flank geometry suggests that the cone was centred on Tirohanga Peak, an andesitic dyke-dome complex (Pta) that marks the upper plumbing of the volcano. The outer flanks of the cone are marked by the Mahaukura and Tahuanui ridgelines, which are broadly symmetrical and indicate that the cone was about five kilometres wide (see cross section C-C' on map). The cone was constructed from a thick succession of basaltic andesite lava flows (Pml), some of which infilled a large collapse scarp in the Paewhenua shield in the area of the Mahaukura bluffs (Fig. 7). Lavas from the base of the bluffs are dated at 2.396 ± 0.05 Ma (new age), indicating that the collapse occurred shortly before Stage II activity. Eruption styles ranged from Hawaiian to Strombolian and Vulcanian activity, the latter associated with late-stage andesite dykes. The Tirohanga Volcano was later broadened by parasitic vents southeast of Tirohanga Peak in the area around Mahaukura, Tihitoetoe and Wharauroa peaks. The location of these vents was structurally controlled by the margins of the underlying sector collapse scarp. The vents were fed by andesitic dyke swarms (Pma), similar in composition to the Tirohanga andesite, that cross cut 2.396 Ma cone lavas (Pml). During the last active phase of the Tirohanga Volcano, an ankaramitic scoria cone fed by

a dyke swarm erupted on the northern flank at Ruapane Peak. The Ruapane vent appears to be relatively young with three separate dates of 1.89 ± 0.06 Ma, 2.06 ± 0.10 Ma, and 2.35 ± 0.20 Ma (Robertson, 1976). The close spatial association to Tirohanga Volcano suggests that the older date of 2.35 Ma (from a plagioclase separate) is the most coherent with respect to the surrounding stratigraphy and it is adopted here.

Stage III – Hihikiwi Volcano (2.3–2.13 Ma)

Following decreased activity at Tirohanga Volcano, another major vent developed on the southern flank of Pirongia in the area surrounding Hihikiwi ridgeline. The cone produced basaltic pyroclastics and lavas (Phb), as well as andesitic dyke swarms (Phr) with coincident orientation. Geomorphic evidence suggests that the main vent location was probably just north of the ridge, within the Oparau River valley. The age of the Hihikiwi Volcano is inferred from dates on two basaltic clasts (2.13 ± 0.10 and 2.25 ± 0.10 Ma) sampled by Robertson (1976) within the Oparau debris avalanche deposit (Odb; 3.4 km west of the proposed vent site).

A fissure vent later opened in the Tiwarawara Peak area. The vent was initially activated with fire fountains of basaltic scoria and tuff, building a prominent scoria cone (Toa). The root of the cone outcrops at Tiwarawara Peak where ankaramite cumulate rocks are exposed. In the late stage of the vent activity, andesite dykes (Twd) were emplaced within the fissure zone, with radial strike to the main Hihikiwi vent. Another radial dyke with subparallel orientation to the Tiwarawara dykes was emplaced at Kohatupiko Peak (Kpa) around this time, erupting through older flank lavas.

Distal lava flows were erupted on the SW flank and periphery of Hihikiwi Volcano around 2.3 Ma. These included a distinct olivine-phyric basalt erupted from a vent above Pirongia West Road (Pob), at least one scoria cone (Psc) and a large dome to its south (Hikurangi vent, Phk; 2.30 ± 0.05 Ma; Briggs et al., 1989). The dome produced a distinct lava flow of phlogopite basaltic andesite comparable in mineralogy and composition only to the (phlogopite-bearing) late-stage lava flow at the summit of the Paewhenua shield (Ptpb).

Stage IV – Hihikiwi sector collapse (~2.1 Ma)

A large sector collapse affecting at least 6 km^2 of the southern flank occurred during the late stages of the Hihikiwi Volcano (Fig. 7). The collapse destroyed part of the older Paewhenua

Table 2: New and existing radiometric age dates for Pirongia Volcano

Lab no.	Location	Rock type	NZ Topo50 GR	Age (Ma) ± 1 sd	Method	Source
P31	Summit	Andesite	BE33 842 935	1.60 ± 0.04	K-Ar	Briggs et al. 1989
P47	Pukehoua	Basalt	BE33 899 907	1.64 ± 0.13	K-Ar	Briggs et al. 1989
277	Oparau	Basalt	BE32 792 917	2.13 ± 0.10	K-Ar	Robertson 1976
278	Oparau	Basalt	BE32 792 917	2.25 ± 0.10	K-Ar	Robertson 1976
P59	Hikurangi	Basaltic andesite	BE33 805 878	2.30 ± 0.05	K-Ar	Briggs et al. 1989
394	Ruapane	Basalt	BE33 859 946	2.06 ± 0.10	K-Ar	Robertson 1976
396a	Ruapane	Basalt	BE33 859 946	1.89 ± 0.06	K-Ar	Robertson 1976
396b	Ruapane	Basalt	BE33 859 946	2.35 ± 0.20	K-Ar	Robertson 1976
PS3	Mahaukura	Basaltic andesite	BE33 857 927	2.396 ± 0.0543	^{40}Ar/^{39}Ar	This study
PT6	Tahuanui	Basaltic andesite	BE33 836 942	2.418 ± 0.0548	^{40}Ar/^{39}Ar	This study
P38	Wharauroa	Basalt	BE33 869 940	2.49 ± 0.09	K-Ar	Briggs et al. 1989
T8	Turitea	Basaltic andesite	BE33 889 800	2.74 ± 0.09	K-Ar	Briggs et al. 1989

edifice, producing a debris avalanche that travelled ~15 km southwards and deposited a large amount of material on to the southern ring plain (Mangakiekie breccia, Mdb). The collapse event was probably triggered by several factors including hydrothermal weakening of the (old) flanks, seismicity associated with regional faults, and/or edifice deformation caused by underlying magma bodies. The head scarp was subsequently infilled by (undated) basaltic lavas from a vent near Te Akeohikopiro peak (Tkb). Vent activity was characterised by Hawaiian fire fountaining episodes that fed relatively fine-grained basaltic lava flows. The lavas flowed southward in channels from the scarp into the southern ring plain.

Stage V – Oparau sector collapse (~1.7 Ma)

The period from 2.1 to 1.7 Ma was characterised by apparent quiescence of the volcano and minor hydrothermal activity. Approximately 1.7 Ma, a large volume sector collapse event destroyed the entire western flank of Pirongia (an area of 10 km^2). The deposits flowed catastrophically for >20 km into the Oparau Graben (the lower reaches of which are now occupied by Kawhia Harbour). The collapse penetrated deeply enough into the subsurface that it rotated the basement rocks underlying Pirongia. The edifice was affected up to summit level. The scarp boundary was closely aligned with the Little Oparau Fault on its northern edge (Fig. 7). The southern scarp boundary was near the present radial valley of Oparau River, where it truncated the Paewhenua shield (Ppe) and the younger Hihikiwi Volcano. The truncated roots of a feeder dyke swarm in the mid-reaches of the Oparau Valley suggest that another vent centre was also destroyed by the collapse.

The probable cause of the collapse was a combination of morphological and seismic factors preconditioned by hydrothermal weakening of the edifice. The close spatial association between the boundary of northern scarp, the alignment of 1.6 Ma vents (see Stage VI) and the Little Oparau Fault suggests that the fault was an important structural control on the sector collapse. It is thus considered probable that the collapse was caused by seismicity along the Little Oparau Fault. The sector collapse occurred on the western flank because of its proximity to the fault and position at the head of the Oparau Graben. The morphological effects of any vertical offset associated with re-activation of the fault have been subdued by subsequent erosion of the edifice. The proposed age of activation on the Little Oparau Fault is significantly younger than that known from its offset of Oligocene strata in the Oparau Graben, and among the youngest fault activations in western Waikato.

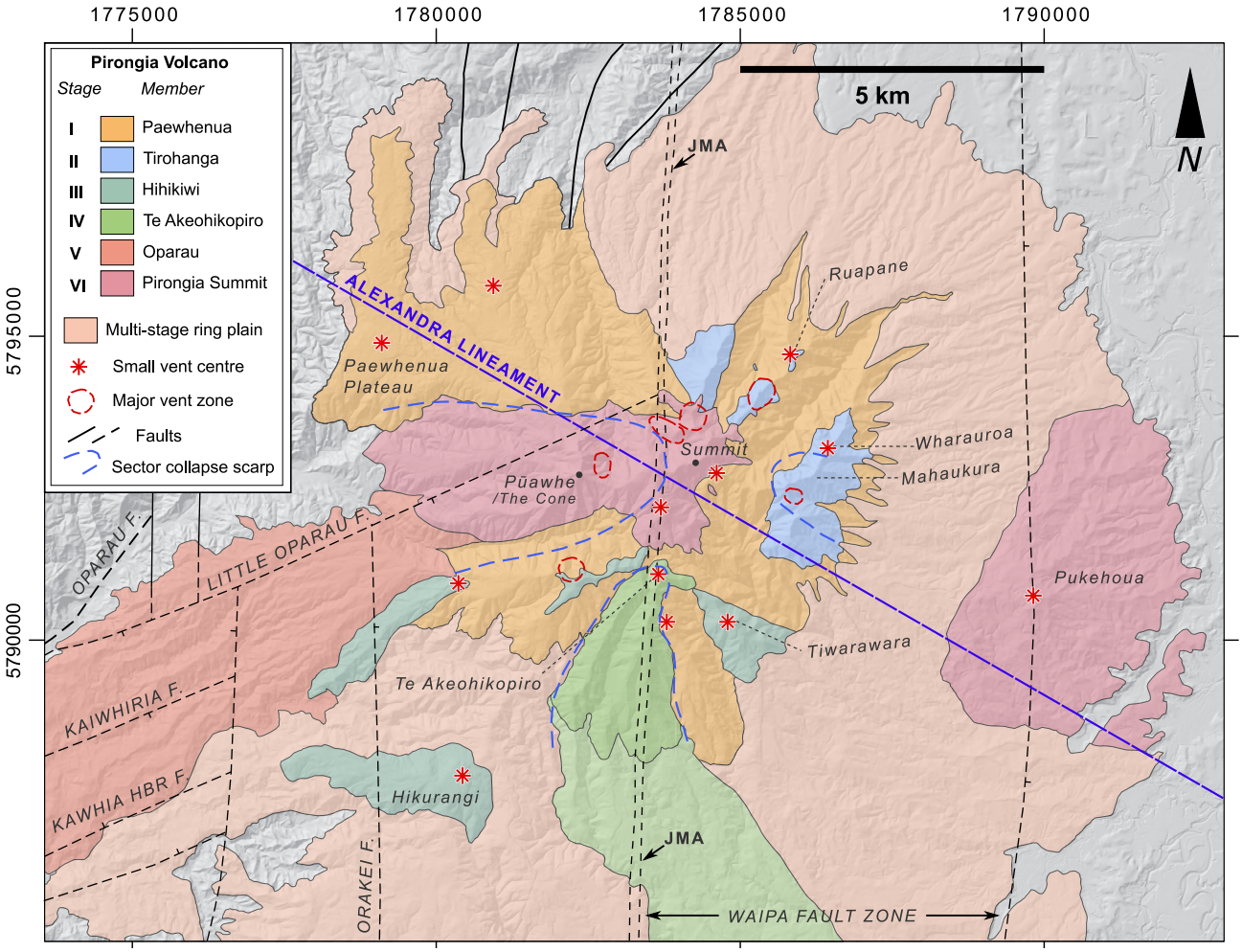

Figure 7. Simplified geological map of Pirongia, colour coded by stratigraphic member. JMA=Junction Magnetic Anomaly.

Stage VI – Pirongia Summit (1.6 Ma)

In the aftermath of the Oparau collapse event, the Pirongia Volcano re-activated around 1.6 Ma with eruptions in the summit zone and lower eastern flank.

Summit eruptions were centred on two major vent sites, Pirongia Summit and Pūawhe/The Cone, within the head scarp. The vents were aligned parallel to the Little Oparau Fault (see Stage V). Mapped deposits suggest that the first vent to activate was near Pirongia Summit. The vent activity likely began with effusions of basaltic lava and breccia (Psul) that were channelled westward into the newly opened scarp. Some ankaramite and basaltic andesite lavas flowed south and southeast as short flows to the area around Hihikiwi Peak. Erupted compositions gradually transitioned towards andesite. A steep-sided cone was constructed from pyroclastic material fed by a swarm of andesitic dykes (Psa; 1.60 ± 0.04 Ma). Dome or small flank collapse within the new cone produced block-and-ash flows that were channelled westwards into the scarp. Some pyroclastic flows also travelled south-eastward towards Hihikiwi Peak. During the later stages of the summit vent, eruptions were mainly basaltic in composition and produced fire-fountains of scoria and effusion of ankaramite lavas (flowing south westward). The flat terrain around Pahautea Hut is formed from a ponded lava flow from this period. Late-stage andesitic dykes were then emplaced, which fed more andesitic eruptions. Most of the dykes were clustered around the Summit Basin. A group of parasitic dykes with similar orientation to the summit dykes (mostly trending NW-SE) erupted around this time in the area around Hihikiwi Peak. The peak itself marks the location of the largest dyke of this group, which fed a parasitic vent cone of which only the root is now exposed.

An isolated batch of basaltic magma, probably related directly to the upwelled summit magmas, erupted along a fissure vent on the lower eastern flank of Pirongia at 1.64 ± 0.13 Ma. The fissure produced a small lava field and a series of scoria cones aligned along the fissure axis. The distal location of the Pukehoua vent may be the result of interplay between edifice loading and structural control by the Waipa Fault Zone.

The last volcanic activity of Pirongia Volcano appears to have been centred just east of Pūawhe/The Cone. The associated lava field was extensive and flowed westward to infill the remainder of the Oparau collapse scarp with fine-grained basaltic lavas (Pcb). The Pūawhe vent produced a steep-sided cone of similar altitude and proportion to the summit cone. It was composed of relatively more basaltic lava, with fire-fountain formed breccias (Pcbr) constructing the uppermost cone. During the last stage of Pūawhe vent, vulcanian andesitic eruptions occurred, which were fed by a dyke swarm (Pcd) of distinct composition to that of the summit dykes.

This reactivation period marked the final eruptive phase of Pirongia, and of the entire Alexandra Volcanic Group.

POST-VOLCANIC DENUDATION

The Pirongia edifice has been intensely modified from its original morphology by over two million years of erosion. In the post-volcanic period, erosion by sector collapses, lahars, mass movement and fluvial incision has reduced the summit height of Pirongia by 300–400 m vertically, such that the sub-surface dyke system is now exposed on the ridgelines. The mountain was described as within the 'planeze stage' of erosion by Kear and Schofield (1978), where sections of the original flanks ('planezes') are preserved between deep radial valleys. The present landform is controlled largely by a fluvial erosion regime that has likely persisted in western North Island since at least Early to Mid-Pleistocene times (as evident in the highly dissected, 1.6–0.9 Ma King Country ignimbrite plateaux). Similar radial drainage networks occur on active North Island volcanoes with high orographic rainfall, e.g. Taranaki and Ruapehu. Unlike these volcanoes, however, glaciation has had no influence on the geomorphology of Pirongia, which is consistent with its warm, coastal location in northern New Zealand and relatively low elevation. A seasonal ice cap may have existed on the (now eroded) summit peaks during glacial periods, when the volcano reached 1200–1400 m (a.s.l.). Pirongia would have been sufficiently eroded by the time of the last glacial cycle (74–18 ka) to avoid glaciation when equilibrium lines for central North Island reached ~1500 m (a.s.l.) (Eaves et al., 2016).

The erosional pattern is defined by numerous radial valleys, of which five are entrenched to depths of several hundred metres (see Fig. 7). Fluvial erosion has progressed headwards up the valleys so that each is separated by only thin ridges of volcanic rock. Two of the presumed oldest valleys of northeastern Pirongia, Mangakara and Rangitukia, have bulbous 'stone arrowhead' morphologies and have incised headwards almost to the point of coalescence. All the main radial valleys likely began incision during the active phase of volcanism, when the summit peaks were taller and radial channels were cut into the loose surficial debris. Debris avalanche deposits below the south and southeast flanks suggest that sector collapses influenced the initial formation of some valleys (e.g. the upper Oparau River valley). At other sites, the heads of valleys coincide with major vent zones (e.g. Kaniwhaniwha stream and Pirongia Summit Basin), suggesting that valley incision began from the (eroded) breached craters. The eastern Alexandra volcanoes of Kakepuku (449 m) and Te Kawa (214 m), though of similar age to Pirongia, are significantly less eroded. The relative degree of erosion is controlled mainly by the edifice height (not erupted age), as shown by the progression in radial valley entrenchment from Te Kawa (single breached crater) to Kakepuku (30–50 m deep) to Pirongia (100–380 m deep).

DESCRIPTION OF MAP UNITS

PREAMBLE

The following section describes the geological units of the Pirongia Volcano map. The geological map delineates 36 new volcanic lithostratigraphic units and integrates 11 existing basement units. Unit descriptions provide details on the field and petrographic characteristics of rocks within those units. Correlation of mapped lithostratigraphic units was based primarily on stratigraphic criteria (unconformities and cross cutting relationships) and lithological (e.g. andesitic) and textural (e.g. % of clinopyroxene megacrysts) grouping of lava units. The large majority of the mapped units are of basaltic lithology (22), with subordinate basaltic andesite (6) and numerous, but volumetrically minor units of andesite (9). Mapping based on geochemical criteria was purposely minimised in favour of field stratigraphy and petrography. Rocks of the Pirongia Volcanic Formation show sufficient lithological diversity to distinguish and correlate them without whole rock chemistry. However, in many cases existing major and trace element data are consistent with the proposed stratigraphic groupings of lavas and dykes (e.g. similar SiO_2 contents). Comprehensive information on the whole-rock geochemistry of Pirongia Volcano is presented in Briggs and McDonough (1990). Several lithostratigraphic units belonging to the Okete Volcanic Formation (Briggs, 1983) occur within the mapped area. Descriptions of these units are provided in the map text because they are important geochronological markers of volcanism and may have petrogenetic associations with Pirongia Volcano.

BASEMENT ROCKS

Triassic-Jurassic metasedimentary rocks belonging to the Murihiku Supergroup outcrop to the north, west, and south of Mount Pirongia. The basement rocks form elongate, north-south trending belts dissected by N-S and NE-SW striking regional faults. The total thickness of the Murihiku Supergroup in the map area probably exceeds 6500 m (Waterhouse and White, 1994).

NEWCASTLE GROUP (Mng)

The oldest rocks of the mapping area comprise a sequence of indurated siltstones, sandstones and rare conglomerates (Kear and Schofield, 1964). The Newcastle Group is the major underlying basement unit of Pirongia and forms mountain ranges to the north (Kapamahunga Range, see Fig. 1) and south of the map area. The stratigraphically youngest rocks of Mng (Pongawhakatiki Mbr.) crop out along the Blue Bull Stream, northwest Pirongia. These rocks are indurated, blue-grey siltstones and sandstones (Kear, 1966).

RENGARENGA GROUP (Mrg)

Rocks of Rengarenga Group outcrop in the northwestern quadrant of the map. They are stratigraphically younger than Newastle Group (Mng). The Mrg rocks underlie Paewhenua Plateau and are exposed within the Blue Bull Stream over a short distance near the Bell Track bridge. These rocks are fine-grained, massively bedded, blue-grey jointed siltstones interbedded with fine layers of sandstone (Putau Mbr). The majority of the plateau is underlain by sandstone of Wilson Sandstone Mbr. (Kear, 1966). It comprises light blue-grey sandstone, overlain by bedded grey siltstone and thin conglomerates. Rocks of the group also outcrop south of the ring plain and underlie parts of the Pekanui breccia (Pdb).

KIRIKIRI GROUP (Mkg)

Kirikiri Group metasediments outcrop as a meridional belt of rocks in the northwest of the map area. Other outcrops occur in the upper Oparau River, overlain by Pirongia Volcanic Formation. These include an upturned block of sandstone (Pakau Fm.) at the base of The Cone lava field (Pcb). Kirikiri Group rocks underlie the western edge of Paewhenua Plateau and the eastern side of Koponui vent. Younger bedded grey siltstones (Moewaka Fm.) with hard sandstone horizons (including volcaniclastic layers) outcrop west of Pakau Formation.

APOTU GROUP (Mag)

The Apotu Group is the most widespread basement unit in the map area. It forms mountainous terrain that rises from sea level at Aotea Harbour to 380 m a.s.l. on the northern side of the Oparau Fault. Apotu Group is overlain by Te Kuiti Group rocks south of the fault. Within the Oparau Graben, Apotu Group comprises most of the basement underlying the Oparau breccia (Odb). North of the graben, Apotu Group is penetrated by the Koponui vent. Rock formations within the map area (oldest to youngest) include massive dark blue grey siltstone or mudstone (Kinohaku Fm.); coarse conglomerates of rounded volcanic and angular siltstone and sandstone clasts (Waiharakeke Fm.); and blue grey siltstone weakly bedded with thin sandstone or tuff (Puti Siltstone).

OLIGOCENE SEDIMENTARY ROCKS

Te Kuiti Group

WAIKATO COAL MEASURES (Tkc)

Coal measures (Tkc) are the basal unit of the Te Kuiti Group (Kear and Schofield, 1959). Small patches of coal (Kawhia coalfield) outcrop north of the Oparau Fault at Pirongia West Road (540 m a.s.l. underlying Odb breccia) and south of Koponui (360 m a.s.l.). Further outcrops occur in the far south of the map, west of the Orakei Fault.

MANGAKOTUKU FORMATION (Tkm)

Mangakotuku Formation rocks are mapped on the northern edge of Paewhenua Plateau, northern Pirongia. The Tkm unit overlies basement rocks (Mrg) and is cut by the Kapamahunga Fault, with another outcrop occurring on the eastern side of the fault. The rocks are overlain by Pirongia Formation lavas (Ppe). They consist of calcareous sandstones with rare shell beds (Pukemiro Sandstone Mbr.).

GLEN MASSEY FORMATION (Tkg)

Limestone (Tkg) outcrops below Ppe lavas north of Pirongia. The limestones form the Kaniwhaniwha Caves, accessed on the Bell Track. Small exposures of limestone occur within the headwaters of Oparau River below Pirongia West Road (~320 m a.s.l.) and on the north side of the river along a serrated ridgeline (200 m a.s.l.). The latter deposit was formerly mapped as overlain by Pirongia Volcanic Formation (Waterhouse and White, 1994). The Tkg unit consists of flaggy limestone (Elgood Limestone Mbr.).

WHAINGAROA FORMATION (Tkw)

Siltstones (Tkw) are mapped on the northern shores of Kawhia Harbour. The unit consists of massive light grey to blue-grey jointed calcareous siltstone (Kotuku Mbr.).

AOTEA FORMATION (Tka)

Aotea Formation outcrops extensively to the south of the Oparau Fault (Fig. 8) and on the shores north and south of Kawhia Harbour. The formation consists of weakly cemented medium to coarse sandstone (Hauturu Mbr.) overlain by massive, bluff-forming calcareous glauconitic silty sandstone (Kihi Mbr.). The sandstones underlie Pirongia ring plain (Odb) within the Oparau Graben (see Fig. 22 A, C) and older ring plain deposits (Pdb) south of the mountain.

ORAHIRI LIMESTONE FORMATION (Olt)

Orahiri Limestone covers much of the southern side of Kawhia Harbour where it overlies Aotea Formation (Tka). It is up to 40 m thick and ranges from flaggy, sandy limestone at its base to coarse bioclastic limestone.

MIOCENE SEDIMENTARY ROCKS

Waitemata Group

WAIKAWAU SANDSTONE (Wws)

Waikawau Sandstone (Henderson and Grange, 1926) forms hills in the northern part of the map area that belong to the Kapamahunga Range. The unit overlies Glen Massey Formation. (Tkg). North-south trending faults cut the unit; it is juxtaposed against basement (Mng) to the west by the Kapamahunga Fault, and dissected by a series of smaller, stepping normal faults immediately east. The unit consists of a thin sandstone (up to 10 m).

Figure 8. View looking south from Okupata Road to pale coloured sandstones of the Aotea Formation (Tka). The sandstones form widespread hill ranges south of the Oparau Graben. The Aotea Formation underlies the Oparau breccia (Odb) of Pirongia just north of this area.

BASALTIC ANDESITE OF TURITEA VENT

Turitea is an isolated vent centre within the southern ring plain of Pirongia (beyond the mapped area), 13.5 km south of the summit. It is included in the mapped units because it consists of the oldest known volcanics of the Pirongia Volcanic Formation, an andesitic dyke (2.74 ± 0.09 Ma; Briggs et al., 1989). The dyke is porphyritic with abundant plagioclase (max. 1.5 mm) and subordinate clinopyroxene (1–2 mm) phenocrysts set in a very fine-grained groundmass. The dyke appears to be associated with a lava flow of similar composition, first noted by Park (1892) as 'tough grey vesicular trachytes that form a thin ridge separating the Mangaone and Maokurarua Streams'. Boulders from the lava flow outcrop on Turoto Road. The Turitea vent centre is unique in that it is adjacent with the location of an Okete vent that produced fine-grained olivine basalt. The Okete basalt is significantly younger than the andesite, with age dates ranging from 2.02 ± 0.09 Ma (Robertson, 1976) to 2.21 ± 0.03 Ma (Stipp, 1968). An older spurious date of 3.03 ± 0.10 Ma was discounted by Briggs et al. (1989). The Turitea vent may be structurally controlled by the Tihiroa Fault, which is projected to directly underlie the unit.

PAEWHENUA MEMBER (2.5–2.42 Ma)

UNDIFFERENTIATED BASALTS OF PAEWHENUA MEMBER (Ppe)

The (Ppe) unit is the largest and oldest (~2.5 Ma) landscape-forming mapped unit of Mount Pirongia. Rocks of the unit collectively define the structure of Paewhenua, a shield-type volcanic structure that is the oldest known edifice of Pirongia. The Paewhenua shield is composed mainly of basaltic lava flows intercalated at various levels with basaltic andesite lavas and fragmental deposits (Fig. 9). The erupted material was sourced from a central vent near to Pirongia Summit that was buried (and probably destroyed) by the 1.6 Ma summit eruptions. The unit is mapped up to 800 m (a.s.l.). The lithology of Ppe is known from outcrops exposed in streams of the largest radial valleys, which have incised several hundred metres into its succession. Numerous younger deposits from other vent centres cross cut and mantle older deposits of the Paewhenua edifice. The Ppe unit is overlain and intercalated with ring plain (Pru) and debris avalanche deposits (Pdb).

NORTHERN PIRONGIA

Breccias

Among the oldest exposed deposits are volcaniclastic breccias that outcrop within the lower reaches of Mangakara Valley (Fig. 9, C). These breccias may underlie much of the lower flanks, although their distribution is poorly constrained. Individual beds are at least 3.5 m thick and outcrop along erosional traces with downslope dips slightly greater than the stream gradient (>4.8º). Clasts are typically angular and vary in size (generally 3–35 mm lapilli, and sparse 65 mm blocks), shape (angular to rounded), colour (grey, pale grey, cream, red, brown), lithology (basalts and plagioclase-rich leucocratic rocks) and abundance (7–10% by volume). The matrix consists of medium-brown clays that contain weathered clinopyroxene crystals (orange coloured, 1–3 mm wide) and coarse ash of the same compositions as the clasts. The predominance of basaltic clasts and matrix constituents indicates they are of basaltic origin. The clay matrix is probably the weathered product of fine-ash. The breccias are cohesive enough to form boulders within the stream.

Undifferentiated rocks in Mangakara Stream valley

A thick succession of undifferentiated basaltic and basaltic andesitic lavas, associated autoclastic breccias and dykes outcrop sporadically within the Mangakara Stream valley (Fig. 9, B). Lavas in the lower reaches of the stream are porphyritic basaltic andesites with fresh phenocrysts of olivine (up to 3 mm), sub-equal amounts of plagioclase and clinopyroxene in fine, purplish groundmass. The lavas contain rare xenoliths of sandstone from the underlying Te Kuiti Group. Intensely weathered cpx-basalt lavas (at least 1 m thick, 80% autobrecciated) with similar texture to the Ruapane dykes (Prb) occur further upstream.

In the mid reaches of the stream, relatively fine-grained basaltic lavas and dykes outcrop sporadically above the gorge and on the northern planeze of Ruapane Peak. Gorge lavas are abundant in glomero-phenocrysts of clinopyroxene (6–9% of rock, 1.5–2.5 mm), sparse plagioclase (≤ 3 mm), olivine (1 mm) and purplish grey groundmass. Higher in the succession, lavas are intercalated with scoriaceous lapilli deposits (individual beds at least 7 m thick) and cross cut by ankaramites of the Ruapane Peak dyke swarm (Prb). Karst-weathered basalt of the unit occurs on the lower flank of the peak. In this area Ppe lavas are overlain by Ruapane (Prb) lavas and breccias. *Upper reaches:* In situ lavas are rarely exposed within the upper Mangakara Stream. Briggs and McDonough (1990) reported in-situ ankaramites (at 570 m a.s.l.) with megacrysts of clinopyroxene and olivine (± vesicles, and similar texture to Ppe ankaramites downstream) and an outcrop of fine-grained basanite (atypical at Pirongia) within the upper catchment area.

Ridges above Mangakara Stream

Highly weathered mounds of ankaramite-type basalt (7% clinopyroxene) of the mid-Ppe succession outcrop up to 650 m (a.s.l.) on the Wharauroa Ridge (Fig. 9, E). The rocks at this site are dated at 2.49 ± 0.09 Ma ('absarokite'; Briggs et al., 1989). Upslope, the unit is overlain by younger lavas (Pml).

NORTHWESTERN PIRONGIA

An expansive and evidently thick (max. ~300 m) basaltic lava field (Ppe) occupies most of the western slopes of the mountain (Fig. 9, A and Fig. 10, A). The lavas form a gently dipping (7–8º) planeze that rises (up to 15º) towards

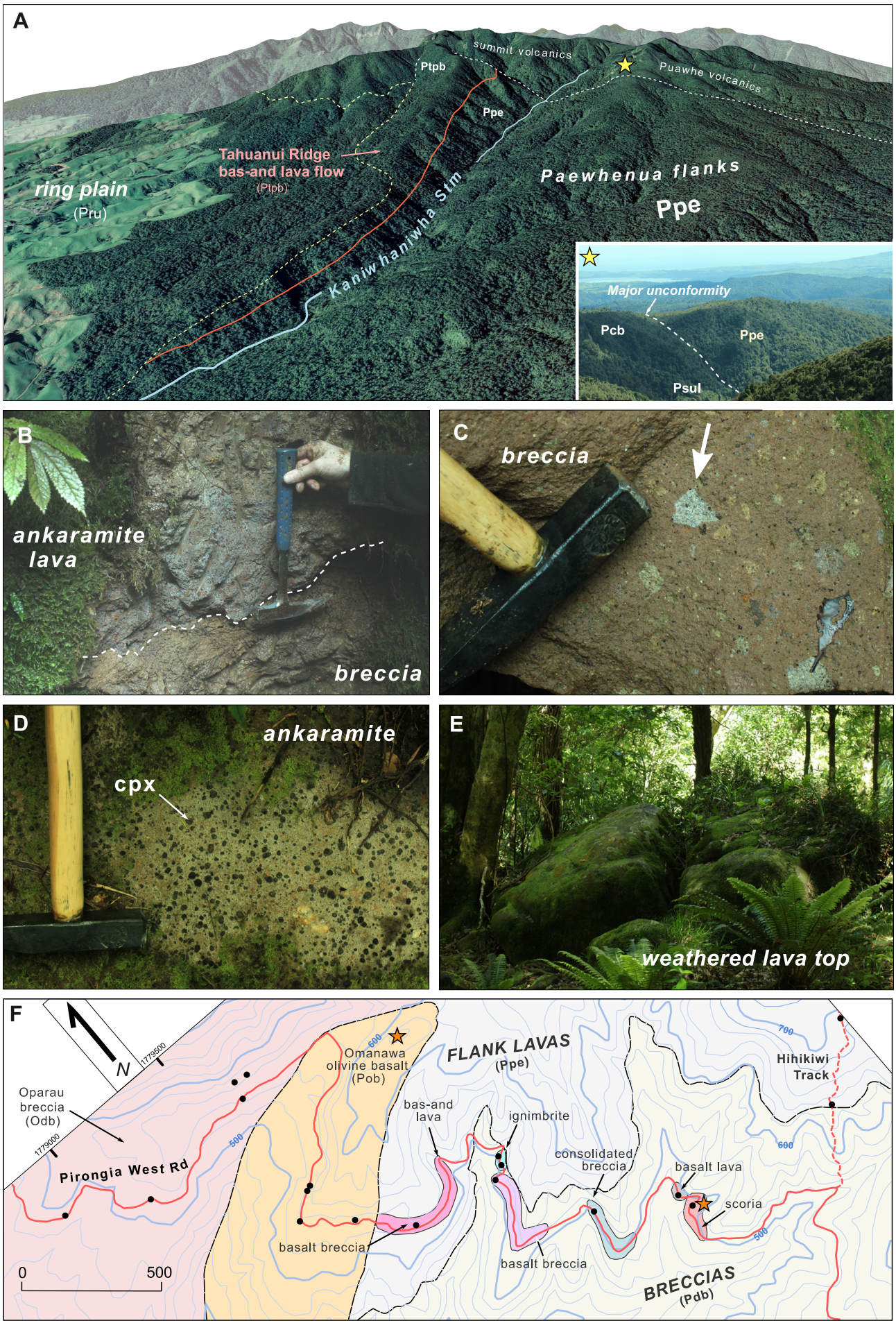
A
summit volcanics
Ptpb
Puawhe volcanics
Ppe
Tahuanui Ridge
bas-and lava flow
(Ptpb)
ring plain
(Pru)
Kaniwhaniwha Stm
Paewhenua flanks
Ppe
Major unconformity
Pcb
Ppe
Psul
B
ankaramite
lava
breccia
C
breccia
D
ankaramite
cpx
E
weathered lava top
F
N
1779500
1779000
Oparau
breccia
(Odb)
Pirongia West Rd
500
Omanawa
olivine basalt
(Pob)
600
FLANK LAVAS
(Ppe)
bas-and
lava
ignimbrite
consolidated
breccia
basalt lava
scoria
basalt breccia
basalt breccia
BRECCIAS
(Pdb)
700
Hihikiwi
Track
600
500
0
500

a round-shaped ridge saddle (770 m a.s.l.) north of The Cone. A major unconformity separates the Paewhenua shield from The Cone volcanics (Fig. 9, A). The planeze surface is well preserved and displays only minor stream incision and rounded ridge structures. To the north, the planeze is deeply truncated by the Kaniwhaniwha Stream.

Ring plain and lavas in the lowest stratigraphic part of the planeze form an expansive surface that directly overlies Murihiku basement to the west and younger sedimentary units to the east (Te Kuiti and Waitemata Groups). These deposits have infilled existing valleys of the country rock. Peripheral areas of the lava field are deeply eroded and topographically inversed. The effect of inversion is most evident in areas where the ring plain deposits overlie soft limestones and mudstones (Tkg, Tkm), such as around the Kaniwhaniwha Caves and Blue Bull Stream.

In-situ basaltic lavas outcrop within the Kaniwhaniwha Stream valley (Briggs, 1986) that become progressively older up stream. All basalts contain large clinopyroxene phenocrysts (maximum size 3–4 mm). The oldest observed lavas are cpx-basalts with large clinopyroxene phenocrysts (7% of rock, ≤ 3.9 mm across) and small amounts of altered olivine. Younger lavas downstream contain relatively more olivine (1 mm), larger phenocrysts of plagioclase (1–2 mm) and more sparse clinopyroxene phenocrysts (4–5% of rock).

Ppe volcanics at the base of the Paewhenua Plateau (60–100 m thick) are overlain by younger ankaramite lavas erupted from a lower flank vent (Ap). The composition of the Ppe lavas here is unknown, but is probably similar to that of the basalts in Kaniwhaniwha Stream. Ppe deposits near to the contact with basement rocks (above the Blue Bull Stream) include red scoria and fine-grained basaltic andesite boulders (light-grey groundmass; plagioclase rich; up to 1 mm; clinopyroxene glomerocrysts 1–2.5 mm, few olivine <1 mm) that could represent buried ring plain material. Younger Ppe lavas are intercalated with, and overlie deposits of the Ap unit above 500 m a.s.l. The unit therefore pre- and postdates emplacement of the (Ap) ankaramites.

SOUTHERN PIRONGIA

Ppe is the major edifice forming unit of southern Pirongia. It is comprised of a thick succession (max. ~250 m thick) of poorly exposed, undifferentiated basaltic, ankaramitic and basaltic-andesitic lavas and volcaniclastic breccias. The unit is prominent south of the Oparau River, forming most of the stratigraphy underlying the Hihikiwi ridgeline and southeastern flank. North of the Oparau River, a large unconformity related to a sector collapse separates Ppe unit from younger lavas of The Cone. Another unconformity separates Ppe and younger lavas of Te Akeohikopiro Peak (Tkb). Younger vent deposits cross cut and overlie Ppe along the Hihikiwi Ridge, Tiwarawara, Kohatupiko and Te Mata vent.

The Ppe unit occupies a planeze (with moderate stream dissection) on the lower Hihikiwi ridgeline. Slope angles of the planeze are 11–13°. Ankaramite lavas and agglomerates of the Hihikiwi ridgeline (Fig. 9, D) contain abundant, large clinopyroxene (glomero-) phenocrysts (10 % of rock, 2–6.5 mm), abundant interstitial plagioclase microphenocrysts and relatively lesser amounts of olivine in fine-grained, dark coloured groundmass. The lower southern flanks of Ppe are buried by ring plain breccias associated with debris avalanches (Odb, Pdb and Mdb).

The oldest Ppe lavas of the area outcrop within the Oparau River. In-situ basaltic lavas contain abundant skeletal hornblende (1–2.5 mm) in an otherwise basaltic-porphyritic assemblage of clinopyroxene (1–2 mm) and plagioclase (1–1.5 mm). The lower Ppe succession lavas are cross cut by an early formed dyke swarm (Dos).

Distal Ppe lavas crop out in road cuttings along Mangati Road, 5.7 km SSE of Te Akeohikopiro Peak. They include highly weathered cpx-basaltic andesite with porphyritic texture (clinopyroxene phenocrysts 1–3 mm; plagioclase 1 mm) and light-grey groundmass that outcrops below a blanket of laharic material (see Fig. 28, E).

Lower flank deposits outcrop discontinuously between thick breccias of the southern ring plain (Pdb and Odb) in road cuttings along Pirongia West Road (Fig. 9, F). A well preserved basaltic andesite lava near the western edge of the forested section of road contains phenocrysts of clinopyroxene (1.5–3 mm; max. 4 mm)>plagioclase (1.5–3.5 mm)>skeletal hornblende (1–3 mm) set within purple-grey groundmass. Further east, an andesitic ignimbrite (the only known ignimbrite deposit on Pirongia) at least two metres thick with constituents of 25% juvenile pumice, 7% hornblende-rich lithics and pale coloured, crystal-rich matrix (clinopyroxene: up to 2 mm) outcrops below unconsolidated laharic material. The unit grades upwards from coarser to finer clast size towards the contact.

Figure 9. Geomorphology and geology of the Paewhenua shield (Ppe) unit. A: View southwest towards the volcanic shield, where it is incised by the Kaniwhaniwha Stream valley. Here, the (Ppe) unit is overlain by a lava flow (Ptpb) sourced from the (proto) summit zone. The lower flanks are mantled by ring plain deposits. A major unconformity separating the Paewhenua shield from younger volcanics of the summit and Pūawhe is marked with a dashed white line (see also inset photo, view northwest). B: Highly weathered ankaramite lava overlying autobreccia in Mangakara Stream. C: Volcaniclastic breccia in Mangakara Stream (arrow shows andesitic clast). D: Ankaramite lava on the lower Hihikiwi ridge, southwestern Pirongia. E: Boulder mound (belonging to Ppe unit) on the Wharauroa ridge, northeastern Pirongia. F: Detailed geological map of volcanic deposits in road cuttings on Pirongia West Road. All lava flows except for the Omanawa basalt (Pob) belong to the Paewhenua shield and are buried by the Pekanui breccia (Pdb).

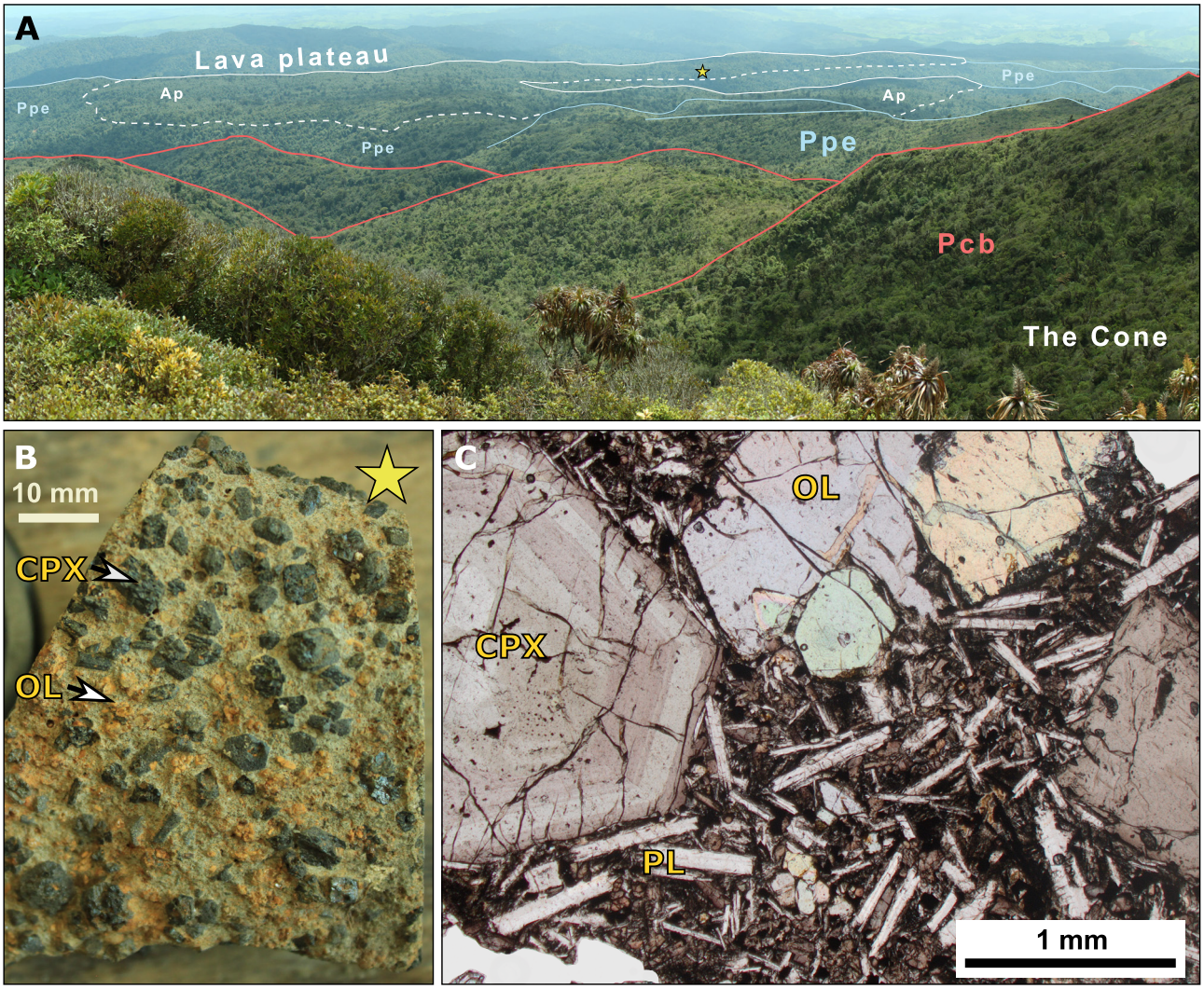

Figure 10. View northwest to the Paewhenua (lava) plateau. The relatively smoothly dipping landscape consists of a thick lava unit of extremely porphyritic ankaramite (Ap). The Ap unit is intercalated with shield-forming lavas of the Paewhenua edifice (Ppe). A major unconformity (concealed in photo) separates these deposits from younger volcanics of Pūawhe/The Cone (Pcb). The yellow star shows the field location of the ankaramite hand specimen shown in (B). The rock is abundant with black zoned (see C) clinopyroxene (CPX) and orange-stained olivine (OL). In thin section (C), these minerals are surrounded by coarse laths of plagioclase (PL).

ANKARAMITE OF PAEWHENUA PLATEAU (Ap)

The (Ap) unit consists of extremely porphyritic (almost doleritic) ankaramite lavas erupted from one or more peripheral vents on the lower north-western flank of Pirongia. The lavas form an elongate, low relief land surface named here as the Paewhenua Plateau (Fig. 10). The unit encompasses two main flow strands, both of which flowed north at very gentle slope angles (4.5–9º to near flat 1.6º) for distances of 3–4 km. Lava thicknesses are estimated as 80 m in medial areas and 20–40 m in the distal portions. Only sporadic outcrops of basalt (in-situ boulders, 1–4 m wide) occur on the edges of the plateau surface, though the unit can be correlated over large distances because of its distinctive texture.

The (Ap) lava flow was emplaced on to older ring plain deposits (Pru) and lavas (Ppe) and is buried by younger lavas of the Paewhenua shield (Ppe), indicating a stratigraphic age older than ~2.5 Ma. The lavas from both units may have originally flowed into and ponded within broad gullies of the country rock that are now intensely eroded/deflated around the (very erosion resistant) lava units.

The ankaramites are dark grey in colour, very dense and hard to fracture. The rocks are extremely porphyritic with large clinopyroxene phenocrysts and glomerocrysts (titanaugite composition; mostly 2–5 mm; 30–35% of rock) up to 1 cm in size that protrude from weathered surfaces (Fig. 10, B). Large olive-green to brown olivine phenocrysts (2–5 mm; 5% of rock) are also abundant, with lesser amounts of plagioclase (up to 1.5 mm) occurring as interstitial laths. The groundmass is only a minor constituent and intergranular in texture; it contains plagioclase, titanaugite, olivine and opaques (Fig. 10, C). Total phenocryst content exceeds 50% and the rock may therefore be considered a magmatic cumulate, although the presence of volumetrically minor groundmass still suggests it was an extrusive volcanic product. Clasts showing distinct

textural similarity to the (Ap) ankaramite occur within vent breccias of The Cone (Pcbr). These clasts, probably entrained from (Ppe) lavas of similar age to (Ap), indicate that these unique lavas occur elsewhere in the lower succession.

DYKES OF OPARAU STREAM (Dos)

Four linear protrusions interpreted as dyke structures crop out at elevations of 520–680 m (a.s.l.) within the headwaters of the Oparau River (see Appendix C for details). The mapped dykes cross cut the lower Ppe succession and show parallel alignment (east-west). The occurrence of the dykes within the base of the valley suggests they are stratigraphically older than ridgetop dykes exposed along Hihikiwi Ridgeline (Phr) and at The Cone (Pcd). The (Dos) dykes crop out adjacent to a major unconformity separating the older Paewhenua shield (Ppe) from younger lavas of The Cone (Pcb). The lowermost dyke (exposed in a landslide above the river) is a porphyritic andesite with abundant phenocrysts of hornblende (1–3 mm), plagioclase (up to 1 mm), and minor glomerocrysts of clinopyroxene (1–2 mm) in a glassy groundmass.

BASALTIC LAVAS AND FRAGMENTAL DEPOSITS OF TIRENI PEAK RIDGE (Pmr)

A complex array of laterally discontinuous basaltic lavas and breccias outcrops over 900 m of ridgeline to the east of Tireni Peak (Fig. 11). The (Pmr) unit surmounts older Paewhenua flank lavas (Ppe) and is cross-cut by younger dykes probably related to the Paewhenua vent centre (Pdr and Ptr). An unconformity separates the (Pmr) unit from younger cone-building basaltic andesite lavas (Pml) to the east.

From east to west, the (Pmr) succession includes: (1) red-coloured, autobrecciated cpx-basaltic lavas (clinopyroxene phenocrysts 1.5–3 mm, weakly to strongly vesicular); (2) Basaltic andesite lava flows with widely spaced phenocrysts of clinopyroxene (3–6 mm), olivine (1–2.5 mm), ± hornblende and plagioclase microphenocrysts in a fine groundmass; (3) glassy basaltic andesite lava with trachytic texture and aligned vesicle trails; overlain by (4) a thicker sequence of dark-grey basaltic lavas (clinopyroxene: 2–3.5 mm, olivine: 1.5–2.5 mm) and associated pyroclastic deposits of cpx-rich, red lapilli-tuffs with scoriaceous clasts and sparse blocks of equivalent texture to the lavas. These basalts are cross-cut by two andesitic dykes (Pdr) striking NE-SW.

DYKES OF TIRENI PEAK RIDGE (Pdr)

Lavas on Tireni Peak ridge (Pmr) are cross-cut by two large rock bodies (Pdr) interpreted as dyke structures (max length ~170 m) with sub-parallel NE-SW strike (Fig. 11). The westernmost dyke forms a steep sided bluff (30 m tall) on the southern edge of the ridge line. The dyke has a doleritic texture with phenocrysts of vitreous hornblende (up to 8 mm), subordinate clinopyroxene and olivine enclosed within a dark-grey matrix of interlocking plagioclase laths.

ANKARAMITE OF TIRENI PEAK (Ptr)

Tireni Peak is a distinctive, flat topped ridge composed of a thick unit of ankaramite lava (Fig. 11). The lava surface is obscured by a swamp and outcrops are limited to the edges of the ridge. The lava flow is associated with (and was probably fed by) a dyke (100 m long, <10 m thick) of similar texture (porphyritic, with large black clinopyroxene 2–6 mm; orange altered olivine 1–2; and abundant plagioclase set within dark grey groundmass) on the western side of the peak. The dyke margin is strongly brecciated. The dyke and lava unit (Ptr) cross cut and overlie nearby ridge lavas (Pmr) of similar age.

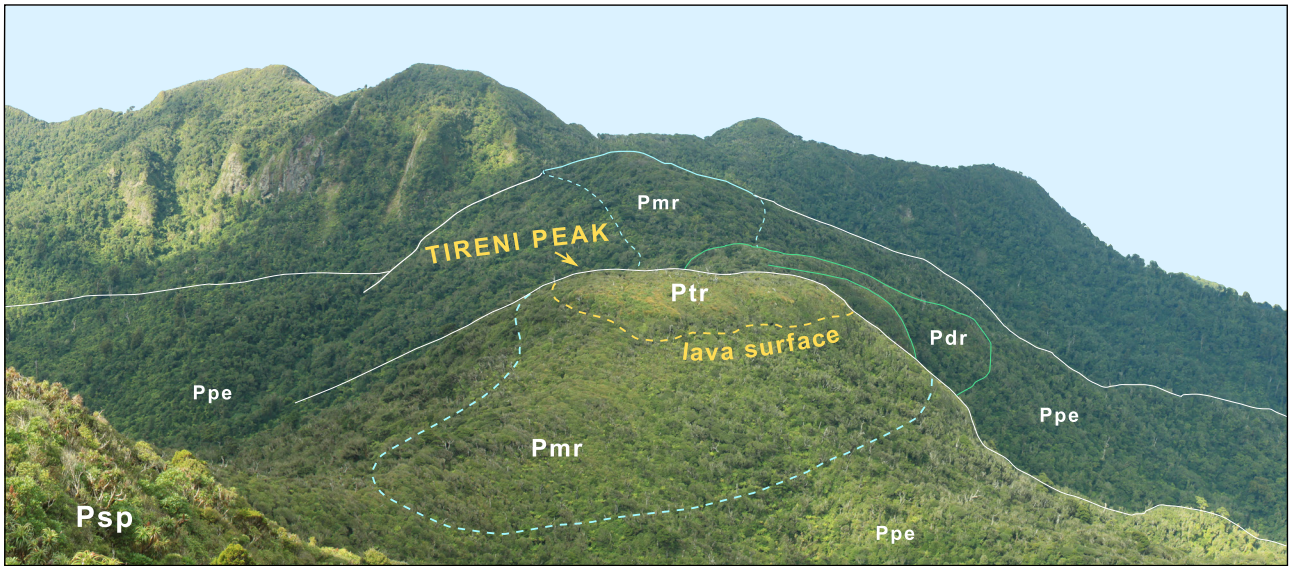

Figure 11. View southeast to Tireni Peak from Pirongia Summit. The peak consists of a large planar surface of ankaramite, probably once a lava lake, that overlies older associated lava flows (Pmr and Ppe)) and dykes (Pdr) of the Paewhenua shield.

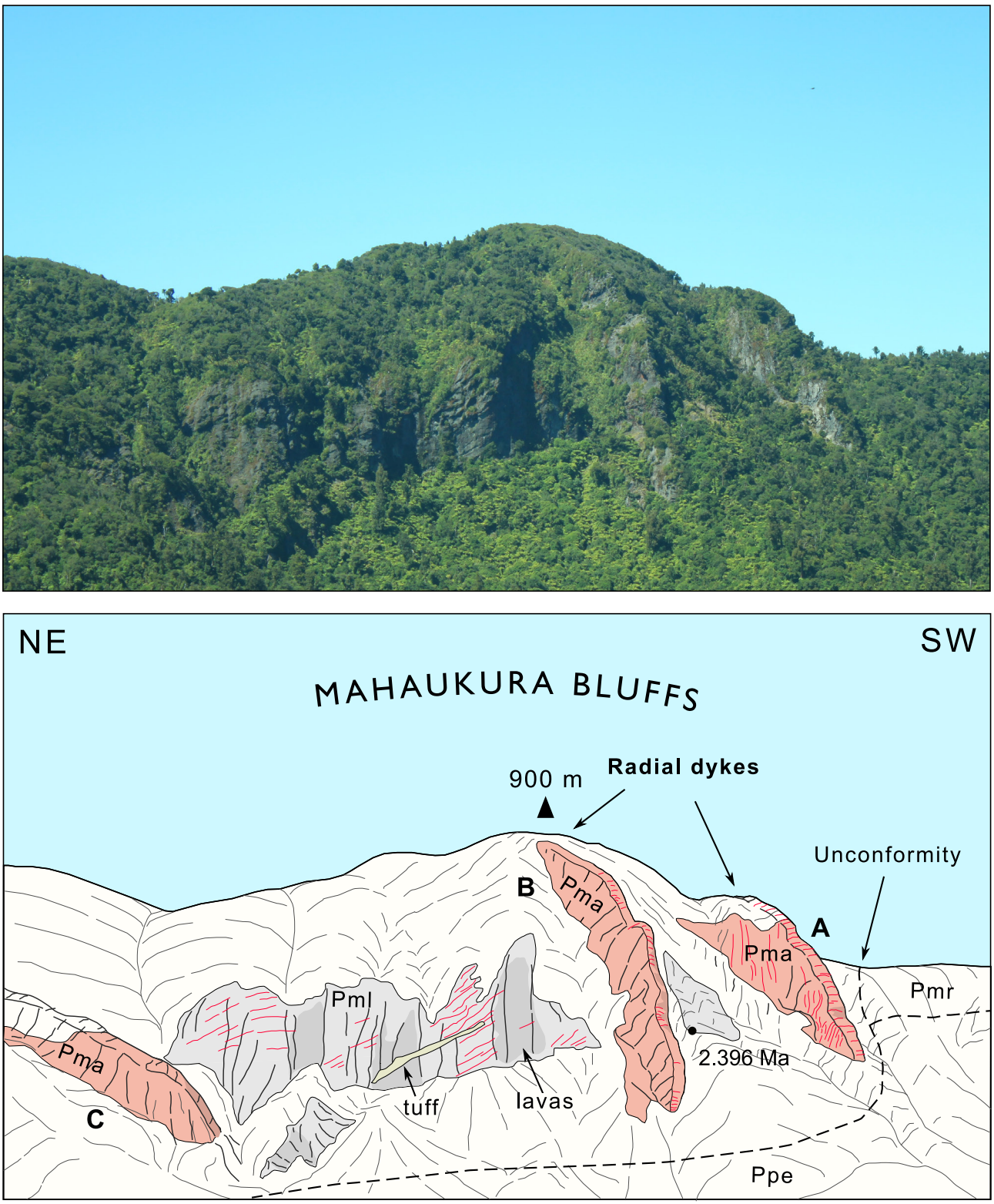

Figure 12. View southeast to the Mahaukura bluffs from Ruapane Peak (photo above) and geological interpretation (sketch below). Field of view is 500 m. The landscape consists of a thick succession of NE-dipping, basaltic andesite lavas (Pml, shown in grey) and a tuff layer (labelled) that overlie older Paewhenua lavas (Ppe). The lavas are cross cut by radial andesitic dykes (Pma, shown in red). Dykes referred to in text are labelled A-C. Joint patterns are shown in red (observed) and geomorphic form lines in black. The location of the (Pml) lava flow dated for this study is marked by a black dot.

BASALTIC ANDESITES OF TAHUANUI RIDGE (Ptpb)

The (Ptpb) unit represents an extensive basaltic andesite lava flow (or group of lavas) that outcrops over 4 km along the Tahuanui ridgeline (780 and 540 m a.s.l.) in northwestern Pirongia (see Fig. 9, A). The lava flow is dated at 2.418 ± 0.05 Ma (this study) and probably originated from a (buried) vent in the area just north of Pirongia Summit. The (Ptpb) unit is associated with late-stage cone-building of the Paewhenua edifice, and overlies older flank lavas of the volcano (Ppe). Slope inclination suggests the lava flowed gently down flank at 7–8º. The lower portions of the lava flow overlie Oligocene-Miocene sedimentary rocks (Tkg and Wws). The unit is overlain by summit group volcanics (Psp and Psp) and at lower elevations (<540 m a.s.l.) by bouldery ring plain debris (Pru).

The lavas are fine-grained basaltic andesites with sub-equal amounts of clinopyroxene (max width 1.5–2.5 mm) and plagioclase (up to 3 mm). Sparse phenocrysts of hornblende (± phlogopite inclusions) and olivine are also present. Small amounts of olivine are present in the groundmass of most (Ptpb) lavas. Portions of the unit above 700 m a.s.l. are slightly coarser-grained and contain more plagioclase phenocrysts than lavas at lower levels on the flank.

PEKANUI BRECCIA (Pdb)

The Pekanui breccia is the oldest and most laterally expansive (>60 km², ~200 m max. thickness) ring plain deposit of Pirongia. The (Pdb) unit is widespread in the southern and southwestern parts of the map area, where it forms a large planar land surface (the Orakei Plateau). The plateau shows progressive entrenchment by valleys to the west towards Kawhia Harbour. The unit (Pdb) is considered the oldest debris avalanche field of Pirongia because of its highly eroded topography. The unit is morphologically older than the Oparau breccias (Odb) to its west. It is separated geomorphically from Odb by the Omanawa lava flow (Pob). The lower parts of the deposit are separated from Odb by the Okupata Stream. The unit probably underlies portions of the Odb breccia, though its main emplacement direction was towards the south of the map area. The (Pdb) breccias are stratigraphically older than the Hikurangi vent lavas (Phk; 2.30 Ma) that erupted through the unit.

Kawhia Road

Isolated portions of the distal ring plain crop out along Kawhia Road SH31, where at 295 m (a.s.l.), Pirongia debris occur on the top of the ridgeline, overlying limestone (Tka). Deep stream incision on either side of the ridge indicates significant erosion of the local topography (100–200 m vertically) since emplacement of the (Pdb) ring plain.

In this area the deposit consists of massive, red weathered clays with relatively sparse lapilli and blocks (up to 70 cm) embedded within the matrix. Clasts include: (1) scoriaceous basalts abundant with clinopyroxene (glomero-) phenocrysts (clay altered, 1–4 mm) and seriate textured plagioclase (≤ 2 mm); and (2) larger blocks of basaltic andesite rich in glomerocrystic clinopyroxene (2–5 mm) and blocky plagioclase (clay altered; ≤ 1.5 mm) within fine-grained groundmass.

Pekanui Road

Polymict breccias typical of the (Pdb) unit outcrop sporadically in road excavations along Pekanui Road (430 m a.s.l.). The largest exposure (50 m long; BE33 816 863) consists of a highly weathered, undulating layer of matrix-supported breccia with abundant basaltic lapilli (angular cpx-basalt, variable texture) and minor andesite (pale-coloured fragments, finely crystalline) in an orange-brown matrix of coarse-ash, loose crystals (mainly orange altered clinopyroxene) and clay. Larger cohesive blocks of basalt typical of the deposit were observed in nearby road cuttings. Finer-grained volcaniclastic deposits, probably of reworked material, and younger tephras mantle the deposits.

Pirongia West Road

Proximal exposures of the (Pdb) unit occur in cuttings along Pirongia West Road, where polymict breccias are interspersed with lavas (Ppe) at the flank-to-ring plain transition zone of Pirongia. The breccias consist of poorly sorted, angular to sub-angular clasts in a weathered, reddish-brown clay matrix. Clasts are continuous in size from very fine lapilli up to blocks. Larger domains of cohesive, jigsaw fractured rock (some >1 m in width) are common within the deposits. Clast compositions reflect the typical lithological variation of Pirongia Volcano and include basalts, basaltic andesites and rare andesites. Basalt is the predominant lithology; typical clasts include dark-grey to reddish cpx-basalt scoria to weakly-vesicular ankaramite (clinopyroxene: 1–2 mm and 2–4+ mm, respectively). The basaltic andesites are finer grained, plagioclase-rich rocks with jigsaw fracturing common in larger blocks. Andesitic lapilli are a minor component of the deposits; clasts are bright white to cream coloured, variably pumiceous, and contain fine hornblende (1–1.5 mm). The matrix contains abundant plagioclase (< 1 mm) and clinopyroxene (up to 2 mm; often fractured), the latter of which is ubiquitous to Pirongia basalts and indicates an overall basaltic composition to the matrix.

Mangati Road

The (Pdb) breccias outcrop in cuttings on Mangati Road, near the intersection with SH39. Large (≤ 1.5 m wide) blocky domains of basaltic andesite are set within polymict, clast supported matrix material comprised mainly of basaltic clasts (width 15 cm down to ash size, i.e. 2 mm), minor hbl-andesite (max. 20–30 cm wide) and interstitial clay. The large blocks of basaltic andesite have plagioclase (max. 1 mm) > clinopyroxene (av. 2 mm) by abundance. All clasts show high degrees of weathering except for the largest blocks.

TIROHANGA MEMBER (2.4–2.35 Ma)

BASALTIC ANDESITE LAVAS OF THE MAHAUKURA AND TAHUANUI RIDGES (Pml)

A thick, landscape-forming succession of basaltic-andesitic lavas belonging to the (Pml) unit are mapped in the northern and eastern parts of Mount Pirongia. The mapped deposits underlie most of the Mahaukura and Tahuanui Peak ridges and form the denuded flanks of an eroded volcanic cone (Tirohanga Volcano) centred on the Tirohanga ridgeline. The unit conformably overlies older flank lavas of the Paewhenua Member (Ppe and Ptpb) in most areas, though a prominent unconformity between Pml and Ppe occurs at the Mahaukura bluffs, associated with a sector collapse scarp. The unit is crosscut by temporally associated dykes of the (Pma) unit and overlain by ring plain (Pru) on its northwestern and eastern flanks. An unconformity separates (Pml) lavas from older basaltic andesites (Pmr) west of the Mahaukura bluffs.

Mahaukura bluffs

The main outcrop locality of the (Pml) unit is at the Mahaukura bluffs (Fig. 12; BE33 858 928), where a lava succession is exposed within the extensive, horseshoe-shaped amphitheatre (300 m wide and 70–100 m tall) enclosed by andesitic dykes (Pma). The succession of at least ten thinly layered basaltic andesite lava flows (each 1–4 m thick) infills a prominent unconformity surface related to a sector collapse scarp within the underlying Paewhenua shield (Ppe) (Fig. 12). Apparent dips on the lavas range from steep (34º at the southern end of the bluffs) to relatively shallow (<7º; northern end). The lavas are all strongly autobrecciated (60–70% breccia) with knobbly surface textures common in weathered outcrops. Lava from near the base of the succession is dated at 2.396 ± 0.05 Ma (this study). This lava has a porphyritic texture with distinctly sparse phenocrysts of green clinopyroxene (up to 3 mm) set within plagioclase-rich groundmass. The lowermost lavas appear to be intercalated with a gently dipping, pale-grey coloured tuff or lapilli-tuff deposit unit (3–4 m thick) that outcrops discontinuously over at least 200 m (and possibly up to 750 m) northwards along the bluffs. The lava succession is overlain by red-coloured scoriaceous deposits visible along the top of the bluff and sporadically across the Mahaukura ridgeline above. The deposits consist of scoriaceous lapilli-tuffs (sub-rounded clasts 2–3 cm wide, clinopyroxene rich) intercalated with ankaramite lavas of similar texture.

BASALTIC PYROCLASTIC DEPOSITS AND LAVAS OF TIROHANGA RIDGE (Ptb)

Basaltic deposits outcrop along the ridgeline surrounding Tirohanga Peak. The (Ptb) unit comprises vent proximal deposits related to the Tirohanga Peak vent zone. The unit cross cuts and overlies older flank lavas of the Paewhenua Member (Ppe). Its deposits are stratigraphically older than those of Ruapane Peak (Prb) to the northeast. The unit is cross cut by andesitic dykes of the Tirohanga Peak unit (Pta). Deposits include lavas, lapilli-tuffs, breccias and rare dykes.

Breccias below Tirohanga Peak

Lapilli-tuff deposits outcrop beneath an intrusive andesite body (Pta) at the base of Tirohanga Peak (Fig. 13, D). The deposit surface dips south (at 18–30º over a length of 50 m) towards Pirongia Summit. It is an erosional disconformity that indicates a time-break between deposition of the lapilli-tuffs and the overlying coulée and dykes. Two sub-units are present. The lower unit is monolithologic and more lithic-rich with abundant vesicular basaltic lapilli and loose clinopyroxene crystals. The upper unit is generally a finer-grained, polymict deposit with lithics of vesicular ankaramite and finer-grained cpx-basalt, andesite and rare greywacke xenoliths. In both units, some basaltic lapilli preserve spindle-bomb shapes with dense cores and vesicular edges.

Ridgeline around Tirohanga

Ankaramites belonging to (Ptb) unit outcrop sporadically over a one kilometre stretch of ridgeline surrounding Tirohanga Peak. Deposits include: (1) in-situ lavas (5–20% clinopyroxene glomerocrysts) with onion skin weathered rinds; (2) bouldery debris fields; and (3) lapilli-tuffs with abundant ankaramite clasts (finely vesicular rocks with ≤13% clinopyroxene and phenocrysts max. 7 mm). Relatively thin, isolated dykes of hornblende basaltic andesite cross cut the ridgeline north of Tirohanga Peak. The dykes have spheroidal jointing patterns and contain acicular hornblende and clinopyroxene (up to 12% of rock) in a fine-grained groundmass.

ANDESITES OF TIROHANGA RIDGE (Pta)

The pinnacle of Tirohanga Peak (770 m a.s.l.) is the eroded central remnant of a large andesitic vent structure spread over 600 m of the Tirohanga ridgeline, northeastern Pirongia (Fig. 13, A). The peak is composed of columnar jointed andesitic lava cross cut by at least one large, NNE-striking dyke (max. 20 m wide, >125 m long) of equivalent composition. The andesitic lava forms a coulée at least 20 m thick that overlies volcaniclastic breccias (see Ptb; Fig. 13, D). Lava at the basal contact displays sheared columnar jointing patterns that indicate a southward flow direction. The cross cutting dyke feeds a splay-jointed dome at the top of Tirohanga Peak (Fig. 13, B). Other andesites of the unit are mapped in the area of the peak. These include: (1) a large body of columnar jointed andesite lava (80 m thick) that outcrops 300 m SSW of the peak (Fig. 13, A); and (2) a radial dyke exposed at the base of the Rangitukia Stream (530 m a.s.l.), 400 m to the northwest. The Tirohanga dyke and lava flow consist of light-grey, porphyritic andesite with abundant plagioclase, vitreous hornblende laths up to 3 mm and clinopyroxene in felted groundmass. Andesite near the lower contact contains large amounts of grey-purple (devitrified) glass within the groundmass. Dispersed spheroidal and angular felsic inclusions (45–120 mm wide) are exposed at Tirohanga Peak (Fig 13, C) and have textural and dimensional similarity to those within the andesites at Mahaukura and Wharauroa peaks. The co-presence of inclusions, along with the texture and joint patterns of the andesite suggests that the andesites of Tirohanga Peak correlate stratigraphically and/or petrogenetically to those 1300 m southeast on the opposite side of Mangakara Valley (Pma).

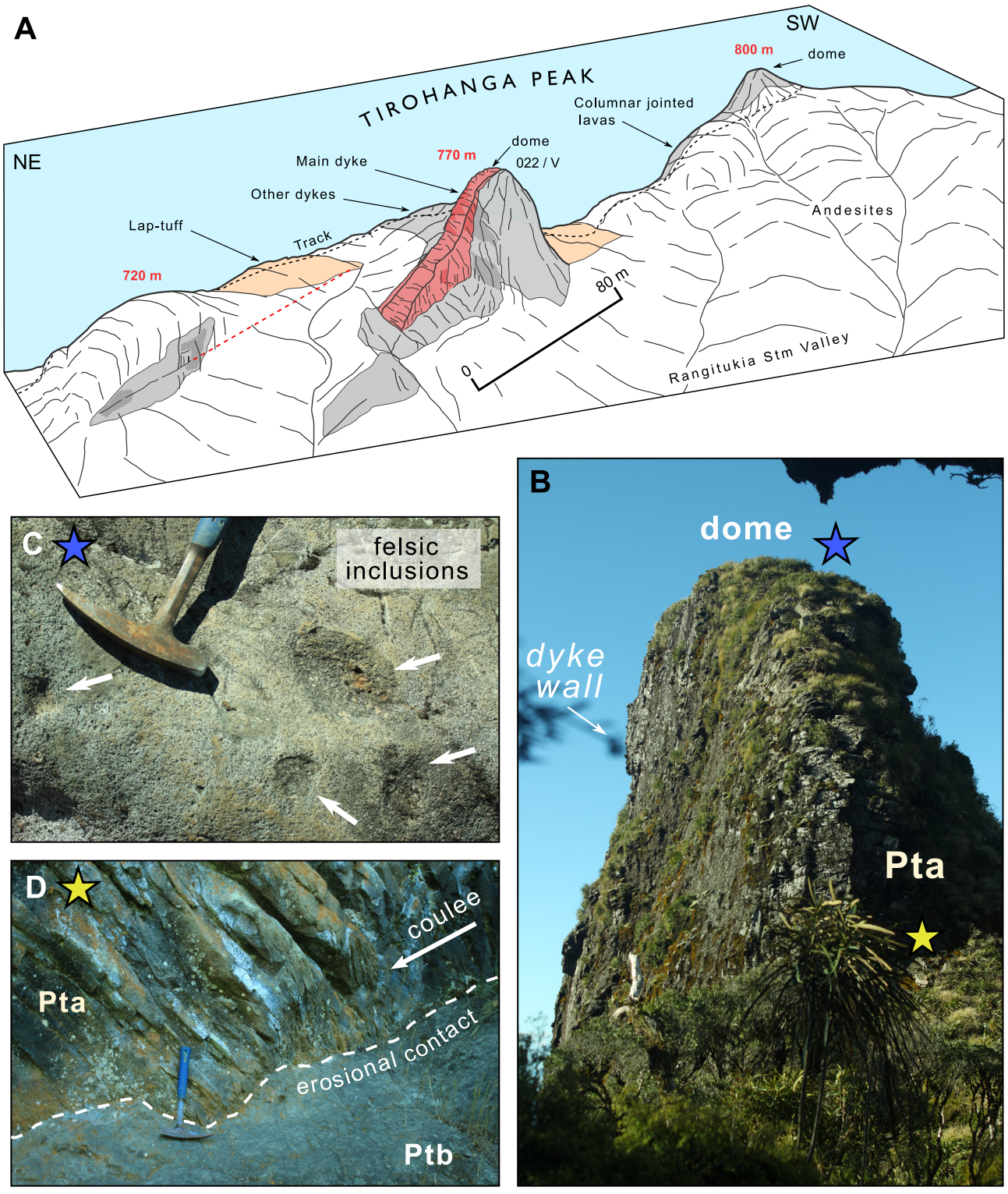

Figure 13. Geological features of the Tirohanga andesite unit (Pta). A: View southeast to Tirohanga Peak showing the structural association of andesitic dykes and lavas of the central vent facies of Tirohanga Volcano. The peak consists of a dome-like structure fed by a prominent dyke (shown in red) that cross cuts other andesites of the unit (shown in grey). B: Southern face of the Tirohanga Peak, showing the steep dyke wall and location of the dome (blue star) and lower contact (yellow star). C: Felsic inclusions in andesite at the top of the Tirohanga dome. D: Lower contact of Tirohanga Peak, where andesitic lava overlies volcaniclastic breccia (Ptb) along an erosional contact.

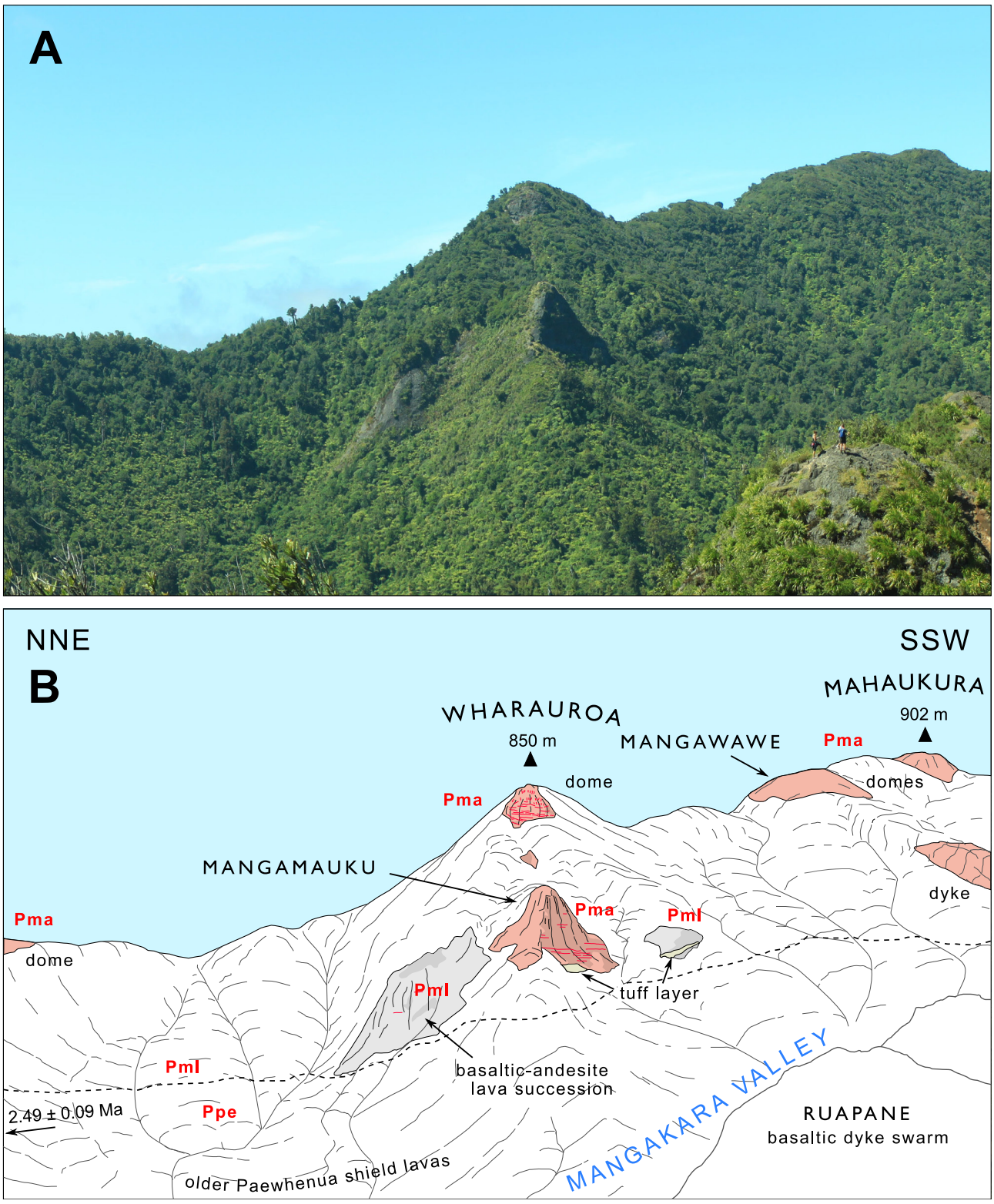

Figure 14. Panoramic view (A) and geological sketch (B) looking eastward from Ruapane to Wharauroa and Mahaukura Peak. Field of view is 1000 m. Note people for scale in foreground, lower right corner. (B) Andesitic dykes and domes of the (Pma) unit (shown in red) crop out at various high points along the ridgeline, including at Wharauroa, Mangawawe and Mahaukura peaks. The andesites intrude through basaltic andesite flank lavas (Pml; shown in grey), such as at Mangamauku Peak. The (Pml) lavas overlie an older flank of the Paewhenua shield (Ppe, dashed line marks approx. contact) with an age of 2.49 Ma near the contact with the (Pml) unit.

Figure 15. Structure and field characteristics of the Wharauroa dome. A: Jointing pattern within the exposed portion of the dome (see also photo D). The dome shows a transition from lower platy jointing to columnar and blocky jointing near its top. B: View northeast to the dome from Mahaukura Peak. C and F: Felsic inclusions within andesite at Mahaukura Peak and their similarity to those of (E:) Felsic inclusions at Wharauroa Peak. G: Relationship between length and width (mm) of felsic inclusions at Mahaukura, Wharauroa and Tirohanga peaks. Inclusions at all three sites show morphological and lithological similarity not observed elsewhere on Pirongia.

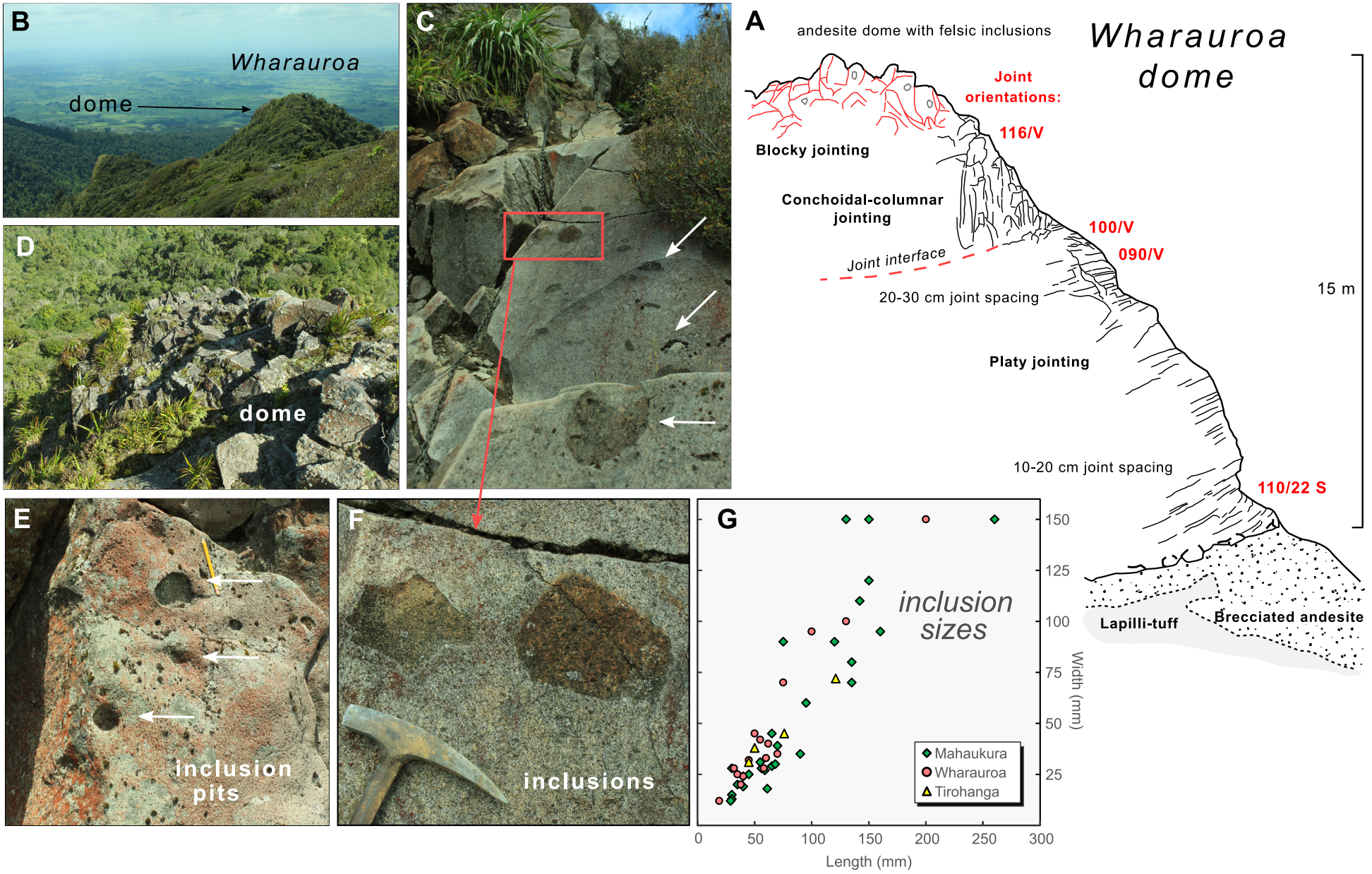
B
Wharauroa
dome
C
D
dome
A
andesite dome with felsic inclusions
Wharauroa
dome
Joint
orientations:
116/V
Blocky jointing
Conchoidal-columnar
jointing
100/V
090/V
Joint interface
20-30 cm joint spacing
15 m
Platy jointing
10-20 cm joint spacing
110/22 S
Lapilli-tuff
Brecciated andesite
E
inclusion
pits
F
inclusions
G
inclusion
sizes
Mahaukura
Wharauroa
Tirohanga
Width (mm)
Length (mm)
0
50
100
150
200
250
300
25
50
75
100
125
150

ANDESITES OF MAHAUKURA RIDGE (Pma)

Andesitic rocks (Pma) form prominent outcrops in eastern Pirongia, along the ridges and cliffs surrounding the peaks of Wharauroa (850 m a.s.l.), Mahaukura (902 m) and Tihitoetoe (845 m). The andesites consist of protruding, eroded dyke structures and associated coulées, lava flows, small domes and tuff breccias. The dykes form radially oriented clusters that each mark a vent domain of either large (e.g. Mahaukura-Tihitoetoe) or moderate (e.g. Wharauroa vent) size. The largest mapped outcrops of the unit are described below.

Mahaukura Bluffs

Four large andesitic dykes (10–15 m thick) of Pma unit crosscut the succession of basaltic andesite lavas (Pml) exposed within the Mahaukura bluffs. (Fig. 12). Three of the dykes form a radial pattern that broadly projects toward a peak (904 m a.s.l) above the bluffs. The dykes display strong horizontal jointing patterns and have brecciated margins (up to 0.5 m wide) along their undulating, sub-vertical contacts with the country rock. The andesites are typically holocrystalline, vesicle-free, light grey, strongly porphyritic rocks with phenocrysts of plagioclase (1.5–2 mm), hornblende (2–5 mm) and less abundant green clinopyroxene (1–3 mm). Dyke A (see Fig. 12) displays strong trachytic alignment of plagioclase on both sides of its dyke structure that parallels the curved entablature within the columnar joints. Dyke B rocks from the inner southern wall are weakly vesicular and contain felsic inclusions equivalent to those observed in andesites at Wharauroa and Mahaukura peaks. The dykes (A-C) feed small, eroded dome and coulée flows on the ridge above the bluff.

Wharauroa Peak

Wharauroa is the remnant of an andesitic dome (refer to Fig. 14) similar to those fed by dykes along the Mahaukura Bluffs. Andesite of the peak overlies basaltic andesite flank lavas (Pml). The top of the dome consists of blocky-jointed lava with splayed, conchoidal joint patterns (Fig. 15; A, B, D). The lower section is marked by a joint interface, below which the jointing patterns are platy, sub-horizontal in orientation and more closely spaced (10–30 cm apart). The cohesive jointed domain overlies brecciated andesite and lapilli-tuff of similar composition. Wharauroa andesite is light-grey and porphyritic with abundant phenocrysts of plagioclase (up to 3 mm), clinopyroxene (1–2 mm), hornblende microphenocrysts (1 mm) and rare olivine (1 mm). Medium-grained, plagioclase-rich felsic inclusions (up to 2% of rock, 19–260 mm long) with spherical to elliptical shapes (Fig. 15, G) are exposed within the upper dome section. The inclusions form pockmarks within the weathered host rock and have rusty-orange alteration colours (Fig. 15, E). A prominent, eroded monolith outcrops 250 m north of Wharauroa Peak (Fig. 14). This feature, informally referred to here as Mangamauku peak (740 m a.s.l.), may represent a dyke or dome of (Pma) andesite, or an older bluff of (Pml) basaltic andesite lavas. The truncated western face of the rock exposes a near-horizontal jointing pattern more typical of lavas rather than the andesite domes or dykes of the Mahaukura ridgeline. Nonetheless, the Mangamauku peak rock is assigned to the (Pma) unit on the basis of geomorphology (erosion resistant, dyke-like structure) and its proximity to the Wharauroa Peak andesite.

Mahaukura Peak

Andesite crops out at Mahaukura Peak as a small, splay jointed dome fed by a large dyke oriented NW-SE. The Mahaukura andesite is light-grey coloured and porphyritic with abundant plagioclase (up to 2.7 mm), visible hornblende (1–1.5 mm) and clinopyroxene (1–2 mm). Felsic inclusions are common (1% of rock) and display both angular and sub-rounded shapes (up to 260 mm in length) with sharply defined margins (Fig. 15, C, F). Their textures are essentially microcrystalline diorites with abundant plagioclase and subordinate clinopyroxene and hornblende. The dome is overlain by small amounts of red, weathered lapilli tuff containing sub-rounded andesitic fragments.

BASALTIC LAVAS AND FRAGMENTAL DEPOSITS OF RUAPANE PEAK (Prb)

The best exposures of ankaramite on the mountain occur along the ridgelines surrounding Ruapane Peak (723 m a.s.l.), northeast Pirongia (Fig. 16). At this site, highly porphyritic basalts form a complex array of agglomerates, lavas and cross cutting dykes that collectively represent proximal deposits of the Ruapane vent. Deposits of the (Prb) unit intrude through and mantle older Paewhenua flank lavas (Ppe).

Ankaramite dykes form two distinct, ridge-parallel groups striking north-south and east-west (Fig. 16, B). The dykes are generally thin (1–1.5 m wide), show platy jointing and have undulating, strongly brecciated margins. Their textures range from moderately to strongly porphyritic with abundant clinopyroxene (glomero-) phenocrysts (1–3 mm; 6–13% of the rock), abundant stubby laths of plagioclase (mostly 1 mm) and subordinate olivine set within dark-grey (or purple) groundmass containing the same minerals. Some dykes are moderately vesicular. The southernmost N-S dyke is notably finer-grained basaltic andesite, with conchoidal jointing similar to that observed in other dykes of the (Ptb) unit further south on the ridgeline.

Figure 16. Ruapane flank vent. A: View northeast to Ruapane Peak and two neighbouring cones (1 and 2). The Ruapane (Prb) deposits overlie Paewhenua (Ppe) shield lavas (yellow dashed line). (B) Map of ridgeline outcrops and structural pattern of dykes related to the Ruapane unit. Dykes and agglomerates at the peak demarcate a fissure zone with vents aligned east-west. Another smaller vent is centred on cone 1, with lavas dipping northwest of the vent and radial dykes situated at cone 2. C: Typical outcrop of vent proximal basaltic agglomerate at cone 2. D: Typical Ruapane-type ankaramite with large phenocrysts of clinopyroxene and microphenocrysts of plagioclase set within purple-coloured groundmass. E: Lava and agglomerate stratigraphy at cone 1 (hammer for scale), including scoriaceous ankaramite (F).

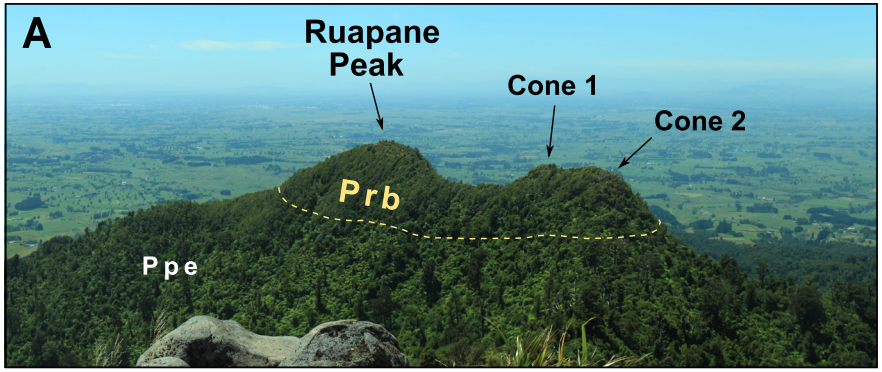
A
Ruapane Peak
Cone 1
Cone 2
Prb
Ppe

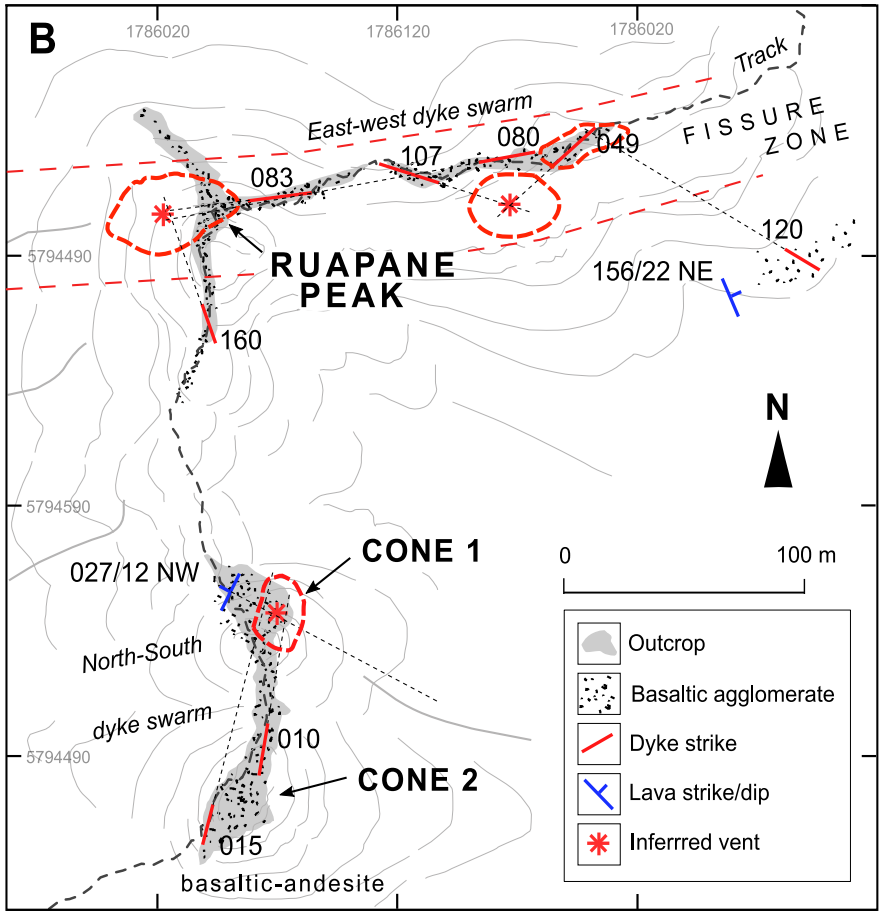
B
1786020
1786120
1786020
Track
East-west dyke swarm
FISSURE ZONE
083
107
080
049
120
RUAPANE PEAK
156/22 NE
160
5794490
5794590
5794490
N
CONE 1
027/12 NW
North-South
dyke swarm
010
CONE 2
015
basaltic-andesite
0
100 m
Outcrop
Basaltic agglomerate
Dyke strike
Lava strike/dip
Inferrred vent

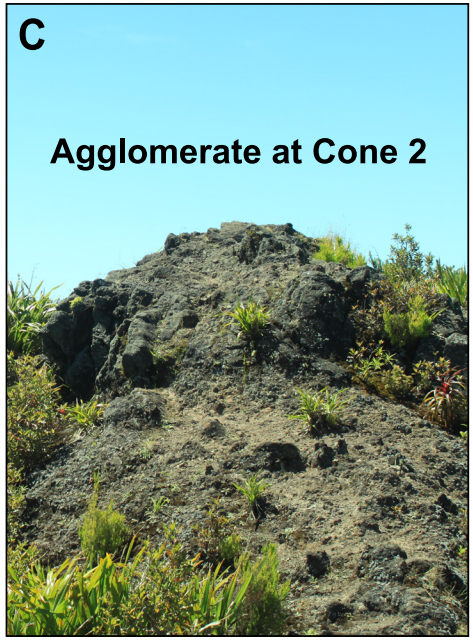
C
Agglomerate at Cone 2


D
ankaramite

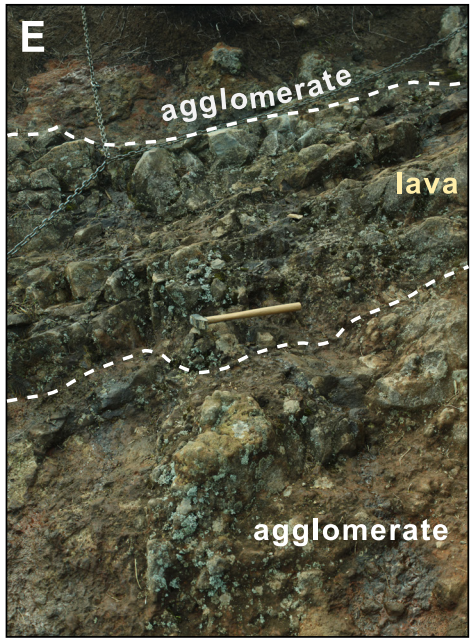
E
agglomerate
lava
agglomerate


F
scoria

Figure 17. View southwest to Hikurangi dome vent (Phk), south of Pirongia. Field of view (foreground) is 400 m.

Ankaramitic agglomerates and lavas are well preserved at Ruapane and its adjacent peaks (Fig. 16, C). The agglomerates consist of highly dense, sub-rounded blocks or bombs (70–100 mm) ranging from scoriaceous to non-vesicular. At Ruapane Peak, the blocks are strongly vesicular with abundant clinopyroxene glomerocrysts (1.5–4.5 mm), stubby plagioclase laths (1–1.5 mm) and subordinate olivine (max. 2 mm, altered red) within fine-grained, dark grey groundmass (Fig. 16, D). At cone 1, the observed succession consists of: (1) relatively thick (>5 m) agglomerate with scoriaceous clasts overlain by (2) a thin (< 1 m thick) northwest-dipping lava flow (clinopyroxene av. 1.5–2 mm, up to 7 mm; 7% of rock; rare olivine (max. 1 mm) and minor plagioclase in a fine dark purple groundmass) that is overlain by another lava flow towards the top of cone 1 (Fig. 16, E). The upper lava unit is more coarsely porphyritic with larger clinopyroxene (av. 3–5 mm, max. 7 mm; 10 % of rock) and abundant, seriate textured plagioclase (max. 1 mm). The lavas are mantled by (3) agglomerate containing weakly vesicular, finer-grained clasts (clinopyroxene 1.5–4 mm).

Lapilli-tuff deposits form the basal succession of the (Prb) unit. Outcrops north and east of Ruapane Peak are matrix supported deposits with coarse angular lapilli (22–45 mm) of vesicular ankaramite and finer-grained red scoria (7–10% clasts) set within a reddish-brown matrix of clay and loose crystals (clinopyroxene and plagioclase). These deposits are intercalated with red-coloured, crystal-rich tuffs containing clinopyroxene. Several sub-vertical, ankaramitic feeder dykes associated with the Ruapane swarm outcrop within the lower Mangakara Valley (600 m a.s.l.), where they cross cut basaltic agglomerates and lavas of the unit.

HIHIKIWI MEMBER (2.3–2.13 Ma)

FLANK SCORIA CONE OF HIHIKIWI RIDGE (Psc)

Deep red coloured scoria deposits (<5 m thick) are exposed along 20 m of road cutting on Pirongia West Road (see scoria in Fig. 9, F). The deposit contains massively sorted, scoriaceous basaltic lapilli with small phenocrysts of clinopyroxene, olivine and plagioclase (all av. 1.5 mm). The lapilli show pervasive hydrothermal alteration with yellow-green vesicle lining (iron oxides) and cream-white amygdales (zeolites).

OMANAWA BASALT (Pob)

The Omanawa basalt is an isolated lava flow on the lower SW flank of Pirongia with distinct olivine-rich texture (see Fig. 9, F). Ridge morphology suggests that the basalt flow has a total length of ~3.1 km, proximal thickness of ~80 m (thinning to 30 m in the distal zone) and erupted from a source zone ~800 m above the Pirongia West Road. In road cuttings, the basalt is pale-grey coloured with typically flaggy jointing and dips 20° to the south. Stratigraphically the unit overlies basaltic andesite lavas of the Paewhenua Member (Ppe; exposed in nearby road cuttings). The (Pob) lava flow forms a topographic barrier to volcaniclastic breccias (Odb) to the west. The Omanawa basalt is a weakly vesicular, fine-grained rock dominated by phenocrysts of olivine (mostly ≤ 1 mm, glomerocrysts max. 4 mm; typically altered) and minor amounts of plagioclase and clinopyroxene set within a trachytic groundmass.

BASALTIC ANDESITES OF HIKURANGI VENT (Phk)

Hikurangi Peak is a flank vent (2.30 ± 0.05 Ma; Briggs et al., 1989) south of Pirongia that produced a single lava flow (three kilometres long) associated with an elongate, flat-topped dome (Fig. 17; 100 m thick; 183 m elevation). The dome was once occupied by a Māori pā site. The lavas produced are distinct phlogopite-bearing basaltic andesites. The dome is centred on the southeastern edge of the Oparau Graben and its lava flowed west into the depression. Distal portions of the flow outcrop on Okupata Road, where bouldery, onion skin weathered lava (at least 5 m thick) is exposed. The (Phk) unit erupted through and overlies older ring plain breccias (Pkb) of the Orakei Plateau. The unit thus provides an age constraint on deposition of the breccias, which must have occurred before 2.30 Ma. Intense erosion of the breccias relative to the (Phk) lavas resulted in the pronounced topography of Hikurangi Peak within the local landscape.

The Hikurangi lavas are mid-grey to purple coloured basaltic andesites with sparse phenocrysts of clinopyroxene (phenocrysts 1–1.5 mm, glomerocrysts 3–6 mm) and hornblende (opaque/skeletal; ≤1 mm) with phlogopite inclusions (<0.5 mm) in very fine-grained groundmass. Rare microphenocrysts of plagioclase and olivine were observed in some samples.

BASALTIC ANDESITE OF KOHATUPIKO PEAK (Kpa)

The sacred 'crooked rock' of Kohatupiko (785 m a.s.l.) is an isolated peak in southern Pirongia (Fig. 18) interpreted as a dyke or dome structure with possible NE-SW strike. The unit intrudes through older Paewhenua (Ppe) flank lavas and is probably coeval in stratigraphic age with andesites of the Tiwarawara ridge (Twd). The Kohatupiko (Kpa) unit covers an area of 160×160 m. The main outcrop consists of a steep bluff (40 m high) with joint striations dipping southwest, and a smaller, less exposed mound to its south.

BASALTIC LAVAS AND SCORIA OF TIWARAWARA RIDGE (Toa)

Voluminous basaltic lavas and interbedded scoriaceous deposits outcrop in the area of Tiwarawara Peak (710 m a.s.l.), SE Pirongia (Fig. 19). The (Toa) unit represents proximal deposits from a flank vent that erupted through older flank lavas of the Paewhenua Member (Ppe). Tiwarawara basalts are cross cut by two andesite dykes (Twd), northwest and southeast of the main peak. The unit is bordered to the north by younger basaltic lavas of Te Akeohikopiro Peak (Tkb).

The Tiwarawara Peak marks a dome of ankaramite lavas with prominent splayed jointing patterns. The ankaramite is unusually coarse-grained and abundant in olivine (1–8 mm; 5% of rock) relative to other Pirongia ankaramites. The rock is dominated by clinopyroxene (1.5–8.5 mm; 15% of rock). Plagioclase is restricted to the groundmass, which is dark grey and poorly vesicular. The dome overlies massive red scoria deposits (± large loose clinopyroxene crystals) of similar composition that outcrop sporadically on steep slopes up to 790 m a.s.l. Lavas downslope of the dome form boulder fields of dark-grey ankaramite with low to medium vesicularity, and with clinopyroxene (1.5–6 mm; 7–12% of rock) more abundant than olivine.

ANDESITES OF TIWARAWARA RIDGE (Twd)

Andesite outcrops at two localities on the Tiwarawara Ridge (southeast Pirongia), where the unit forms dyke structures orientated parallel (northwest-southeast) to the ridgeline (Fig. 19). The dykes comprise fresh, finely-porphyritic andesite with abundant plagioclase (1–2.5 mm) and vitreous black hornblende (generally acicular, 1–2 mm, few 4–13 mm) in medium-light grey, glassy groundmass. The upper dyke (at 670 m a.s.l.) is weakly vesicular. Dyke measurements for the (Twd) unit are summarised in Appendix D.

BASALTIC LAVAS AND FRAGMENTAL DEPOSITS OF HIHIKIWI RIDGE (Phb)

The (Phb) unit includes a diverse and stratigraphically complex sequence of lava flows and volcaniclastic breccias that mantle older flank lavas (Ppe) over a two kilometre stretch of the Hihikiwi ridgeline, southwestern Pirongia. The unit outcrops up to 900 m a.s.l, although it is poorly exposed. Deposits of the unit are cross cut and overlain by more siliceous dykes and lavas (Phr). The two units are probably intercalated as an overall vent facies succession associated with Hihikiwi Volcano. Basaltic breccia belonging to the (Phb) unit is exposed at 810 m a.s.l. in a landslide scarp at the southern

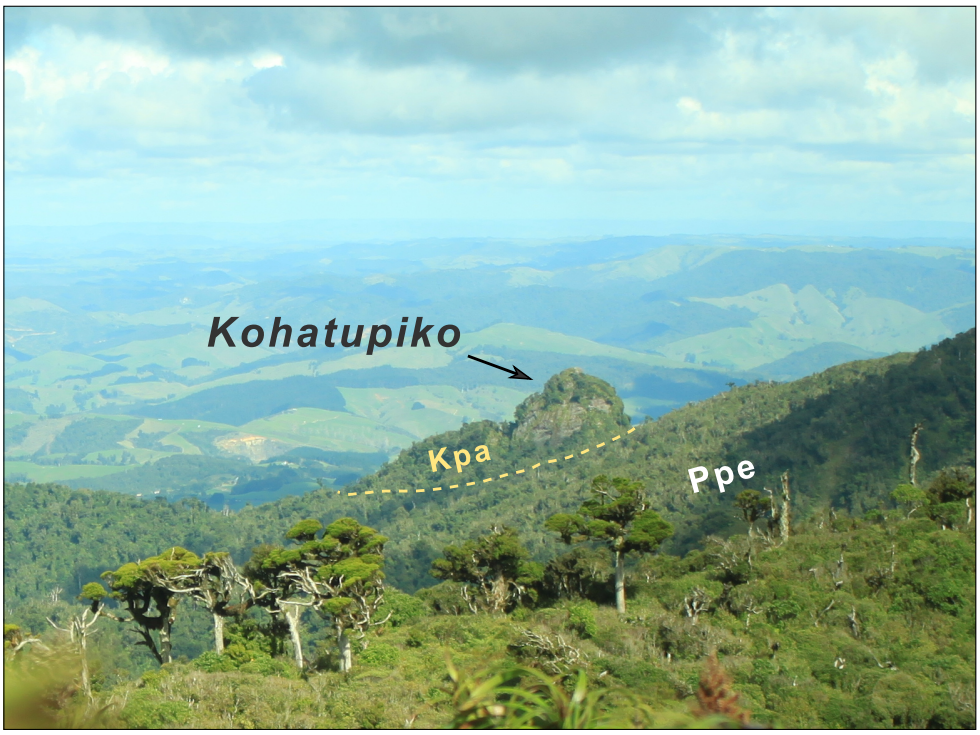

Figure 18. View south (from summit ridge) to the monolith of Kohatupiko. The (Kpa) unit consists of a dyke that cross cuts older shield lavas (Ppe).

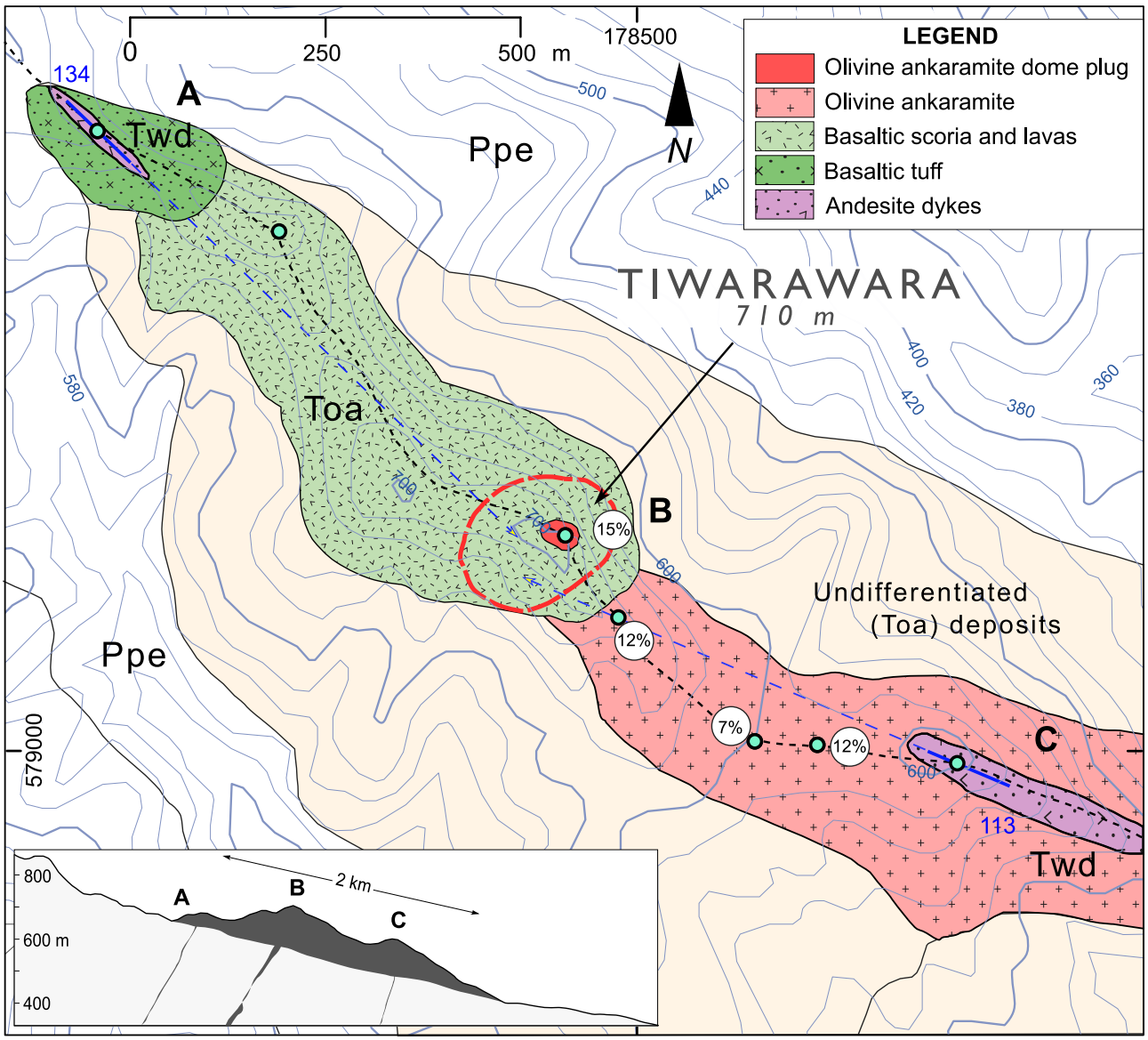

Figure 19. Map: basaltic tuffs and scoria surrounding the Tiwarawara Peak vent, southeastern Pirongia. The vent area is shown by a red dashed line surrounding the dome. Radial dykes project towards the vent centre. The percentage of clinopyroxene in the basaltic deposits is shown by % symbols. Inset: topographic profile showing (Toa) unit (dark grey) overlying older flank lavas (Ppe).

extent of the unit (Fig. 20; A-D). The deposit is conformably overlain by basaltic andesite dome lavas (see Phr, below). The breccia contains unsorted basalt clasts of lapilli to block size within fine red matrix material. The clasts contain weathered clinopyroxene (1.5–4 mm) and lesser amounts of phenocrystic to microlitic plagioclase in purple to red groundmass. At higher elevations, cpx-basalt (clinopyroxene 3%; 2–4 mm) and ankaramite (clinopyroxene: 9–10 % volume; 3–5 mm) lavas and dykes outcrop sporadically.

ANDESITES OF HIHIKIWI RIDGE (Phr)

Intrusive domains of mainly andesitic composition outcrop along the ridgeline southwest of Hihikiwi Peak (Fig. 20; A, F) at lateral intervals of ~700 m. From south to north, these domains are described as follows. (1) [BE33 818 905] Platy-jointed basaltic andesite lava (~20 m thick) that overlies intensely weathered basaltic block-and-tuff deposits within a 12 m tall landslide scarp. The lava is pale-grey in colour, fine-grained and abundant with plagioclase phenocrysts and microcrysts interspersed with black clinopyroxene

Figure 20. Hihikiwi ridge volcanics, southern Pirongia. A: Panorama of Hihikiwi ridge, looking south from The Cone (Pcd, foreground) across the Oparau River valley. The ridge consists of Paewhenua shield lavas cross cut and mantled by basaltic (Phb) and andesitic (Phr) deposits of the Hihikiwi vent zone (contact is yellow dashed line). Scale of vent zone is 400 m. B: Stratigraphic relationship between Hihikiwi vent deposits in a landslide scarp (behind main ridge in photo). C: Basaltic block-and-ash deposits (Phb, see inset photo D) are overlain by basaltic andesite dome lavas (Phr). Some Phr lavas are highly porphyritic andesites (E) with large hornblende crystals. The (Phr) dykes form sharp peaks along Hihikiwi ridgeline (F; view looking northeast to Pirongia Summit).

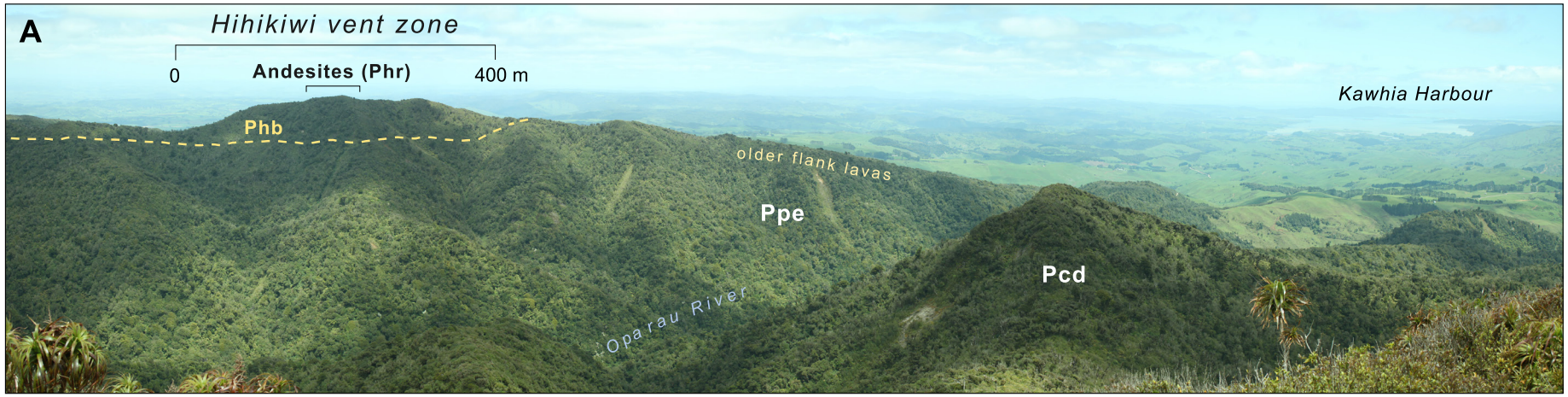

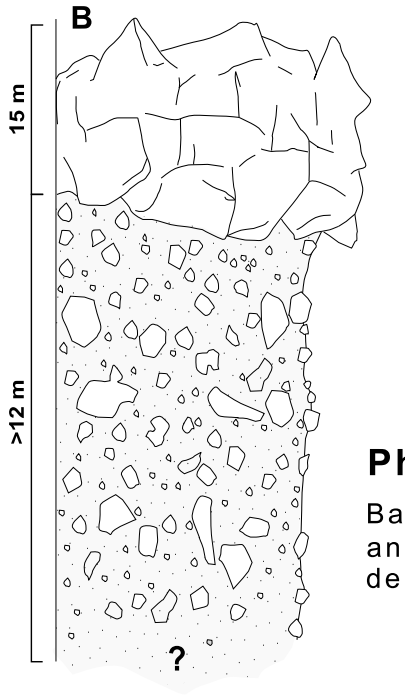

Phr
Basaltic-andesite dome lavas

Phb
Basaltic block and ash flow deposits

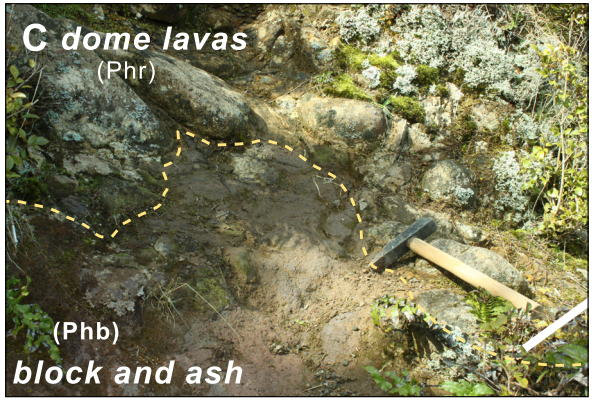

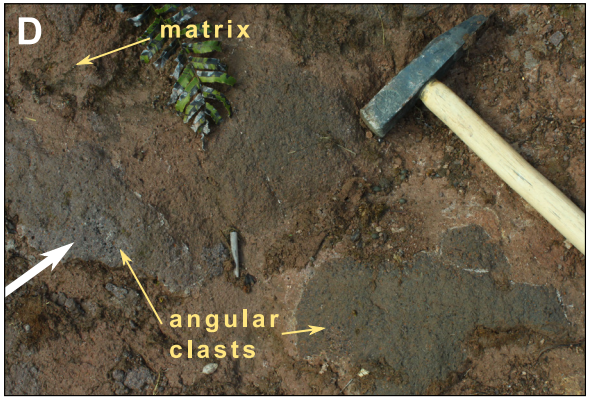

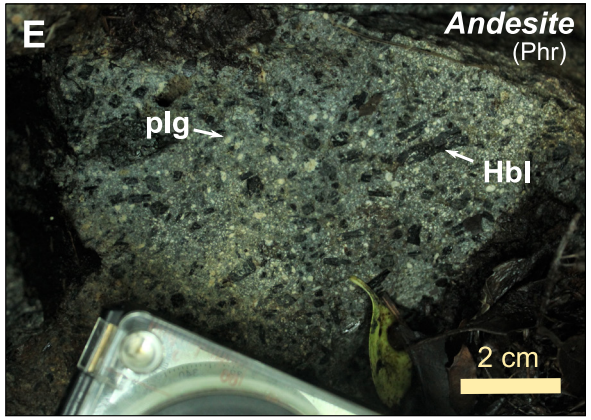

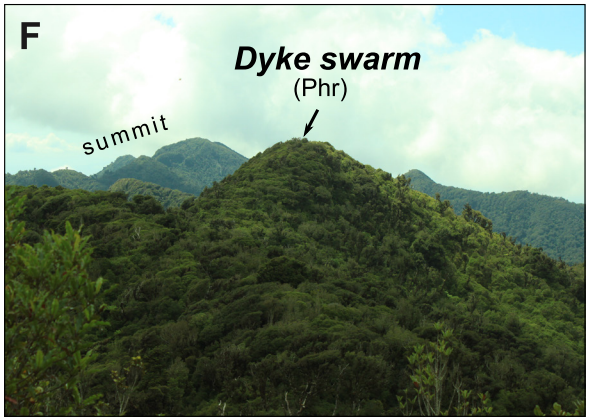

phenocrysts (1.5 mm) and glomerocrysts (that include plagioclase; 2–3 mm). (2) [BE33 824 909] A prominent lava and dyke complex (450 m wide) of basaltic andesites that outcrops at a peak at the converging point of two prominent ridges, 2 km northeast of Pirongia West Road. Overall, these erupted products are more mafic than other members of the unit, with clinopyroxene the main phenocryst phase and hornblende (up to 4 mm) restricted to a single dyke at the north end of the complex. (3) [BE33 832 912] Ridge capping lavas of light-grey coloured, highly porphyritic andesite with abundant phenocrysts of vitreous hornblende (1.5–3.5 mm; rare megacrysts up to 17 mm; Fig. 20; E) and black clinopyroxene (1–4 mm). Plagioclase is restricted to microphenocrysts and is abundant in the groundmass. The rock is weakly vesicular (av. 1.5 mm wide). The unit overlies basaltic andesite agglomerates without hornblende.

TE AKEOHIKOPIRO MEMBER (2.1 Ma)

MANGAKIEKIE BRECCIA (Mdb)

The Mangakiekie breccia is a laterally extensive unit mapped over the southern flanks and ring plain of Pirongia. The (Mdb) unit is poorly exposed over most of its area and has an indistinct surface expression (low rolling hills). It extends over 10 kilometres SSE of the mountain. Thickness of the unit on the lower flanks is at least 100 m. Previous mapping by Henderson and Grange (1926) identified volcaniclastic breccias in the southern ring plain that stratigraphically belong to the unit. These breccias outcropped in road cuttings along a six kilometre stretch of the Kawhia Road. Further south, the (Mdb) unit outcrops along the edge of the Moakurarua Stream and at Turoto Road.

The (Mdb) unit is considered younger than the plateau-forming Pekanui breccia (Pdb) to its west on geomorphological grounds. The unit infills lowlands on the dissected edge of the (Pdb) plateau. The (Mdb) breccia is stratigraphically overlain by lavas of Te Akeohikopiro Peak (Tkb; see Fig. 21).

Blocky domains proximal to the volcano outcrop sparsely near the top of Mangati Road at a small waterfall. The deposits consist of loose boulders of andesite up to two metres wide. The andesite is dominated by plagioclase phenocrysts, with sub-equal amounts of hornblende (1–4.6 mm) and clinopyroxene (<1–1.5 mm) in plagioclase-rich groundmass. More andesite boulders occur scattered in farm paddocks adjacent to where the road crosses Whakarautawa Stream.

BASALTIC LAVAS OF TE AKEOHIKOPIRO (Tkb)

The (Tkb) unit defines an extensive basaltic lava flow field (Fig. 21) erupted from a flank vent in the area of Te Akeohikopiro Peak (869 m a.s.l.). The unit encompasses three remarkably linear, morphologically young ridges (oriented SSW-NNE). These ridges are the remnants of channelized (Tkb) lava flows now inverted topographically by fluvial erosion (see Fig. 21; inset sketch). Measurements of ridge slope suggest that the lavas flowed at low angles (4.4–6.2°) and travelled three to four kilometres from the peak. A sector-collapse-related unconformity separates the (Tkb) unit from older Paewhenua shield lavas (Ppe) and vent deposits of Hihikiwi Member (Phb and Phr). The proximity of the Tkb and Hihikiwi Member central vents suggests that the Tkb lava flow was emplaced rapidly after the edifice collapse event and therefore has a stratigraphic age slightly younger than 2.2 Ma.

The composition of (Tkb) lavas is inferred from (poorly exposed) outcrops at Te Akeohikopiro Peak. At the peak, red basaltic-lapilli tuff (containing 7–8% clinopyroxene; 2–4 mm) is overlain by two lava units: (1) relatively fine-grained basalt with sparse phenocrysts of clinopyroxene (2–3, max. 5 mm) and olivine (≤ 2.5 mm) and scarce plagioclase (≤ 1 mm); and (2) basalt with relatively coarser groundmass (plagioclase-rich overall) and greater abundance of clinopyroxene (1–3.5 mm, 10% of rock), olivine (≤ 2 mm, glomerocrystic) and plagioclase (mostly ≤ 1 mm, max. 2 mm) phenocrysts in dark grey groundmass.

OPARAU MEMBER (1.7 Ma)

OPARAU BRECCIA (Odb)

A large-volume (~3 km^3), laterally expansive unit (31 km^2) of undifferentiated, volcaniclastic breccia (Odb) extends from the southwestern flanks of Pirongia to Kawhia Harbour, 20 km southwest of the volcano. The distribution of Odb breccia is confined to the Oparau Graben, where it partially overlies basement rocks (Mkg, Mag), Oligocene sedimentary rocks (Tka, Tkg) and older Pirongia Formation breccias (Pkb). The breccia is overlain in the northeast by younger lavas of Pūawhe/The Cone (Pcb).

The Oparau breccia (Odb) is interpreted as a debris avalanche deposit sourced from a large-scale sector collapse of the western flank of Pirongia. Edifice stratigraphy indicates that the deposit consists mainly of rubble from the Paewhenua shield (Ppe) and smaller amounts of material from the overlying Hihikiwi Member (Phb, Phr).

The maximum age of breccia deposition is constrained by the sector collapse scarp that truncates the Paewhenua shield (Ppe; 2.5 Ma) and younger Hihikiwi Member (Phb, Phr; 2.3–2.2 Ma). The minimum deposition age is given by Kauroa Ash bed K3 (1.68 ± 0.12 Ma; Lowe et al., 2001) that overlies the breccia at Tiritirimatangi Peninsula (Horrocks, 2000). At this site, the upper two metres of Odb unit are weathered and have formed a paleosol (20 cm thick) below the K3 bed. The degree of weathering suggests a modest time break between Odb breccia and deposition of the K3 tephra. An emplacement age of 1.7 Ma is thus adopted here which closely predates eruption of the Pirongia Summit Member lavas (1.6 Ma) that infill the collapse scarp associated with Odb breccia.

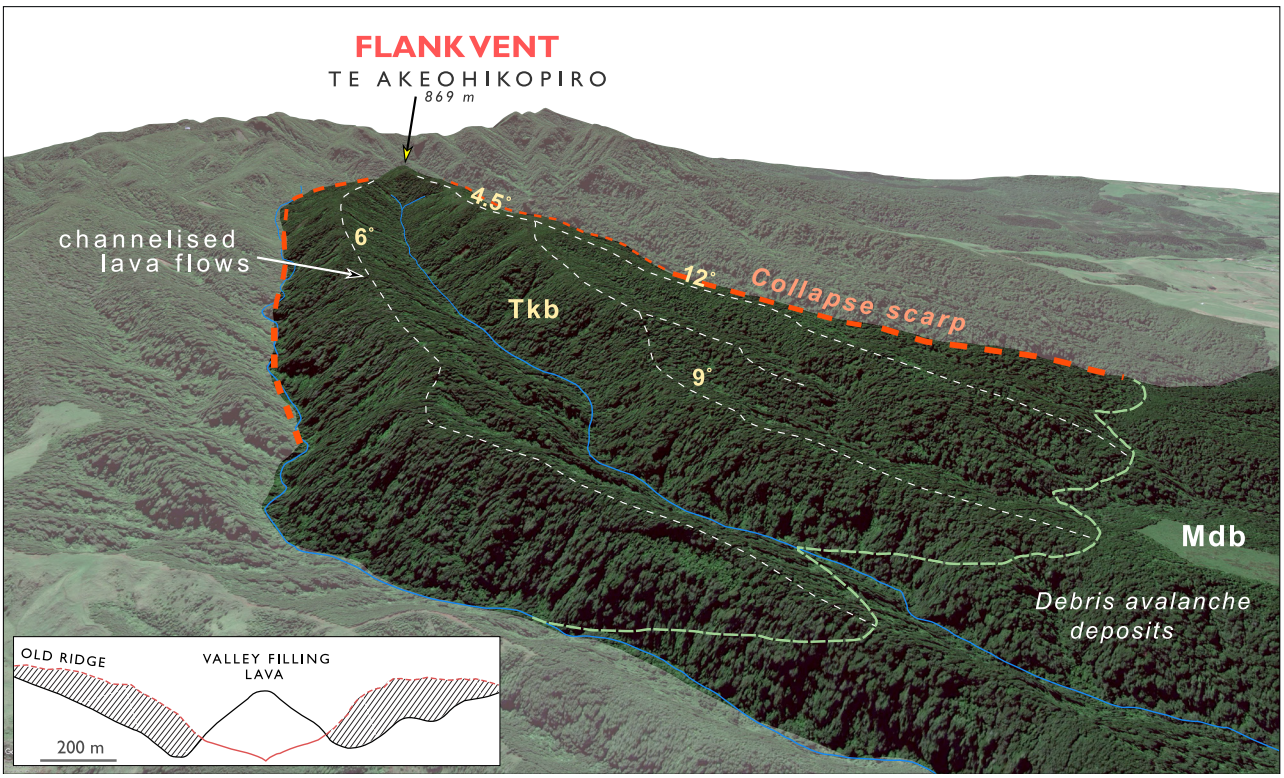

Figure 21. View northeast to Te Akeohikopiro flank vent, southern Pirongia (Google Earth image). The (Tkb) lavas originate from a vent at the peak and have infilled a collapse scarp (orange dashed line). They overlie debris avalanche deposits (Mdb) associated with the collapse event (contact is green dashed line). The lavas are channelised and flowed at generally low slope angles of 4.5–12°. Topographic inversion has formed ridges and removed any older valley walls (see inset cross section).

Proximal deposits

The composition of proximal deposits is known from limited outcrops on the upper planeze surface of (Odb) breccia. Boulder fields weathered from the unit are widespread on the planeze. They consist of large (1–2 m) blocks of basalt and basaltic andesite weathered from the underlying breccia.

Farm track cuttings (at ~530 m a.s.l.) expose small-scale vertical variations in the (Odb) breccia. A well-preserved outcrop shows: (1) a lower polymict, block-rich domain (clasts up to 35 cm) overlain by (2) a lapilli-rich domain containing red scoria (total deposit is 1 m thick), overlain by (3) a larger deposit (>2 m thick) of clast-supported breccia with jigsaw fractured boulders of basalt and basaltic andesite (up to 1.5 m wide). Hydrothermal alteration (clay altered plagioclase) is evident in some boulders. Two dates for boulders from this area yield ages of 2.13 ± 0.10 and 2.25 ± 0.10 Ma (Robertson, 1976). The boulders are correlated stratigraphically to lavas from the Hihikiwi Member, 2.6 km east upslope.

The top of the (Odb) breccia outcrops on Pirongia West Road between 510 and 490 m a.s.l. The deposits here consist of highly weathered, polymict breccia with clast sizes ranging from lapilli to small blocks (<30 cm). The clasts are set within a matrix of reddish-brown clay and loose clinopyroxene crystals. Larger cohesive blocks (1–2 m) are scattered in the surrounding paddocks. The boulders are typically Pirongia-type basalts and basaltic andesites but also include finer-grained, melanocratic basanites (with euhedral olivine). Occurrence of the latter in the (Odb) deposit indicates that alkali-basalt (Okete-type) lavas exist in the local edifice succession (i.e. within the Ppe unit of Paewhenua shield) further upslope.

Distal deposits

Distal portions of the (Odb) breccia form prominent crags (below 70 m a.s.l.) along the Oparau River valley where the unit overlies Aotea Formation sandstone (Tka; Fig. 22, A, C). At the best exposed bluff (base height ~38 m a.s.l.) the breccia is vertically continuous over 40 m (Fig. 22, B) and forms scattered outcrops to the top of the ridge line (~95 m a.s.l.). Deposits in this area consist of poorly sorted, matrix supported diamictons of volcanic rock (Fig. 22, D). Clasts range from angular, coarse lapilli up to large metre-sized blocks. Many of the blocks show jigsaw fracturing infilled by matrix material (Fig. 22, E). The clastic component is polymict and dominantly basaltic in composition. Lithologies range from ankaramite to finer-grained basaltic andesite. Andesite is relatively uncommon and occurs mainly as lapilli, including pale-coloured pumice. Hydrothermal alteration is prevalent in many clasts (e.g. zeolite amygdales). Deformed blocks of sandstone (Tka) and angular basement (metasedimentary) clasts are relatively common in the breccia (Fig. 22, F).

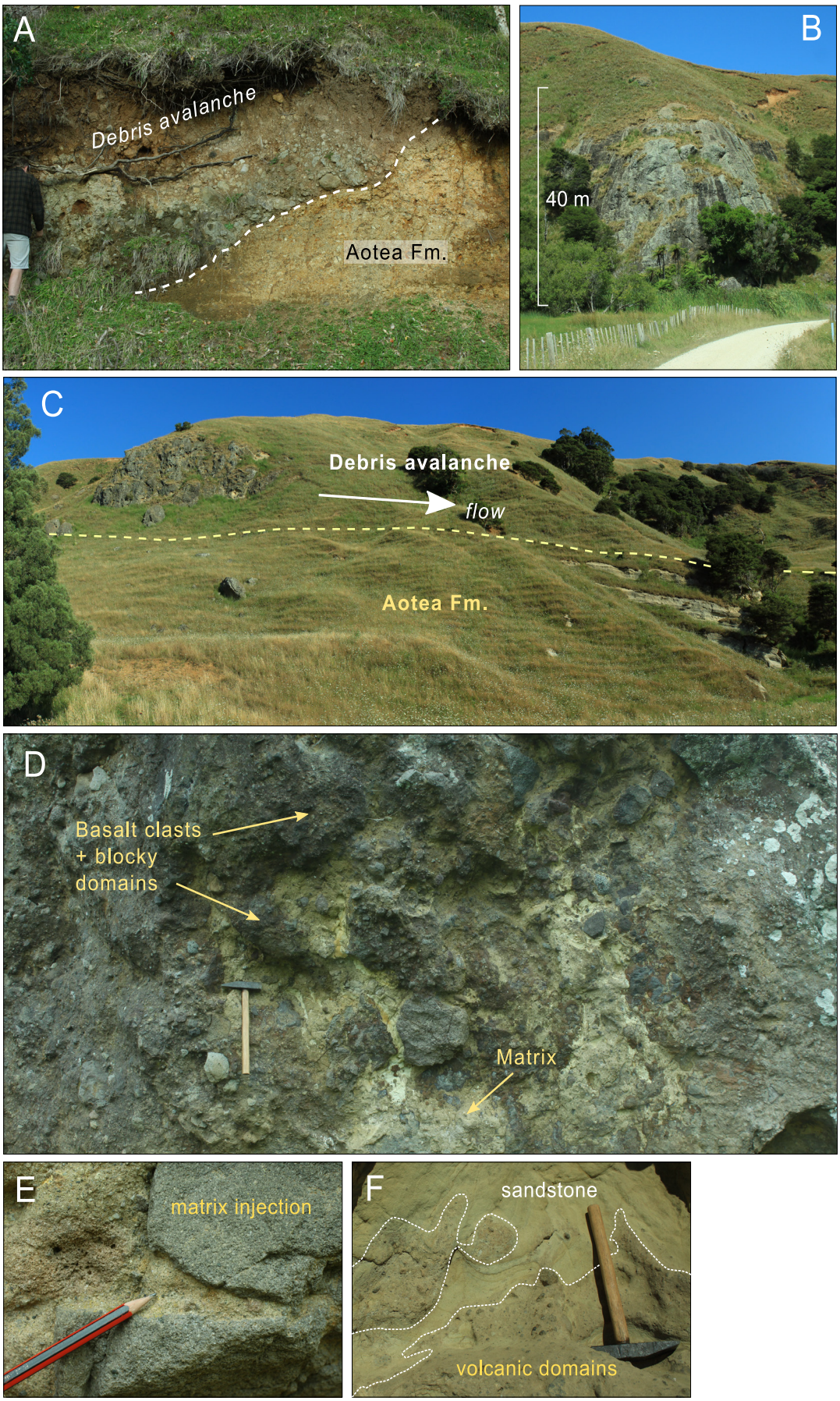

Figure 22. Outcrops of Oparau breccia (Odb) along Pirongia West Road. A: Deposition contact with Aotea Formation mudstone breccia. B: Prominent bluff with 42 m of vertical exposure, 13 km from Pirongia Summit. C: Deposition contact between Odb breccia and flaggy sandstone of Aotea Formation. D: Outcrop photo of poorly sorted, matrix supported diamicton with basaltic clasts. Hammer for scale. E: Jigsaw fractured basaltic clast showing matrix injection texture. Pencil for scale. F: Block of Aotea Formation sandstone with fluidal-type deformation within diamicton domains of Odb breccia.

PIRONGIA SUMMIT MEMBER (1.6 Ma)

BASALTS OF PUKEHOUA VENT (Poa)

The Pukehoua volcanics are among the youngest erupted deposits of Pirongia (1.64 ± 0.13 Ma; Briggs et al., 1989), emplaced from a prominent satellite vent on the lower eastern flank of the volcano. The deposits cover an area of ~15 km^2. The Pukehoua vent(s) appear to represent a fissure system that produced fire fountains of scoria and ash intercalated with a number of texturally distinct lavas (collectively Poa unit) that flowed at least 3 km. Rock exposures are limited to sparse boulder fields and track cuttings. The (Poa) unit cross cuts and overlies the eastern flank of Pirongia (Ppe) and is intercalated with ring plain deposits (Pru) of the volcano. The Poa unit is cross cut by basaltic dykes (Pkoa) of the Pukehoua vent system. Relatively young landslide deposits from Tihitoetoe peak (845 m a.s.l.) have buried the western edge of Pukehoua (Fig. 23; A).

Distinct lavas of the (Poa) unit include a relatively large flow (covering ~0.25 km^2) of platy-jointed lava, exposed in boulder fields one kilometre southeast of the Trig (Fig. 23, D). The rocks are fresh and contain sparse, dark green clinopyroxene (1–3 mm, 3% of rock) in dense, non-vesicular purplish-grey groundmass. Another lava unit, 500 m SSE of the trig contains fine-grained basalt with small phenocrysts of clinopyroxene (1–2 mm, max. 5), olivine (1–2 mm) and hornblende (mostly 1 mm, max 4 mm) in light-grey, weakly vesicular groundmass.

Pukehoua-derived, red scoriaceous lapilli-tuffs and highly weathered, massive red clays outcrop sporadically in road cuttings over distances of 0.5–3.5 km from Pukehoua trig. A proximal vent deposit contains a succession of bedded lapilli-tuffs with blocks (75–130 mm in width) in the lowest horizon (Fig. 23, E). Clasts include dark-grey, fine-grained basalts and coarser-grained basalts (4–7 mm clinopyroxene; coarse plagioclase microlites) in a generally vesicular groundmass. Towards the distal zone, scoria and massive clay beds occur buried beneath weathered lava flows. Further downslope, deposits include: (1) red scoria buried beneath a platy-jointed lava flow (see Fig. 23, D); (2) massive red clay with quartz grains, apparently a weathered basaltic ash, beneath a basaltic lava flow (onion skin weathered, clinopyroxene ≤5 mm); and (3) polymict breccia on Sainsbury Road (110 m a.s.l.) with basaltic lapilli and blocks (20–80 mm, max. 200 mm) intercalated with a thin horizon (~100 mm) of red basaltic ash.

BASALTIC PLUGS OF PUKEHOUA VENT (Pkoa)

Olivine ankaramites with textures ranging from highly porphyritic to sub-doleritic outcrop along the three tallest peaks of Pukehoua (Fig. 23; B), cross cutting Pukehoua (Poa) lavas. The rocks probably represent volcanic plugs associated with the Pukehoua vent. In outcrop they display unusual karstic weathering features (such as closely spaced, fluted crevasses; see Fig. 23; C) and are very dense due to their high crystal contents. Their phenocryst assemblage is dominated by large, blackish-green coloured clinopyroxene (1–10 mm; mostly 6–12%, max. ~25% of rock) and olivine (1–4.5 mm) set within a fine-grained dark-grey/black groundmass (± plagioclase microlites). The dolerites of Pukehoua resemble the coarse-grained ankaramite lavas of the Paewhenua Plateau (Ap), in north-western Pirongia.

UNDIFFERENTIATED LAVAS AND FRAGMENTAL DEPOSITS OF PIRONGIA SUMMIT (Psul)

Widespread but poorly exposed volcanic deposits related to the lowest part of the summit succession occupy most of the Summit Basin and the headwaters of the Kaniwhaniwha (see Fig. 24, F and exposures in Fig. 25 and Fig. 26), Oparau and Hihikiwi river valleys. The unit overlies older Mahaukura lavas (Pmu) although the contact can only be defined topographically due to poor exposure. It is overlain by breccias, dykes and lavas of the summit, Hihikiwi and Tahuanui areas. It appears to also be overlain by lavas and breccias of The Cone (Pcb), which form an extensive lava field to the northwest.

ANDESITIC FRAGMENTAL DEPOSITS OF PIRONGIA SUMMIT (Psp)

Andesitic block-and-ash flows are interbedded with polymict breccias within the upper stratigraphy of the Summit Basin and south of the Pirongia Summit ridge (Fig. 24). The (Psp) unit deposits are overlain by basaltic scoria and lavas, and are cross cut by younger dykes of the summit succession (Psb and Psa).

The best exposure of the (Psp) unit occurs in a landslide scarp (270 m southeast of Pahautea Hut; Fig. 24; stratigraphic section and images A-D). At this site, recent collapses have polished the underlying rocks over a steep (~30°) section of terrain (120 m in length). The lower part of the succession comprises poorly sorted, andesitic block-and-tuff deposits (possibly >45 m thick) with pale-grey, angular clasts within a pale-brown matrix of tuff. Andesitic clasts range in size from small lapilli to blocks up to 460 mm in diameter.

Four main clast lithologies are recognised in the block-and-ash flow deposits: (1) light-grey andesite with abundant plagioclase and hornblende; (2) andesite with equivalent mineralogy to that of Type-1 with tan to dark brown (devitrified) glassy groundmass; (3) dark-grey mafic blebs within Type-1 andesite blocks (see Fig. 24; D); and (4) rare clasts of polymict breccia (andesite pumice + minor basaltic material) of the same texture as the intercalated and overlying unit (see below). Medium-grained diorite of equivalent mineralogy to the andesites is present in small amounts. A summary of the clast types and sizes is given in Appendix E1.

Polymict breccias are intercalated with, and overlie, andesite block and tuff deposits in the highest stratigraphic level of the (Psp) unit (Fig. 24; stratigraphic section). The total unit

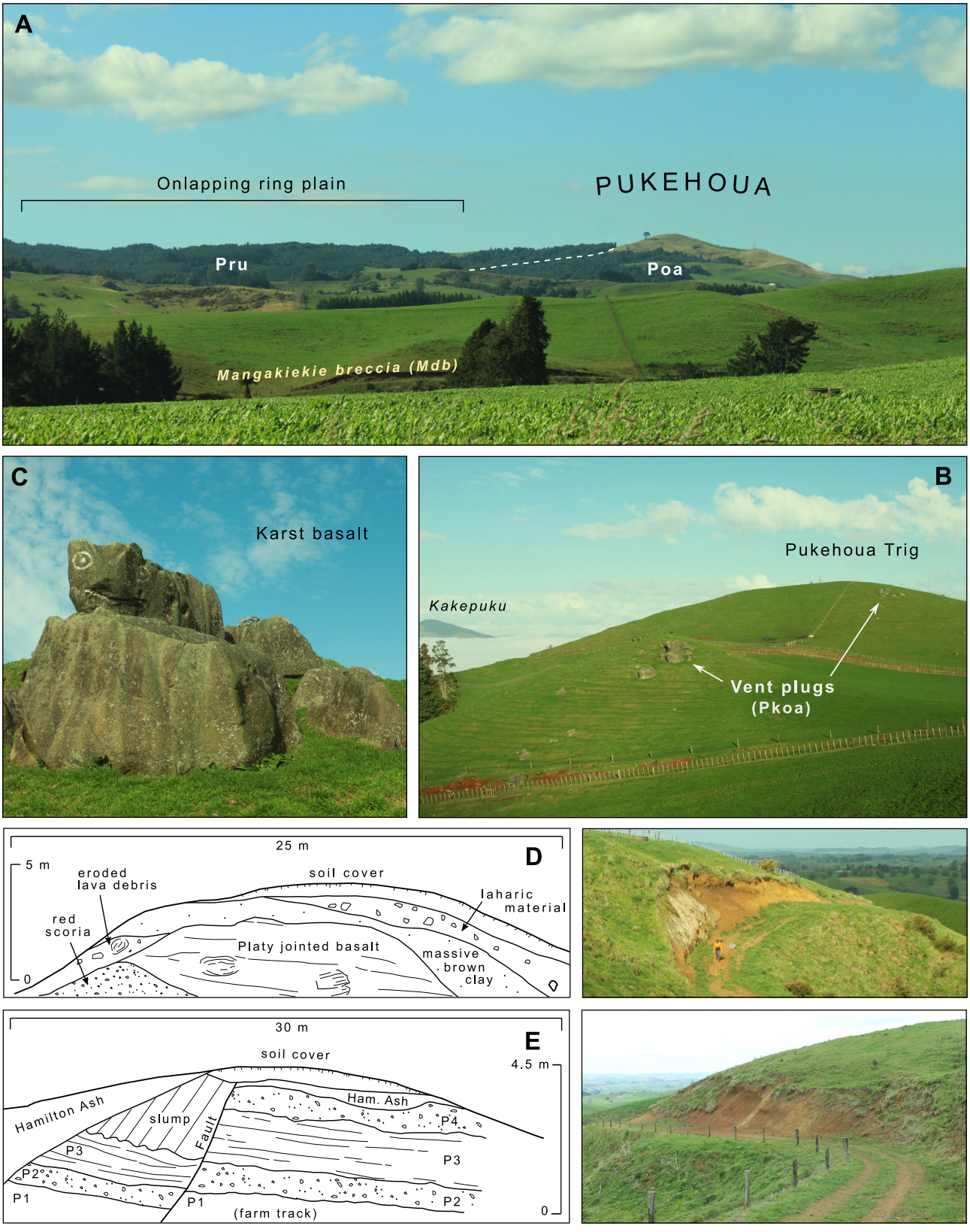

Figure 23. Volcanic features of Pukehoua flank vent, eastern Pirongia. A: Panorama looking northeast towards Pukehoua from the Mangakiekie breccia (Mdb) plains. Pukehoua is a subdued hill formation onlapped by ring plain (Pru) to the west (contact is white dashed line). B: View south to Pukehoua Trig. The main peak and another smaller hillock are vent plugs with coarsely porphyritic basalt, which show (C) karst weathering features. D: Mid flank stratigraphy from track cutting (see photo right) showing red scoria overlain by a distinct platy jointed lava flow and mantled by clays and laharic material. E: Vent proximal track cutting (see photo right) consisting of weathered lapilli-tuff beds cross cut by a small fault. Deposit descriptions: P1 – undifferentiated lapilli-tuff; P2 – scoriaceous lapilli-tuff with bombs 75–130 mm; P3 – finely bedded lapilli-tuff, lapilli up to 20 mm; P4 – lapilli-tuff, lapilli av. 8–15 mm.

thickness is probably <20 m, with individual intercalated deposits as thin as 17 cm. The breccias are clast supported with equidimensional lapilli and blocks (~10–200 mm). The main lithology of the lapilli and blocks is andesitic pumice (11–90 mm), with lesser amounts of non-vesicular andesite (13–208 mm), relatively larger basalt (fine-grained and ankaramite-type; 14–90 mm) and rare andesitic block and tuff clasts (63–171 mm) sourced from the underlying unit. Larger, sub-rounded boulders (0.3–1 m wide) of andesite are scattered over the surface of the deposit (Fig. 24; B) that appear to be weathered out from the polymict breccia. The boulders are typically glassy (devitrified) with abundant phenocrysts of plagioclase (1.5–2.6 mm), and lesser amounts of hornblende laths (1.9–2.9 mm) and clinopyroxene (1–1.9 mm). A summary of clast types and sizes is given in Appendix E2.

BASALTIC LAVAS AND FRAGMENTAL DEPOSITS OF PIRONGIA SUMMIT (Psb)

Basaltic deposits with complex stratigraphy outcrop at high elevations (780–959 m a.s.l.) in the area surrounding Pirongia Summit (refer to Fig. 25). Deposits of the (Psb) unit include cohesive lava flows, dykes and agglomerates of scoriaceous material that overlie older andesitic deposits (Psp) of the summit group (Fig. 24, stratigraphic section). The deposits are cross cut in places by andesitic dykes (Psa), which appear to have contributed clasts for overlying (Psb) agglomerates that post-date the dykes.

Lavas and dykes

Poorly exposed basaltic lava flows (2–5 m thick) appear interspersed with agglomerates and cross cutting basaltic dykes in the summit area. The lavas range from scoriaceous to non-vesicular. Phenocrysts consist of clinopyroxene (1–4.5 mm; glomerocrysts ≤ 10 mm) and lesser amounts of olivine (1–4 mm) in dark-grey glassy to plagioclase-rich groundmass. Basalts with abundant, relatively small clinopyroxene phenocrysts (1.5–2 mm, up to 20% of rock) are ubiquitous of the (Psb) unit. Basaltic lavas form a broad plateau covering 0.18 km^2 to the west of Pahautea Hut (see basaltic lavas, Fig. 25). The lava unit consists of poorly vesicular ankaramite with abundant phenocrysts of clinopyroxene (8–12 % of rock; av. 2 mm and up to 7 mm in glomerocrysts) set in medium-grey, fine-grained groundmass. A probable correlative of this lava flow occurs south of Hihikiwi Peak (see Fig. 26), where ankaramite (~12% clinopyroxene) overlies basaltic andesite lavas between 850 and 790 m (a.s.l.). In the northern part of the unit, ankaramite lava (clinopyroxene up to 1 cm wide, vesicular) overlies basaltic lapilli-tuff at 880 m (a.s.l.)

Lapilli-tuffs

Laterally and vertically discontinuous basaltic lapilli-tuffs are widespread on the ridgelines surrounding the summit area (Fig. 25; see basaltic fragmental deposits). The deposits consist of angular lapilli and occasional blocks (10–30 cm wide). Clasts range from non-vesicular to moderately vesicular. The basaltic clasts are abundant in euhedral, vitreous clinopyroxene (phenocrysts 1.5–3 mm; glomerocrysts 2.5–4.5 mm) that comprise 6–20% of the deposit. The ash matrix is typically dark red and rich with clinopyroxene crystals of the same size (1–3 mm) as in the clasts. Andesitic lapilli and blocks with hornblende and abundant plagioclase phenocrysts occur in some lapilli-tuffs near to andesite dykes, but are always less abundant than the basaltic-constituents.

ANDESITIC DYKES OF PIRONGIA SUMMIT (Psa)

At least fourteen bodies of ridge-forming andesite outcrop at high elevations (860–900 m a.s.l.) within the Pirongia Summit area (Fig. 25). The (Psa) unit includes the youngest dated rock of Mount Pirongia (1.60 ± 0.04 Ma; Briggs et al., 1989), an andesite dyke (906 m a.s.l.) that crops out 600 m north of the summit peak. Andesites of the unit occur as dykes (see Fig. 24; E, F) and associated domes, short lava flows and breccias that cross cut and mantle older summit deposits (Psul, Psp and Psb). The easternmost mapped deposits, which crop out at lower elevations (700–760 m a.s.l.), directly cross cut Paewhenua Member lavas (Ppe).

The (Psa) dyke orientations form two distinct groups oriented NW-SE and W-E. Both groups strike perpendicular to their respective ridgelines. The projection of dyke orientations indicates that they converge on an oval-shaped zone within the Summit Basin (Fig. 25). This area is inferred to mark the central vent zone of the late-stage summit cone associated with the dyke swarm.

A summary of the physical dimensions of the dykes is given in Appendix F. The andesites are fine-grained, dark-grey glassy rocks (pale grey in weathered outcrops) with phenocrysts and glomerocrysts of plagioclase, hornblende (1–4 mm) and (±) clinopyroxene in sub-equal amounts. Andesitic breccias (for their distribution, see Fig. 25) range from well-consolidated, lithified breccias with rounded clasts of lapilli to block size, to unsorted debris piles with a clay matrix. The last deposits are associated with collapse of the dykes along their jointed margins, and are commonly mixed with basaltic clasts of the underlying (Psb) unit.

BASALTIC ANDESITE DYKES OF HIHIKIWI PEAK (Php)

Basaltic andesite and andesite dykes outcrop to the south of Pirongia Summit at Hihikiwi Peak (905 m a.s.l.) and its surrounding ridges (refer to Fig. 26; A). The (Php) unit consists of an older, mainly andesitic dyke swarm with NE-SW orientation and a younger basaltic-andesitic group striking NNW-SSE. The dykes cross cut older deposits of the Paewhenua shield (Ppe) and summit group (Psul, Psp, Psb; see Fig. 26; B).

Andesites in the older dyke group range from fine-grained to coarsely porphyritic. Their general assemblage is dominated by greenish-clinopyroxene (glomero-) phenocrysts (1–2 mm; 2% of rock), less abundant vitreous hornblende

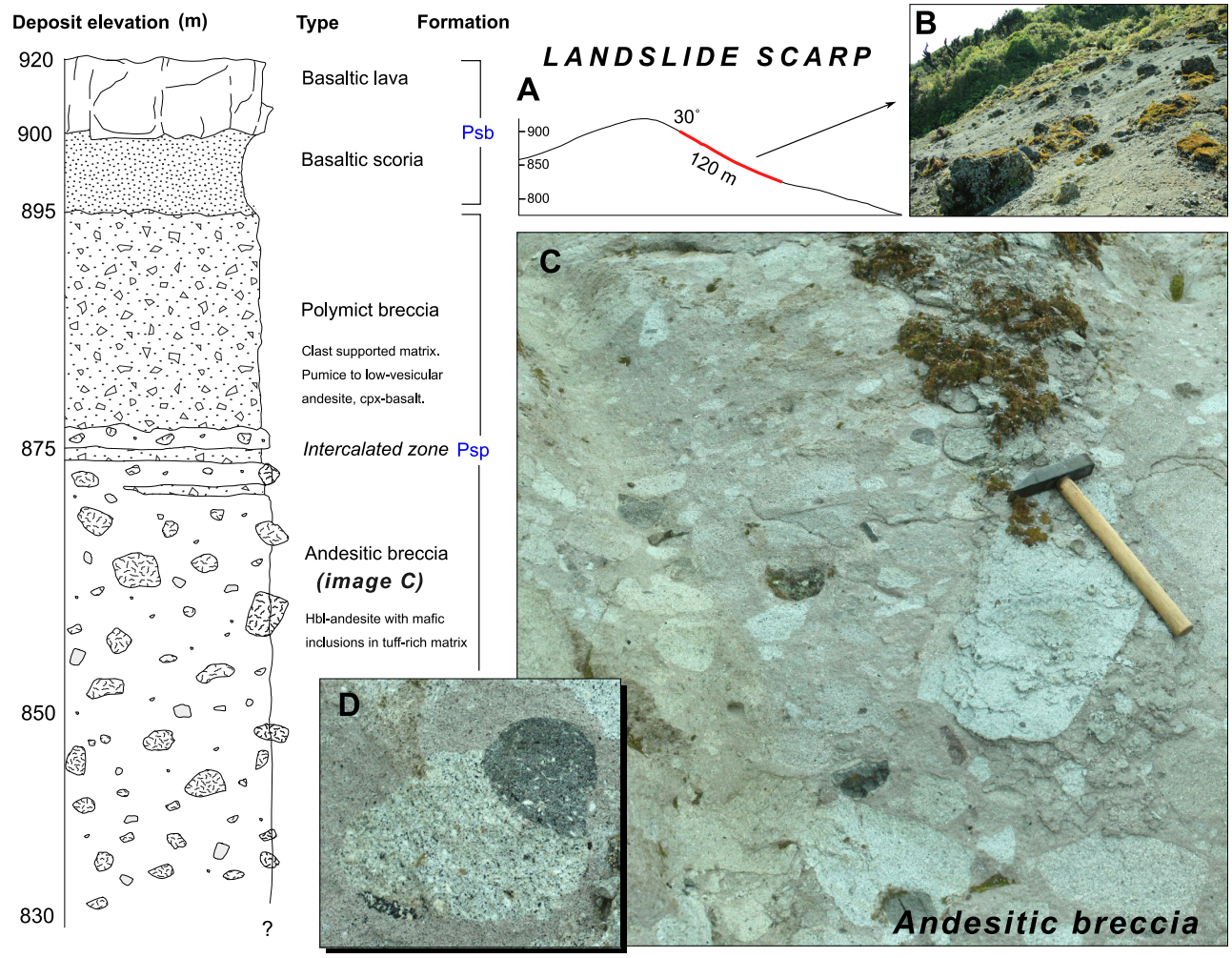
Deposit elevation (m)
Type
Formation
920
900
895
875
850
830
?
Basaltic lava
Basaltic scoria
Psb
Polymict breccia
Clast supported matrix.
Pumice to low-vesicular
andesite, cpx-basalt.
Intercalated zone Psp
Andesitic breccia
(image C)
Hbl-andesite with mafic
inclusions in tuff-rich matrix
LANDSLIDE SCARP
A
30°
120 m
900
850
800
B
C
D
Andesitic breccia


E
dykes
NW
SE
170 m
dome
dyke
dyke
columnar
jointing
Psa
Psa
Psa

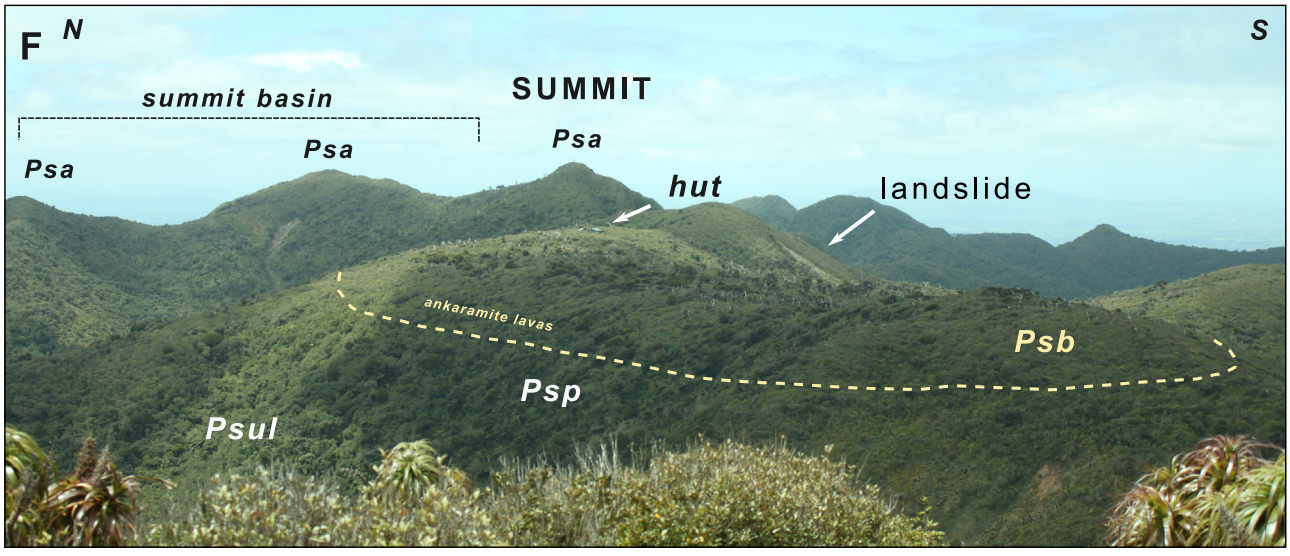
F
N
S
summit basin
SUMMIT
Psa
Psa
Psa
hut
landslide
ankaramite lavas
Psb
Psp
Psul

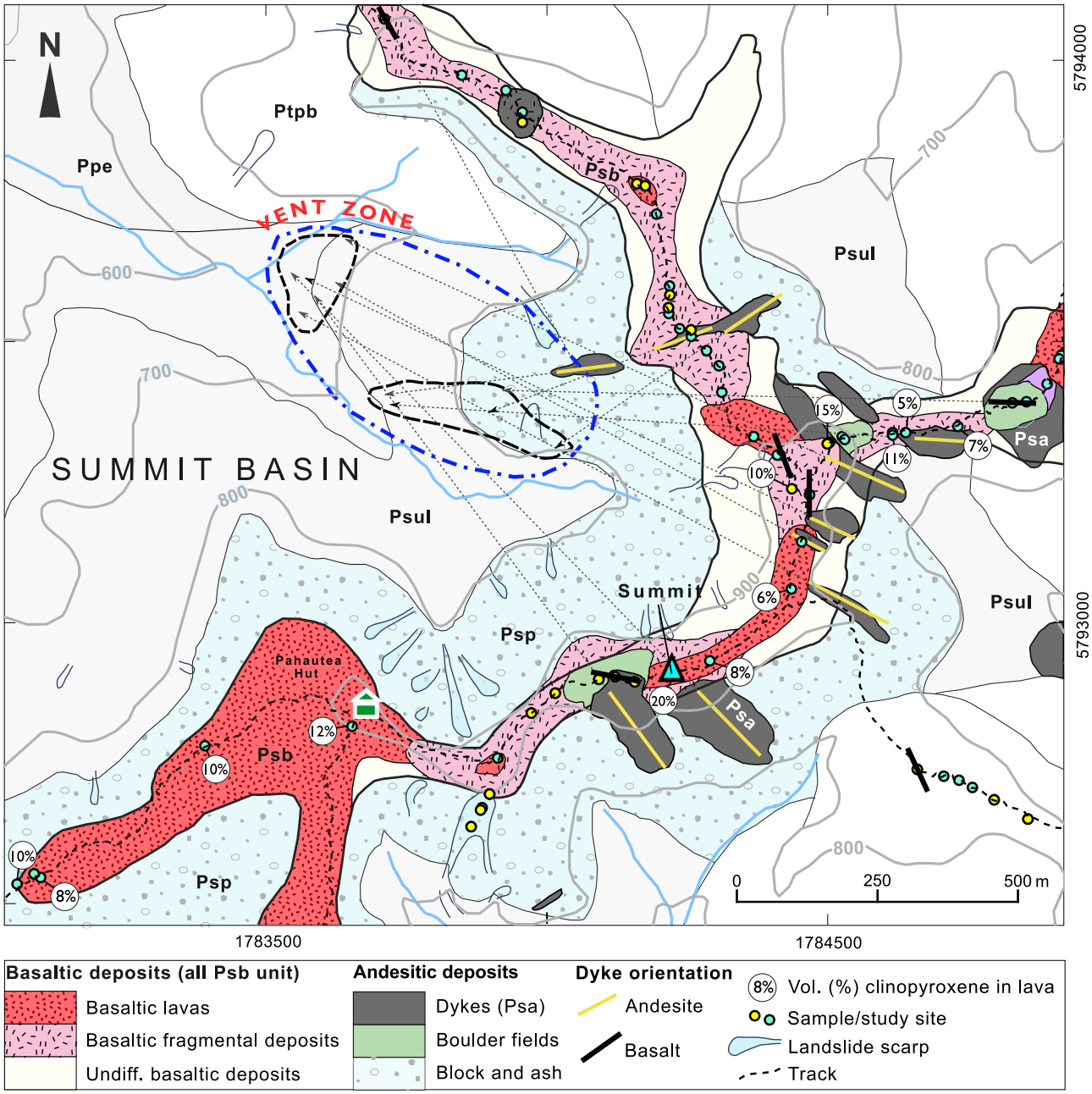

Figure 25. Map showing the stratigraphy of Pirongia Summit. The vent proximal association consists of block-and-ash flows, overlain by basaltic deposits that are cross cut by an andesitic dyke swarm. The andesite dykes are oriented radially and project towards two vent centres (black dashed ovals) within a broader vent zone (blue dashed line), located in the Summit Basin. Basaltic ring dykes (black) occur sparsely on the surrounding ridgelines.

laths (1–2 mm) and plagioclase microphenocrysts (<1 mm) within a devitrified glassy groundmass. In the most porphyritic andesite, very large hornblende (up to 11 mm) and clinopyroxene crystals (5 mm) occur. The lower dyke at Hihikiwi Peak (strike 065º) is a porphyritic basaltic andesite with phenocrysts of hornblende (av. 3–4 mm, max. 7 mm) and clinopyroxene (often 4–5 mm). The dyke feeds a lava flow that underlies most of the peak. Dykes of the younger group outcrop at Hihikiwi Peak and at another smaller peak 500 m to the southeast. The dyke at the peak has a higher ratio of hornblende to clinopyroxene than in the older basaltic andesite it cross cuts.

Figure 24. Volcanic deposits of Pirongia Summit. The upper stratigraphy (see stratigraphic section, left) exposed in a landslide scarp (A-B) consists of andesitic breccias (C; hammer for scale) with occasional mafic inclusions (D). The breccias are intercalated with and overlain by polymict breccias. Basaltic scoria deposits and lavas form the top of the succession. The basalts are intercalated with and cross-cut by andesitic dykes (Psa). Typical dyke outcrops are shown in panoramic view (E-F). In photo (E), the summit andesites form platy spines (dykes), columnar jointed domains, and ridge-top domes. The landscape around Pahautea Hut (F) includes a broad plateau of ankaramite lavas (Psb, yellow dashed line is contact) that overlies other summit group deposits (Psp and Psul). Andesite dykes (Psa) form sharp peaks in the background. The landslide referred to above is also labelled.

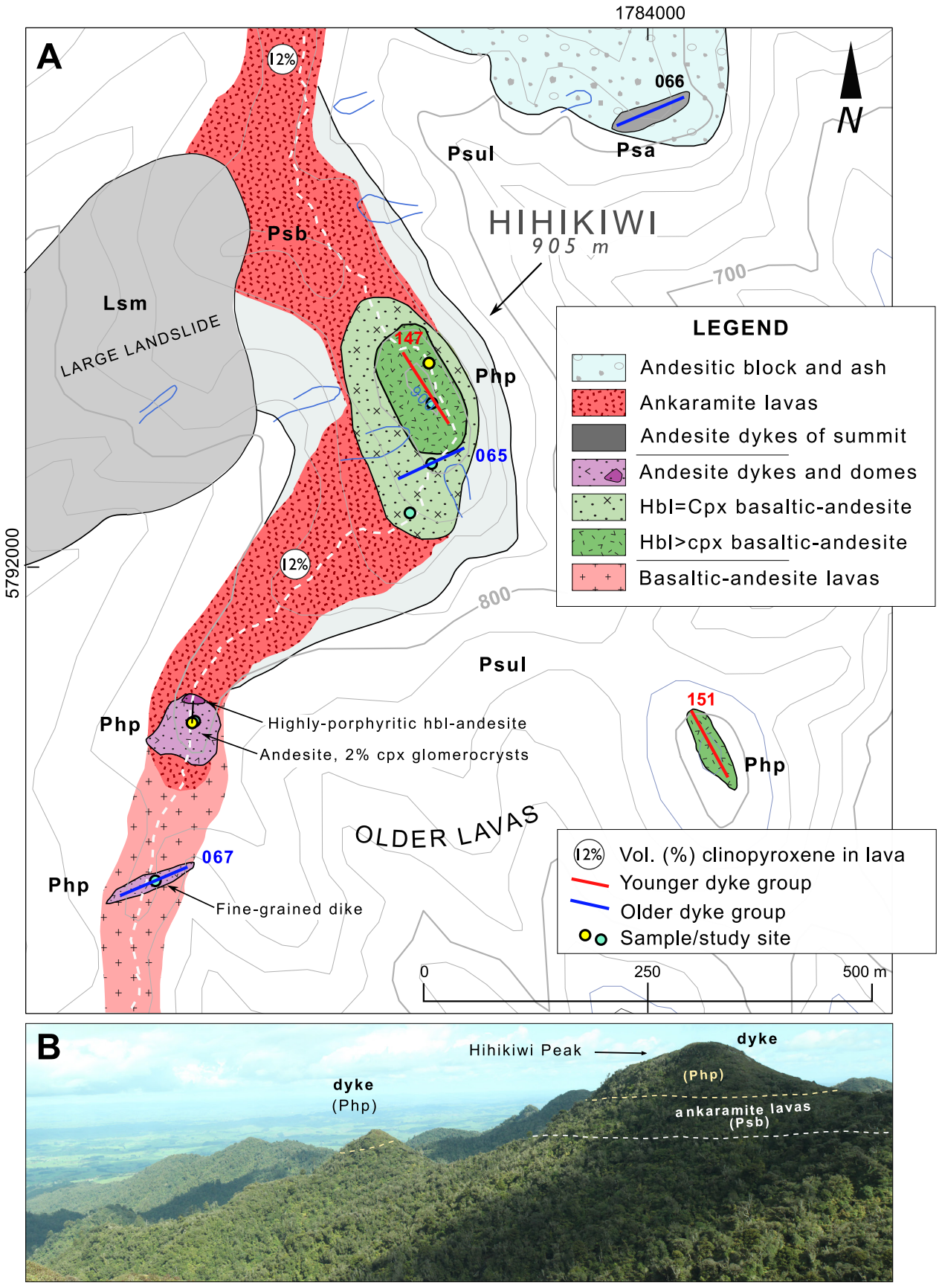

Figure 26. Stratigraphy of Hihikiwi Peak, central Pirongia. A: Detailed map showing lithological variation across the peak and surrounding ridgeline (white dashed line is Hihikiwi Track). Much of the peak is underlain by ankaramite summit lavas (Psb; red stippled – see map Fig. 25 and image panel B) associated with the lava plateau near Pahautea Hut. Dyke formations consist of an older group striking NE-SW and a younger group striking NW-SE. The top of the peak is marked by a (younger group) dyke of basaltic-andesitic composition that is oriented radially to the Pirongia Summit vent (see Fig. 25).

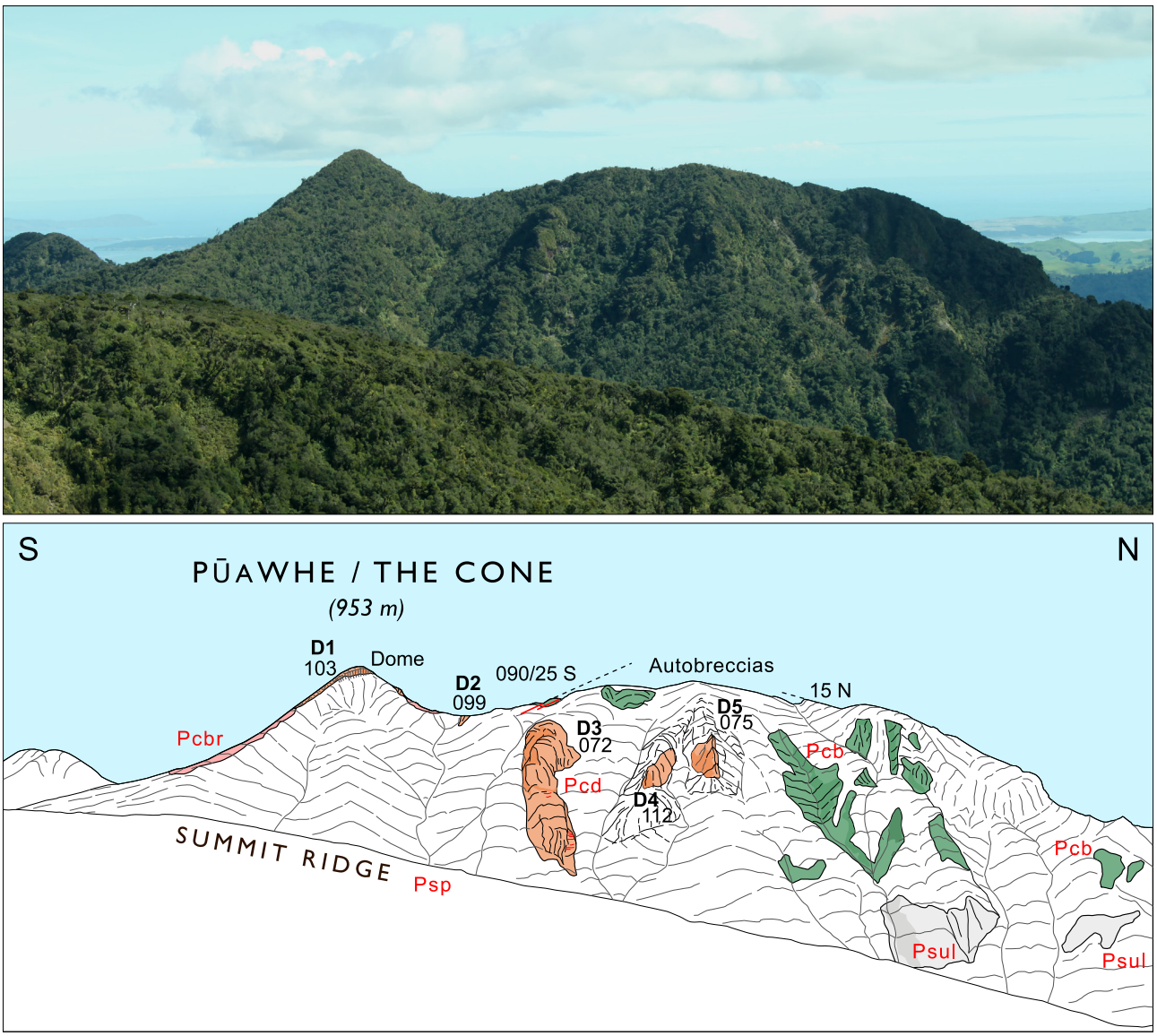

Figure 27. Panoramic view southwest to Pūawhe/The Cone from Pirongia Summit ridge (photo above) and geological interpretation (sketch below). Field of view is 850 m. The main peak is composed of breccia (Pcbr; pale red) intruded by an andesitic dyke (D1; all andesite is orange). The broad ridge to the north is dominated by a thick basaltic lava succession (Pcb; green) cross cut by other andesite dykes of the (Pcd) unit. Dyke labels (D1-D5) relate to their physical dimensions in Appendix G. Basaltic lavas at the ridge top project towards the centre of the ridge, (dashed lines) and indicate that the main vent centre was somewhere in the foreground valley, east of the ridge line. Joint patterns are shown in red (observed) and geomorphic form lines in black.

BASALTIC LAVAS OF PŪAWHE/THE CONE (Pcb)

Late-stage basalts associated with cone-building of the major vent at Pūawhe form an extensive lava field in southwestern Pirongia. The lavas are thick (~120 m) and steeply dipping (~25º) in the proximal zone and flowed westwards (at slope angles 6–8º) over distances of up to 3.5 km into the Oparau Graben. A major unconformity related to sector collapse of the edifice separates (Pcb) lavas from older flank deposits (Ppe) to the north and south of the unit (see Fig. 9, A-inset, and Fig. 10, A). Stratigraphic relationships show that (Pcb) lavas infill an existing scarp in (Ppe) flank lavas. The distal portions of the lava field directly overlie upturned basement rocks and ring plain breccias (Odb) associated with a major debris avalanche. At the bluffs north of Pūawhe (refer to Fig. 27), the (Pcb) lavas mantle slightly older cone-building deposits of the summit area (Psul). The lavas are cross cut by associated vent breccias (Pcbr) and dykes (Pcd).

Basaltic lava crops out at a few locations on the ridge north of Pūawhe. Lavas on the ridge appear to be the top of a thick succession of autobrecciated a'a lava flows (0.7–1 m thick). The flows dip steeply south towards Pūawhe Peak, indicating a source vent to the north or northeast. The lavas are moderately vesicular and porphyritic with phenocrysts of clinopyroxene (1–1.5 mm; 4–5% of rock), abundant plagioclase and minor olivine in a fine-grained groundmass.

FRAGMENTAL DEPOSITS OF PŪAWHE/THE CONE (Pcbr)

Vent associated basaltic breccias intercalated with thin basaltic lava flows and fragmental andesitic deposits crop out at Pūawhe Peak (Fig. 27). The (Pcbr) unit cross cuts and mantles Pūawhe cone-building lavas (Pcb). It is cross cut by andesitic dykes of the peak (Pcd). The breccia consists of scoriaceous to weakly-vesicular basaltic lapilli (10–50 mm) in a deep red-coloured matrix abundant with loose, black clinopyroxene crystals. Clast lithology includes ankaramite (clinopyroxene: euhedral, vitreous, 3–5 mm, 5–8% of rock; sparse olivine: <1 mm; abundant plagioclase: 0.7–2 mm) and finer-grained basalts with clinopyroxene and dark-grey to red groundmass.

ANDESITES OF PŪAWHE/THE CONE (Pcd)

A cluster of andesitic dykes and domes outcrop at the peak and ridgeline surrounding Pūawhe (953 m a.s.l.), the second tallest peak on Pirongia (refer to Fig. 27). The (Pcd) dykes are inferred to be the youngest stratigraphic unit of Pirongia Volcanic Formation, formed during the final stage of eruptions at Pūawhe vent around 1.6 Ma. The dykes show marked west-east orientation and form two subgroups striking WNW-ESE and ENE-WSW (see Appendix G for details). Another isolated dyke situated ~600 m southwest of Pūawhe strikes NE-SW and is oriented radially to the peak. The dykes cross cut volcaniclastic breccias (Pcbr) and lavas (Pcb) associated with Pūawhe volcanics.

Andesite at the top of Pūawhe forms a 30 m thick, massive extrusion of platy-jointed lavas fed by a subvertical dyke. On the ridgeline north of the peak, other (Pcd) dykes cross cut the ridgeline and form platy-jointed spines and bluffs of light-grey coloured, fine-grained holocrystalline andesite equivalent to the peak. The andesites contain sparse phenocrysts of acicular hornblende (1–1.5 mm), clinopyroxene (≤ 2.5 mm), plagioclase and alkali-feldspar (mostly <1 mm, few 1–1.5 mm).

UNDIFFERENTIATED RING PLAIN (Pru)

Undifferentiated deposits of the Pirongia ring plain (Pru) are widespread in the northern and eastern parts of the map area. The constitution and extent of the ring plain deposits are known from sparse roadside outcrops, boulder fields and geomorphological interpretation of slope profiles on the lower flanks (see Fig. 28). Included in this unit are (1) unconsolidated to poorly consolidated polymict (basaltic to andesitic) diamictons, and (2) massive clay beds of weathered, Pirongia volcano-derived tephra (see summary below). Collectively the unit (Pru) represents the accumulation of deposits by lahars, small landslides, tephra fall and river/stream sedimentation. Correlation of outcrops with slope morphology indicates the ring plain is thickest on slopes dipping 5–10º (av. 7.6º), at elevations between 40–60 and 500–650 m (a.s.l.). In some areas the ring plain deposits comprise only a thin veneer mantling distal lava flows (e.g. Mangati Road, 145 m a.s.l., Fig. 28, E). The ring plain underwent deposition continuously during the volcanic and post-volcanic periods. The depositional apron is now deeply incised by fluvial erosion, and several large planezes exist between radial valleys (e.g. below Ruapane Peak).

Ring plain (Pru) deposit types

(1) The ring plain of the northern, eastern and southern sectors of Pirongia is characterised by expansive boulder fields and massive, weathered clay beds that are exposed on the surface of farm paddocks and in road cuttings. The boulder fields are volumetrically the largest component of the ring plain, and their constituents reflect the lithology upslope. The deposits mantle older volcanics and infill paleo valleys. Younger ring plain deposits occur within the actively eroding radial valleys of Pirongia; these massive, unsorted, unconsolidated, polymict boulder deposits consist of rounded cobbles to boulders. Their thicknesses range from metres to tens of metres at lower elevations. The source of the boulders appears to be re-worked talus fans from collapses in the headwaters of the valleys.

(2) Massive, weathered reddish-brown to orange clay beds are ubiquitous in Pirongia road cuttings where they mantle older volcanic deposits (Fig. 28, D). Clayey beds were noted as being possible basaltic ash deposits derived from eruptions of Pirongia Volcano by Kear and Schofield (1978), but Briggs (1983) considered only centimetre-thick tephra layers had originated from Pirongia. The lower clay horizons are intercalated in some areas with unambiguous (Pirongia-derived) red basaltic tuffs and lapilli-tuffs comparable to those observed at higher elevations on the volcano. This stratigraphic relationship suggests that greater thicknesses of Pirongia-derived tephra beds are preserved than previously recognised. Clear identification of Pirongia-derived tephra deposits is complicated by the presence of quartz in most clay horizons (quartz does not occur in any Pirongia lavas). Quartz was also observed in basaltic tephras of the Karioi Volcano, intercalated with basaltic lavas (Goles et al., 1996). The source of the quartz was attributed to eolian sedimentation, possibly windblown from the exposed continental shelf or Australia, such as occurs during glacial periods (e.g. Alloway et al., 1992). At Pirongia, only those deposits with basaltic fragments can be directly correlated to the volcano (Fig. 28, B) but it is likely similar eolian processes have distributed quartz into associated tephra deposits. The overlying clay-rich beds (containing quartz from rhyolitic eruptions), in contrast, represent the thick Kauroa and Hamilton Ash Formations, as described by Ward (1967), Pain (1975), Briggs et al. (1989, 1994a), Horrocks (2000) and Lowe (2019).

A well exposed depositional sequence (Pru) outcrops laterally over 200 m near the base of Te Tahi Road, eastern Pirongia (Fig. 28, C). The sequence includes at least seven highly weathered volcaniclastic breccia layers (each 0.35 m to >1.3 m thick), some of which are separated by thin clay horizons. The breccia layers are clast supported (lapilli to blocks) and appear to be monolithologic. A representative

part of the succession is defined by (from the base upwards): (1) ankaramite dominated breccia with variably weathered clinopyroxene and olivine (both 2–6 mm) and acicular plagioclase (1–1.5 mm) in medium grey groundmass with large spheroidal vesicles (2–7 mm); overlain by a (2) light brown clay layer (20–25 mm) possibly of weathered basaltic tuff; overlain by (3) basaltic breccia with clasts rich in equant plagioclase and clinopyroxene (weathered orange; 3–4 mm) in dark-grey, highly vesicular groundmass. The breccia succession is mantled by massive and banded clays, younger Pirongia laharic debris, and younger tephra deposits of late Quaternary age in which modern soils are formed.

A broad distinction is made between undifferentiated (Pru) ring plain and the consolidated, widespread breccia formations of southern (Pdb, Mdb) and southwestern Pirongia (Odb) of probable debris avalanche origin (which are *sensu stricto* part of the ring plain). The debris avalanche deposits occur as very thick, landscape/bluff forming units with large angular, jigsaw fractured blocks. In numerous road cuttings (e.g. Pirongia West Road and Mangati Road) these breccias are mantled by poorly consolidated diamictons of clay and (sub-)rounded cobbles and boulders of the Pru unit.

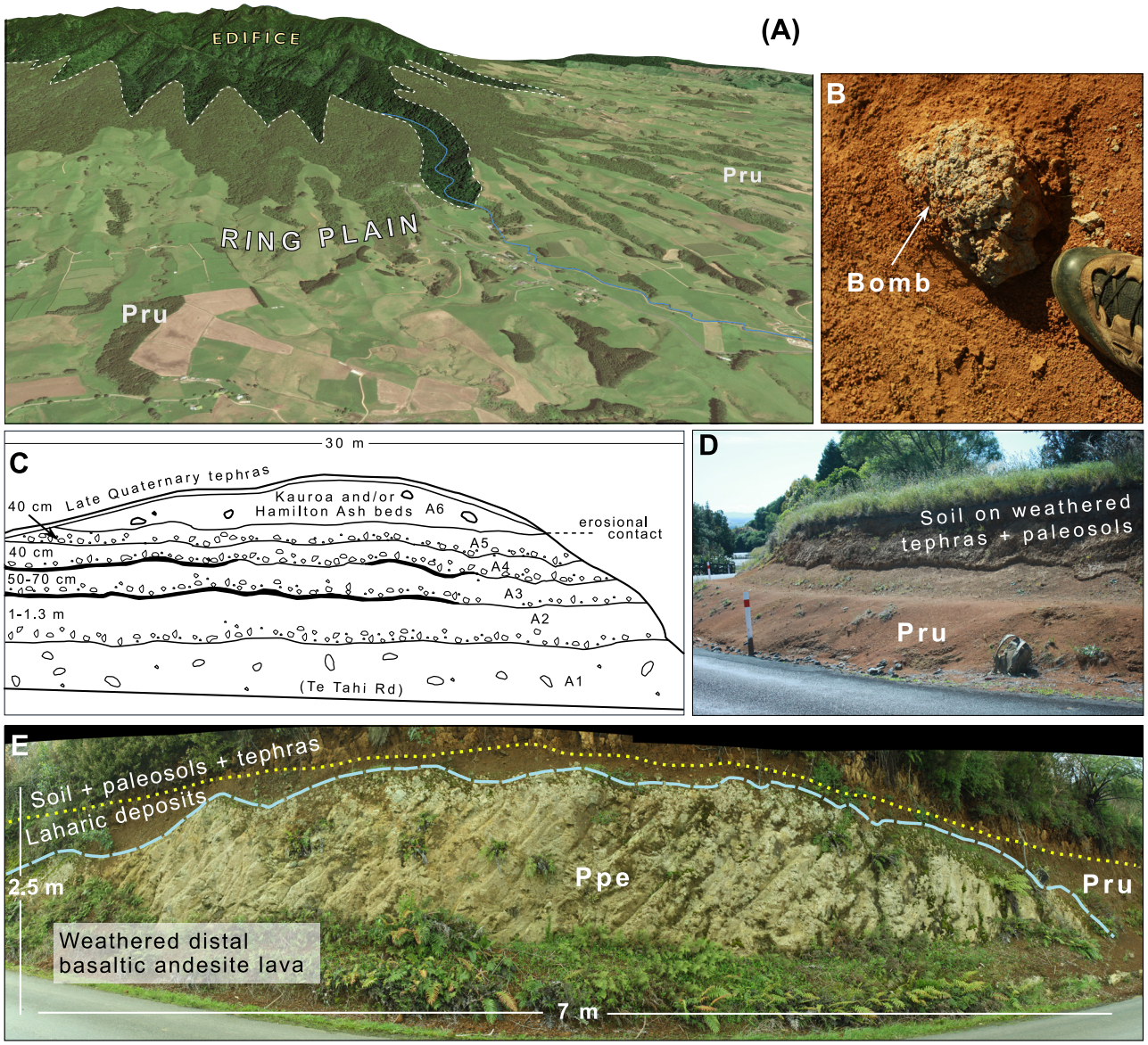

Figure 28. Features of the Pirongia ring plain (Pru). A: Ring plain distribution pattern on the lower northeastern slopes of the volcano. B: Basaltic bomb within red clay matrix of a weathered lapilli-tuff deposit on the lower flanks. C: Succession of ring plain deposits in road cutting on Te Tahi Road. Breccia deposit descriptions (by clast type): A1 - laharic undifferentiated; A2 – vesicular rock, acicular plagioclase, weathered clinopyroxene capped by a clay layer, 2–2.5 cm thick, light brown; A3 – equant plagioclase (25% of rock; av. 3–4 mm) capped by a clay layer, 2 cm thick, brown rind with black interior clay; A4 – similar constituents to A2; A5 – undifferentiated Pirongia-derived deposit; A6 – undifferentiated Kauroa and/or Hamilton Ash deposits, overlain by late Quaternary deposits. D: Reddish clay (weathered basaltic tuff) on Sainsbury Road overlain by weathered Kauroa and Hamilton Ash deposits and paleosols overlain by late Quaternary tephras. E: Highly weathered basaltic andesite lava flow mantled by laharic ring plain deposits on Mangati Road.

OKETE VOLCANIC FORMATION

BASALT OF VANDY ROAD VENT (Ovv)

Eroded basaltic vent of the Okete Volcanic Formation, 13 km NW of Pirongia Summit. The landform consists of a weathered lava field. The lavas are fine-grained basanites with abundant olivine phenocrysts (+ minor clinopyroxene) set within sub-trachytic plagioclase-rich groundmass (Briggs and Goles, 1984).

BASALT OF KOPONUI VENT (Oko)

The Koponui vent (2.23 ± 0.09 Ma; Briggs et al., 1989) produced a plateau (11.7 km^2) of hawaiitic lavas on top of mountainous terrain (Apotu Group; Mag), 10 km northwest of Pirongia Summit. Koponui Peak (554 m a.s.l.) is clearly visible on the Pirongia skyline looking south from Hamilton Basin and the Kapamahunga Range. The unit is densely covered by forest, poorly exposed and largely inaccessible. Limited sampling indicates that its basalts are texturally equivalent to those of Vandy Road, with abundant (altered) olivine set within a fine plagioclase-rich groundmass (Briggs and Goles, 1984). The map unit colour is green in recognition of its temporal association with Hihikiwi Member volcanism.

BASALT OF KARAMU VENT (Okv)

The (Okv) unit forms a highly eroded basaltic hill (188 m a.s.l.) of the Okete Formation (2.03 ± 0.03 Ma; Briggs et al., 1989) in the northern edge of the map area. The Karamu vent is structurally controlled by a N-NE trending fault (Briggs, 1983). Outcrop at Harker's Quarry shows a large mass of columnar jointed basanite interbedded with tuffs (Kear and Schofield, 1978). Rocks are fine-grained and melanocratic with abundant olivine (0.5–1 mm) and subordinate clinopyroxene.

QUATERNARY COVER BEDS

LANDSLIDE MATERIAL OF SUMMIT (Lsm)

Undifferentiated landslide deposit extending 1.1 km southwest from the saddle between Hihikiwi Peak and Pahautea Hut. The pronounced ridge morphology of the unit suggests it is relatively young, perhaps of Holocene age.

OPARAU TEPHRA (Ot)

Pale coloured, sandy rhyolitic tephra. Oparau Tephra is well preserved around the eastern shores of Kawhia Harbour and has its type locality near Oparau settlement, where the unit is a maximum of 3 m thick (Pain, 1975). The unit (Ot) mantles Oparau breccia (Odb). It is a correlative of the Ongatiti Ignimbrites (1.34–1.21 Ma; Briggs et al., 2005) and equivalent to unit K12 of the Kauroa Ash sequence (Horrocks, 2000) (1.28 ± 0.11 Ma; Lowe et al., 2001).

IGNIMBRITE, ALLUVIUM AND TEPHRA-FALL DEPOSITS (Qa)

Undifferentiated ignimbrites, alluvium and tephra-fall deposits of Quaternary age occupy lowland areas (Hamilton Basin) to the north and east of Mount Pirongia. The Hamilton Basin consists of the following. (1) An older landscape of low rolling hills (Walton Subgroup; Pleistocene; e.g. Kear and Schofield, 1978) mantled by Hamilton Ash (0.34 Ma to >50 ka; Lowe et al., 2001), overlain by late Quaternary tephras (<50 ka; Lowe, 1988, 2019) and infilled by (2) large volumes of volcanogenic alluvium (Hinuera Fm; ~22 to 17.5 ka) and younger deposits (e.g. McCraw, 2011; Lowe, 2020). The Pirongia ring plain (Pru) is deeply buried by these deposits (Qa), probably to depths of >100 m north of the mountain. Kauroa and Hamilton Ash formations (≤3 m thick) crop out in road cuttings up to at least 200 m a.s.l. on the northern and eastern flanks but are too thin to map as Qa. Alluvium deposited contemporaneously with Pirongia Formation is evident on Sainsbury Road (west of Pirongia township), where Walton Subgroup (Qa) is overlain by Pukehoua vent deposits (Poa; volcaniclastic breccia; 1.64 ± 0.13 Ma). The Walton Subgroup deposits consist of (1) a lower unit (42 m a.s.l.) of finely laminated, sandy, light cream and orange layers of lithics and pumice, overlain along an erosional contact by (2) orange coloured conglomerate (50 m a.s.l.) with abundant clasts of argillite and subordinate pumice. Walton Subgroup is overlain at lower elevations by flood plain terrace deposits of the Waipa River.

The Kauroa and Hamilton Ash formations (too thin to map) mantle Oparau breccia (Odb) southwest of Pirongia. These deposits thicken toward the eastern shore of the harbour and weather to distinct red and pink clays. Thick (>8 m) deposits of the Oparau Tephra (Ot; Pain, 1975) around Kawhia Harbour are the correlative of Kauroa Tephra bed K12, in turn correlated with Ongatiti Ignimbrite aged 1.28 Ma (Horrocks, 2000; Lowe et al., 2001).

Among the youngest Qa deposits are river and stream sediments, including the Waipa River floodplain and gravel fans from the radial valleys of Pirongia (e.g. Mangakara and Kaniwhaniwha streams). The most extensive Pirongia-related gravel deposits are those of the Oparau River floodplain (southwestern Pirongia), which form terraces of progressively younger age towards Kawhia Harbour (Kear and Schofield, 1978). The terraces and present river gravels are predominantly volcanogenic in lithology (Pirongia Formation) with subordinate greywacke and Te Kuiti Group sediment from the surrounding hills. Blocks of volcaniclastic breccia and lava (1–4 m wide) eroded from the Oparau breccia (Odb) are embedded sparsely within the riverbed.

ACKNOWLEDGMENTS

The author Oliver McLeod thanks his wife Julieta and his parents who supported publication of this work. This research is dedicated to his late grandmother Lorna McLeod who introduced him to the Waikato volcanoes. Representatives of Tainui are thanked for allowing scientific access to the sacred peaks of Pirongia, Karioi and Kakepuku. Landowners of the Pirongia and Oparau areas kindly provided access to field sites. Selwyn and Dianne June, Tom Davies, Steve McClunie, Clare St Pierre and other members of the Pirongia Restoration Society are acknowledged for their support, as is Nardene Berry (NZ Landcare Trust) for connection to landowners. Fieldwork assistance: C. Morcom, M. House, R. Wenzlick, S. Kosik, G. McQuillan, R. Hughes, A. Harpur. Technical assistance: R. Radosinsky, A. Rodgers, K. Vincent. Alan Hall at Pirongia Heritage and Information Centre is especially thanked for his help and addition of the Foreword to this text. Tom Roa of Maori and Indigeneous studies (University of Waikato) is thanked for providing a valuable cultural framework to the study. Scientific discussions were held with D. J. Lowe, PJ.J. Kamp, S. Cronin, I.E.M. Smith, C.J.N. Wilson, M. Garcia, D. Karatson, M. Baulks, N. Mortimer, H. Campbell, B. Hayward, L. Pure, C. Rees, F. Spinardi, M. Prentice, J. Mering and B. Andrews. Drone photography was facilitated by D. Schmale at the property of J. Fulton. We also thank Jo Horrocks for allowing us to cite data from her thesis. Credits for aerial photos used in figures or morphological work: S. Frimmel, M. Baptist, S. June, D.J. Lowe and J. Greenwood. We especially acknowledge Phil Moore and Gianluca Groppelli for their detailed reviews of the manuscript and geological map, which enabled us to improve them substantially. This research was funded by a University of Waikato Doctoral Scholarship. Additional publication costs were sponsored by the Waipa District Council Pirongia and Te Awamutu ward committees. Finally, we thank the Geoscience Society of New Zealand for enabling this bulletin and map to be published.

REFERENCES

Anderson G 2001. The merchant of the Zeehaen: Isaac Gilsemans and the voyages of Abel Tasman. Te Papa Press, Wellington. 162 p.

Adams CJ, Graham IJ, Seward D, Skinner DNB 1994. Geochronological and geochemical evolution of late Cenozoic volcanism in the Coromandel Peninsula, New Zealand. New Zealand Journal of Geology and Geophysics 37, 359-379.

Alloway BV, Stewart RB, Neall VE, Vucetich CG 1992. Climate of the last glaciation in New Zealand, based on aerosolic quartz influx in an andesitic terrain. Quaternary Research 38, 170-179.

Briggs RM 1983. Distribution, form and structural control of the Alexandra Volcanic Group, North Island, New Zealand. New Zealand Journal of Geology and Geophysics 26, 47-55.

Briggs RM 1986. Volcanic rocks of the Waikato Region, western North Island, and some possible petrologic and tectonic constraints on their origin. Royal Society of New Zealand Bulletin 23, 76-91.

Briggs RM and McDonough WF 1990. Contemporaneous convergent margin and intraplate magmatism, North Island, New Zealand. Journal of Petrology 31, 813-851.

Briggs RM, Goles GG 1984. Petrological and trace element geochemical features of the Okete Volcanics, western North Island, New Zealand. Contributions to Mineralogy and Petrology 86, 77-88.

Briggs RM, Houghton BF, McWilliams M, Wilson CJN 2005. $^{40}Ar/^{39}Ar$ ages of silicic volcanic rocks in the Tauranga-Kaimai area, New Zealand: dating the transition between volcanism in the Coromandel Arc and the Taupo Volcanic Zone. New Zealand Journal of Geology and Geophysics 48, 459-469.

Briggs RM, Itaya T, Lowe DJ, Keane AJ 1989. Ages of the Pliocene-Pleistocene Alexandra and Ngatutura Volcanics, western North Island, New Zealand, and some geological implications. New Zealand Journal of Geology and Geophysics 32, 417-427.

Briggs RM, Lowe DJ, Goles GG, Shepherd TG 1994a. Intra-conference tour day 1: Hamilton-Raglan-Hamilton. In: Lowe DJ (ed) Conference Tour Guides. Proceedings Inter-INQUA Field Conference on Tephrochronology, Loess and Paleopedology. University of Waikato, Hamilton, 24-44.

Briggs RM, Okada T, Itaya T, Shibuya H, Smith IEM 1994b. K-Ar ages, paleomagnetism, and geochemistry of the South Auckland Volcanic Field, North Island, New Zealand. New Zealand Journal of Geology and Geophysics 37,143-153.

Briggs RM, Rosenberg MD, de Lange PJ, Itaya PR, King PR, Price RC 1997. Geology and geochemistry of Gannet (Karewa) Island, Tasman Sea: a rift-related nephelinitic tuff ring. New Zealand Journal of Geology and Geophysics 40, 263-273.

Brown SJA, Smith RT, Cole JW, Houghton BF 1994. Compositional and textural characteristics of the strombolian and surtseyan K-Trig basalts, Taupo Volcanic Centre, New Zealand: implications for eruption dynamics. New Zealand Journal of Geology and Geophysics 37, 113-126.

Clarkson B, Merrett M, Downs T 2002. Botany of the Waikato. Waikato Botanical Society, Hamilton. 136 p.

Coombs DS, Landis CA, Norris RJ, Sinton JM, Borns DJ, Craw D 1976. The Dun Mountain Ophiolite Belt, New Zealand; its tectonic setting, constitution and origin, with special reference to the southern portion. American Journal of Science 276, 561-603.

Cox SH 1877. Report on Waikato District. New Zealand Geological Survey Report, Geological Exploration 10, 11-26.

Davidson J and de Silva S 2000. Composite volcanoes. In Sigurdsson H (ed), Encyclopedia of volcanoes, first edition. Academic Press, San Diego, pp, 663-681.

Eaves SR, Mackintosh AN, Winckler G, Schaefer JM, Alloway BV, Townsend DB 2016. A cosmogenic ^{3}He chronology of late Quaternary glacier fluctuations in North Island, New Zealand (39° S). Quaternary Science Reviews 132, 40-56.

Eccles JD, Cassidy J, Locke CA, Spörli KB 2005. Aeromagnetic imaging of the Dun Mountain Ōphiolite Belt in northern New Zealand: insight into the fine structure of a major SW Pacific terrane suture. Journal of the Geological Society, London 162, 723-735.

Edbrook SW 2001. Geology of the Auckland area: scale 1:250000. Lower Hutt: Institute of Geological and Nuclear Sciences. Geological map 3, 74 p. + 1 folded map.

Edbrooke SW 2005. Geology of the Waikato area: scale 1:250000. Lower Hutt: Institute of Geological and Nuclear Sciences. Geological map 4, 68 p. + 1 folded map.

Edbrooke SW, Sykes R, Pocknall DT 1994. Geology of the Waikato Coal Measures, Waikato Coal Region, New Zealand. Institute of Geological and Nuclear Sciences Monograph 6. Institute of Geological and Nuclear Sciences, Lower Hutt, New Zealand: 236 p.

Edbrooke SW 2017. The geological map of New Zealand. Lower Hutt: Institute of Geological and Nuclear Sciences. Geological map 2, 183 p. + 2 maps.

Fergusson DA 1986. Geology of inland Kawhia: emphasis on Te Kuiti Group stratigraphy and sedimentation. Unpublished M.Sc. thesis lodged in the Library, University of Waikato, Hamilton.

Fisher M 2014. The environmental management of Pirongia Forest Park with a focus on the period since 1970. A report commissioned by the Waitangi Tribunal for the Te Rohe Pōtae Inquiry District.

Gamble JA, Smith IEM, Graham IJ, Kokelaar BP, Cole JW, Houghton BF, Wilson CJN 1990. The petrology, phase relations and tectonic setting of basalts from the Taupo Volcanic Zone, New Zealand and the Kermadec Island Arc – Havre Trough, SW Pacific. Journal of Volcanology and Geothermal Research 43, 235-270,

Gamble JA, Smith IEM, McCulloch MT, Graham IJ and Kokelaar BP 1993. The geochemistry and petrogenesis of basalts from the Taupo Volcanic Zone and Kermadec Island Arc, SW Pacific. Journal of Volcanology and Geothermal Research 54, 265-290.

Gamble JA, Wright IC, Woodhead JD, McCulloch MT 1995. Arc and back-arc geochemistry in the southern Kermadec arc-Ngatoro Basin offshore Taupo Volcanic Zone, SW Pacific. In: Smellie JL (Ed), Volcanism Associated with Extension at Consuming Plate Margins. Geological Society Special Publication No. 81, 193-212.

Goles GG, Briggs RM, Rosenberg MD 1996. Late Pliocene stratigraphic succession and volcanic evolution of Karioi volcano, western North Island, New Zealand. New Zealand Journal of Geology and Geophysics 39, 283-294.

Gómez-Vasconcelos MG, Villamor P, Cronin S, Procter J, Palmer A, Townsend D, Leonard G 2017. Crustal extension in the Tongariro graben, New Zealand: Insights into volcano-tectonic interactions and active deformation in a young continental rift. Geological Society of America Bulletin 129, 1085-1099.

Hayward BW 1975. Lower Miocene geology of the Waitakere hills, west Auckland, with emphasis on the paleontology. Unpublished PhD thesis, lodged in the Library, University of Auckland, Auckland.

Hayward BW, Black PM, Smith IEM, Balance PF, Itaya T, Doi M, Takagi M, Bergman S, Adams CJ, Herzer RH, Robertson DJ 2001. K-Ar ages of early Miocene arc-type volcanoes in northern New Zealand. New Zealand Journal of Geology and Geophysics 44, 285-311.

Henderson J and Grange LI 1926. The geology of the Huntly-Kawhia Subdivision. New Zealand Geological Survey bulletin 28, 112 p.

Horrocks JL 2000. Stratigraphy, chronology and correlation of the Plio-Pleistocene (c. 2.2–0.8 Ma) Kauroa Ash sequence, western North Island, New Zealand. Unpublished Ph.D. thesis lodged in the Library, University of Waikato, Hamilton,

Houghton BF, Wilson CJN, McWilliams MO, Lanphere MA, Weaver SD, Briggs RM, Pringle MS 1995. Chronology and dynamics of a large silicic magmatic system: central Taupo Volcanic Zone, New Zealand. Geology 23, 13-16.

Hume TM, Sherwood AM, Nelson CS 1975. Alluvial sedimentology of the Upper Pleistocene Hinuera Formation, Hamilton Basin, New Zealand. Journal of the Royal Society of New Zealand 5, 421-462.

Hunt TM 1978. Stokes Magnetic Anomaly System. New Zealand Journal of Geology and Geophysics 21, 595-606.

Hutton FW 1867. Geological report on the lower Waikato district (with maps and sections). New Zealand Geological Survey Report, Geological Exploration 2, 8 p.

Johnston M and Nolden S 2011. Travels of Hochstetter and Haast in New Zealand 1858-186. Nikau Press, Nelson. 336 p.

Kear D 1960. Sheet 4 Hamilton. Geological Map of New Zealand 1:250 000. N.Z. Department of Scientific and Industrial Research, Wellington.

Kear D 1964. Volcanic alignments north and west of New Zealand's Central Volcanic Region. New Zealand Journal of Geology and Geophysics 7, 24-44.

Kear D 1966. Geological map of New Zealand, 1:63,360 Sheet N55 Te Akau. Department of Scientific and Industrial Research, Wellington.

Kear D and Schofield JC 1959. Te Kuiti Group. New Zealand Journal of Geology and Geophysics 4, 685-717.

Kear D and Schofield JC 1978. Geology of the Ngaruawahia Subdivision. New Zealand Geological Survey Bulletin 88, 167 p.

La Croix A 1916. Sur quelques roches volcaniques melanocrates des possessions Francaises de l'ocean Indien et du Pacifique. Comptes redus de L'Academie des Sciences 158, 177-183.

Leonard GS, Calvert AT, Hopkins JL, Wilson CJ, Smid ER, Lindsay JM and Champion DE 2017. High-precision $^{40}Ar/^{39}Ar$ dating of Quaternary basalts from Auckland Volcanic Field, New Zealand, with implications for eruption rates and paleomagnetic correlations. Journal of Volcanology and Geothermal Research 343, 60-74.

Lowe DJ, Tippett JM, Kamp PJJ, Liddell IJ, Briggs RM, Horrocks JL 2001. Ages on weathered Plio-Pleistocene tephra sequences, western North Island, New Zealand. Les Dossiers de l'Archeo-Logis 1, 45-60.

Lowe DJ 1988. Stratigraphy, age, composition, and correlation of Late Quaternary tephras interbedded with organic sediments in Waikato lakes, North Island, New Zealand. New Zealand Journal of Geology and Geophysics 31, 125-165.

Lowe DJ 2019. Using soil stratigraphy and tephrochronology to understand the origin, age, and classification of a unique Late Quaternary tephra-derived Ultisol in Aotearoa New Zealand. Quaternary 2, 1-34.

Lowe DJ 2020. Introduction to the landscapes and soils of the Hamilton Basin and South Waikato. Field notes, School of Science, University of Waikato, Hamilton. 36 p.

Marshall P 1907. Geology of centre and north of North Island. Read before the Otago Institute, 10th September, 1907.

Matheson SG 1981. The volcanic geology of the Mt Karioi region. Unpublished M.Sc. thesis. Lodged in the Library, University of Waikato, Hamilton.

McCraw J 2011. The wandering river: landforms and geological history of the Hamilton Basin. Guidebook 15. Lower Hutt, NZ: Geoscience Society of New Zealand.

Mortimer N and Scott JM 2020. Volcanoes of Zealandia and the Southwest Pacific. New Zealand Journal of Geology and Geophysics 63, 371-377.

Mortimer N, Smith Lyttle B, Black J 2020. Tectonic map of Te Riu-a-Māui / Zealandia. Lower Hutt (NZ): GNS Science. 1 poster, scale 1:8,500,000. GNS Science poster 8.

Nelson CS 1978. Stratigraphy and paleontology of the Oligocene Te Kuiti Group, Waitomo County, South Auckland, New Zealand. New Zealand Journal of Geology and Geophysics 21, 553-594.

O'Brien JP and Rodgers KA 1973. Alpine-type Serpentinites from Auckland province – the Wairere Serpentinite. Journal of the Royal Society of New Zealand 2, 169-190.

Pain CF 1975. Some tephra deposits in the south-west Waikato area, North Island, New Zealand. New Zealand Journal of Geology and Geophysics 18, 541-550.

Park J 1882. On the occurrence of granite and gneissic rocks in the King-Country. Transactions and Proceedings of the Royal Society of New Zealand 25, 353-362.

Park J 1885. On the Geology of the Auckland provincial district. Reports New Zealand Geological Survey 136.

Pittari A, Danišík M, Vincent KA 2016. New (U-Th)/He and U-Pb zircon ages across the Tauranga and Kaimai Volcanic Centres: strengthening the age framework of the Coromandel–Taupo transition. In: Riesselman C and Roben A (eds). Abstracts, Geosciences 2016, Wanaka, Geoscience Society of New Zealand Miscellaneous Publication 145A, p65.

Pilaar WFH and Wakefield LL 1978. Structural and stratigraphic evolution of the Taranaki basin, offshore North Island, New Zealand. The APPEA Journal 18, 93-101.

Player RA 1958. The Geology of North Kawhia. Unpublished M.Sc. thesis lodged in the Library, University of Auckland, Auckland.

Robertson DJ 1976. A paleomagnetic study of volcanic rocks in the South Auckland area. Unpublished M.Sc. thesis, lodged in the Library, University of Auckland, Auckland.

Robertson DJ 1983. Paleomagnetism and geochronology of volcanics in the northern North Island. Unpublished PhD thesis, lodged in the Library, University of Auckland, Auckland.

Selby MJ and Lowe DJ 1992. The middle Waikato Basin and hills. In Soons JM and Selby MJ (eds). Landforms of New Zealand second edition, Longman Paul, Auckland 233-255.

Sharp A 1968. The voyages of Abel Janszoon Tasman. University of Michigan: Clarendon Press. 375 p.

Smith IEM, Okada T, Itaya T, Black, PM 1993. Age relationships and tectonic implications of late Cenozoic basaltic volcanism in Northland, New Zealand. New Zealand Journal of Geology and Geophysics 36, 385-393.

Spörli KB 1989. Tectonic framework of Northland, New Zealand. Royal Society of New Zealand Bulletin 26, 3-14.

Stern TA 1985. A back-arc formed within continental lithosphere: the Central Volcanic Region of New Zealand. Tectonophysics 112, 385-409.

Stipp JJ 1968. The geochronology and petrogenesis of the Cenozoic volcanics of the North Island, New Zealand. Unpublished PhD thesis, lodged in the Library, Australian National University, Canberra.

Timm C, de Ronde CEJ, Hoernle K, Cousens B, Wartho JA, Caratori Tontini F, Wysoczanski R, Hauff F, Handler M 2019. New age and geochemical data from the Southern Colville and Kermadec Ridges, SW Pacific: insights into the recent geological history and petrogenesis of the Proto-Kermadec (Vitiaz) Arc. Gondwana Research 71, 169-193.

Trewick SA and Bland KJ 2012. Fire and slice: paleogeography for biogeography at New Zealand's North Island/South Island juncture. Journal of the Royal Society of New Zealand 42, 153-183.

Tripathi ARP, Kamp PJJ, Nelson CS 2008. Te Kuiti Group (Late Eocene-Oligocene) lithostratigraphy east of Taranaki Basin in central-western North Island, New Zealand. Ministry of Economic Development, New Zealand, unpublished Petroleum Report PR3900, 70 p.

Utting AJ 1986. The petrology and geochemistry of the Ngatutura Basalts. Unpublished M.Sc. thesis, lodged in the Library, University of Waikato, Hamilton.

von Hochstetter F and Petermann A 1864. Geological and topographical atlas of New Zealand: six maps of the provinces of Auckland and Nelson. Auckland: T. Delattre.

von Hochstetter F and Sauter E 1867. New Zealand, its physical geography, geology and natural history: with special reference to the results of government expeditions in the provinces of Auckland and Nelson.

Ward WT 1967. Volcanic ash beds of the lower Waikato Basin, North Island, New Zealand. New Zealand Journal of Geology and Geophysics 10, 1109-1135.

Waterhouse BC and White PJ 1994. Geology of the Raglan-Kawhia area. Lower Hutt: Institute of Geological and Nuclear Sciences. Institute of Geological and Nuclear Sciences geological map 13, 48 p.

Wilmshurst JM, Anderson AJ, Higham TFG, Worthy TH 2008. Dating the late prehistoric dispersal of Polynesians to New Zealand using the commensal Pacific rat. Proceedings of the National Academy of Sciences 105, 7676-7680.

Wilson CJN, Houghton BF, McWilliams MO, Lanphere MA, Weaver SD, Briggs RM 1995. Volcanic and structural evolution of Taupo Volcanic Zone, New Zealand: a review. Journal of Volcanology and Geothermal Research 68, 1-28.

Wilson CJN, Gravley DM, Leonard GS and Rowland JV 2009. Volcanism in the central Taupo Volcanic Zone, New Zealand: tempo, styles and controls. Studies in volcanology: the legacy of George Walker. Special Publications of IAVCEI 2, 225-247.

Wilson CJN, Blake S, Charlier BLA, Sutton AN 2006. The 26.5 ka Oruanui Eruption, Taupo Volcano, New Zealand: development, characteristics and evacuation of a large rhyolitic magma body. Journal of Petrology 47, 35–69.

APPENDICES

APPENDIX A

Volcanic facies	Mapping criteria
Intrusive bodies	Dykes and other intrusive bodies were mapped according to their distinctive morphological characteristics, namely the tendency to outcrop as clusters of erosion resistant peaks and platy-jointed ridge structures. In most cases, the intrusive bodies with pronounced topography are of andesitic composition. Lithostratigraphic dyke groups were defined according to their spatial distribution, stratigraphic height, altitude, orientation, lithology (texture, mineralogy and presence of inclusions).
Edifice forming succession	The major landscape-forming unit of the mountain is a thick succession of basaltic lavas and interlayered breccias, sourced from numerous vent sites. Lithostratigraphic correlation of the succession is generally difficult because of the lack of outcrop at lower levels on the volcano. Flank-building lava packages were defined as broad, lithostratigraphic units within lithosomes where there was compelling geomorphological evidence linking flank and vent facies (e.g. flanks radiating from a central vent facies zone). Further refinement of the flank stratigraphy was possible where outcrops allowed correlation based on lithology (rock composition or mineralogy) or major unconformities were mapped (providing constraints on the distribution of flank lavas). Petrographic correlation of lava units was possible over distances of several kilometres where a distinctive tracer mineral was present (e.g. phlogopite flakes within resorbed hornblende).
Flank vents	Lava flows/fields associated with flank vents were identified on the grounds of morphology, facies and lithology. Flank vents typically form isolated peaks at mid to upper levels on the edifice associated with vent facies deposits (dykes and pyroclastic material). In most cases, flank vent deposits are basaltic in composition and show a narrow range in texture and mineralogy. They are therefore mapped as a single lithostratigraphic unit based on the following criteria: (1) field evidence of localised vent facies (e.g. pyroclastic deposits, dykes) within the mid to lower flank zones; (2) evidence of lateral extent of lavas – both from direct field evidence and continuous ridge geomorphology associated with (topographically inversed) lava flows and (3) mafic composition, preferably with a distinctive texture (e.g. extremely porphyritic) or lithology (olivine-phyric basalt) that is traceable over the deposit.
Distal vents	Volcanic vents situated in the peripheral zone of the volcano (6–7 km from the summit) were mapped as separate lithostratigraphic units. The vents are topographically pronounced (i.e. hill forming) in comparison to the subdued ring plain that surrounds them. They have field characteristics similar to flank vents (see above). The extent of peripheral vent units was interpreted from their geomorphology and facies (generally lava dominated) that distinguish them from older and younger deposits of the ring plain.
Ring plain	Deposits of the ring plain facies were subdivided into lithostratigraphic units on the basis of deposit type (sector collapse breccias or undifferentiated laharic debris, tephras and stream sediments). Sector collapse breccias were mapped as separate units where there was clear topographic control on their distribution (i.e. infilling a graben) or geomorphological evidence of their extent (plateau forming, high elevation relative to other breccias, intensely eroded) with respect to their probable source areas (upslope on the edifice). Ring plain deposits other than the breccias were grouped together as a single lithostratigraphic unit. The extent of the undifferentiated breccia unit is based on geomorphological criteria (low elevation slope breaks on gently dipping flanks) supported by field observations (outcrops in road cuttings, stream sections and boulder fields).

FACIES MODEL

The complex array of volcanic units presented in the Pirongia map can be synthesised into a simple volcanic facies model, following Davidson and de Silva (2000). The facies are: (1) central vent facies; (2) flank facies; and (3) ring plain facies.

Central vent facies encompasses vent-proximal deposits including breccias, lavas, dykes and domes that occur near to interpreted vent sites. These sites typically occur on ridges at the upper elevations of Pirongia.

Flank facies consist of thick successions of generally autobrecciated basaltic to basaltic-andesitic lava flows (1–2 m thick) and interlayered volcaniclastic breccias. Typical flank lavas dip 15–20° and steepen to 25–28° near well-preserved ridges. Also included in the flank facies are numerous flank vents. Flank vents are defined as topographically prominent peaks with vent proximal deposits located relatively far from the summit zone of Pirongia. On Pirongia, the flank vents occur within two zones situated 2.4 km and 6–7 km from Pirongia Summit. Erupted compositions are primarily basaltic with textures ranging from fine-grained to coarsely porphyritic, and are typically abundant in augite and olivine phenocrysts. Their vent proximal deposits are scoriaceous and form eroded mounds cross cut by dykes or doleritic plugs of similar composition. Associated lava flow fields are typically expansive and reach 3–4 km in length.

Ring plain facies encompass all fragmental material (volcaniclastic breccias, diamictons, tuff) present on the gentle lower flanks of Pirongia (with slopes of 5–10°). Deposits include diamictons associated with large volume debris avalanches (length >12 km), as well as basaltic block-and-ash flow deposits, andesitic ignimbrites, bouldery laharic material and alluvial gravels.

APPENDIX B

Summary of previous geological mapping work in the Pirongia area.

Author	Map area	Map scale
von Hochstetter and Petermann (1864)	First geological map of North Island, showing Pirongia as a volcano. Detailed map of Kawhia and Aotea Harbour, showing Pirongia ring plain.	1:700,000 1:120,000
Hutton (1867)	Raglan area stratigraphy	1:126,720*
Cox (1875–1877)	Kawhia district	?
McKay (1884)	Kawhia district	?
Park (1885)	Kawhia Harbour to Pirongia	?
Henderson & Grange (1926)	Districts of Pirongia, Alexandra, Puniu, Kawhia and Karioi.	1:63,360*
Kear (1960)	Hamilton - Pirongia	1:250,000
Kear & Schofield (1978)	Ngaruawahia subdivision	1:63,360*
Matheson (1981)	Mt Karioi area	1:20,000
Waterhouse & White (1994)	Raglan-Kawhia-Oparau	1:50,000
Edbrooke (2005)	QMap Waikato	1:250,000

*1:63,360 = 1 inch to 1 mile; 1:126720 = ½ inch to 1 mile

APPENDIX C

Dyke measurements (Dos unit) from aerial imagery.

ID (from west to east)	Strike	Length (m)	Thickness (m)	Elevation (m asl)
1	078	115	52	520
2	096	110	31	640
3	094	103	13	670
4	103	100	13	640

APPENDIX D

Dyke measurements for Tiwarawara andesite (Twd) from aerial imagery.

ID (from west to east)	Strike	Length (m)	Thickness (m)	Elevation (m asl)
1	134	163	21	670
2	113	296	42	600

APPENDIX E1

Summary of main lithologies and clast sizes within andesite block and tuff unit (Psp) at Pirongia Summit.

		Clast sizes (mm)[1]				
Lithology	Description	Min	Max	Median	Mean	Std dev
Type-1 andesite	Light-grey hornblende andesite	10	464	43	52	48
Type-2 andesite	Andesite with tan to dark brown groundmass	9	80	28	31	16
Melanocratic inclusions within Type-1 andesite	Dark-grey coloured rock with phenocrysts of plagioclase and hornblende.	10	82	35	38	24
Type-4 breccia	Clasts of polymict breccia from intercalated and overlying unit.	-	-	-	-	

[1]Data based on 180 clast measurements. Studied area was approximately 4×4 m.

APPENDIX E2

Representative clast sizes in polymict breccia of the Psp unit near Pirongia Summit[1].

Lithology	Description	Clast sizes (mm)[1]				
		Min	Max	Median	Mean	Std dev
Andesite Type A	Moderately to highly vesicular pumice (?), with phenocrysts of hornblende and sparse phenocrysts of plagioclase. Colours of clasts range from: tan to dark brown and red.	10	89	28	32	16
Andesite Type B	Non-vesicular plagioclase rich andesite. Minor groundmass component with pale-grey to cream colour.	13	208	43	59	51
Basalt Type 1	Dark grey cpx-basalt with small augite phenocrysts and relatively larger plagioclase (up to 11 % of rock).	17	89	39	44	23
Basalt Type 2	Ankaramite with abundant large, black augite phenocrysts (up to 10 mm) in fine-grained groundmass of light grey to deep red colour.	13	87	32	43	26
Other 1	Clasts or clasts and matrix of the underlying andesitic block and tuff unit.	63	171	170	135	62

[1]Data based on 90 clast measurements. Measurements represent maximum diameter of clasts and are interpreted from scaled outcrop photographs from an area of approximately 4×4 m. Note: Fine lapilli (<10 mm) within the matrix were not measured.

APPENDIX F

Measurement data for andesitic dykes of the Pirongia Summit (Psa) unit.

Group	Strike	Length (m)	Thickness (m)	NZ topo 50 G.R.
NW-SE	092	80	21	BE33 848 934
	135	101	23	BE33 845 934
	Unclear	83	22	BE33 845 932
	120	43	15	BE33 845 931
NE-SW	071	300	24	BE33 843 935
	066	58	15	BE33 840 925

APPENDIX G

Dyke or shallow plumbing system measurements for (Pcd) andesites from aerial imagery.

Dyke ID (refer to Fig. 25)	Strike	Length (m)	Thickness (m)	Elevation (m a.s.l.)
D1	103	279	26	950
D2	099	117	19	900
D3	072	123	35	880
D4	112	158	30	890
D5	075	80	33	870
n/a	051	162	18	860

Chapter 3

Evidence of mixing between island arc and intraplate basaltic magmas in the Alexandra Volcanic Group, New Zealand

'The rocks differ markedly from all other volcanic material of the North Island'
Patrick Marshall, 1907

O.E. McLeod
M.B. Brenna
R.M. Briggs
A. Pittari

Introduction

Island arc basalts (IAB) and ocean island basalts (OIB) are two classical endmembers of oceanic basalt that form the main eruptive products of the subduction-margin and intraplate settings respectively (Keleman et al. 2014; Sun and McDonough, 1989). The key geochemical and isotopic differences between IAB and OIB are the result of a complex interplay between the tectonic environment of magma formation, its source characteristics, conditions of magma generation, and mixing of mantle source regions (e.g. Sun and McDonough, 1989; Zheng, 2019).

Strong consensus exists linking the source of IAB magmas to partial melting of metasomatized mantle wedge above the subducted slab (e.g. Kushiro, 1987; Morris et al. 1990; McCulloch and Gamble, 1991; Stern, 2002; Plank, 2005). These ultramafic metasomatites carry the elemental 'signature' of IAB (i.e. enrichment in LILE, Pb and LREE, but strong depletion of HFSE) (Hawkesworth et al. 1991) and are more susceptible to melting than normal asthenospheric peridotite (e.g. Kushiro, 2001; Kogiso et al. 2004). Melting may occur either directly by fluid fluxing from the slab (e.g. Stolper and Newman, 1992), or through decompression of the mantle wedge (Bartels et al. 1991; Grove et al. 2002).

Compared to IAB, the origin of OIB is complicated by its presence in both pure intraplate settings as well as the back-arcs of convergent margins. Most of the Earth's OIB volcanism is associated with mantle plumes which produce age-progressive seamount tracts, e.g. the Hawaiian-Emperor chain (Wilson, 1963). Relatively smaller volume melting events in the asthenosphere or lithosphere (Sun and McDonough, 1989; Ringwood, 1990, Panter et al. 2006) typically produce non-age-progressive seamounts (e.g. Zindler et al. 1984) and continental volcanic fields (e.g. Scott et al. 2020). Continental OIBs show geochemical similarities to IABs (i.e. enrichment of LILE, LREE, depletion of Pb) but also distinct differences, i.e. HFSE enrichment (Zindler and Hart, 1986) which arise from their petrogenesis through decompression melting of the metasomatized asthenosphere (e.g. Hoernle et al. 2006; McGee et al. 2013) and/or melting of veined mantle lithosphere (e.g. Panter et al. 2006; Pilet et al. 2005).

Despite their occurrence in generally distinct tectonic settings, the spatial and temporal overlap of IAB with OIB is documented in some volcanic fields. In Europe, such overlap typically manifests as a systematic evolution from IAB to OIB volcanism over time in response to changing tectonic conditions. Examples are found in the Mediterranean (Agostini et al. 2007; Beccaluva et al. 2011) and Carpathian-Pannonian region (Lexa et al. 2010; Harangi et al. 2015). Other sites include Fiji in the South Pacific (Gill and Whelan, 1989) and Baja California, Mexico (Storey et al. 1989). In contrast, most sites of spatially and temporally overlapping IAB-OIB volcanism are clustered on or near the Pacific margin; e.g. the Cascades Arc of western USA (Ormerod et al. 1988; Strong and Wolff, 2003; Hildreth, 2007; Wanke et al. 2019), the Trans Mexican Volcanic Belt (Verma and Nelson, 1989; Márquez et al. 1999; Ferrari et al. 2001), the Caribbean and Central America (Wadge and Wooden, 1982; Reagan and Gill, 1989), Japan (Morris, 1986; Mashima, 2009; Sakuyama et al. 2009; Mahony et al. 2011) and Vanuatu in the South Pacific (Sorbadere et al. 2013). The causes of OIB volcanism in arc settings have been linked broadly to changes in plate motion and evolution of plate margins (Wadge and Wooden, 1982; Sorbadere et al. 2013), accompanied by back-arc extension, fracture zones or slab tears, which allow OIB magmas to ascend via vertical or lateral flow from the asthenosphere. In most cases, OIB represents only a fraction (<5%) of the total erupted material within the arc, but vents may be dispersed over a wide area.

The Alexandra Volcanic Group of North Island, New Zealand is a prime example of a continental back-arc setting where IAB-related stratovolcanoes are surrounded by, and intercalated with, the eruptive deposits of an OIB-type intraplate volcanic field. The field contains arguably the

best-preserved successions of IAB-OIB stratigraphy at any site globally, and is therefore a crucial reference site for such bi-modal volcanism. In this study, we present the first complete geochemical and isotopic dataset for the Alexandra Volcanic Group and apply this data in a stratigraphic sense to answer fundamental questions related to the IAB-OIB transition in subduction settings. Understanding the transition from arc to intraplate volcanism provides valuable information to explain the changing magmatic response to subduction at sub-arc (80–160 km) to post-arc (>200 km) depths.

Geological setting

History of North Island volcanism and tectonism

The 30 Myr history of North Island volcanism is the manifestation of a continuous and evolving interaction between the Pacific and Australian plates (e.g. Mortimer et al. 2010; Reyners, 2013) that has ultimately shaped the tectonic and volcanic setting of Zealandia since the Late Cenozoic (Mortimer and Scott, 2020). The main convergent margin, defined by oblique westward subduction of the Pacific Plate under the Australian Plate, has been in existence since ~16 Ma (Mortimer et al. 2010) and stabilised into its present-day configuration of the Hikurangi-Kermadec-Tonga Trench in the last ~5 Ma (e.g. Seebeck et al. 2014)(Fig. 1).

Arc volcanism occurred initially along the NNE-trending proto-Kermadec (Vitiaz) Arc between Tonga and North Island (Mortimer et al. 2007), where on shore it corresponds to age-progressive andesitic volcanism that has migrated southeastwards from Northland to the Coromandel Volcanic Zone (Herzer, 1995; Wilson et al. 2008; Seebeck et al. 2014). The Vitiaz Arc was disrupted around 6 Ma by slab-rollback which induced back-arc opening of the southern Havre Trough (Walcott, 1987; Wright et al. 2006) and rifting of the former arc chain (post- 4.4 Ma) into the Colville and Kermadec ridges (Wysoczanski et al. 2010; Timm et al. 2019). This led to development of the active intra-rift, submarine Tonga-Kermadec Arc which extends ~2500 km from Samoa into the central North Island (Wright et al. 1996).

The present foci of North Island arc activity, the Taupo Volcanic Zone (TVZ), is an extremely productive site of silicic volcanism (Wilson et al. 1995) that marks the onshore (~300 km) extension of the Tonga-Kermadec Arc and Havre Trough (Fig. 1). The TVZ and its tectonic structure, the Taupo Rift (Villamor and Berryman, 2001; 2006; Wilson et al. 2009; Stern, 2009) are dislocated from the back-arc region to its west by ~65 km of rift-related extension within the active Hauraki Rift and older Hamilton Basin. Back-arc extension manifests as age-progressive, alkaline basaltic volcanic fields (Briggs et al. 1989; 1994; Leonard et al. 2017) and localised, antecedent arc-type basaltic strato-volcanism (i.e. Alexandra Volcanic Group, the subject of this paper) between 100 and 170 km from the arc front.

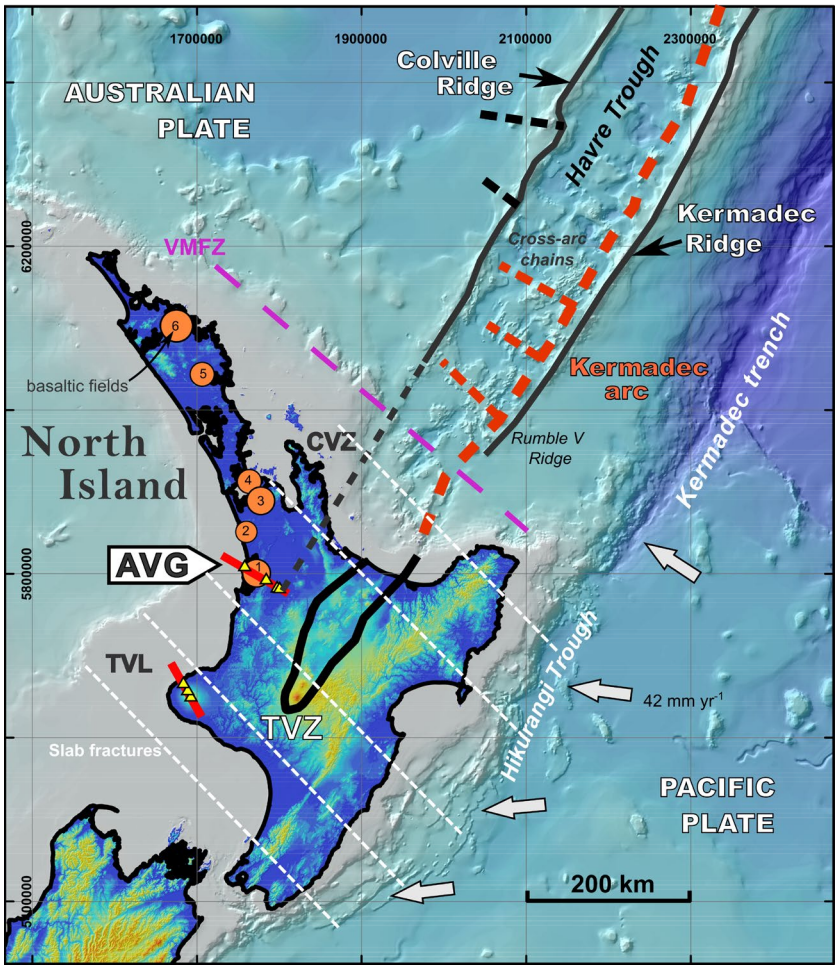

Figure 1. Volcanic setting of North Island, New Zealand in the context of the Tonga-Kermadec-Hikurangi subduction zone, where the Pacific Plate is obliquely subducting beneath the Australian Plate. Slab-rollback has rifted apart an older arc chain to form the Kermadec and Colville ridges, the latter connecting onshore to the extinct Coromandel Volcanic Zone (CVZ). The active Kermadec arc extends from the Havre Trough into the Taupo Volcanic Zone (TVZ) of continental Zealandia. Emerging from the arc are NW-SE striking 'cross-arc' volcanic chains, which include the Alexandra Volcanic Group (AVG) and the Taranaki Volcanic Lineament (TVL). These chains are sub-parallel to fractures on the subducted slab (interpreted from Reyners, 1989) and to the Vening Meinesz Fracture Zone (VMFZ). The back-arc zone is characterised by OIB-type basaltic volcanic fields (orange circles), which are: (1) Okete (of Alexandra Volcanic Group), (2) Ngatutura, (3) South Auckland, (4) Auckland, (5) Whangarei and (6) Kaikohe-Bay of Islands.

Alexandra Volcanic Group

The Quaternary age Alexandra Volcanic Group (AVG) (2.74–1.60 Ma; Briggs et al. 1989) is the most expansive (1000 km^2) and voluminous (~50 km^3) basaltic volcanic field in North Island, comprising ~50% of all basalt erupted on the island since 17 Ma. The field is located on the western edge of the Hamilton Basin, a major rift-related depression within the back-arc of the Taupo Volcanic Zone, ~100 km northwest of the active front arc (Fig. 1).

The field (Fig. 2) consists of a chain of arc-type basaltic cones and stratovolcanoes (Karioi, Pirongia, Kakepuku and Te Kawa; Briggs, 1983), termed the Alexandra Volcanic Lineament (AVL), that show pronounced NW-SE (300°) alignment perpendicular to the strike of the Taupo Volcanic Zone. These centres are interspersed with an intraplate-type basaltic volcanic field (Okete Volcanic Formation; Briggs, 1983) that is most prevalent towards the northwest of the field. The key volcanoes in the field are described below.

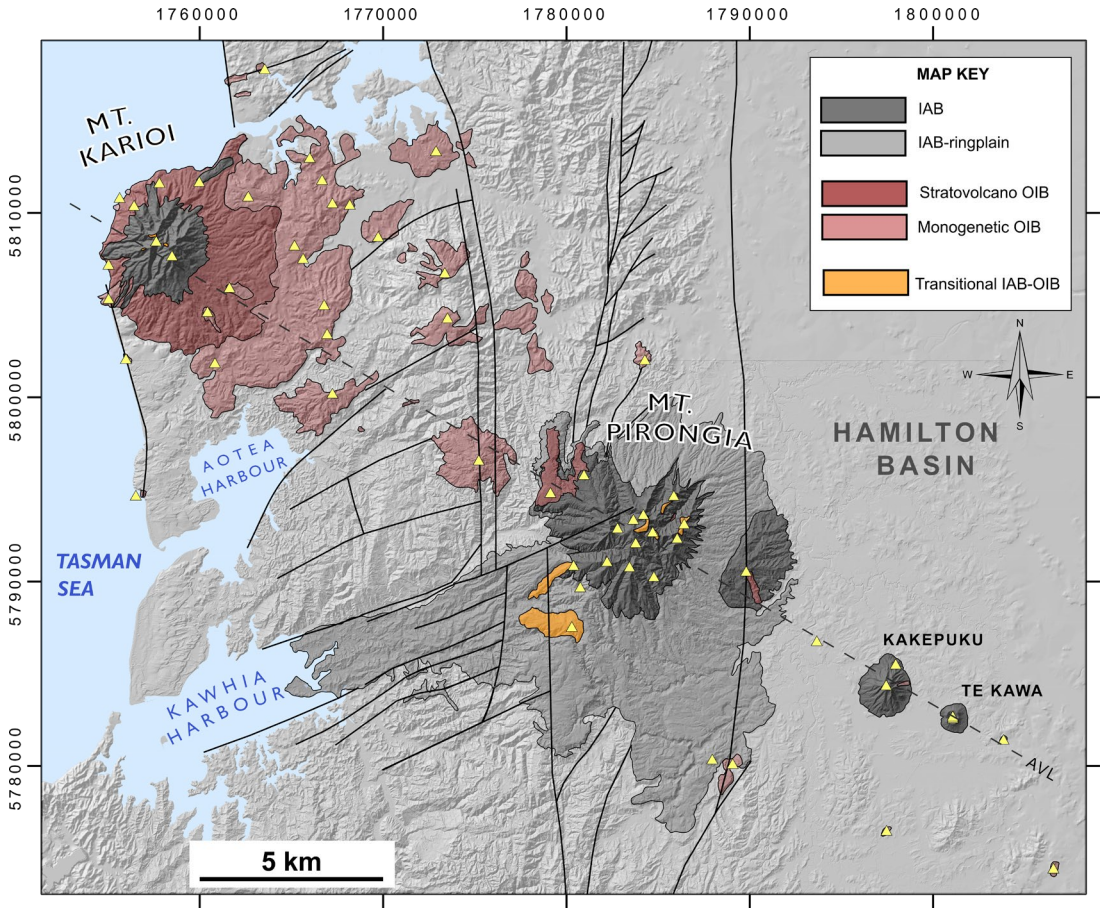

Figure 2: Hillshaded map of the Alexandra Volcanic Group and surrounding faulted terrain of western Waikato, North Island, New Zealand. The field consists of arc-type stratovolcanoes, domes and cones that span a 60 km zone, termed the Alexandra Volcanic Lineament (AVL) that stretches from the southern Hamilton Basin to the Tasman Sea. An intraplate basaltic field, the Okete Volcanics, is interspersed with the volcanic terrain and is most prominent in the area surrounding Mt Karioi. The volcanoes are colour-coded according to erupted composition, showing the predominance of IAB across the stratovolcanoes, prevalence of OIB in the northwest of the field, and low-volume distribution of transitional IAB-OIB lavas at Pirongia and Karioi.

Karioi

Mount Karioi is an eroded basaltic stratovolcano, 8×11 km wide and 756 m tall, on the Tasman coast at the north western edge of the volcanic field (Fig. 2). It has a post-erosional volume of 15 km^3, about half that of Mount Pirongia. The western flanks of Karioi are incised by sea cliffs (e.g. Te Toto Gorge), which provide excellent exposures of the mid to lower stratigraphy (Matheson, 1981; Goles et al. 1996). Upper edifice stratigraphy is less well constrained due to the extreme topography and forestation. The edifice consists of four stratigraphic members emplaced between 2.48 and 2.28 Ma (Goles et al. 1996)(see Fig. 3). Initial eruptions formed a phreatomagmatic tuff ring and lavas of OIB composition (Pauaeke Member), later overlain by a thin succession of IAB-type lavas and tuffs (Te Toto Member) that mark the base of the Karioi Volcanic Formation. Major shield-building then commenced (Whaanga Member), with a thick succession of OIB-type lavas and tephras emplaced from central and flank vents. In the final phase of volcanism, the OIB shield was surmounted by a high-angle stratovolcano (Wairake Member) composed of lava flows, dikes, breccias and associated laharic deposits with mainly IAB-type compositions.

Pirongia

Mount Pirongia is the largest basaltic volcano (15×17 km, elev. 959 m, 30 km^3) in the Alexandra Volcanic Group and the wider North Island. The mountain lies in the middle of the volcanic field, straddling an up-faulted block to the west of the Hamilton Basin. The Pirongia Volcano was constructed from numerous vents on the central, flank and peripheral zones of the edifice over a period of ~1 Ma (2.7–1.6 Ma; Briggs et al. 1989), which relate to six principle stages of edifice growth and collapse (McLeod et al. 2020)(Fig. 3). Most of Pirongia formed during Stage 1 volcanism (Paewhenua Member; 2.5–2.42 Ma) which constructed an expansive shield composed of IAB-type ankaramites and subordinate OIB basalts. Following partial sector collapse of the shield, Stage II vent activity shifted northeast of the summit where IAB-type andesites and basaltic andesites were erupted to form the Tirohanga Member stratovolcano. Late Stage 2 eruptions produced a high-K basaltic flank vent. In Stage III, the foci of eruptions shifted to the southern flank of Pirongia where a large stratovolcano and two lower flank vents with diverse alkaline compositions were emplaced, collectively forming the Hihikiwi Member. The Stage 3 edifice was partly destroyed by a sector collapse event around 2.1 Ma and subsequently infilled by basaltic lavas of Stage 4 Te Akeohikopiro Member. Another larger sector collapse of the western flank occurred between 2.2 and 1.7 Ma. This collapse displaced 3.3 km^3 of material and formed the deposit of the Oparau breccia (Stage 5, Oparau Member). Around 1.6 Ma, resurgent volcanism associated with Stage 6 emplaced the Pirongia Summit Member, with eruptions centred on two major vents in the summit zone and on a lower flank vent on the eastern side of the mountain.

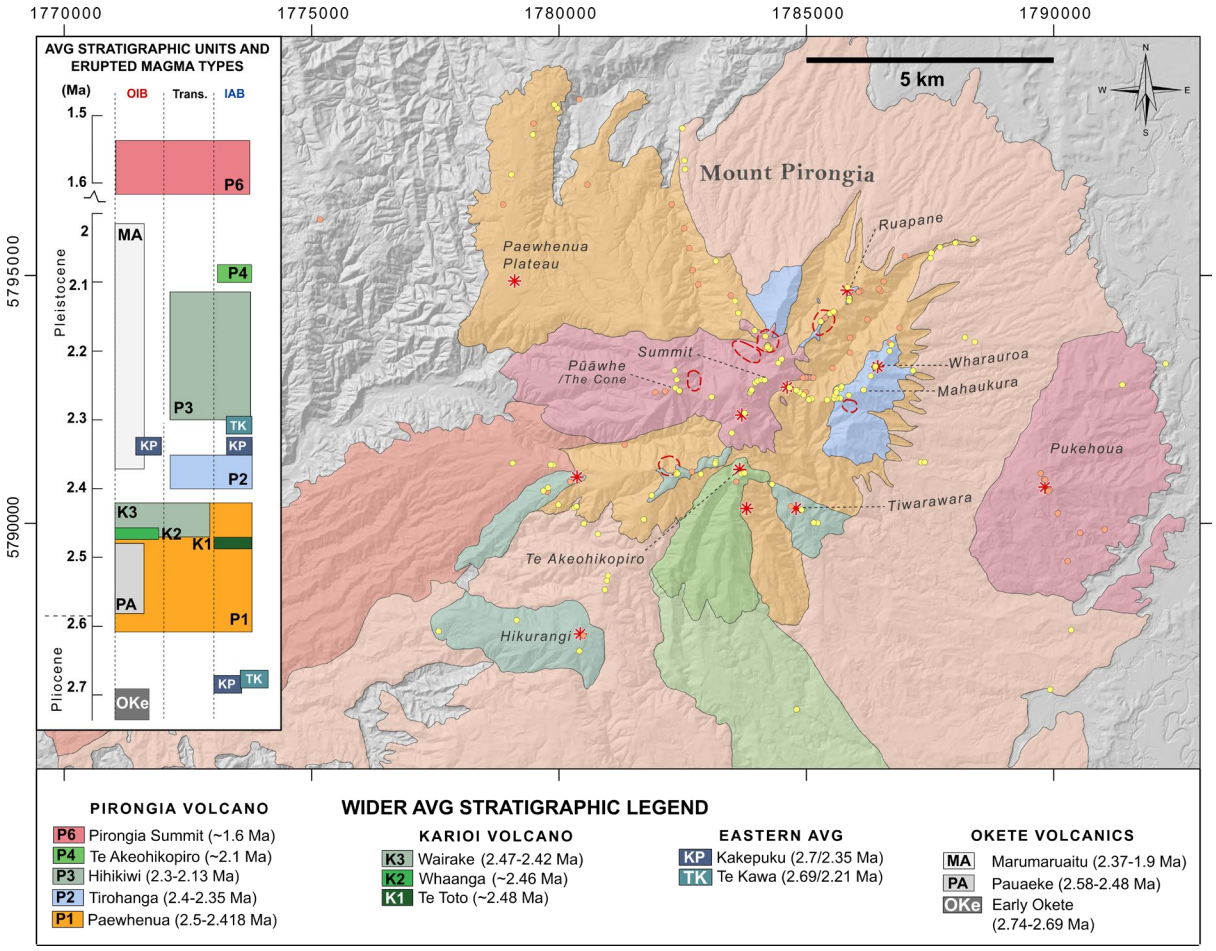

Figure 3. Simplified geological map of Pirongia Volcano, adapted from McLeod et al. (2020). Stratigraphic members of Pirongia are defined in the bottom legend, along with the stratigraphic members of the wider volcanic field. Vent symbols are shown by red dashed lines (major vents) and red asterisks (minor vents). Locations of analysed samples are shown by coloured circular symbols (yellow or orange). The temporal relationship between AVG stratigraphic members and their erupted compositions (IAB, OIB or transitional) are summarised in top left panel.

Kakepuku

Kakepuku (elev. 449 m) is a perfectly formed basaltic dome southeast of Pirongia, located within the downfaulted block of the Hamilton Basin (Fig. 2). The main phase of dome-building at 2.7 Ma produced crystal-rich ankaramite and sporadic lava flows of OIB-type basalt, which constructed a 3×3 km edifice. Radiometric dating indicates that another vent activated at 2.3 Ma on the northern flank at Ongaru, following an apparent 350 ka hiatus of eruptions.

Te Kawa

The Te Kawa volcano (elev. 214 m) is a small basaltic dome (1.6×1.9 km wide) at the southeastern edge of the Alexandra Volcanic Group (Fig. 2). The volcano has a distinct semi-circular crater structure, which is the only preserved crater in the volcanic field. Edifice construction occurred from two separate but spatially overlapping vents active at 2.69 ± 0.20 Ma (Robertson, 1976) and 2.21 ± 0.08 Ma (Briggs et al. 1989), mirroring the eruptive pulses of Kakepuku (Fig. 3). Both Te Kawa eruptions produced ankaramite lavas, with the earlier eruption notably more enriched in olivine than the latter.

Okete and Auckland Province volcanism

The Okete Volcanic Formation (Briggs, 1983) defines a group of alkaline (OIB) basalts erupted from ~27 vents across the Alexandra Volcanic Group. These eruptions produced tuff rings, scoria cones and lava fields that are most prominent on the inland areas of Mount Karioi, but cover a total area of ~1000 km^2 extending to the far eastern and southern edges of the field (Fig. 2). Based on their distribution, Goles et al. (1996) proposed the subdivision of Okete Volcanic Formation into stratigraphic members that pre-date (Pauaeke Member) and post-date (Marumaruaitu Member) Karioi Volcano (see Fig. 3). Erupted compositions range from basanites and alkali olivine basalts to olivine tholeiites and hawaiites (Briggs and Goles, 1984), with mafic and ultramafic xenoliths (5–20 mm, max. 25 cm) common in the former two groups (Rodgers and Brothers, 1969). Amphibole-bearing ultramafic wehrlites and pyroxenites indicative of mantle metasomatism occur within Okete lavas at Te Toto Gorge (Sanders, 1994).

The Okete Volcanics (2.69–1.9 Ma) are the earliest manifestation of back-arc, intraplate volcanism established in western North Island. During the Quaternary, monogenetic intraplate volcanic fields have migrated northward from Okete to Ngatutura (1.83–1.54 Ma; Briggs et al. 1989; 1990) and South Auckland (1.59–0.51 Ma; Briggs et al. 1994; Cook et al. 2005) towards the active Auckland Volcanic Field (0.26 Ma–present; Leonard et al. 2017; McGee et al. 2013). Collectively, these fields define the Auckland Province (Weaver and Smith, 1989) and are similar in terms of their overall volcanic style (Strombolian and phreatomagmatic eruptive deposits), longevity (≤1 Ma), total erupted volume (<2.5 km^3) and alkalic to sub-alkalic OIB compositions (e.g. Smith and Cronin, 2020).

Methods

All rock samples analysed in this study (n=195) were collected by the authors and combined with a subset of published analyses (n=74) from Briggs & Goles (1984), Briggs (1986) and Briggs and McDonough (1990). From our samples, 156 rocks were sectioned and analysed by petrographic microscope.

Microprobe analyses of crystals within polished sections (n=10) were performed on the JEOL JXA-8230 SuperProbe with Wavelength Dispersive Analysis at Victoria University of Wellington. An accelerating voltage 15 kV, beam current of 12 nA and a focused beam with a 2 μm diameter were used for analyses.

Major and minor element concentrations were analysed by X-ray fluorescence (XRF) on fused disks using a Bruker S8 TIGER at the University of Waikato. Fused disks were prepared with 12:22 Fusion Flux (XRF Scientific). Standards used were OREAS 24C (Ore Research & Exploration) and USGS specimens BHVO-1, BHVO-2, AGV-1 and AGV-2. Loss on ignition (LOI) was calculated after firing sample powders to 1100 °C for one hour. Values obtained for standards are accurate to within 2% of the published values for Si, Al, Ti, Ca and K, 3% for Mg, 6% for Na and 10% for P. Duplicate analyses indicate precision of better than 1% for Al, Ti, Mn, Fe, Mg and Ca, but lower precision for Si (3%), K (5%) and P (10%). Karioi whole-rock data was collected at the Victoria University of Wellington XRF Facility by Ken Palmer in 1992. Unfortunately, no information on accuracy or precision is available.

Trace elements were measured using a RESOlution-SE Compact 193nm excimer laser ablation (LA) system in tandem with an Agilent 8900 Inductively Coupled Plasma – Mass Spectrometer (ICP-MS) at University of Waikato. Analyses were conducted by pulsing the laser at 10 Hz with a 30 μm spot size and energy density of 5.0 J/cm^2 with an ablation time of 45s. Ultra-high purity helium was used as the carrier gas (370 mL/min) to deliver the ablated sample from the LA system to the ICP-MS. The ICP-MS was optimized to maximum sensitivity daily. Background counts (gas background, measured with the laser off) were collected for 30 seconds between samples. NIST glass standards (610, 612) were analysed after every 10 samples to account for any instrument drift. Analysis of BHVO-2 and AGV-2 indicates that LA-ICPMS data is accurate to within 10% of the published values for most trace elements, with lower accuracy for Cu (21%), Rb (23%), Y (15%), Zr (13%), Nb (15%), Pr (15%), Gd (12%), Yb (13%), Lu (12%), Th (29%) and U (16%). Karioi trace element data was collected by XRF (ANALABS facility, Perth, Australia, 1994) and INAA (University of Oregon). Precision for INAA trace elements is ±5 % of the accepted value for primary solution standards and secondary USGS standards.

Whole-rock Sr-Nd isotope ratios were measured on a ThermoFinnigan Triton thermal ionization mass spectrometer (TIMS) at the Geochemistry Lab, Victoria University of Wellington. A single digestion was made for each sample using standard HF-HNO_3 digestion techniques, following the method of Pin et al. (2014). Total procedural blanks were less than 100 pg for both Sr and Nd respectively. Sr samples were loaded on single Re filaments with a Ta_2F_5 activator and measured using a static collection routine for 240 ratios using 16 sec. integrations. The NBS 987 standard (500 ng) gave averages of $^{87}Sr/^{86}Sr$ = 0.7102559 ± 0.000004 (2SE max; n=2) and 0.7102642 ± 0.000004 (2SE max; n=4) for the two analytical sessions respectively. The values were identical to the long-term instrument average $^{87}Sr/^{86}Sr$ = 0.7102560 ± 0.000006 (2SD, n=16). AGV-2 was run as a secondary standard. Data were corrected for fractionation to $^{86}Sr/^{88}Sr$ = 0.1194 using the exponential law.

Nd samples were dissolved in 2.5 M HCl, then loaded on double Re filaments in a 0.25 M H_3PO_4 emitter solution. Ratios were measured using a static collection routine and 270 ratios with 8.389 sec. integrations. Runs of the 'in house' J&M standard gave averages of $^{143}Nd/^{144}Nd$ = 0.511818 ± 0.000004 (2SD max; n=2) and 0.512101 ± 0.000002 (2SE; n=4) for the two analytical sessions respectively. These values were identical to the long-term average for the J&M standard

$^{143}Nd/^{144}Nd$ = 0.511818 ± 0.000004 (2SD, n=34). It should be noted that this standard is distinct from the value of La Jolla, which yields an average value of $^{143}Nd/^{144}Nd$ = 0.511847 ± 0.000004 (2SD, n=6).

The Karioi Sr-Nd isotope data was analysed at Analabs, Western Australia in 1994. Sr samples were loaded in 1 Ml 1 M H_3PO_4 onto single Ta filaments; stable ion beams of 2-4x10-11A ^{88}Sr were obtained at filament temperatures of 1300–1450C. Mass fractionation was corrected by normalizing to $^{86}Sr/^{88}Sr$ = 0.1194. Typically, 5-7 blocks of 10x8 sec integrations produced in-run precisions (2SE) of +0.003%. $^{87}Sr/^{86}Sr$ (±2SD) for SRM987 (n=100) is 0.71023 ± 7 (0.01%), BCR-1 (n=6) is 0.70500 ± 4, BHVO-1 (n=19) is 0.70348 ± 6.

Nd was loaded in H_3PO_4-doped 1M HNO_3 onto the Ta side of a Ta-Re double filament assembly; stable ion beams of 1-3x10-11 A ^{144}Nd were obtained at Re filament temperatures of around 1700C. Mass fractionation was corrected by normalizing to $^{146}Nd/^{144}Nd$ = 0.7219. Typically, 5-7 blocks of 10x8 sec integrations produced in-run precisions (2SE) of ± 0.0025%. $^{143}Nd/^{144}Nd$ (±2SD) for La Jolla (n=100) is 0.511860±16, BCR-1 (n=7) is 0.512634±18, BHVO-1 (n=5) is 0.512989±13. Present day CHUR was taken as 0.512631.

Results

Petrography and mineral chemistry

OVERVIEW

The erupted material of the Alexandra Volcanic Group is overwhelmingly basaltic (~95%) in composition. Most basalt is contained within the Pirongia and Karioi stratovolcanoes (94%), with minor additional contributions from Kakepuku and Te Kawa (2%), and the Okete Volcanics (4%). Previous classification of the Alexandra suite was based on geochemical criteria (Briggs and McDonough, 1990; Briggs and Goles, 1984), which defined six arc-type rock groups; (1) ankaramite, (2) transitional olivine basalt, (3) olivine-tholeiite, (4) high-Al basalt, (5) andesite and (6) K-rich basalt, and four intraplate groups; (1) basanite, (2) alkali olivine basalt, (3) olivine tholeiite and (4) hawaiite, respectively. For this study, we propose a simplified geochemical classification based on the TAS diagram (Fig. 4, see section below). However, we retain use of the name 'ankaramite' to differentiate megacrystalline basalts from finer-grained basalts of similar composition. Overall, the rock suite can be broadly subdivided into arc-type (IAB) and intraplate-type (OIB) rocks based on their texture, mineralogy and compositional characteristics. A third group is also present which shows transitional properties between the IAB and OIB endmembers. In the following section, we describe the rocks of these three groups. Mineral symbols are: Cpx=clinopyroxene, Pl=plagioclase (feldspar), Hbl=hornblende (amphibole), Ol=olivine, Mag=magnetite, Phl=phlogopite (mica).

Rock classification

According to TAS classification (Fig. 4), Alexandra Volcanics range from low-Si basanites (44 wt%) to silicic andesites (60 wt%) of sub-alkalic to transitional affinity. Of the Karioi lavas (n=76), most plot within the basalt field. However, the observed variation may reflect incomplete sampling of the upper stratigraphy of Karioi compared to Pirongia, where silicic rocks are widely exposed on ridgelines. More silicic basaltic-andesite and andesite rocks occur within the upper stratigraphy, ranging up to 60 wt% SiO_2 at the Karioi summit peak. Pirongia lavas (n=146) span roughly the same silica range as Karioi (45–59 wt%), but many rocks have higher total alkali contents at a given SiO_2 concentration and span into the trachybasalt and (basaltic-) trachyandesite fields. Further sub-classification define all Pirongia basaltic-trachyandesites as shoshonites, and trachyandesites as both benmoreites and latites. Kakepuku and Te Kawa are composed entirely of basalt. All rocks of the Okete Volcanics plot within or near to the basalt and basanite fields.

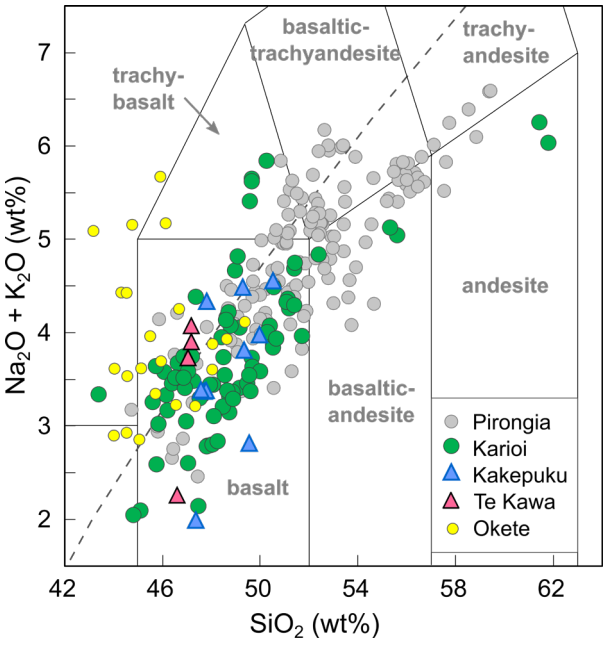

Figure 4: TAS classification diagram (Le Bas et al. 1992) for all new and published AVG whole-rock data (n=270). Published data is from Briggs & Goles (1984), Briggs (1986) and Briggs & McDonough (1990). Alkalic/sub-alkalic line (dashed) is from Irvine and Baragar (1971).

Petrography

In this section, the petrography of the key volcanic rock groups in the field are described and illustrated (Fig. 5). Detailed notes on the petrography of rocks within individual stratigraphic members are presented in Table 1.

THE IAB ROCKS

Ankaramites

Ankaramite is the most widespread and ubiquitous rock-type in the volcanic field, forming the foundational lithology of Karioi, Pirongia, Kakepuku and Te Kawa (Table 1). They are dense, dark-grey basalts with abundant megacrysts of Cpx and Ol that protrude from weathered surfaces (Fig. 5B). Variations in the overall abundance of megacrysts in lavas is observed at the outcrop scale. The megacrysts are set within an intergranular groundmass of Cpx±Ol±Pl±Mag dominated by coarse Pl (Fig. 5A). Most ankaramite lavas are very weakly vesicular, in contrast to scoriaceous ankaramites in pyroclastic deposits which generally have hyalopilitic textures.

Ankaramite is relatively uniform in texture across the volcanic field but the following distinctions are notable: (1) Ol appears to be more modally abundant within Karioi, Kakepuku and Te Kawa lavas compared to Pirongia. Many Pirongia ankaramites contain almost no Ol as phenocrysts or within the groundmass. (2) Cpx megacrysts are more diopsidic at Karioi (dark green) than Pirongia (dull black).

Cpx forms pale green to pale brown (mega-) phenocrysts and glomerocrysts typically ranging in size from 1–8 mm and rarely up to 20 mm wide. Phenocrysts are mainly euhedral, while glomerocrysts are subhedral and consist of fractured mosaics of clinopyroxene with inclusions of Mag±Pl±Ol. Red-altered Ol form kernels in the centres of some glomerocrysts. Many glomerocrysts mimic the euhedral forms of phenocrysts (e.g. hexagonal shape) and often have rounded edges that appear to be abrasion features from transport in their host magmas. Cpx megacrysts show weak to intense zonation with >50 concentric zone bands observed in some crystals. Zonation from green cores to brownish-green rims is common.

Ol forms euhedral microphenocrysts ± phenocrysts and glomerocrysts with honey-brown appearance in outcrop. In nearly all cases, Ol is less abundant than Cpx and forms relatively smaller phenocrysts (typically ≤3 mm, but up to 9 mm). Ol commonly shows alteration to red iddingsite, occasionally with fresh outer rims apparently unaffected by alteration. Similar alteration has been documented in some oceanic island lavas and was attributed to surface degassing of water-oversaturated magmas following rapid magma ascent (Caroff et al. 2000). Brown fibrous bowlingite alteration occurs in some Ol from Te Kawa. Pl forms sparse, tabular phenocrysts (1–3 mm) and is always abundant either as microphenocrysts or microlites. Complex sieve-textured zones with abundant glass inclusions occur in some ankaramites. The groundmass is typically composed of an intergranular array of abundant Pl (acicular to anhedral) + interstitial Cpx (colourless to pale green) + Mag + minor to moderate amounts of Ol + sporadic patches of chlorite/smectite. Subtle flow alignment of plagioclase is evident in some lavas.

The intermediate rocks

These rocks are relatively fine-grained, porphyritic basalts and basaltic-andesites with the assemblage Pl+Cpx+Hbl+Mag±Ol. Typical modal abundance is Cpx≥Pl>Hbl, with Pl more abundant than Cpx in some lavas, and Hbl always sparse (Fig. 5C). Groundmass textures range from felty-trachytic to glassy and intergranular to sub-ophitic. Cpx is pale-green to pink-brown, forming euhedral phenocrysts (1–3 mm) and sparse, sub-rounded glomerocrysts (max. 5 mm, ± Mag and Ol inclusions) in some lavas. Some Cpx shows green core to brown rim zonation, and is in some cases resorbed and embayed. Pl shows seriate distribution from phenocrysts (1–3 mm) to microlites, with common zonation and sieve core texture common. Hbl phenocrysts (1–3 mm) are skeletal with opaque rims and replaced by Mag, Phl, Cpx and Pl. Cumulates of Hbl+Cpx+Pl occur in some lavas. Ol is uncommon overall and restricted to the groundmass where it forms altered, reddish microlites.

Andesites

IAB-related andesites occur at Pirongia and Karioi (see also transitional andesites in section below). The andesites appear pale-grey in outcrop and contain phenocrysts of Pl (1–2.5 mm) + Hbl (1–5 mm) + Cpx (1–3 mm) + Mag set within glassy to holocrystalline groundmass (Fig. 5D). Hbl crystals have opaque rims and form sporadic megacrysts up to 13 mm long. Pale green-brown Cpx is rare as phenocrysts but widespread in the groundmass. Groundmass textures range from intergranular to sub-ophitic to trachytic.

THE OIB ROCKS

Typical OIB-type basalts are exemplified by the Okete Volcanics, which consists of fine-grained porphyritic alkali basalts with high groundmass to phenocryst ratios (Fig. 5F,H). Phenocrysts (1–2 mm) have the assemblage Ol (12–17%) + Cpx (5–10%) + minor Pl (<3.5%) and Mag (<1 %), where Cpx is invariably subordinate to Ol (Briggs and Goles, 1984). Calcite and apatite are accessory minerals. Most Cpx is purplish-brown titanaugite, with green core-to-rim zonation in some rocks. Phenocrysts are generally 1–2 mm and set within intergranular groundmass. Comparable fine-grained OIB rocks occur within the stratigraphy of Karioi (Pauaeke, Whaanga and Wairake members) and Pirongia (Paewhenua Member) (Table 1). Non Okete-type OIBs are also present at the stratovolcanoes, including trachytic Pl-rich basalt with minor Ol (Whaanga and Wairake members), and ankaramite-type basalts with titanaugite and Ol megacrysts that occur on flank vents of Pirongia (Paewhenua Member) and Kakepuku (Fig. 5G).

TRANSITIONAL ROCKS

Rocks with transitional IAB-OIB compositions (as defined by trace element chemistry, see geochemistry section) occur in the flank and cone stratigraphy of Pirongia and Karioi (Table 1).

Most of these rocks are indistinguishable from IAB-type rocks in the field, i.e. diopsidic-ankaramites (Fig. 5I), Hbl-basalts and glassy Hbl-andesites. However, some transitional rocks have distinct mineralogy and texture (i.e. Phl-bearing basaltic-andesites (Fig. 5J), Ol-rich basalts and finely trachytic basalt (Fig. 5K)) that are atypical of the IAB-suite and more similar to OIB-rocks.

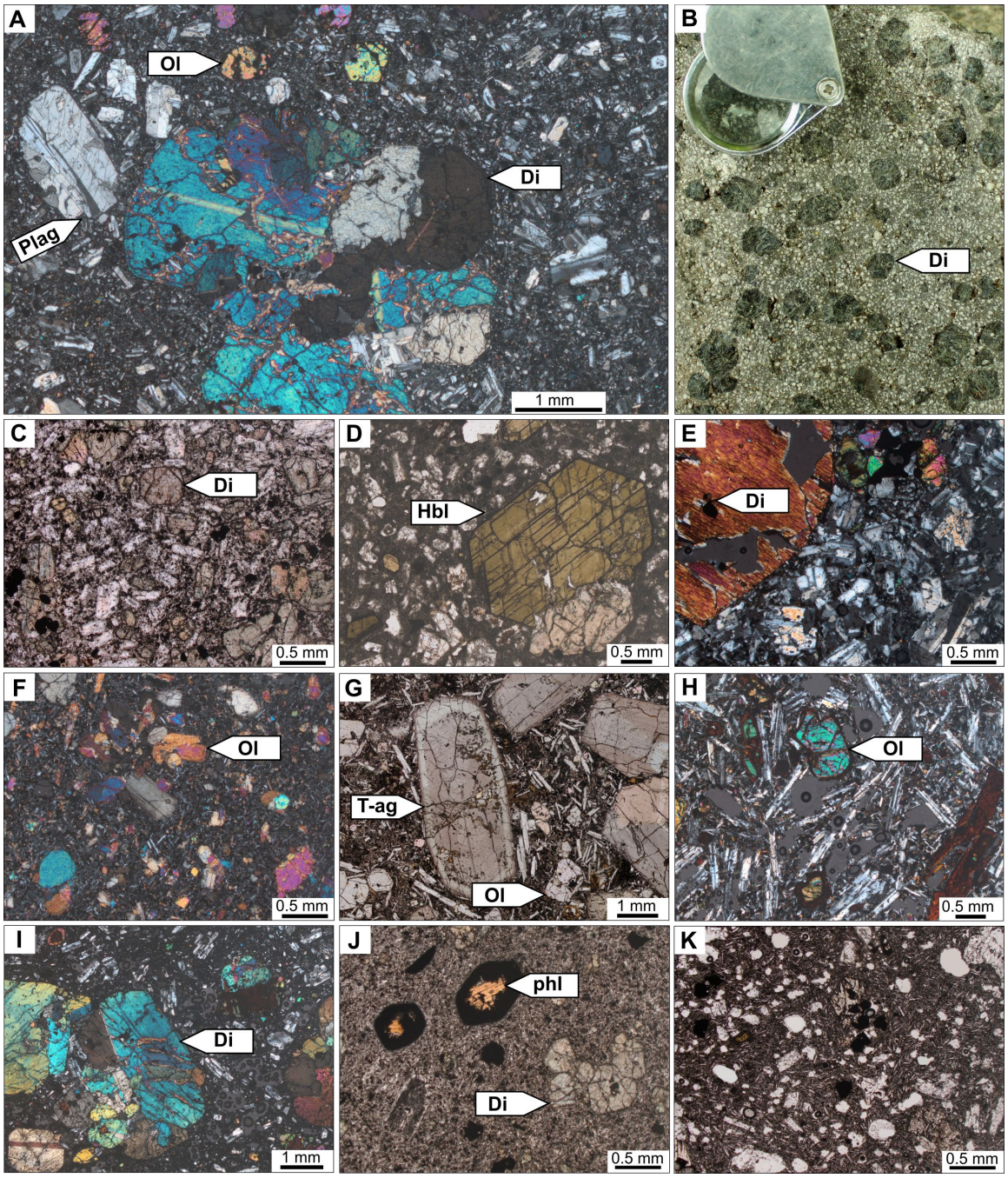

Figure 5. Petrographic characteristics of Alexandra Volcanic Group rocks. (A-E) IAB-type rocks. (A) ankaramite microphoto in cross-polarised light show typical clinopyroxene glomerocrysts. (B) ankaramite hand sample with diopside (glomero-) phenocrysts. (C) Pirongia basaltic-andesite. (D) hornblende-andesite. (E) Karioi ankaramite. (F-H) OIB-type textures for typical Okete basanite (F), Pirongia basanite-ankaramite (G) and Karioi Whaanga Member basalt (H). (I-K) transitional lavas, showing Pirongia ankaramite from Ruapane Peak with rounded diopside glomerocrysts (I), phlogopite shoshonite from Hikurangi dome (J), and basaltic-trachyandesite from Tireni ridge (K). Mineral abbreviations: Di=diopside, Plag = plagioclase, Ol=olivine, Hbl=hornblende, T-ag=titanaugite, phl=phlogopite.

Table 1. Summary of petrographic information for individual volcanic-stratigraphic members of the Alexandra Volcanic Group in relation to major geochemical groups (IAB, OIB and transitional). Mineral symbols: Cpx=clinopyroxene, Pl=plagioclase (feldspar), Ol=olivine, Hbl=hornblende (amphibole), Mag=magnetite, Phl=phlogopite (mica), Chl=chlorite, Cal=calcite.

Geochemical group	Volcanic formation	Rock type
IAB	Karioi Pirongia Kakepuku Te Kawa	*General description:* Includes a diverse suite of rocks ranging from Cpx-basalts to ankaramites, basaltic andesites and andesites. In the basalt suite, the assemblage is Cpx+Pl+Ol, set within an invariably holocrystalline groundmass of Pl+Cpx+Ol+Mag. Cpx is generally pale-green diopside. In the basaltic andesites, the ratio of Pl to Cpx is higher and Cpx phenocrysts are generally smaller. Hbl is common as microphenocrysts and Ol is rare or absent. The groundmass is invariably holocrystalline. The most silicic rocks, the andesites, are moderately porphyritic with prominent phenocrysts of Hbl and Pl>Cpx set within glassy to microcrystalline groundmass. Atypical examples include the Cpx-dominated andesites of Tireni ridge and the summit dyke of Pūawhe Peak, which contains sanidine rims on Pl phenocrysts (the only known occurrence of alkali feldspar in the AVG). ▪ IAB-type ankaramites comprise all of the Te Toto Mbr (Karioi), more than half of Paewhenua Mbr (Pirongia), and almost all of Te Kawa and Kakepuku. Basaltic-andesites occur in Wairake Mbr (Karioi) and throughout the Pirongia Fm. Andesites occur in Wairake Mbr (Karioi) and the Paewhenua, Tirohanga, Hihikiwi and Pirongia Summit members (Pirongia).
OIB	Okete Karioi	▪ *Pauaeke Mbr:* Typical 'Okete-type' fine-grained basalts with sparse Ol phenocrysts (honey brown, av. 1–2 mm, max 4–6 mm) and Pl visible in hand specimen. In thin section, Ol is either dominant or sub-equal in proportion to titanaugite and set in intergranular groundmass of Ol+Cpx+Pl laths+Mag±chloritized glass±Cal. Ol is unaltered, in contrast to the Whaanga Mbr lavas. Some pyroxenes show green core to brown rim zonation. Weakly vesicular. ▪ *Marumaruaitu Mbr:* Equivalent to Pauaeke Mbr. ▪ *Whaanga Mbr:* Two types occur: (1) fine-grained, Okete-type basalts with small phenocrysts (1–2 mm) and moderate vesicularity. Ol-rich assemblage with equal to subordinate Cpx, which is mainly purplish-red titanaugites ± green core zonation. Colourless augite occurs in some lavas. Pl forms tabular microphenocrysts and rare phenocrysts (≤ 8 mm) in some lavas. Fe-Ti oxides are abundant. Some larger cpx have Ol inclusions. Cpx forms sparse megacrysts (8–10 mm, max. 20 mm wide) ± inclusions of Ol, and glomerocrysts with Ol. Ol (up to 10 mm) is euhedral, pervasively altered to iddingsite and contains fluidal embayment structures. (2) Pl-phyric basalts with relative coarse, flow-aligned Pl (up to 7 mm) and minor Ol set within intergranular groundmass. ▪ *Wairake Mbr:* Two types occur: (1) basalt with phenocrysts of titanaugite+Ol+Pl set within an interstitial, plag-rich groundmass, and (2) basalt dominated by Pl phenocrysts (tabular, 2–4 mm, max. 8 mm) with subordinate Ol (red altered)+pale greenish Cpx+Mag set in groundmass of Pl+Cpx+Mag+chloritized glass.

	Pirongia Kakepuku	▪ *Pirongia and Kakepuku*: Coarse-grained alkali basalts occur on a western flank vent of Pirongia (Paewhenua Mbr) and at Kakepuku (Fig. 5G). Extremely abundant with megacrysts (sometimes >50% of rock) of pale brown titanaugite (2–6 mm, max. 10 mm) and Ol (2.5–3.6 mm), with interstitial Pl laths (~1 mm) and Mag microcrysts set within intergranular groundmass (Pl>titanaugite>Ol>Mag). Titanaugite shows prominent oscillatory zoning and is rich with inclusions of Ol and glass.
Transitional IAB-OIB	Karioi	▪ *Wairake Mbr:* Two types occur: (1) Coarse-grained, vesicular basalts with abundant (glomero-) phenocrysts of colourless, euhedral Cpx and red-altered Ol. The groundmass contains Pl+Mag+devitrified glass+colourless Cpx+Ol+Chl. (2) Andesite with phenocrysts of Hbl+Pl+Cpx set within very fine-grained, felted to trachytic groundmass of Pl+Mag+isolated Cpx and Hbl. Cpx is pale green to colourless (max. 2 mm). Hypersthene occurs in a summit dyke.
	Pirongia	▪ *Paewhenua Mbr:* On Tireni Ridge, an atypically glassy, weakly-vesicular lava occurs (Fig. 5K). It contains flow-aligned Pl microlites, sparse Pl phenocrysts (max. 1.4 mm), pale green-brown augite (max. 2 mm) and accessory Hbl in the groundmass. ▪ *Tirohanga Mbr:* Two types occur: (1) andesites at Tirohanga-Wharauroa peaks with abundant Pl (1–2.7 mm, zoned, sieve textured), Hbl (1–2 mm, opaque rims), Cpx (pale green (glomero-) phenocrysts, 1–5 mm) and Mag set within holocrystalline to glassy groundmass containing Pl+Mag+Cpx. Felsic glomerocrysts of Hbl+Pl+Mag±Cpx are common. Hbl in glassy andesites lacks opaque rims. (2) Ankaramite at Ruapane Peak (Fig. 5I) is abundant with pale green-brown diopside glomerocrysts (2–8 mm), surrounded by tabular Pl microcrysts (1–1.5 mm) and subordinate Ol (≤ 2 mm, altered red) in coarse, intergranular groundmass of Pl+Ol+Mag. ▪ *Hihikiwi Mbr:* Hikurangi flank vent lavas (Fig. 5J) are fine-grained shoshonites with sparse phenocrysts of titanaugite (light green-brown, zoned, 1–3.5 mm, max. 6 mm) and skeletal Hbl (max. 1 mm). Phl, Cpx or Mag pseudomorph the latter. Pl phenocrysts are up to 1.5 mm wide. Ol is a rare accessory mineral. Omanawa flank vent basalt is dominated by Ol (glomero-) phenocrysts (av. < 1 mm, max. 4 mm) set within flow-aligned, Pl-rich groundmass. Rare accessory phenocrysts of Pl and microcrysts of Cpx occur. ▪ *Pirongia Summit Mbr:* Transitional rocks at Pirongia Summit include porphyritic Cpx-basalts of similar mineralogy to Ruapane ankaramite but finer-grain size, and glassy andesites with Hbl phenocrysts (≤ 4 mm) ± Phl inclusions.

Mineral chemistry

We present new major and trace element mineral chemistry for Pirongia in the context of a wider compilation of published/thesis data for the Alexandra Volcanic Group (see Appendix 1 for full dataset).

Clinopyroxene is ubiquitous as (mega-)phenocrysts in all Alexandra IAB-type basalts, with strongly calcic compositions ranging from high-Wo augite to diopside (Fig. 6A). The diversity of Cpx compositions at Pirongia is equivalent to that of the entire field, with Mg# of 59–90 (median 76), compared to Karioi (67–77, max. 84), Kakepuku (66–77.5), Te Kawa (69–73) and Okete (68–82). The present dataset suggests that Cpx at Karioi is less Mg-rich than at Pirongia, though more mineral data for Karioi basalts is required to confirm this relationship.

Pirongia IAB-hosted Cpx shows low, decreasing TiO_2 (1.5–1 wt%) with increasing MgO and CaO, concordant with the available Cpx data for Kakepuku and Te Kawa (Fig. 6C-D). In contrast, Pirongia OIB-hosted Cpx is TiO_2-rich titanaugite (1–5 wt%) which shows a steep negative correlation with increasing MgO. Much of this variation relates to the concentric zonation of titanaugite megacryst from Ti-rich to Ti-depleted zones. Calcium contents are uniformly high (22–23 wt%) but subtly lower than OIB-related Cpx in the Okete Volcanics (CaO=23–24 wt%). The IAB and OIB trends for Cpx intersect at 15 wt% MgO.

Olivine data is available only for Pirongia and Okete Volcanics (Fig. 6B). IAB-hosted olivine has relatively low Fo contents (mainly 58–77) in contrast to OIB-hosted olivine (79–91.6). The highest Fo values occur in Okete basalts and in olivine cores from two lavas from Pirongia (Paewhenua Plateau OIB and an IAB-type Cpx-basalt at the summit). These olivines overlap with the Fo values of local mantle olivine (from xenoliths in Okete lavas) but are more enriched in CaO (>1.5 wt%) than is typical of dunite or lherzolite (<1.5 wt%).

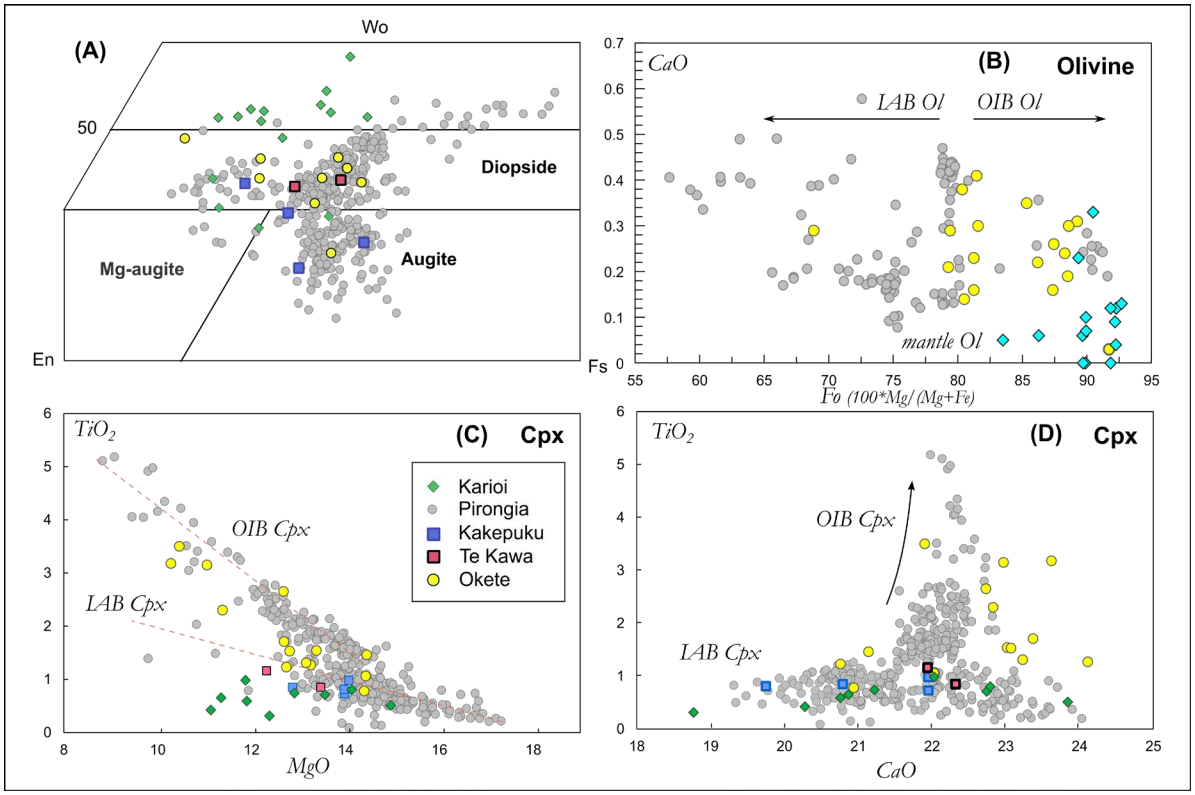

Figure 6. Mineral chemistry for the Alexandra Volcanic Group. (A) clinopyroxene compositions (n=429) in relation to the Cpx classification diagram of Morimoto (1988). (B) Olivine compositions (n=144) for Pirongia and Okete Volcanics compared to Okete-hosted olivine mantle xenoliths (all available data). (C-D) MgO vs TiO_2 and CaO vs TiO_2 bivariate plots for clinopyroxene, illustrating the TiO_2-rich nature of phenocrysts in OIB relative to IAB rocks. Compiled data sources: Karioi (Matheson, 1981); Okete (Matheson, 1981; Briggs and Goles, 1984; Sanders, 1994); Pirongia, Kakepuku and Te Kawa (Briggs and McDonough, 1990), and Okete mantle olivine data (Sanders, 1994).

Pyroxene trace elements

Clinopyroxene (mega-)phenocrysts in Pirongia basalts have distinct trace element patterns which correspond to the IAB or OIB composition of their host rock (see Appendix 1 for data). In Fig. 7, IAB-hosted Cpx shows strong depletions in La, Sr, Zr, Hf and Ti compared to megacrysts within our Pirongia OIB-rock (Paewhenua Plateau ankaramite), which also exhibits a steeper REE pattern. Interestingly, the trace element pattern of Cpx hosted in transitional (IAB-OIB) rocks falls within the overlap zone of the two suites, suggesting that this Cpx crystallised within the hybrid magma and was not inherited from either endmember.

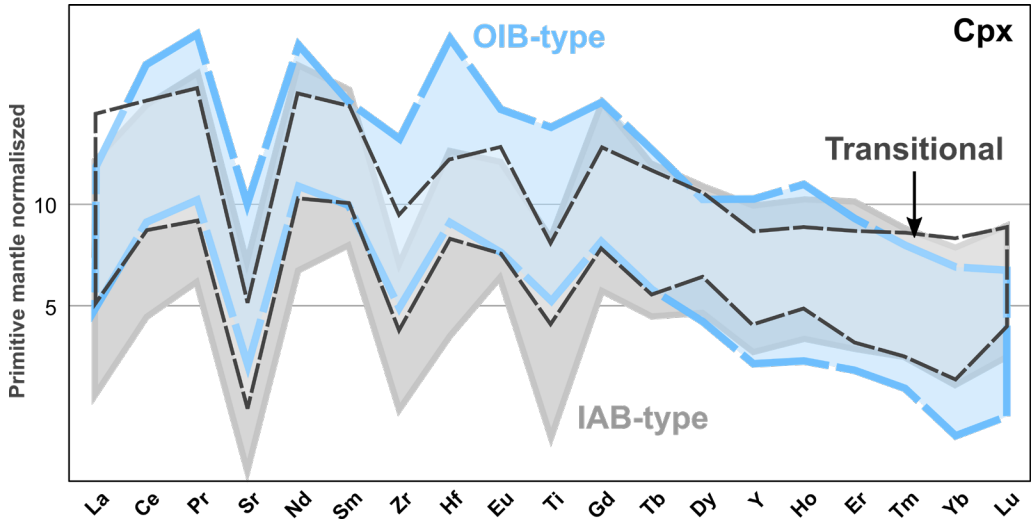

Figure 7. Clinopyroxene trace element patterns of phenocrysts (n=138) within IAB, OIB and transitional rocks of Pirongia. Normalising values from Sun and McDonough (1989).

Whole-rock chemistry

Major elements

Major element variation for the AVG is shown in Fig. 8 using MgO variation diagrams (see Appendix 2 for full dataset). Systematic decreases in SiO_2, Al_2O_3 Na_2O and K_2O contents occur with increasing MgO abundance, whereas CaO and Fe_2O_3 contents increase. The Pirongia and Karioi suites show similar overall variation in MgO, SiO_2, Al_2O_3, CaO, Fe_2O_3 and K_2O, though MgO-poor, SiO_2-rich rocks are underrepresented in the Karioi dataset compared to Pirongia. The majority of Karioi lavas thus have high, yet restricted ranges for Fe_2O_3 (10–13 wt%) and CaO (9–12 wt%) that show little variation with increasing MgO contents (Fig. 8G). Kakepuku and Te Kawa basalts show remarkable variation in MgO (4.5–15.5 wt%) and Al_2O_3 (10–19.7 wt%), with higher Al_2O_3 at a given MgO content than Pirongia. K_2O variation (Fig. 8F) is complex across the AVG with a large total range (0.3–2.52 wt%) that reflects numerous MgO-K_2O lineages within the Karioi and Pirongia suites. The most potassic rocks are high-K and shoshonitic dykes at Pirongia (2.4–2.5 wt%). Kakepuku and Te Kawa lavas have low K_2O contents (0.4-1.5 wt%) relative to Pirongia. Okete Volcanics are MgO-rich (8–15 wt%), SiO_2-poor rocks with high Fe_2O_3 and CaO, moderate to low K_2O and very low Al_2O_3 contents typical of continental alkaline basalts. Sodium contents show large variation (1.8–4.6 wt%) across a narrow range of MgO (10–13 wt%).

TiO_2 contents for AVG rocks (Fig. 8D) fall within three distinct groups: low (0.5–1.1 wt%); moderate (1.1–1.5 wt%) and high (1.6–2.8 wt%). Within these groups, TiO_2 shows negligible variation with increasing MgO. The low-Ti group contains most of the IAB-suites of Pirongia and Karioi, while the high-Ti group consists of OIB-type rocks from the Okete Volcanics, Karioi, Pirongia and Kakepuku. The moderate group contains transitional rocks from Karioi and Pirongia, and most rocks from Kakepuku and Te Kawa.

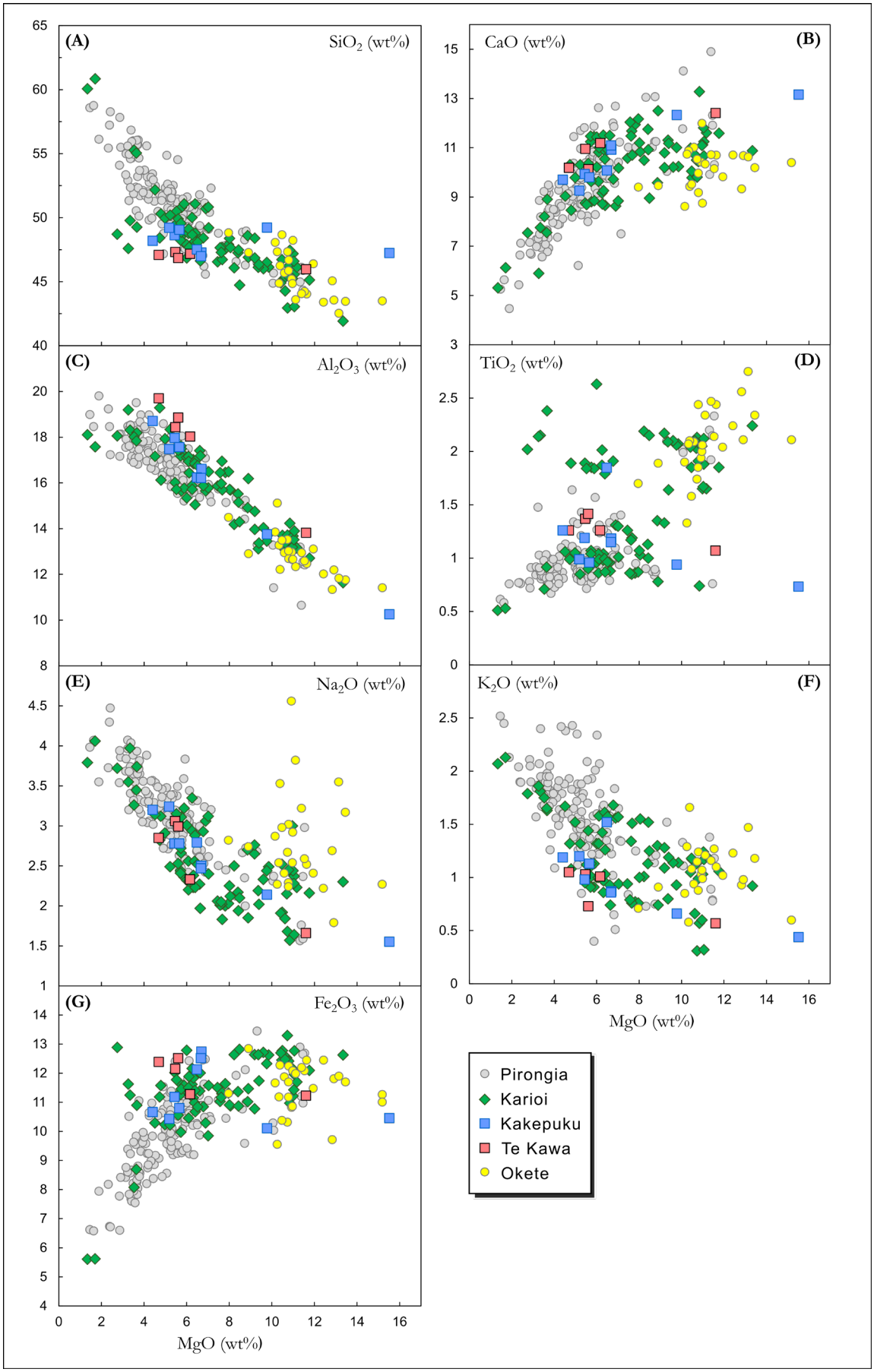

Figure 8. Major element variation against MgO (wt%) for Alexandra Volcanic Group rocks. Additional data for Kakepuku, Te Kawa and Okete rocks is from Briggs and Goles (1984), Briggs (1986) and Briggs and McDonough (1990).

Trace elements

Primitive mantle normalised element patterns for the Alexandra Volcanic Group are presented in Fig. 9 (see Appendix 2 for complete dataset). The element patterns of all analysed rocks form a transitional spectrum between IAB and OIB end members. The observed IAB pattern consists of enrichment in LILE, Pb and LREE, but depletion in HFSE (e.g. Nb and Ta), and less enrichment in HREE relative to the primitive mantle (i.e. the typical element abundances of IAB globally; Hawkesworth et al. 1991). The overall OIB pattern demonstrates elevated LILE, LREE and HFSE relative to IAB, with general depletion in Pb (i.e. typical of continental OIB; Sun & McDonough, 1989).

The IAB endmember predominates at Pirongia, showing a typical IAB pattern with strong depletion in the HFSEs Nb, Ta and Ti (Fig. 9A). In contrast, Pirongia OIB has a humped pattern (Fig. 9B) with elevated LILE, LREE and HFSE, but depletion in Pb. A subset of Pirongia rocks show transitional IAB-OIB patterns defined by relative enrichment of the HFSEs (Nb, Ta and Ti) compared to the IAB endmember.

Similar IAB, OIB and transitional element patterns occur within the Karioi suite. Karioi rocks with IAB-type patterns occur within the Te Toto Member and selected Wairake Member samples (Fig. 9C). Karioi IAB patterns are defined by: (1) lower abundances of HREEs compared to Pirongia IAB; (2) less pronounced Nb and Ta anomalies; (3) weak negative Ti-anomaly in most rocks and (4) strong Pb-enrichment and P-depletion. Karioi transitional rocks are restricted to the Wairake Member, where they are similar to Karioi IABs but have subdued Nb-anomalies. Transitional andesites show positive spikes in K, Zr and Hf, but very strong Ti-depletion. OIB-type patterns define all rocks of the Whaanga Member and selected rocks of the Wairake Member (Fig. 9D). Their patterns are characterised by very pronounced positive spikes in Ba and Ta and Pb.

Kakepuku and Te Kawa volcanics (Eastern AVG, Fig. 9E) display IAB-type patterns with very strong depletions of Nb and Ta but no negative spikes in Ti. Overall, the IABs of the Eastern AVG contain lower abundances of LILE and LREE than Pirongia, and lack the positive Nd spike observed in Pirongia and Karioi IABs. A single basalt from Kakepuku displays an OIB-type pattern, with typical elevated abundances LREE, LILE and HFSE, and depletion in Pb.

The Okete Volcanics all have OIB patterns (Fig. 9F). Their patterns are subdivided into pre-(Pauaeke) and post-Karioi (Marumaruaitu) Members. Among Pauaeke Member lavas, those from Te Toto Gorge show extreme positive spikes in Ba, Ta, Pb and Sr that are similar to OIBs of the overlying Karioi units (Whaanga and Wairake Members) but distinct from the other Okete OIBs of Marumaruaitu Member and those of Pirongia and Kakepuku. Compared to Pauaeke Member, OIBs of Marumaruaitu Member are more diverse in their element patterns, with the most LILE and LREE depleted patterns corresponding to hawaiites.

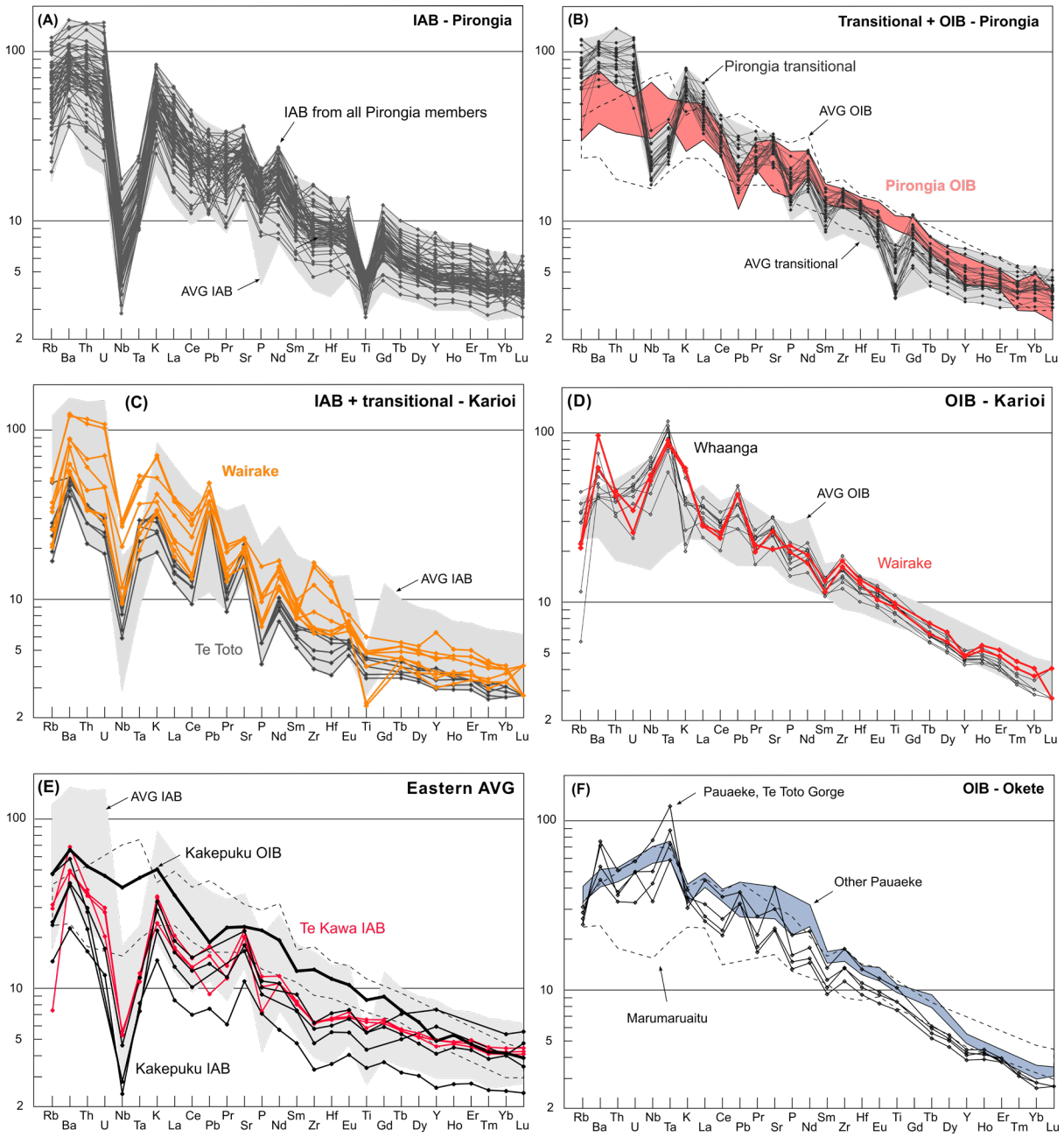

Figure 9. Primitive mantle normalised diagrams for the Alexandra Volcanic Group (normalising values from Sun & McDonough (1989)). (A): IAB-type eruptives from all stratigraphic members of Pirongia. (B): Transitional IAB-OIB and OIB eruptives from Pirongia. (C) IAB and transitional IAB-OIB from Te Toto and Wairake members of Karioi. (D) OIB from the Whaanga and Wairake members of Karioi. (E) IAB and OIB of the Eastern Alexandra Volcanic Group showing the IAB affinity of Kakepuku and Te Kawa, and a single OIB lava from Kakepuku. (F) OIB from the Okete Volcanics, subdivided into pre-(Pauaeke) and post-Karioi (Marumaruaitu) members. The Pauaeke Member is further sub-divided into basal Karioi lavas from Te Toto Gorge, and those of the wider volcanic field (blue). Grey fields define the total compositional variation for all AVG rocks, for IAB (AVG IAB) and OIB (AVG OIB).

Isotopes

The Sr-Nd isotope array of the Alexandra Volcanic Group is shown in Fig. 10 and the dataset presented in Table 2 (see also Appendix 3 for details). Isotopic ratios occur along a roughly linear trend from $^{87}Sr/^{86}Sr$ = 0.70542–0.70304 and $^{143}Nd/^{144}Nd$ = 0.512686–0.512952, with OIB and IAB 'endmember' compositions defined by the Okete Volcanics and Pirongia Volcano, respectively. There is no systematic variation of Sr-Nd ratios with rock-type, except for basalts with strong alkalic affinity (i.e. OIB-related) which consistently show high $^{143}Nd/^{144}Nd$ (≤0.512856) and low $^{87}Sr/^{86}Sr$ (<0.7039).

The Pirongia suite clusters into three groups (G1, G2 and G3) ranging from $^{87}Sr/^{86}Sr$ = 0.705047–0.703570 and $^{143}Nd/^{144}Nd$ = 0.512736–0.512890. The G1 field (n=14) is the most Sr-radiogenic suite in the AVG ($^{87}Sr/^{86}Sr$ = 0.705047–0.704485) and is representative of the majority of Pirongia edifice-forming deposits. Intermediate $^{87}Sr/^{86}Sr$ (0.704056–0.704363) and $^{143}Nd/^{144}Nd$ (0.512820–0.512854) ratios define G2 volcanics (n=8), which consist mainly of silicic dykes (52.9–56 wt% SiO_2) and basaltic flank vent (~50 wt% SiO_2) deposits, as well as basaltic lavas at Pirongia Summit. The most Nd-radiogenic Pirongia rocks form the G3 field (n=3), which comprise low-silica (45–46 wt% SiO_2), TiO_2-rich basalts of OIB affinity.

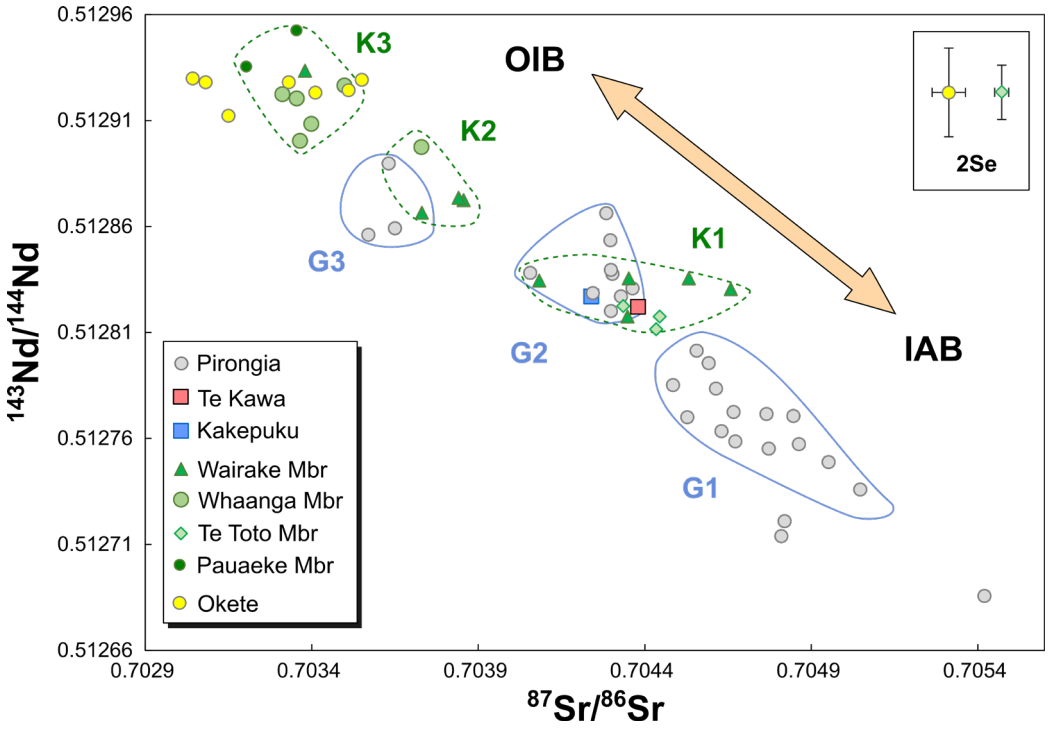

Figure 10. Sr-Nd isotope systematics of the Alexandra Volcanic Group. The arrows point towards the endmember OIB and IAB compositions of the isotopic array.

As observed at Pirongia, Sr-Nd ratios for Karioi Volcanics also cluster into three groups (K1–3), with overall higher $^{143}Nd/^{144}Nd$ (0.512811–0.512952) and lower $^{87}Sr/^{86}Sr$ (0.704658–0.703203) than Pirongia. The two oldest stratigraphic members of Karioi, Pauaeke (alkali basalt) and Te Toto (ankaramite), plot within the K3 and K1 end member fields respectively. The overlying Whaanga Member shield lavas plot mainly within the K3 field but extend into the transitional K2 field. Late-stage Wairake Member volcanics show marked Sr-Nd isotopic variation, spanning across all three fields (K1–3). There is overlap between the fields of K1 and Pirongia G2, and also K2 and Pirongia G3. The K3 group overlaps with the Okete Volcanics field.

Two samples from Te Kawa and Kakepuku have intermediate isotopic ratios ($^{87}Sr/^{86}Sr$: 0.70424–0.70438; $^{143}Nd/^{144}Nd$: 0.512822–0.512827) similar to the Pirongia G2 and Karioi K1 fields. Okete Volcanics have uniformly high $^{143}Nd/^{144}Nd$ (0.512912–0.512930) coupled with low and more variable $^{87}Sr/^{86}Sr$. (0.70304–0.70355). There is close overlap between Okete lavas and the most alkalic Karioi K3 lavas.

Table 2. Sr-Nd isotope ratios for Pirongia and Karioi volcanoes.

Sample ID	Location	Member	Rock-type	$^{87}Sr/^{86}Sr$	$^{143}Nd/^{144}Nd$
PIRONGIA					
PZ3	Paewhenua plateau	Paewhenua	Basalt	0.703631	0.512890
PKH1	Pukehoua	Summit	Basalt	0.704298	0.512820
PN4	Pūawhe/The Cone	Pirongia Summit	Basalt	0.704773	0.512755
PTW3	Tiwarawara Peak	Hihikiwi	Basalt	0.704667	0.512773
PH5	Hihikiwi Track ridge	Hihikiwi	Basalt	0.705420	0.512686
PR3	Pirongia Summit	Pirongia Summit	Basalt	0.704672	0.512759
PX6	Ruapane Peak	Tirohanga	Trachybasalt	0.704279	0.512866
PV4	Mangakara Valley wall	Tirohanga	Trachybasalt	0.704328	0.512827
PR2	Pirongia Summit	Summit	Bas-trachyandesite	0.704244	0.512829
PW10	Lower Pirongia West Rd	Oparau	Basalt	0.705047	0.512736
PH2	Hihikiwi Track ridge	Hihikiwi	Basalt	0.704631	0.512763
PS5	Mahaukura bluffs	Tirohanga	Bas-trachyandesite	0.704556	0.512801
PW6	Pirongia West Rd	Paewhenua	Bas-andesite	0.704846	0.512771
PT6	Tahuanui Ridge	Paewhenua	Bas-trachyandesite	0.704592	0.512796
PK6	Hikurangi dome	Hihikiwi	Bas-trachyandesite	0.704485	0.512785
PC2B	Hihikiwi Track ridge	Hihikiwi	Bas-andesite	0.704863	0.512757
PG5	Upper Mahaukura Track	Paewhenua	Bas-trachyandesite	0.704056	0.512838
PTW1	Tiwarawara Track	Hihikiwi	Bas-trachyandesite	0.704765	0.512772
PX3	Base of Tirohanga Peak	Tirohanga	Bas-andesite	0.704298	0.512839
PN1	Pūawhe/The Cone	Pirongia Summit	Bas-trachyandesite	0.704952	0.512749
PD2	Wharauroa Peak	Tirohanga	Bas-andesite	0.704297	0.512854
PJ2	Tahuanui Track ridge	Pirongia Summit	Bas-trachyandesite	0.704363	0.512831
PG4	Upper Mahaukura Track	Paewhenua	Bas-andesite	0.704613	0.512784
PX5+PA1	Tirohanga Peak	Tirohanga	Bas-andesite	0.704303	0.512838
PS6	Mahaukura bluffs	Tirohanga	Trachyandesite	0.704528	0.512770
KARIOI					
NIK-37	North Wall, Te Toto	Pauaeke	Basalt	0.703354	0.512936
NIK-62	South Wall, Te Toto	Pauaeke	Basanite	0.703203	0.512919
NIK-5	East Wall, Te Toto	Te Toto	Basalt	0.704434	0.512795
NIK-21	South Wall, Te Toto	Pauaeke	Basalt	0.704445	0.512801
NIK-23	South Wall, Te Toto	Te Toto	Basalt	0.704335	0.512806
NIK-9	East Wall, Te Toto	Whaanga	Basalt	0.703498	0.512910
NIK-14	East Wall, Te Toto	Whaanga	Basalt	0.703365	0.512884
NIK-25	East of Whaanga Rd	Whaanga	Trachybasalt	0.703399	0.512892
NIK-45	South Wall, Te Toto	Whaanga	Basalt	0.703355	0.512904
NIK-46	South Wall, Te Toto	Whaanga	Basalt	0.703312	0.512906
NIK-47	South Wall, Te Toto	Whaanga	Basalt	0.703729	0.512881
NIK-29	East of Whaanga Rd	Wairake	Basalt	0.703856	0.512856
NIK-63	Bay south of Te Toto	Wairake	Basalt	0.704352	0.512819
NIK-78	Wairake Track	Wairake	Basalt	0.704532	0.512819
NIK-55	South of Te Toto	Wairake	Trachybasalt	0.703731	0.512850
NIK-53	Ridge south of Te Toto	Wairake	Basalt	0.704348	0.512801
NIK-58	Te Hutewai Stream	Wairake	Basalt	0.704083	0.512818
NIK-232	Summit ridge	Wairake	Basalt	0.703841	0.512857
NIK-52	Ridge south of Te Toto	Wairake	Basalt	0.70338	0.512917
NIK-79	Wairake Track	Wairake	Andesite	0.704658	0.512814

Spatio-temporal relationships

The relationship between volcanic stratigraphy and the geochemical-isotopic groups identified in Figs. 9 and 10 is summarised in Fig. 11.

Stratigraphy

Karioi

The base stratigraphy of Karioi is prominently exposed at Te Toto Gorge (Fig. 11A), where an ancient landslide has cut cliffs up to 100 m high (Goles et al. 1996, reference therein). At this site, the oldest volcanic deposits are lavas and (lapilli-) tuffs with OIB compositions (Pauaeke Member, Okete Volcanics) that overlie carbonaceous sandstone.

An erosional unconformity separates Pauaeke Member from Te Toto Member, the base unit of Karioi Formation (*sensu stricto)*, which at the southern wall of the gorge consists of a basal surge deposit and three ankaramite lavas with IAB-type compositions.

Te Toto Member is overlain by Whaanga Member along a westward dipping erosion surface mantled by the 'main marker horizon' (Mmh; see Fig. 11A), a distinct red-coloured tuff (≤2 m) that marks the onset of Whaanga Member volcanism. The Mmh is overlain by ~15 thin, shield-building lava flows extending to the top of the southern gorge wall. Both the Mmh and all overlying lavas have OIB compositions distinct from the IAB-type Te Toto Member.

Above the gorge amphitheatre (on Whaanga Rd), the base of the Wairake Member cone is marked by laharic deposits (~4 m thick) overlying Whaanga Member lavas. At this site, the oldest Wairake lavas and tuffs are IABs erupted at modest recurrence intervals, indicated by weathered flow tops. Discontinuous stratigraphy for the upper cone indicates that OIB-type lavas are interspersed at various levels within the IAB-dominated succession, though their relative volume is apparently insubstantial. Lavas and dykes with transitional IAB-OIB compositions crop out near Karioi summit. The main summit dyke, an andesite of transitional affinity, crosscuts an older IAB cone succession and indicates that the late-stage (or even last stage) eruptive activity was transitional rather than IAB-type.

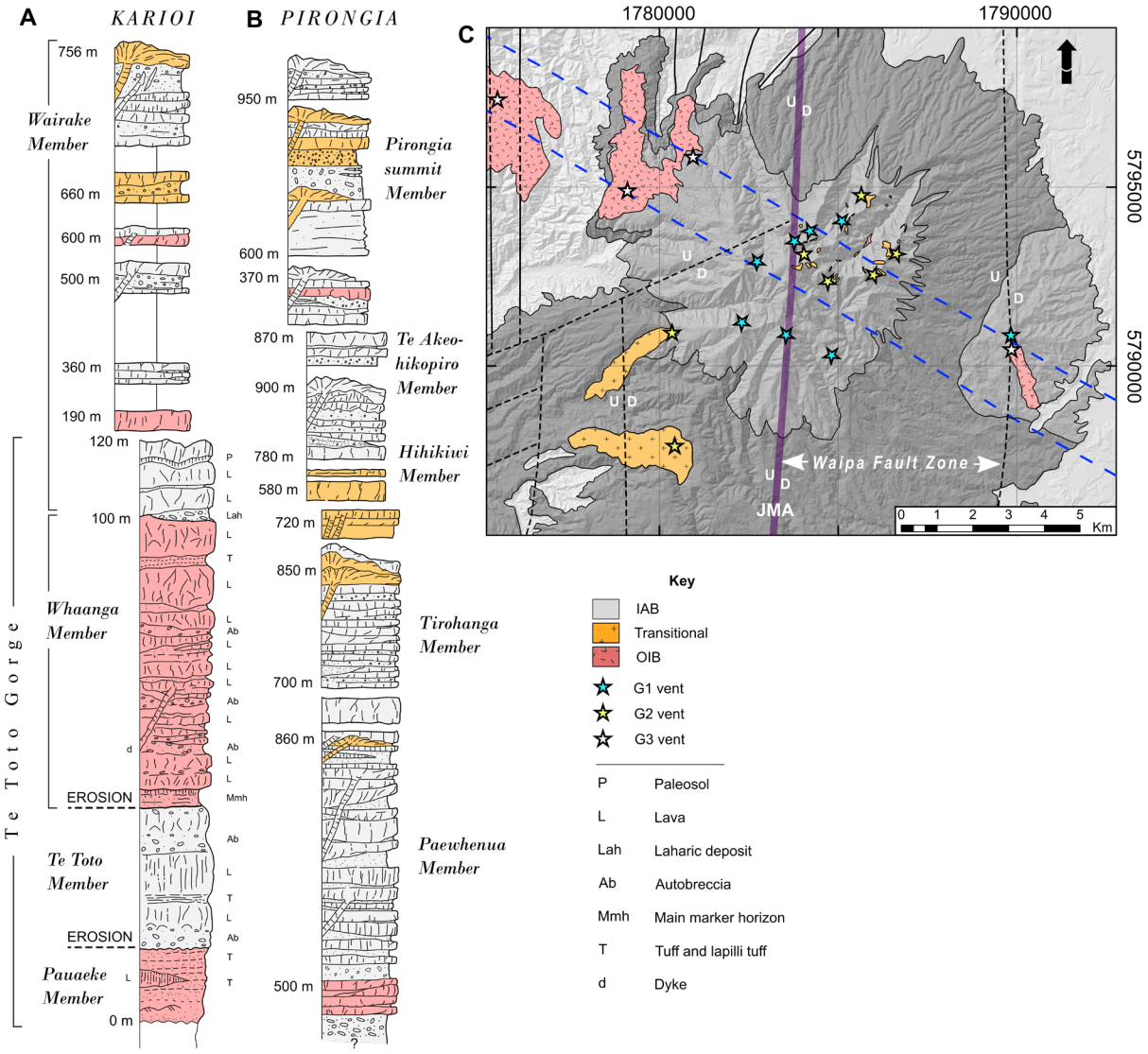

Figure 11. Stratigraphy of Karioi and Pirongia, colour-coded by geochemical group (OIB, IAB and transitional). (A) The complete base succession of Karioi (Pauaeke, Te Toto and Whaanga members) crops out within a single cliff section on the south wall of Te Toto Gorge. The upper stratigraphy of Wairake Member is based on sparse outcrops on the forested mountain. (B) Composite stratigraphy for Pirongia established through detailed mapping by McLeod et al. (2020). (C) Spatial distribution of Pirongia geochemical groups and their corresponding vent sites (G1=IAB, G2=Transitional, G3=OIB). The ring plain (dark grey) consists mainly of redeposited G1 material. Linear features are regional faults (solid black lines), the Alexandra Volcanic Lineament (dashed blue lines) and Junction Magnetic Anomaly (thick purple line).

Pirongia

The composite stratigraphy of Pirongia Volcano is shown in Fig. 11B. The earliest volcanic activity (Stage 1, Paewhenua Member) was characterised by coeval eruptions of IAB and OIB from dispersed vents in the central and flank zones. Subsequent shield-building was exclusively IAB-type. In late Stage 1 activity, transitional dykes in the central vent zone punctured the shield. These dykes are post-dated stratigraphically by a late-stage lava lake and basaltic-andesite lava flow of IAB composition.

Stage 2 (Tirohanga Member) activity constructed another IAB-type cone offset to the northeast from the main vent zone. Late-stage andesitic dykes and domes with transitional affinities subsequently crosscut the IAB cone over a wide area extending from Tirohanga to Mahaukura peak. Another large andesitic dyke with IAB composition was emplaced from the same vent system during this phase. The last Stage 2 eruption produced a basaltic flank vent at Ruapane Peak with high-K transitional affinity.

Stage 3 (Hihikiwi Member) activity began from two southern flank vents that produced a shoshonitic dome and olivine basalt lava flow, both of transitional affinity. Central edifice volcanism then constructed an IAB-type cone. Late-stage, resurgent volcanism following sector collapse of the Hihikiwi cone (Stage 4, Te Akeohikopiro Member) produced a voluminous IAB-type lava field on the southern side of Pirongia.

Following another massive sector collapse event, late-stage eruptive activity (Stage 6, Pirongia Summit Member) began initially at an eastern flank vent (Pukehoua) that produced an IAB-type basaltic lava field intercalated with at least one OIB lava flow from the same vent. Around this time, eruptions from two vents at Pirongia Summit produced ~5 km^3 of material that infilled the central collapse scarp. Transitional silicic dykes, scoria and basaltic lavas are intercalated with IAB-deposits in the upper stratigraphy of the cone, including the Pirongia summit dyke. The last eruptions of Pirongia occurred at Pūawhe/The Cone, producing andesites of IAB affinity.

Spatial distribution of Pirongia IAB, OIB and transitional volcanism

The spatial distribution of IAB, OIB and transitional rocks on Pirongia is shown in Fig. 11C. The IAB (G1) suite are the most abundant geochemical group, erupted from numerous vents dispersed in the central zone of the volcano. The main summit vents, which represent the centres of highest magma output, cluster at the intersection point of the Junction Magnetic Anomaly (a principle slip surface of the Waipa Fault Zone) and the Alexandra Volcanic Lineament. We thus consider the foci of IAB (G1) eruptions to be strongly controlled by the lineament, with secondary structural influence from upper crustal faults (i.e. the Waipa Fault Zone).

OIB (G3) occurs mainly as peripheral vents on the NW and SE flanks of Pirongia. These vent sites are closely aligned with the Alexandra Volcanic Lineament. Koponui vent (Okete Volcanics) also lies along the lineament to the NW of Pirongia (Fig. 11C). Rare outcrops of OIB within the Mangakara Valley (NE Pirongia) also appear to be associated with vents centred along the volcanic lineament. The presence of OIBs (albeit texturally diverse) in Pirongia debris avalanche deposits further suggests that a larger volume of OIB (G3) lies buried in the lower stratigraphy. This may amount to a small basal shield or lava field, as observed at the base of Karioi (Pauaeke Member).

Transitional (G2) lavas are confined to two zones, on the NE quadrant of the upper edifice and on the lower SW flank. The volume erupted from the SW flank vents appears to be significantly higher than the NE quadrant, though summit erosion makes this uncertain. The NE quadrant deposits consist of andesitic dyke swarms and basaltic eruptives, sourced from vents that fall broadly within the Alexandra Volcanic Lineament and which all occur east of the Junction Magnetic Anomaly. In contrast, the SW flank deposits are located far south of the lineament, and west of the Junction Magnetic Anomaly, but near to another meridional normal fault. Thus, the general pattern of transitional vents sites on the down-faulted side of major faults suggests that their distribution is largely controlled by upper crustal faults.

Stratovolcano time-chemistry

The temporal-geochemical evolution of Karioi and Pirongia is defined by the interplay of IAB and OIB volcanism, which is preserved in the stratigraphic record of both volcanoes (see above section). In this section, we use key isotopic and geochemical criteria ($^{143}Nd/^{144}Nd$ and Nb/La) to distinguish the relative influences of IAB and OIB on overall erupted composition through time.

Karioi

The Karioi stratigraphy is characterised by four abrupt shifts in erupted composition (Fig. 12), each separated by erosional unconformities (i.e. time breaks). Pre-Karioi volcanism (Pauaeke Member) defines a 'background' of OIB activity with typical high $^{143}Nd/^{144}Nd$ (max. 0.512936) and Nb/La (~1). All of these lavas show reversed polarity and erupted during the Gauss chron, up to 2.58 Ma (Goles et al. 1996). Lava compositions then abruptly change to IAB-type ankaramite (Te Toto Member), with uniformly low $^{143}Nd/^{144}Nd$ (0.512795–0.512806) and Nb/La (~0.3). After cessation of IAB volcanism at ~2.40 Ma, lava compositions revert to OIB (Whaanga Member) with high $^{143}Nd/^{144}Nd$ (~0.5129) and Nb/La (~1) comparable to the Pauaeke Member. Subtle enrichment of Nb/La (from 0.79 to 1.11) occurs from the oldest to youngest Whaanga lavas, consistent with the observed pattern within $^{143}Nd/^{144}Nd$. During the last stage of volcanism, a complex and more silicic stratovolcano formed (Wairake Member) with eruptions spanning from IAB to OIB compositions. Stratigraphy indicates that initial eruptions were transitional (K2), with elevated $^{143}Nd/^{144}Nd$ (0.51286), followed by widespread IAB (K1) cone-building that was capped by OIB and transitional lavas (~2.3 Ma). The second (inferred) stage of cone building, centred on Karioi summit (~2.29 Ma) produced another IAB (K1) basaltic cone capped by late-stage transitional (K2) dykes and lavas.

Pirongia

In contrast to the 'on/off' IAB-OIB systematics of Karioi, the Pirongia stratigraphy is OIB-poor and characterised by subtle, cyclical enrichment of its IAB deposits towards more Nd-radiogenic compositions with higher Nb/La ratios (Fig. 12).

Stage 1 volcanism (Paewhenua Member, ~2.6–2.42 Ma) began with coeval eruptions of IAB (G1) and OIB (G3) that transitioned into IAB-only shield building. IABs from Stage 1 and Stage 2 (Tirohanga Member) show steady and continuous enrichment from low initial values of $^{143}Nd/^{144}Nd$ (0.512770) and Nb/La (0.15) to peak values at 2.36 Ma ($^{143}Nd/^{144}Nd$=0.512801, Nb/La=0.35). The 2.36 Ma spike coincides with major eruptions of transitional (G2) composition (mainly basaltic-andesites) from the Stage 2 Tirohanga vent, which follow earlier transitional eruptions at the end of Stage 2. The convergence of the IAB (G1) and transitional (G2) trends at 2.36 Ma suggests that they are petrogenetically related, and that IAB (G1) magmas grade compositionally into transitional (G2) magmas. Isotopically, the latter show an apparent enrichment of their $^{143}Nd/^{144}Nd$ ratios from Stage 1 to Stage 2, progressing to higher ratios towards the 2.36 Ma spike.

The post-2.36 Ma spike consists of transitional (G2) flank eruptions followed by IAB cone building on the southern flank (Stage 3, Hihikiwi Member). Initial IAB lavas have low Nb/La ratios (0.12), equivalent to the early Stage 1 eruptions, indicating a 'reset' of the IAB system prior to the beginning of Stage 3 activity. Lava compositions show a similar ramping up of $^{143}Nd/^{144}Nd$ and Nb/La towards 2.2 Ma, however unlike earlier phases no transitional lavas were erupted from the central vent. Edifice collapse and resurgent volcanism at 2.1 Ma (Te Akeohikopiro Peak) was also strictly IAB type.

Late-stage resurgent volcanism occurred ~1.65 Ma with fissure eruptions on the lower eastern flank (Pukehoua). Initial erupted products were IAB (G1) type basalts with low Nb/La=0.13, overlain by at least one OIB (G3) ankaramite lava flow (high Nb/La=1.13) erupted from the same vent system. Contemporaneous vent activity at Pirongia Summit (~1.64–1.55 Ma) produced IAB (G1) basaltic dykes, pyroclastic and ankaramite lavas flows that show continuation

of the IAB (G1) enrichment trend defined by Pukehoua eruptives. The summit vent was punctuated by a switch to G2 andesitic dyke injection at 1.6 Ma. Subsequent cone-building alternated between G1 and G2 deposits, culminating with the G2 Pirongia summit dyke. Most G1 eruptives from this period, including the last-stage eruptives from the Pūawhe vent, show uniform Nd-isotope ratios ($^{143}Nd/^{144}Nd$: 0.512749–0.512759) and Nb/La (av. 0.22).

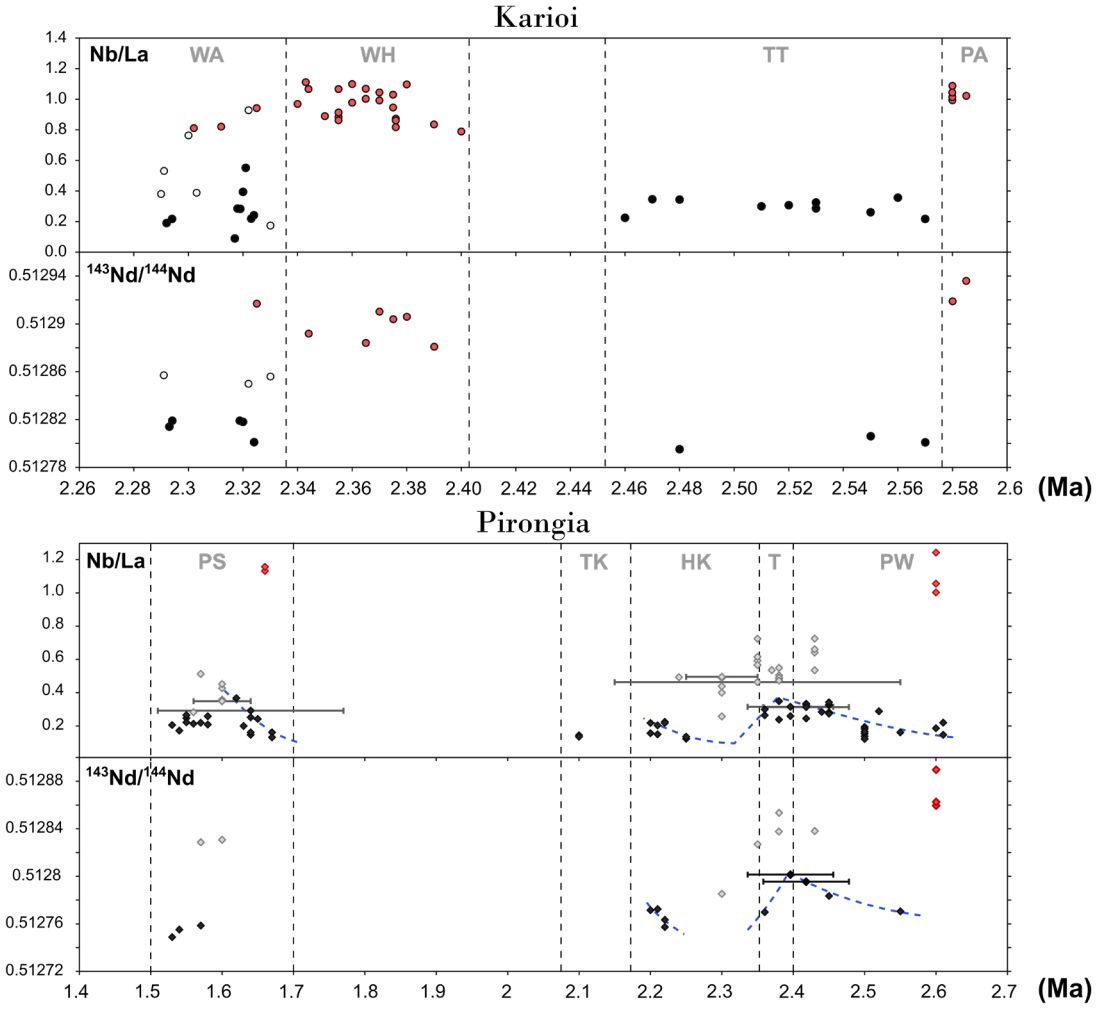

Figure 12. Temporal variations in erupted compositions (IAB, OIB and transitional) at Karioi and Pirongia stratovolcanoes. Approximate stratigraphic ages (Ma) were assigned to all volcanic rock samples using an age calibrated stratigraphy established with radiometric (K-Ar and $^{40}Ar/^{39}Ar$) dating (see Appendix 4 for all radiometric dates). Error bars are for radiometric dates. Symbols: black circles/diamonds = IAB, red circles/diamonds = OIB, grey circles/diamonds = transitional IAB-OIB. Karioi stratigraphic members: PA = Pauaeke, TT = Te Toto, WH = Whaanga and WA = Wairake. Pirongia stratigraphic members: PW = Paewhenua, T = Tirohanga, HK = Hihikiwi, TK = Te Akeohikopiro, PS = Pirongia Summit.

Spatio-chemical plots

The spatio-temporal relationships between volcanic vents and rock-chemistry within the Alexandra Volcanic Group is shown in Fig. 13. Volcanic vents are closely aligned to the Alexandra Lineament in the southeast of the field, but show progressive dispersal to the northwest, such that the Okete vents near Karioi occur up to ~12 km from the lineament (Fig. 13B). A secondary chain of vents in the far southeast of the field have an unclear relationship to the main lineament.

In general, whole-rock isotope compositions (Fig. 13C) increase in $^{143}Nd/^{144}Nd$ towards the northwest of the field (i.e. towards Karioi). The data is symbolised according to the isotopic groups (Pirongia G1–3, and Karioi K1–K3) identified in Fig. 10. Two important enrichment trends are observed: (1) the IAB-suite shows strong enrichment from Pirongia to Karioi, such that average $^{143}Nd/^{144}Nd$ increases from 0.512770 to 0.512806; and (2) the more Nd-radiogenic suite

(consisting of OIB and transitional rocks) shows a gradual enrichment of $^{143}Nd/^{144}Nd$ from Te Kawa and Kakepuku through Pirongia to Karioi. The most Nd-radiogenic Karioi rocks are isotopically equivalent to the Okete Volcanics, which exhibit uniformly high $^{143}Nd/^{144}Nd$ (~0.512930) over the 25 km segment.

The Nb/La ratio (Fig. 13D) is a useful proxy for $^{143}Nd/^{144}Nd$ systematics and allows a larger subset of samples to be compared using trace elements. Nb/La ratios for the IAB-suite are uniform from Te Kawa to Kakepuku to Pirongia (av. 0.22), but show notable enrichment in Karioi lavas (av. 0.5). Similar northwestward enrichment is observed in the transitional suite from Pirongia (av. 0.51) to Karioi (av. 0.8). The OIB suite shows progressive increases in Nb/La from Kakepuku and Pirongia (av. 1.16) through to the Okete Volcanics (~1.5) and edifice-forming Karioi lavas (1.36–2.04).

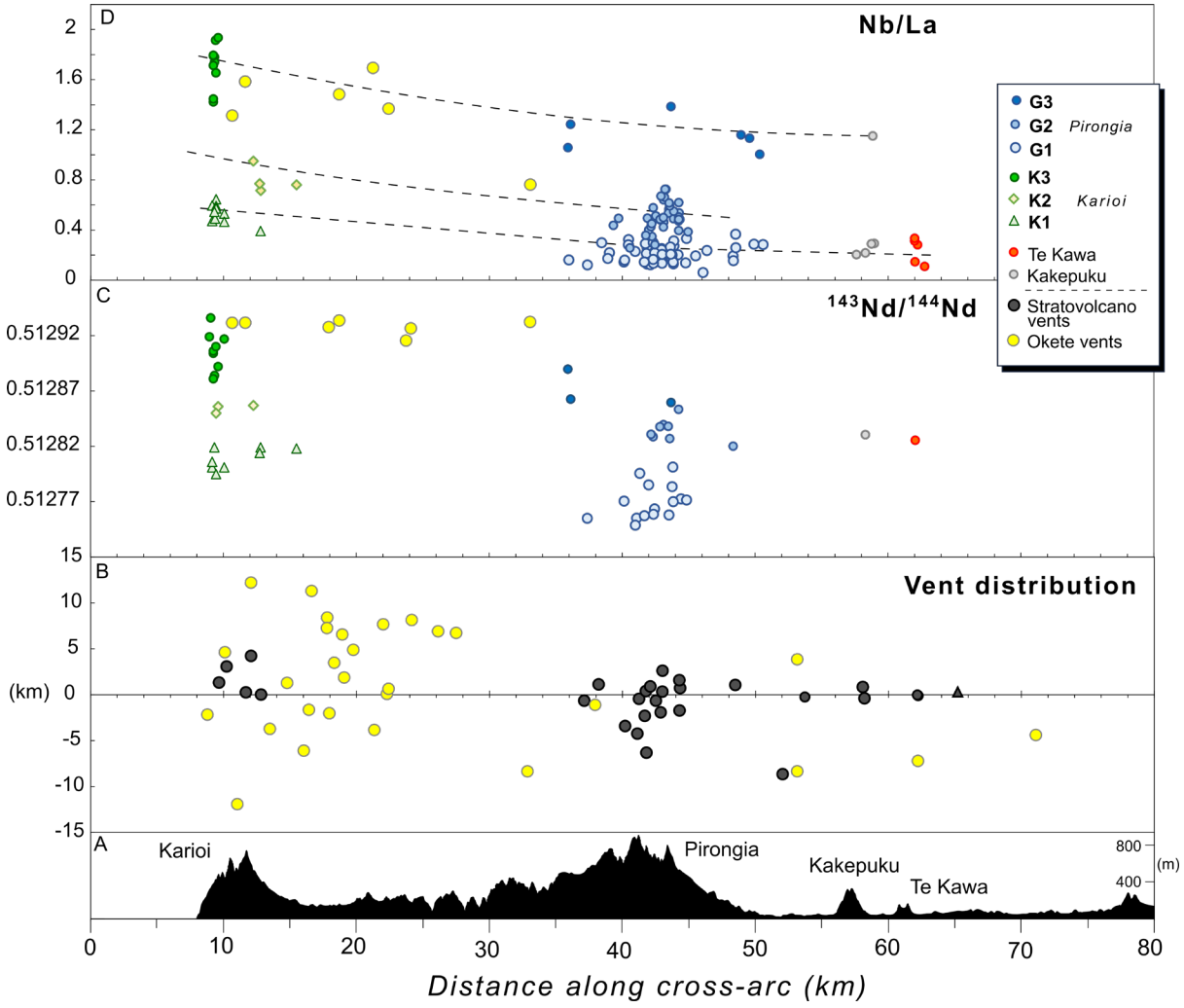

Figure 13. Spatio-chemical systematics of the Alexandra Volcanic Group, with all data plotted relative to 'distance along cross-arc' on the bottom x-axis. (A) Volcanic topography along the lineament axis. (B) Volcanic vent distribution. (C) $^{143}Nd/^{144}Nd$ along-axis variation. (D) Nb/La trace element ratio along-axis variation.

Interpretation and discussion

Source processes

IAB PETROGENESIS - OVERVIEW

The IAB elemental signature (i.e. enrichment of LILE, Pb and LREE, with depletion of HFSE) observed in the Alexandra Volcanic Group is broadly characteristic of all continental arc basalts and silicic derivatives in North Island, from the extinct Coromandel Volcanic Zone to the modern Taupo Volcanic Zone (TVZ).

There is strong consensus globally linking the source of IAB to partial melting in the mantle wedge above the subducted oceanic lithospheric slab (e.g. Kushiro, 1987; McCulloch and Gamble, 1991; Stern, 2002). During subduction, the wedge is metasomatised by hydrous subduction fluids and melts derived from metamorphic dehydrations in the down going slab (e.g. Morris et al. 1990; Plank, 2005). The resultant ultramafic metasomatites have a lower solidus temperature than normal asthenospheric peridotite (e.g. Kushiro, 2001; Kogiso et al. 2004), which may lead to partial melting either directly by fluid fluxing from the slab (e.g. Stolper and Newman, 1992; Grove et al. 2001), or through decompression of the mantle wedge (Bartels et al. 1991; Grove et al. 2002). The LILE and Pb components are added to the mantle source of IAB by the subduction fluids (e.g. Hawkesworth et al. 1991), while trace elements with higher charge density such as the HFSEs (Nb, Ta, Ti, Zr and Hf) are largely immobile in subduction zone fluids (Ringwood, 1974; Tatsumi et al. 1986; Pearce et al. 1995).

All arc volcanism in the TVZ is fundamentally a product of the active subduction margin, where fluid fluxing on the down going slab instigates partial melting of the metasomatised mantle wedge to produce IAB magmas. Rapid extension in the Taupo Rift (8 mm/yr, Darby and Meertens, 1995), caused by rotation of the Hikurangi margin (Stern et al. 2006) coupled with rollback of the Pacific Plate and subduction of the Hikurangi Plateau (Ballance et al. 1999, Reyners 2013), and accompanied by high heat flow (Rowland and Sibson, 2001) has led to extremely productive rhyolitic arc-volcanism (Wilson et al. 1995, Stern et al. 2010). These silicic magmas are ultimately fuelled by IAB parent magmas (Hildreth, 1981; Gamble et al. 1993, Wilson et al. 1995), which evolve through assimilation, fractionation and mixing to produce arc andesites and rhyolites. The near absence of arc-basalt (<1%) in the eruptive output of the TVZ (Gamble et al. 1990) may be explained by density filtering, whereby a thick underplate of low-density silicic rocks prohibits (dense) basaltic magmas from ascending to the surface (Wilson et al. 1995, Price et al. 2016).

While the Alexandra Volcanic Group IABs are more mafic than most TVZ eruptives, they follow the same trend of systematic K_2O-enrichment (Fig. 14A) observed in the modern back-arc (i.e. Egmont Volcano) relative to the arc front (i.e. Tongariro-Ruapehu) (Price et al. 1992; 1999). The Alexandra Volcanic Group shows close affinity with Egmont Volcano in terms of high-K, low SiO_2 systematics, with erupted compositions that are intermediate between Egmont andesite and its gabbroic parental rocks (Price et al. 2016). Globally, high-K volcanism is common in back-arc extensional settings where IAB and OIB magmas may interact, and can also relate to cross-arc fractures (Foden and Varne, 1983) or tears in the subducted slab (Agostini et al. 2007). Both the Alexandra and Egmont fields are similar in terms of their back-arc setting, respective volcanic alignments (NW-SE), mafic compositions (basalt to basaltic andesite) and mineralogy (Cpx+Hbl), which suggests that they share a common petrogenesis and similar structural controls (i.e. slab tear; see section below).

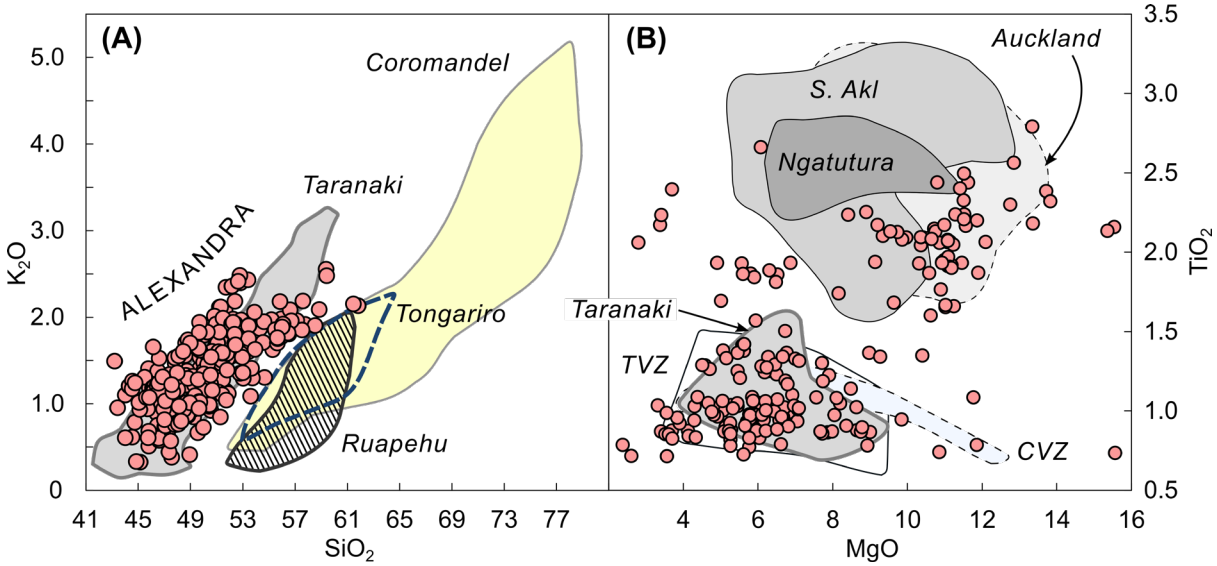

Figure 14. Regional geochemical data compilation for North Island volcanics. (A) SiO_2 v K_2O plot of arc-related mafic to silicic eruptive products of the North Island compared to Alexandra Group rocks. (B) Comparison of MgO v TiO_2 for arc and intraplate basalts. Field references: Tongariro (Hobden, 1997; Pure, 2020), Ruapehu (Conway et al, 2015; Tost et al, 2016), Coromandel (Rabone, 1975; Stokes et al, 1992; Adams et al, 1994; Krippner et al. 1998; Lindsay et al, 1999; Booden et al, 2012), Taranaki (Neall et al, 1986; Lowe, 1988; Price et al. 1992; 1996; 1999; 2016; Platz et al, 2007; Turner et al. 2008), TVZ (GEOROC database), Ngatutura (Sanders, 1994; Briggs et al. 1990), South Auckland (Rafferty et al. 1979; Cook, 2002), Auckland (McGee et al. 2013, Smith and Cronin, 2020).

OIB PETROGENESIS – OVERVIEW

OIB-type alkaline volcanism is widespread across the South Pacific (Mortimer and Scott, 2020), varying widely in terms of magnitude and longevity from large seamount chains and shield volcanoes (e.g. Thompson et al. 1998, Coombs et al. 2008, Gamble et al. 2018) to small-volume, short lived monogenetic fields (e.g. McGee et al. 2013). The composition of Alexandra OIBs is typical of Zealandia intraplate basalt (e.g. high-TiO_2 contents, Fig. 14B), which over the last 100 million years have been characterised by remarkable homogeneity in terms of geochemistry and isotopic composition (Scott et al. 2020). Two main models have been proposed to explain the petrogenesis of Zealandia OIBs. (1) Decompression melting of asthenosphere (Hoernle et al. 2006), where detachment of garnet bearing peridotite blocks at the base of the lithosphere trigger deep upwelling of a heterogeneous mantle source. (2) Shallower melting of veined mantle lithosphere (Panter et al. 2006), in which hydrous 'metasomes' are triggered to melt by conductive heating from the asthenosphere, either as a result of lithospheric delamination, thinning, or injection of hot magma into the lithosphere. A third model, proposed to explain geochemical and Sr-Nd-Pb variation of OIB within the Auckland and South Auckland volcanic fields, suggests that melting begins in the fertile, garnet-bearing asthenosphere and instigates secondary melting of metasomatised lithospheric mantle (Cook et al. 2005, McGee et al. 2013).

ISOTOPE SYSTEMATICS OF IAB AND OIB

The Sr-Nd isotope systematics of North Island volcanic fields are illustrated in Fig. 15. The isotope data define a linear array for the 'Main Arc Volcanoes' (IAB) of the CVZ and TVZ, with separate fields for Ruapehu and Taranaki, and the offshore Kermadec and Colville Ridges. Isotope compositions for this group range from $^{87}Sr/^{86}Sr$ (0.7060–0.7035) and εNd (0–8), which partially overlaps with the metasedimentary Waipapa terrane field. Intraplate (OIB-type) volcanic fields (Okete, Auckland, South Auckland and Northland) plot within a relatively small zone that has lower $^{87}Sr/^{86}Sr$ for a given εNd value than the Main Arc Volcanoes.

The Alexandra Volcanic Group have distinct Sr-Nd compositions that are transitional between the Main Arc Volcanoes and the intraplate OIB fields. The highest $^{87}Sr/^{86}Sr$ and lowest εNd values occur within Pirongia IAB (G1) rocks, which overlap with the lower edge of the TVZ basalt and Waiapapa terrane fields but are otherwise distinct from all the fields of the Main Arc

Volcanoes. Okete Volcanics have higher $^{87}Sr/^{86}Sr$ and lower εNd (~5) than the Auckland or South Auckland intraplate fields.

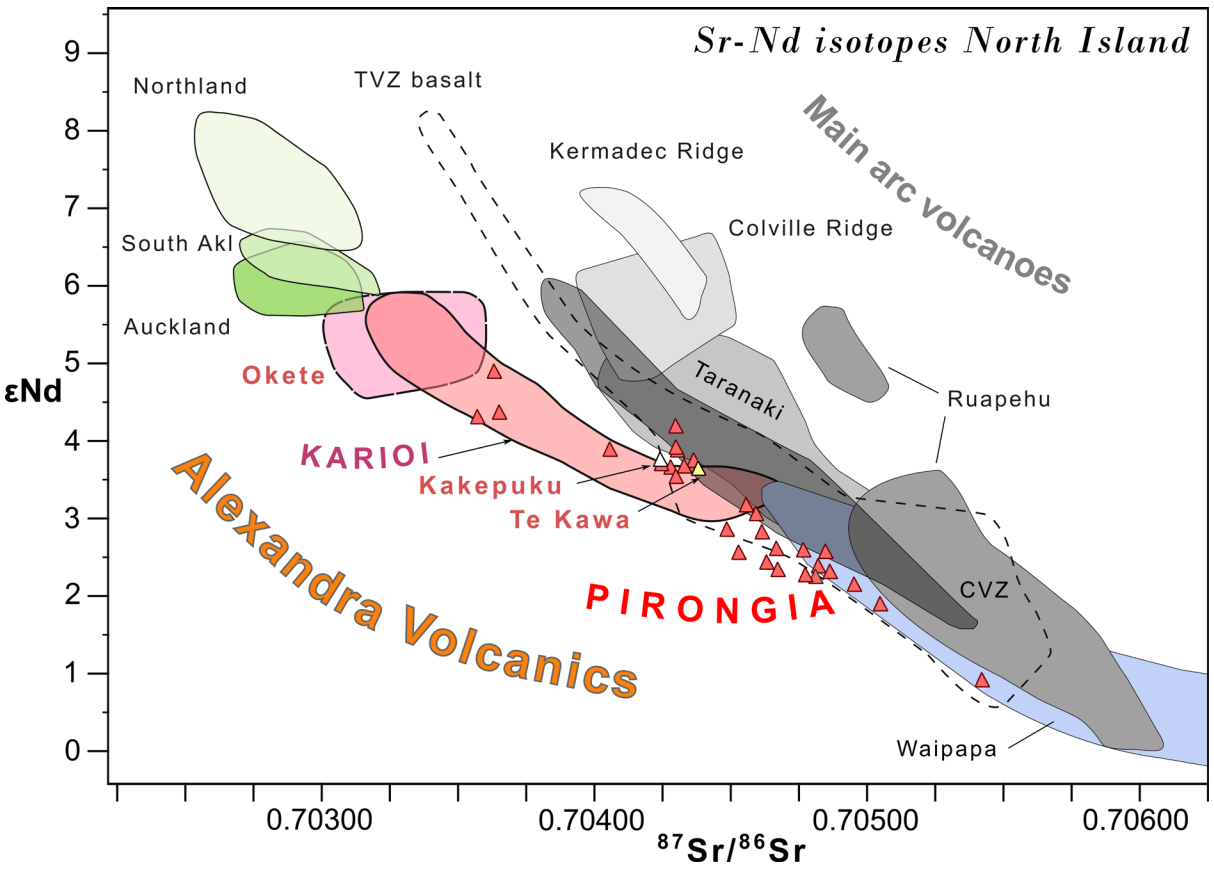

Figure 15. Regional array of Sr-Nd data for North Island volcanics, in relation to the Alexandra Volcanic Group. Isotope data sourced for non-Alexandra rocks is from the GEOROC database.

IAB-OIB magma mixing

The rock suites of Pirongia and Karioi have gradational geochemical (Fig. 9) and isotopic (Fig. 10) compositions between IAB and OIB that may relate to mixing of these two endmember magmas.

A two-component mixing model is proposed to explain the linear array of isotope values of lavas from Pirongia Volcano (Fig. 16B) for which the most data is available. Endmember compositions selected were 'average Okete' ($^{87}Sr/^{86}Sr$=0.703338, $^{143}Nd/^{144}Nd$=0.512929) and the most Sr-radiogenic IAB basalt of Pirongia (PW10; $^{87}Sr/^{86}Sr$ =0.705047, $^{143}Nd/^{144}Nd$ =0.512736). Note: another more Sr-radiogenic sample (Ph5 basalt) was not used due to possible alteration.

The model shows that isotopic variation in the Pirongia suite can be explained by small amounts of mixing for G1 (5–32% OIB), moderate mixing for G2 (43–58% OIB) and high mixing for G3 (70–81% OIB). The relatively low degree of scatter along the mixing line suggests that a simple two component mixing model is appropriate. The scatter may be explained by heterogeneity of the true Okete OIB end member(s), which show variation in terms of $^{87}Sr/^{86}Sr$ (see Fig. 10). Heterogeneity of the IAB endmember(s) is also likely, though this variation is probably small or equivalent to that of the Okete field, which already accounts for the overall deviation of some Pirongia samples from the mixing line.

Application of the mixing model to trace elements (Fig. 16A) shows that intermediate trace element patterns can be generated by mixing variable amounts of the IAB (PW10) and OIB (average Okete) endmember compositions. In particular, mixing of 25–30% OIB with IAB is able to replicate the characteristic subdued Nb-Ta anomalies observed in Pirongia transitional (G2)

rocks (see average G2 line in Fig. 16B). Total variation in Nb-Ta for the G2 suite (see Fig. 9B) amounts to 20–45% mixing of OIB with IAB. The mixing model is able to replicate the overall G2 pattern, except for the incompatible elements (Cs, Rb, Ba, Th) which have higher abundances in the natural G2 average line. Such enrichment is likely the result of fractional crystallisation processes that are not accounted for in the mixing model.

There is a moderate discrepancy between the isotope and trace element mixing proportions (43–58% and 25–45% respectively) required to generate transitional (G2) compositions. This discrepancy stems from selection of the IAB endmember PW10, which may not equate directly to the true IAB endmember composition of Pirongia Volcano. The natural endmember likely contains slightly higher $^{87}Sr/^{86}Sr$, lower $^{143}Nd/^{144}Nd$ and a more pronounced Nb-Ta anomaly. A possible IAB endmember is Kakepuku ankaramite, which contains the extreme Nb and Ta anomalies (see Fig. 9E) required to couple the trace element and isotopic mixing proportions on Pirongia.

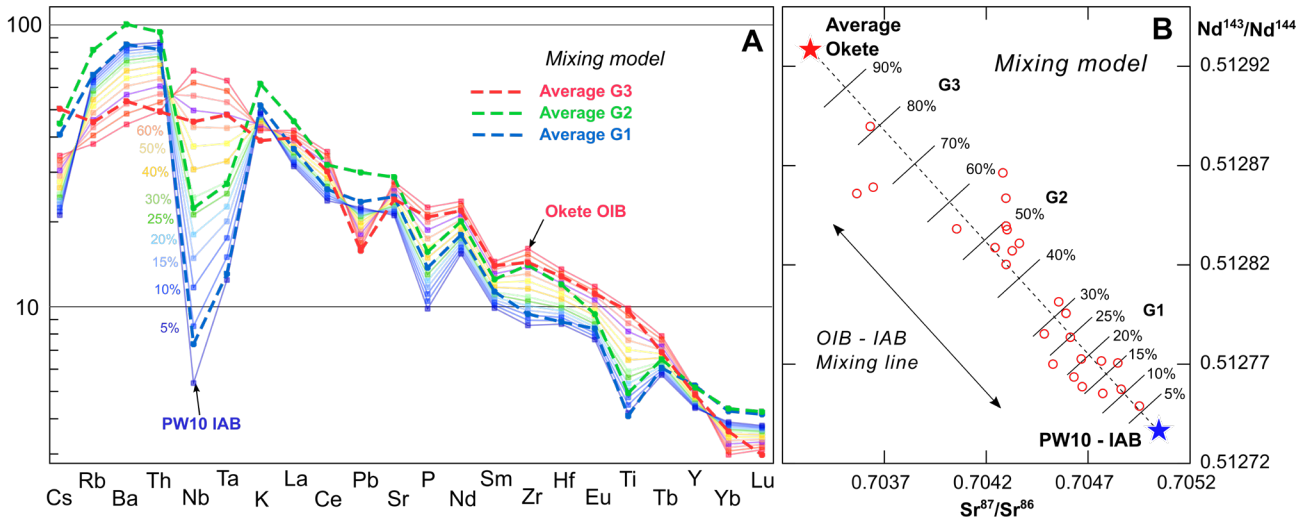

Figure 16: Two component linear mixing model for IAB-OIB to explain the (A) trace element variation and (B) isotopic variation of lavas from Pirongia Volcano. Trace element data are normalised to Primitive Mantle (Sun and McDonough, 1989).

IAB-OIB eruption cyclicity in the AVG

Both Karioi and Pirongia volcanoes exhibit chemical cyclicity in terms of IAB-OIB eruptive composition, with each volcano displaying subtle yet contrasting modes of behaviour (see Fig. 10). At both volcanoes, we observe early bi-modal IAB-OIB volcanism, which implies a close source or triggering relationship between the two magma types.

At Pirongia, erupted IABs show gradual enrichment in $^{143}Nd/^{144}Nd$ and Nb/La ratios towards transitional compositions that we interpret as signs of progressive contamination by OIB magmas recharging the magmatic system over time. Not only does this imply the omnipresence of OIB in the volcanic system, but this pattern suggests that the source of the OIB magmas is deeper, and fundamentally driving, IAB volcanism.

In contrast to Pirongia, Karioi shows 'on/off' switches between OIB and IAB, with IAB phases showing no signs of progressive contamination by OIB. Transitional (K2) compositions are restricted to the Wairake Member and are most prominent near the summit of the volcano. This indicates that transitional magmas at Karioi are linked to late-stage, large volume edifice-building phases, and may be related to progressive contamination as observed on Pirongia. With finer detailed sampling in the future, this trend may become apparent.

The proportion of IAB relative to OIB shows significant variation between the two stratovolcanoes, such that OIB constitutes ~45% of the Karioi edifice but only ~5% of Pirongia.

We conclude that the productivity of OIB magmatism exerts a first order control on the magma system, with lower output leading to progressive contamination of the IAB magmas, and higher output generating more pure 'on/off' bi-modal IAB-OIB volcanism.

Evidence for spatial variation in mantle-wedge chemistry

Spatio-chemical variation in lava compositions along the Alexandra cross-arc is a useful indicator of mantle source heterogeneity and the metasomatic influence of the subducted slab on the mantle wedge. Among the IAB suite, we observed systematic enrichments in $^{143}Nd/^{144}Nd$ and Nb/La from southeast to northwest (Fig. 13) that correspond to increasing slab depth. We argue that the observed enrichment pattern reflects a metasomatic gradient in the mantle wedge, where IABs generated further from the trench (i.e. Karioi) have lower subduction components (high $^{143}Nd/^{144}Nd$ and Nb/La) than IABs generated closer to the trench (i.e. Pirongia). Conversely, OIB lavas of the Okete and Karioi volcanics display uniformly high $^{143}Nd/^{144}Nd$ across the volcanic field that indicate a homogeneous source zone for these magmas that is independent from the (gradient controlled) metasomatized mantle wedge. Interestingly, ankaramite-type OIBs within the Pirongia stratigraphy are less Nd-radiogenic than other OIBs of the AVG, suggesting low-degree contamination by IAB melts and thus some influence from the gradient controlled mantle wedge in their formation.

Storage and formation of ankaramites

Megacrystalline basalts (i.e. ankaramites) comprise ~70% of all material erupted in the AVG and are thus crucial rocks for interpreting the petrogenesis of IAB and OIB in the volcanic field. Most, but not all AVG ankaramites have strong IAB compositions, with rare examples of OIB-ankaramite occurring at flank vents on Pirongia and Kakepuku, and transitional high-K ankaramites on the upper Pirongia flanks.

While ankaramites do not occur outside of the AVG in New Zealand, these rocks are widespread in the South Pacific on (OIB-type) ocean islands, e.g. Tahiti (McBirney and Aoki, 1968), Rarotonga (Thompson et al. 1998) and Samoa (Stice and McCoy, 1968), and IAB-type ankaramites also occur in some local arcs, e.g. Vanuatu (Peate et al. 1997) and Indonesia (Elburg et al. 2007).

In the AVG, texturally distinct ankaramites have erupted along a 50 km transect at four separate volcanoes, which range widely in edifice volume (0.1–30 km^3). Stratigraphy presented in this study and in McLeod et al. (2020) indicates that ankaramites erupt in large volumes during the initial stages of volcanism, e.g. Paewhenua Member (Pirongia) and Te Toto Member (Karioi), and eruptions may occur contemporaneously at more than one volcano (e.g. Pirongia and Karioi (2.5 Ma), or Kakepuku and Te Kawa (2.7 and 2.3 Ma). This indicates that ankaramite petrogenesis is irrespective of edifice size or size of the sub-edifice plumbing system and is instead related to sub-crustal processes capable of generating large volumes of megacrystalline magma. Ankaramite formation has been previously linked to clinopyroxenites, which either disaggregate into basaltic melts (Foden and Varne, 1983) or melt directly (Georgiev et al. 2009). These dense, crystal-laden magmas are then upwelled to the surface during extension or rifting events (Maaloe et al. 1986, Hammer et al. 2016), or following massive sector collapse (Longpré et al. 2009).

We envisage that AVG ankaramites began formation as IAB-type basaltic magmas that underplated the crust along the entire ~50 km length of the volcanic field. The underplate zone was characterised by variations in thickness associated with block faulting in the crust, which acted as traps to pool the magmas. Prolonged crystallisation of mafic, hydrous IAB-type magma (and some OIB magmas) formed clinopyroxene-rich mushes with the assemblage Cpx+Ol+Mag. Trace element chemistry indicates that Cpx-megacrysts have inherited the distinct IAB, OIB or transitional compositions of their host magmas (Fig. 7), which implies that mixing of IAB-OIB occurred at greater depths in the mantle prior to underplating. Underplating is supported by

preliminary thermobarometry experiments on megacrysts (using the Cpx-liquid barometer of Putirka, 2008), which indicate maximum formation pressures of 5–6 kbar and depths of 20–23 km, corresponding to the base of the crust (25±3 km thick; Stern, 1985)

Eruption of the crystal-mushes was triggered by major extensional tectonic events, probably associated with normal faulting along the horst graben structures of western Waikato (e.g. Hamilton Basin). These events destabilised the crystal-mushes spread across the underplate zone and prompted rapid upwelling and eruption of crystal-laden magmas across a wide zone in the volcanic field. Evidence of rapid magma ascent is preserved in Cpx-megacrysts which were physically abraded and rounded during transport (see Fig. 5I).

Link to tectonics

Local structural controls on IAB-OIB magmatism

The AVG stratovolcanoes are situated at major junctions in the crust where the volcanic lineament (AVL) is intersected by north-south striking regional faults (McLeod et al. 2020). The two largest stratovolcanoes of Pirongia and Karioi directly overlie major graben boundaries (Hamilton Basin and the offshore west coast respectively) on opposing sides of the Karioi horst block, while Kakepuku and Te Kawa lie along subsidiary strands of the Waipa Fault Zone. This tectono-magmatic relationship suggests that the volume of IAB magma erupted at any AVG vent is proportional to the magnitude of normal faulting.

Finer-scale variation is observed in the distribution of OIB and transitional vents. The OIB vents show close alignment to the AVL in the southeast of the field, but become increasingly dispersed to the northwest of Pirongia, where they occur along normal faults and have higher eruptive volumes and vent densities. This pattern suggests that the structural influence of the AVL on OIB vent diminishes to the northwest, and the role of crustal faults increases. The exception to this trend is Karioi Volcano, the locus of large-volume OIB eruptions in the volcanic field, which lies directly on the AVL in the north-western edge of the field. This suggests a space-volume relationship for OIB, where the large-volume, sustained fluxes of OIB magma (i.e. at Karioi) are controlled by the AVL, while smaller volume fluxes produce scattered vents in the proximal area.

Transitional IAB-OIB vents occur in the summit zones of Karioi and Pirongia. At Pirongia, strong fault control is evident in the location of transitional (G2) summit vents, which occur within the down faulted (eastern) block of the Waipa Fault Zone. A similar structural control is proposed for Pirongia G2 flank vents. Transitional (K2) vents at Karioi summit appear to also show structural preference for the downfaulted (western) block. Further mapping is required to confirm this relationship.

The Alexandra Volcanic Lineament – caused by slab tear?

Historical explanations for the AVL included fault control along a NW-SE striking crustal fault (Henderson and Grange, 1926), possibly deep-seated within the Mesozoic basement rocks (Kear, 1960), that formed in response to extensional stress perpendicular to the subduction margin (Briggs, 1983). However, no major NW-SE striking faults are mapped within the AVG – or even within the wider western North Island – that are concordant with the AVL. The possibility of a concealed fault in the lower crust appears unlikely, given the clear surface manifestation of deep crustal structures within the field area (e.g. the Hamilton Basin graben, and Karioi horst block).

Instead, the AVL may have formed in response to a deeper zone of weakness within the mantle, such as a linear tear on the subducted Pacific slab, as proposed by Briggs & McDonough (1990). A necessary precondition for this explanation is that the slab must have existed beneath the AVG during the main period of volcanism (2.7–2.0 Ma). In the present configuration, the slab terminates at the eastern edge of the field, where it is vertical and 300 km deep (Reyners et al. 2011).

The south-eastward migration of volcanic front arcs in Northern New Zealand since 16 Ma indicates temporal changes in the geometry of the subducted Pacific slab. Based on the present depth to slab of the modern TVZ (90±15 km), we assume that the ancient arc fronts mark the 90 km slab contour wherever they occur. Since 7 Ma, the arc migration rate has been 18±3 mm a^{-1} (Seebeck et al. 2014), which corresponds to the arc being ~45 km northwest of the TVZ at 2.5 Ma. This is temporally consistent with rhyolitic volcanism in the Tauranga area (3–2 Ma, Briggs et al. 2005) marking the front arc at time of the AVG activity, which occurred 20–75 km behind this arc front. Based on modern slab geometry, the position of the Tauranga arc implies that the slab would be subvertical (>200 km deep) 75 km west of the arc, which corresponds exactly to the distance from the arc front to Karioi, i.e. the western extent of back-arc volcanism.

If the AVG is related to a major slab tear, this tear will have migrated southwest since volcanism ceased at ~2 Ma). Assuming a constant motion vector for the Pacific Plate of 42 mm yr^{-1} (DeMets, 1994), this amounts to 84 km of net migration to the WSW. This would place the modern tear position ~50 km south of Pirongia, which very closely corresponds to the position and strike (313º) of a regional-scale slab tear proposed by Reyners (1989), one of five tears proposed on the basis of discontinuities in the distribution of earthquakes in mid to lower North Island (refer to Fig. 1). We argue that the AVL is consistent with a slab tear control, where the tear edge coincides with scattered vent distribution (i.e. Karioi-Okete area) and the inner part of the tear corresponds with sharply aligned vents (i.e. Pirongia, Kakepuku, Te Kawa and adjacent Okete vents). The tear in the down going Pacific Plate has formed a linear zone of focused melting (60 km long) in the mantle wedge above the slab leading to volcanism.

Subduction-related volcanic alignments of similar size and orientation occur elsewhere in North Island (Kear, 1964, see Fig. 1)), including the Taranaki volcanics (330º), Kiwitahi (300º) and Maungatautari (295º) and offshore in the Colville Ridge and Kermadec Arc (306–309º; Wysoczanski et al. 2010). In the Kermadec Arc, these 'cross-arc' chains, e.g. Rumble V Ridge, have been related broadly to monotonic migration of the melt source eastward across the back-arc (Wright et al. (1996; 1997) but this has been discredited in more recent bathymetric surveys (Wysoczanski et al. 2010). The mantle 'hot-finger' model, originally applied to explain the anomalous thermal regimes of the mantle wedge in the Japan Arc (Tamura et al. 2002; Tamura 2003), was used to explain the thermal structure and composition of the Kermadec cross arcs (Todd et al. 2011). Although the northwestward (down-slab) transition from IAB to OIB in the AVG is broadly consistent with the pattern observed in the Japan Arc, the AVG is far more geographically isolated from its neighbouring cross arcs (170 km to the Taranaki Volcanics) than in Japan (22±16 km) or the Kermadec arc (~80 km).

Existing models for IAB-OIB volcanism

OIBs in volcanic arcs occur at various locations around the Pacific Rim, including western USA and Mexico, the Caribbean, Japan and Vanuatu (see introduction), where their occurrence generally coincides with zones where the arcs meet back-arc extension (e.g. Reagan and Gill, 1989, Hildreth 2007), or are defined by complex tectonic-magmatic settings, e.g. triple-junctions (e.g. Márquez et al. 1999). Outside of the AVG, examples of OIB intercalated with IAB in the stratigraphy of stratovolcanoes are very rare globally, occurring on flank vents of Mt St Helens, western USA (Leeman and Smith, 2018; Wanke et al. 2019) and in the oldest and youngest stages of volcanism at Turrialba, Costa Rica (Reagan and Gill, 1989). In both cases, OIB appears to constitute only a minute fraction of the total erupted volume. There is broad consensus linking the source of bi-modal IAB-OIB volcanism to the melting of compositionally heterogeneous mantle wedge material (Ferrari et al. 2001, Hildreth, 2007), where the slab-flux metasomatised mantle lies interspersed with HFSE-enriched domains or sheets that are little affected by slab flux. The latter may be introduced to the wedge either laterally by wedge corner flow or vertically

through fractures, tears or gaps in the subducted slab (Hildreth 2007, Mullen et al. 2017). In the case of wedge corner flow, the upwelling of asthenosphere may occur following slab rollback, which induces a lateral flow of asthenosphere into the mantle wedge (Ferrari et al. 2001). Melting of both heterogeneous mantle wedge components may occur by direct fluid-flux melting from the slab (e.g. Ferrari et al. 2001; Strong and Wolff, 2003) or the depleted-MORB component may melt via decompression melting associated with asthenospheric advection (Hochstaedter et al. 1996; Luhr, 1997). As an alternative, the source of OIB has been linked to mantle plumes in the back-arc rift setting of the western Trans Mexican Volcanic Belt (Moore et al. 1994; Márquez et al. 1999). However, the plume model is inconsistent with the overall low volume of OIB relative to IAB in the arc, which indicates the IAB mantle source has not been displaced, as well as the lack of OIB age progression predicted by plate motion (Ferrari et al 2001).

Model for bimodal IAB-OIB volcanism in the AVG

We propose a new tectono-magmatic model to explain bimodal IAB-OIB volcanism in the AVG that is consistent with the field observations, geochemistry and isotope data presented in this paper.

In our model (Fig. 17), the down going Pacific Plate underlies the volcanic field and reaches sub-vertical inclination (>200 km depth) at Karioi. The slab in this area contained a prominent tear with 300º (NW-SE) orientation. The mantle wedge above the slab was metasomatized over millions of years by slab fluid-fluxing, with the degree of metasomatism decreasing to the northwest (i.e. away from the trench). Back-arc extension in the crust caused by slab roll back was ongoing from 4–3 Ma, forming horst and graben structures exemplified by the Hamilton Basin and Karioi horst block. Slab roll back, and associated extension within the block-fault structures, triggered the sub-slab asthenosphere to upwell laterally around the edge of the slab, and to flow vertically through the slab tear. Decompression of the upwelling asthenosphere led to partial melting, forming OIB-type magmas above the slab. OIB generation was most prolific near the edge of the slab (i.e. below Karioi) where lateral flow was highest. Some OIB magmas ascended through the wedge and were channelled along crustal faults, erupting as monogenetic vents that increased in volume and vent density away from the trench. The thermal anomalies caused by OIB magma generation led to secondary conductive melting of the metasomatized mantle wedge, forming IAB-type magmas. The IAB (and some OIB and mixed-transitional) magmas ascended to the base of the crust and formed an underplated zone, ~50 km long, that was thickest where fault-controlled steps in the crust occurred (i.e. below Pirongia and Karioi). This led to the prolonged crystallisation and the formation of clinopyroxene-rich crystal mushes. During major extensional events in the back-arc, these mush zones were destabilised and entrained to the surface by fresh, upwelling IAB magmas. The resultant megacrystalline basaltic lavas (ankaramites) were erupted in large volumes, closely spaced in time across multiple vents in the volcanic field. Both IAB and OIB magmas continued to feed the system, developing complex sub-volcanic magma chambers beneath the main loci zones of magma flux (i.e. the stratovolcanoes) where fractional crystallisation occurred. The continual flux of OIB into the Pirongia IAB reservoirs led to progressive mixing/contamination and the formation of transitional IAB-OIB magmas, while at Karioi, the effects of back-arc extension led to large volume generation of OIB which then triggered secondary IAB-type magmatic activity.

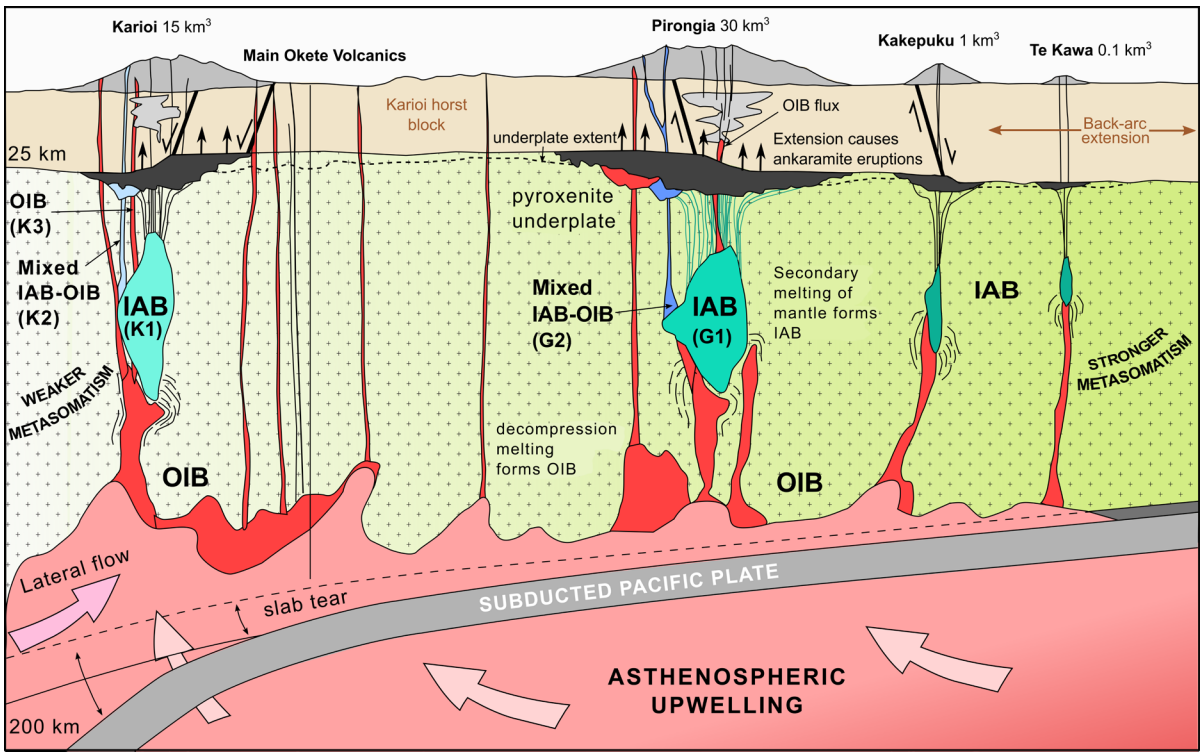

Figure 17. Schematic model of slab interactions and magma petrogenesis in the Alexandra Volcanic Group. The model begins with subduction and fluid fluxing of the Pacific Plate, which produces a metasomatic gradient in the mantle wedge. Regional-scale slab tearing results in asthenospheric upwelling and lateral flow through and around the slab in the back-arc region. This asthenosphere decompresses and melts to form OIB, which ascends and erupts sporadically. Areas of high OIB-magma productivity generate secondary melting of the mantle wedge, forming IAB magmas. These magmas ascend and underplate the crust, forming crystal mush zones. Extensional tectonic events associated with back-arc extension trigger the release of these mushes along with fresh melt, leading to large-scale ankaramite eruptions. Mixing of IAB and OIB magmas occurs in the mantle wedge, and also in crustal magma chambers of the largest stratovolcanoes, forming transitional magmas. Continued OIB fluxes manifest as periods of OIB shield building (i.e. Karioi) or as progressive contamination of IAB sources (i.e. Pirongia).

Conclusions

The Alexandra Volcanic Group of North Island, New Zealand is a classic site of back-arc volcanism, where island arc (IAB) and ocean island (OIB) basalt occur closely intercalated in space and time. In this study we have used detailed stratigraphy, petrography, mineral chemistry, whole-rock geochemistry and isotope data to resolve fine details of IAB-OIB systematics at basaltic stratovolcanoes and their surrounding monogenetic fields.

Our results show that all eruptives in the AVG have geochemical and isotope compositions falling on a spectrum between IAB and OIB endmembers. With increasing distance from the trench, the arc signature wanes and OIB becomes increasingly prevalent in terms of erupted composition and volume.

In the AVG, OIB forms dispersed monogenetic vents, but also influences the compositions of the stratovolcanoes. In the far back-arc, this OIB volcanism manifests as distinct 'on/off' eruption pulses alternating with IAB, whereas further trenchward it exhibits a more cryptic influence through progressive contamination of IAB by continuous injection into the sub-volcanic magma system. In either case, OIB magmas appear to be the fundamental driver of volcanic activity.

We identify slab tear and back-arc extension as fundamental tectonic factors responsible for the juxtaposition of distinct mantle sources that give rise to IAB and OIB. This is broadly consistent with the tectonic-magmatic setting of other co-magmatic suites globally.

This study may have important implications for the inception of intraplate volcanism in Northern New Zealand. It may be that lateral flow around the edge of the subducted slab, established during the time of AVG volcanism around 2.7 Ma, has continued to propagate north-westward to the present day, where OIB-activity continues in the active Auckland Volcanic Field.

Acknowledgements

This paper benefited from unpublished stratigraphic-chemical work on Karioi (1991–1996) by the late Gordon Goles (University of Oregon). OEM was supported by a University of Waikato Doctoral Scholarship. Additional funding came from the Hutton Fund (Royal Society of New Zealand). Isotope analyses were conducted by Bruce Charlier, Victoria University. XRF and LA-ICPMS were facilitated by A. Rodgers and K. Vincent, and A. French (University of Waikato) respectively.

References

Adams CJ, Graham IJ, Seward D, Skinner DNB, Adams CJ, Skinner DNB, Moore PR 1994. Geochronological and geochemical evolution of late Cenozoic volcanism in the Coromandel Peninsula, New Zealand. New Zealand Journal of Geology and Geophysics 37(3), 359–379.

Agostini S, Doglioni C, Innocenti F, Manetti P, Tonarini S, Savasçin MY 2007. The transition from subduction-related to intraplate Neogene magmatism in the Western Anatolia and Aegean area. Special Papers - Geological Society of America, 418.

Balance PF, Ablaev AG, Pushchin IK, Pletnev SP, Birylina MG, Itaya T, Follas HA, Gibson GW 1999. Morphology and history of the Kermadec trench-arc-backarc basin-remnant arc system at 30 to 32°S: geophysical profile, microfossil and K–Ar data. Mar. Geology 159, 35–62.

Bartels KS, Kinzler RJ, Grove TL 1991. High pressure phase relations of primitive high-alumina basalts from Medicine Lake volcano, northern California. Contributions to Mineralogy and Petrology 108, 253–270.

Beccaluva L, Bianchini G, Natali C, Siena F 2011. Geodynamic control on orogenic and anorogenic magmatic phases in Sardinia and Southern Spain: Inferences for the Cenozoic evolution of the western Mediterranean. Lithos 123(1-4), 218–224.

Booden MA, Smith IEM, Mauk JL, Black PM 2012. Geochemical and isotopic development of the Coromandel Volcanic Zone, northern New Zealand, since 18 Ma. Journal of Volcanology and Geothermal Research 219, 15–32.

Briggs RM 1983. Distribution, form and structural control of the Alexandra Volcanic Group, North Island, New Zealand. New Zealand Journal of Geology and Geophysics 26, 47–55.

Briggs RM 1986. Volcanic rocks of the Waikato Region, western North Island, and some possible petrologic and tectonic constraints on their origin. In: Smith IEM Late Cenozoic volcanism in New Zealand: a collection of papers dealing with the nature and distribution of Late Cenozoic volcanic activity in New Zealand. 76-91.

Briggs RM and Goles GG 1984. Petrological and trace element geochemical features of the Okete Volcanics, western North Island, New Zealand. Contributions to Mineralogy and Petrology 86, 77–88.

Briggs RM, Houghton, BF, McWilliams M, Wilson CJN 2005. $^{40}Ar/^{39}Ar$ ages of silicic volcanic rocks in the Tauranga-Kaimai area, New Zealand: Dating the transition between volcanism in the Coromandel Arc and the Taupo Volcanic Zone. New Zealand Journal of Geology and Geophysics 48(3), 459–469.

Briggs RM, Itaya T, Lowe DJ, Keane AJ 1989. Ages of the Pliocene-Pleistocene Alexandra and Ngatutura Volcanics, western North Island, New Zealand, and some geological implications. New Zealand Journal of Geology and Geophysics 32, 417–427.

Briggs RM, McDonough WF 1990. Contemporaneous convergent margin and intraplate magmatism, North Island, New Zealand. Journal of Petrology 31(4), 813–851.

Briggs RM, Okada T, Itaya T, Shibuya H, Smith IEM 1994. K-Ar ages, paleomagnetism, and geochemistry of the South Auckland Volcanic Field, North Island, New Zealand. New Zealand Journal of Geology and Geophysics 37,143-153.

Caroff M, Maury RC, Cotten J, Clément JP 2000. Segregation structures in vapor-differentiated basaltic flows. Bulletin of Volcanology 62(3), 171–187.

Conway CE, Townsend DB, Leonard GS, Wilson CJN, Calvert AT, Gamble JA 2015. Lava-ice interaction on a large composite volcano: a case study from Ruapehu, New Zealand. Bulletin of Volcanology 77(3), 21.

Cook C 2002. Petrogenesis and evolution of alkalic basaltic magmas in a continental intraplate setting: the South Auckland volcanic field, New Zealand (Doctoral dissertation, University of Waikato).

Cook C, Briggs RM, Smith IEM, Maas R 2005. Petrology and geochemistry of intraplate basalts in the South Auckland Volcanic field, New Zealand: evidence for two coeval magma suites from distinct sources. Journal of Petrology 46(3), 473–503.

Coombs DS, Adams CJ, Roser BP, Reay A 2008. Geochronology and geochemistry of the Dunedin Volcanic Group, eastern Otago, New Zealand. New Zealand Journal of Geology and Geophysics 51(3), 195–218.

Darby DJ, Meertens CM 1995. Terrestrial and GPS measurements of deformation across the Taupo back arc and Hikurangi forearc regions in New Zealand. Journal of Geophysical Research: Solid Earth 100(B5), 8221–8232.

DeMets C, Gordon, RG, Argus DF, Stein S 1994. Effect of recent revisions to the geomagnetic reversal time scale on estimates of current plate motions. Geophysical research letters 21(20), 2191–2194.

Elburg MA, Kamenetsky VS, Foden JD, Sobolev A 2007. The origin of medium-K ankaramitic arc magmas from Lombok (Sunda arc, Indonesia): Mineral and melt inclusion evidence. Chemical Geology 240(3–4), 260–279.

Ferrari L, Petrone CM, Francalanci L 2001. Generation of oceanic-island basalt–type volcanism in the western Trans-Mexican volcanic belt by slab rollback, asthenosphere infiltration, and variable flux melting. Geology 29(6), 507–510.

Foden JD, Varne R 1983. Arc ankaramites, Sangeang Api xenoliths and cordilleran ultramafic to dioritic intrusive complexes: an updated concept of arc growth and development. Abst 6th Aust Geol Conven, Canberra, 153–154.

Gamble JA, Adams CJ, Morris PA, Wysoczanski RJ, Handler M, Timm C 2018. The geochemistry and petrogenesis of Carnley Volcano, Auckland Islands, SW Pacific. New Zealand Journal of Geology and Geophysics 61(4), 480–497.

Gamble JA, Smith IEM, Graham IJ, Kokelaar BP, Cole JW, Houghton BF, Wilson CJ 1990. The petrology, phase relations and tectonic setting of basalts from the Taupo Volcanic Zone, New Zealand and the Kermadec Island Arc-Havre Trough, SW Pacific. Journal of Volcanology and Geothermal Research 43(1–4), 253–-270.

Gamble JA, Smith IEM, McCulloch MT, Graham IJ, Kokelaar BP 1993. The geochemistry and petrogenesis of basalts from the Taupo Volcanic Zone and Kermadec Island Arc, SW Pacific. Journal of Volcanology and Geothermal Research, 54(3–4), 265–290.

Georgiev S, Marchev P, Heinrich CA, Von Quadt A, Peytcheva I, Manetti P 2009. Origin of nepheline-normative high-K ankaramites and the evolution of Eastern Srednogorie arc in SE Europe. Journal of Petrology 50(10), 1899–1933.

GEOROC geochemical database. Max Planck Institute for chemistry, Mainz, Germany. http://georoc.mpch-mainz.gwdg.de/georoc/.

Gill J and Whelan P 1989. Postsubduction Ocean Island Alkali Basalts in Fiji. Journal of Geophysical Research 94 (B4), 4579–4588.

Goles GG, Briggs RM, Rosenberg MD 1996. Late Pliocene stratigraphic succession and volcanic evolution of Karioi volcano, western North Island, New Zealand. New Zealand Journal of Geology and Geophysics 39, 283-294.

Grove T, Parman S, Bowring S, Price R, Baker M 2002. The role of an H_2O-rich fluid component in the generation of primitive basaltic andesites and andesites from the Mt. Shasta region, N California. Contributions to Mineralogy and Petrology 142(4), 375–396.

Hammer J, Jacob S, Welsch B, Hellebrand E, Sinton J 2016. Clinopyroxene in postshield Haleakala ankaramite: 1. Efficacy of thermobarometry. Contributions to Mineralogy and Petrology 171:7.

Harangi S, Jankovics MÉ, Sági T, Kiss B, Lukács R, Soós I 2015. Origin and geodynamic relationships of the Late Miocene to Quaternary alkaline basalt volcanism in the Pannonian basin, eastern–central Europe. International Journal of Earth Sciences 104(8), 2007–2032.

Hart SR, Zindler A 1986. In search of a bulk-Earth composition. Chemical Geology 57(3–4), 247–267.

Hawkesworth CJ, Hergt JM, Ellam RM, McDermott F 1991. The Behaviour and Influence of Fluids in Subduction Zones. Philosophical Transactions of the Royal Society of London 335, 393–405.

Henderson J, Grange LI 1926. The geology of the Huntly-Kawhia Subdivision. New Zealand Geological Survey bulletin 28, 112.

Herzer RH 1995. Seismic stratigraphy of a buried volcanic arc, Northland, New Zealand and implications for Neogene subduction. Marine and petroleum geology 12(5), 511–531.

Hildreth W 1981. Gradients in silicic magma chambers: implications for lithospheric magmatism. Journal of Geophysical Research: Solid Earth 86(B11), 10153–10192.

Hildreth W 2007. Quaternary magmatism in the Cascades: Geologic perspectives (No. 1744). US Geological Survey.

Hobden BJ 1997. Modelling magmatic trends in time and space: eruptive and magmatic history of Tongariro volcanic complex. Unpublished PhD thesis, University of Canterbury.

Hochstaedter AG, Ryan JG, Luhr JF, Hasenaka T 1996. On B/Be ratios in the Mexican volcanic belt. Geochimica et Cosmochimica Acta 60(4), 613–628.

Hoernle K, White JDL, van den Bogaard P, Hauff F, Coombs DS, Werner R, Timm C, Garbe-Schönberg D, Reay A, Cooper AF 2006. Cenozoic intraplate volcanism on New Zealand: Upwelling induced by lithospheric removal. Earth and Planetary Science Letters 248(1–2), 350–367.

Irvine TNJ, Baragar WRA 1971. A guide to the chemical classification of the common volcanic rocks. Canadian journal of earth sciences 8(5), 523–548.

Kear D 1960. Sheet 4 Hamilton. Geological Map of New Zealand 1:250 000. N.Z. Department of Scientific and Industrial Research, Wellington.

Kear D 1964. Volcanic alignments north and west of New Zealand's central volcanic region. New Zealand Journal of Geology and Geophysics 7(1), 24–44.

Keleman PB, Hanghøj K, Greene AR 2014. One View of the Geochemistry of Subduction-Related Magmatic Arcs, with an Emphasis on Primitive Andesite and Lower Crust. In: Holland HD, Turekian KK (eds), Treatise on Geochemistry, 1–70.

Kogiso T, Hirschmann MM, Pertermann M. 2004 High-pressure Partial Melting of Mafic Lithologies in the Mantle. Journal of Petrology 45(12), 2407–2422.

Krippner SJ, Briggs RM, Wilson CJ, Cole JW 1998. Petrography and geochemistry of lithic fragments in ignimbrites from the Mangakino Volcanic Centre: implications for the composition of the subvolcanic crust in western Taupo Volcanic Zone, New Zealand. New Zealand Journal of Geology and Geophysics 41(2), 187–199.

Kushiro I 1987. A petrological model of the mantle wedge and lower crust in the Japanese island arcs. In : Mysen BO (ed), Magmatic process: physicochemical principles, 165–181.

Kushiro I 2001. Partial melting experiments on peridotite and origin of mid-ocean ridge basalts. Annual Review of Earth and Planetary Sciences 29, 71–107.

Le Bas MJ, Le Maitre RW, Woolley AR 1992. Mineralogy and Petrology 46, 1–22.

Leeman WP, Smith DR 2018. The role of magma mixing, identification of mafic magma inputs, and structure of the underlying magmatic system at Mount St. Helens. American Mineralogist: Journal of Earth and Planetary Materials 103(12), 1925–1944.

Leonard GS, Calvert AT, Hopkins JL, Wilson CJ, Smid ER, Lindsay JM and Champion DE 2017. High-precision $^{40}Ar/^{39}Ar$ dating of Quaternary basalts from Auckland Volcanic Field, New Zealand, with implications for eruption rates and paleomagnetic correlations. Journal of Volcanology and Geothermal Research 343, 60–74.

Lexa J, Seghedi I, Németh K, Szakács A, Konečny V, Pécskay Z, Fülöp A, Kovacs M 2010.-Quaternary volcanic forms in the Carpathian-Pannonian Region: a review. Central European Journal of Geosciences 2(3), 207–270.

Lindsay JM, Worthington TJ, Smith IEM, Black PM 1999. Geology, petrology, and petrogenesis of Little Barrier Island, Hauraki Gulf, New Zealand. New Zealand Journal of Geology and Geophysics 42(2), 155–168.

Longpré MA, Troll VR, Walter TR, Hansteen TH 2009. Volcanic and geochemical evolution of the Teno massif, Tenerife, Canary Islands: Some repercussions of giant landslides on ocean island magmatism. Geochemistry, Geophysics, Geosystems 10(12).

Lowe DJ 1988. Stratigraphy, age, composition, and correlation of late Quaternary tephras interbedded with organic sediments in Waikato lakes, North Island, New Zealand. New Zealand Journal of Geology and Geophysics 31(2), 125–165.

Luhr JF 1997. Extensional tectonics and the diverse primitive volcanic rocks in the western Mexican Volcanic Belt. The Canadian Mineralogist 35(2), 473–500.

Maaløe S, Sørensen IB, Hertogen J 1986. The trachybasaltic suite of Jan Mayen. Journal of Petrology 27(2), 439-466.

Mahony SH, Wallace LM, Miyoshi M, Villamor P, Sparks RSJ, Hasenaka T 2011. Volcano-tectonic interactions during rapid plate-boundary evolution in the Kyushu region, SW Japan. GSA Bulletin, 123(11–12), 2201–2223.

Márquez A, Oyarzun R, Doblas M, Verma SP 1999. Alkalic (ocean-island basalt type) and calc-alkalic volcanism in the Mexican volcanic belt: A case for plume-related magmatism and propagating rifting at an active margin? Geology 27(1), 51–54.

Mashima H 2009. Genesis of high-magnesium andesites and associated basalts from Saga–Futagoyama, northwest Kyushu, southwest Japan. Journal of Volcanology and Geothermal Research, 187(1–2), 106–116.

Matheson SG 1981. The volcanic geology of the Mt Karioi region. Unpublished M.Sc. thesis. Lodged in the Library, University of Waikato, Hamilton.

Mcbirney AR, Aoki KI 1968. Petrology of the island of Tahiti. Geological Society of America Memoirs 116, 523–556.

McCulloch, M.T., Gamble, J.A., 1991. Geochemical and geodynamical constraints on subduction zone magmatism. Earth and Planetary Science Letters 102, 358–374.

McGee, L. E., Smith, I. E., Millet, M. A., Handley, H. K., & Lindsay, J. M. (2013). Asthenospheric control of melting processes in a monogenetic basaltic system: a case study of the Auckland Volcanic Field, New Zealand. Journal of Petrology, 54(10), 2125–2153.

McLeod OE, Pittari A, Brenna M, Briggs RM 2020. Geology of the Pirongia Volcano, Waikato: 1:30,000 Geological Map. Wellington, New Zealand, Geoscience Society of New Zealand, Miscellaneous Publication 156, 60 p.

Moore GM, Carmichael ISE, Marone C, Renne PR 1994. Basaltic volcanism and extension near the intersection of the Sierra Madre volcanic province and the Mexican volcanic belt: Geological Society of America Bulletin 106, 383–394

Morimoto N, Fabries J, Ferguson AK 1988. Pyroxene nomenclature. Mineralogy and Petrology 39, 55–76.

Morris JD, Leeman WP, Tera F 1990. The subducted component in island arc lavas: constraints from Be isotopes and B–Be systematics. Nature 344(6261), 31–36.

Morris PA 1986. Geochemistry of some Miocene to Quaternary igneous rocks bordering an ensialic marginal basin-an example from eastern Shimane Prefecture and Oki Dozen Island, Southwest Japan. Memoir of the Faculty of Science, Shimane University 20, 115–133.

Mortimer N, Herzer RH., Gans PB, Laporte-Magoni C, Calvert AT, Bosch D 2007. Oligocene–Miocene tectonic evolution of the South Fiji Basin and Northland Plateau, SW Pacific Ocean: evidence from petrology and dating of dredged rocks. Marine Geology 237, 1–24.

Mortimer N, Scott JM 2020. Volcanoes of Zealandia and the Southwest Pacific. New Zealand Journal of Geology and Geophysics, 1-7.

Mortimer N., Gans PB, Palin JM, Meffre S, Herzer RH, Skinner DNB 2010. Location and migration of Miocene-Quaternary volcanic arcs in the SW Pacific region. Journal of Volcanology and Geothermal Research 190, 1–10.

Mullen EK, Weis D, Marsh NB, Martindale M 2017. Primitive arc magma diversity: New geochemical insights in the Cascade Arc. Chemical Geology 448, 43–70.

Neall VE, Stewart RB, Smith IEM 1986. History and petrology of the Taranaki volcanoes. Royal Society of New Zealand Bulletin 23, 251–263.

Ormerod DS, Hawkesworth CJ, Rogers NW, Leeman WP, Menzies MA 1988. Tectonic and magmatic transitions in the Western Great Basin, USA. Nature 333(6171), 349–353.

Panter KS, Blusztajn J, Hart SR, Kyle PR, Esser R, McIntosh WC 2006. The origin of HIMU in the SW Pacific: evidence from intraplate volcanism in southern New Zealand and subantarctic islands. Journal of Petrology 47, 1673–1704.

Pearce JA, Baker PE, Harvey PK, Luff IW 1995. Geochemical evidence for subduction fluxes, mantle melting and fractional crystallization beneath the South Sandwich island arc. Journal of Petrology 36(4), 1073–1109.

Peate DW, Pearce JA, Hawkesworth CJ, Colley H, Edwards CM, Hirose K 1997. Geochemical variations in Vanuatu arc lavas: the role of subducted material and a variable mantle wedge composition. Journal of Petrology 38(10), 1331–1358.

Pilet S, Hernandez J, Sylvester P, Poujo M 2005. The metasomatic alternative for ocean island basalt chemical heterogeneity. Earth and Planetary Science Letters 236, 148–166.

Pin C, Gannoun A, Dupont A 2014. Rapid, simultaneous separation of Sr, Pb, and Nd by extraction chromatography prior to isotope ratios determination by TIMS and MC-ICP-MS. Journal of Analytical Atomic Spectrometry 29(10), 1858–1870.

Plank T 2005. Constraints from Th/La on sediment recycling at subduction zones and the evolution of the continents. Journal of Petrology 46, 921–944.

Platz T, Cronin SJ, Cashman KV, Stewart RB, Smith IEM 2007. Transition from effusive to explosive phases in andesite eruptions—A case-study from the AD 1655 eruption of Mt. Taranaki, New Zealand. Journal of Volcanology and Geothermal Research 161(1–2), 15–34.

Price RC, McCulloch MT, Smith IEM, Stewart RB 1992. Pb-Nd-Sr isotopic compositions and trace element characteristics of young volcanic rocks from Egmont Volcano and comparisons with basalts and andesites from the Taupo Volcanic Zone, New Zealand. Geochimica et Cosmochimica Acta 56(3), 941–953.

Price RC, Smith IEM, Stewart RB, Gamble JA, Gruender K, Maas R 2016. High-K andesite petrogenesis and crustal evolution: Evidence from mafic and ultramafic xenoliths, Egmont Volcano (Mt. Taranaki) and comparisons with Ruapehu Volcano, North Island, New Zealand. Geochimica et Cosmochimica Acta 185, 328–357.

Price RC, Stewart RB, Woodhead JD, Smith IEM 1999. Petrogenesis of high-K arc magmas: evidence from Egmont volcano, North Island, New Zealand. Journal of petrology 40(1), 167–197.

Pure L 2020. The volcanic and magmatic evolution of Tongariro volcano, New Zealand. Unpublished PhD thesis, Victoria University of Wellington.

Putirka KD 2008. Thermometers and barometers for volcanic systems. Reviews in mineralogy and geochemistry 69(1), 61–120.

Rabone SDC 1975. Petrography and hydrothermal alteration of Tertiary andesite-rhyolite volcanics in the Waitekauri Valley, Ohinemuri, New Zealand. New Zealand Journal of Geology and Geophysics 18(2), 239–258.

Rafferty WJ, Heming RF 1979. Quaternary alkalic and sub-alkalic volcanism in South Auckland, New Zealand. Contributions to Mineralogy and Petrology 71(2), 139–150.

Reagan MK, Gill JB 1989. Coexisting calcalkaline and high-niobium basalts from Turrialba Volcano, Costa Rica: Implications for residual titanates in arc magma sources. Journal of Geophysical Research: Solid Earth 94(B4), 4619–4633.

Reagan MK, Gill JB 1989. Coexisting calcalkaline and high-niobium basalts from Turrialba Volcano, Costa Rica: Implications for residual titanates in arc magma sources. Journal of Geophysical Research: Solid Earth 94(B4), 4619–4633.

Reyners M 1989. New Zealand seismicity 1964–87: an interpretation. New Zealand Journal of Geology and Geophysics 32(3), 307–315.

Reyners M 2013. The central role of the Hikurangi Plateau in the Cenozoic tectonics of New Zealand and the Southwest Pacific. Earth and Planetary Science Letters 361, 460–468.

Reyners M, Eberhart-Phillips D, Bannister S 2011. Tracking repeated subduction of the Hikurangi Plateau beneath New Zealand. Earth and Planetary Science Letters 311(1–2), 165–171.

Ringwood AE 1974. The petrological evolution of island arc systems: Twenty-seventh William Smith Lecture. Journal of the Geological Society 130(3), 183–204.

Ringwood AE 1990. Slab-mantle interactions: 3. Petrogenesis of intraplate magmas and structure of the upper mantle. Chemical Geology 82, 187–207.

Robertson DJ 1976. A paleomagnetic study of volcanic rocks in the South Auckland area. Unpublished MSc thesis, lodged in the Library, University of Auckland, Auckland.

Sakuyama T, Ozawa K, Sumino H, Nagao K 2009. Progressive melt extraction from upwelling mantle constrained by the Kita-Matsuura basalts in NW Kyushu, SW Japan. Journal of Petrology 50(4), 725–779.

Sanders RJ 1994. Ultramafic and mafic xenoliths from the Okete, Ngatutura and South Auckland Volcanics. Unpublished M.Sc. thesis, lodges in the Library, University of Waikato, New Zealand.

Sanders RJ 1994. Ultramafic and mafic xenoliths from the Okete, Ngatutura and South Auckland Volcanics, northern North Island, New Zealand (Doctoral dissertation, University of Waikato).

Scott JM, Pontesilli A, Brenna M, White JDL, Giacalone E, Palin JM, le Roux PJ 2020. The Dunedin Volcanic Group and a revised model for Zealandia's alkaline intraplate volcanism. New Zealand Journal of Geology and Geophysics, 1–20.

Seebeck H, Nicol A, Giba M, Pettingam J, Walsh J 2014. Geometry of the subducting Pacific plate since 20 Ma, Hikurangi margin, New Zealand. Journal of the Geological Society 171, 131–143.

Smith IEM and Cronin SJ 2020. Geochemical patterns of late Cenozoic intraplate basaltic volcanism in northern New Zealand and their relationship to the behaviour of the mantle. New Zealand Journal of Geology and Geophysics, DOI: 10.1080/00288306.2020.1757470.

Sorbadere F, Schiano P, Métrich N, Bertagnini A 2013. Small-scale coexistence of island-arc- and enriched-MORB-type basalts in the central Vanuatu arc. Contributions to Mineralogy and Petrology 166, 1305–1321.

Stern RJ 2002. Subduction zones. Reviews of Geophysics 40(4), 3–1.

Stern T, Benson A 2011. Wide-angle seismic imaging beneath an andesitic arc: Central North Island, New Zealand. Journal of Geophysical Research: Solid Earth 116(B9).

Stern TA 2009. Reconciling short- and long-term measures of extension in continental back-arcs: Heat flux, crustal structure and rotations within the central North Island, New Zealand. In: Extending a Continent: Architecture, Rheology and Heat Budget, Geological Society of London, Special Publication 321, 73–87.

Stern TA, Stratford WR, Salmon ML 2006. Subduction evolution and mantle dynamics at a continental margin: Central North Island, New Zealand. Reviews of Geophysics 44(4).

Stice GD, McCoy Jr FW 1968. The geology of the Manu'a Islands, Samoa. Pacific Science 22, 427–457.

Stokes S, Lowe DJ, Froggatt PC 1992. Discriminant function analysis and correlation of late Quaternary rhyolitic tephra deposits from Taupo and Okataina volcanoes, New Zealand, using glass shard major element composition. Quaternary international 13, 103–117.

Stolper EM, Newman S 1992. Fluids in the source region of subduction zone magmas: clues from the study of volatiles in Mariana Trough magmas. Reports, Geological Survey of Japan 279, 161–169.

Storey M, Rogers G, Saunders AD, Terrell DJ 1989. San Quintin volcanic field, Baja California, Mexico: 'within-plate' magmatism following ridge subduction. Terra Nova 1(2), 195–202.

Strong M and Wolff J 2003. Compositional variations within scoria cones. Geology 31(2), 143–146.

Sun SS, McDonough WF 1989. Chemical and isotopic systematics of oceanic basalts: implications for mantle composition and processes. Geological Society, London, Special Publications 42(1), 313–345.

Tatsumi Y, Hamilton DL, Nesbitt RW 1986. Chemical characteristics of fluid phase released from a subducted lithosphere and origin of arc magmas: evidence from high-pressure experiments and natural rocks. Journal of Volcanology and Geothermal Research 29(1–4), 293–309.

Thompson GM, Malpas J, Smith IEM 1998. Volcanic geology of Rarotonga, southern Pacific Ocean. New Zealand Journal of Geology and Geophysics 41(1), 95–104.

Timm C, de Ronde CEJ, Hoernle K, Cousens B, Wartho JA, Caratori Tontini F, Wysoczankski R, Hauff F, Handler M 2019. New Age and Geochemical Data from the Southern Colville and Kermadec Ridges, SW Pacific: Insights into the recent geological history and petrogenesis of the Proto-Kermadec (Vitiaz) Arc. Gondwana Research 71, 169-193.

Todd E, Gill JB, Wysoczanski RJ, Hergt J, Wright IC, Leybourne MI, Mortimer N 2011. Hf isotopic evidence for small-scale heterogeneity in the mode of mantle wedge enrichment: Southern Havre Trough and South Fiji Basin back arcs. Geochemistry, Geophysics, Geosystems 12(9).

Tost M, Price RC, Cronin SJ, Smith IEM 2016. New insights into the evolution of the magmatic system of a composite andesite volcano revealed by clasts from distal mass-flow deposits: Ruapehu volcano, New Zealand. Bulletin of Volcanology 78(5), 38.

Turner MB, Cronin SJ, Smith IEM, Stewart RB, Neall VE 2008. Eruption episodes and magma recharge events in andesitic systems: Mt Taranaki, New Zealand. Journal of Volcanology and Geothermal Research 177(4), 1063–1076.

Verma SP, Nelson SA 1989. Isotopic and trace element constraints on the origin and evolution of alkaline and calc-alkaline magmas in the Northwestern Mexican Volcanic Belt. Journal of Geophysical Research: Solid Earth 94(B4), 4531–4544.

Villamor P, Berryman K 2001. A late Quaternary extension rate in the Taupo Volcanic Zone, New Zealand, derived from fault slip data. New Zealand Journal of Geology and Geophysics 44(2), 243–269.

Villamor P, Berryman KR 2006. Evolution of the southern termination of the Taupo Rift, New Zealand. New Zealand Journal of Geology and Geophysics 49(1), 23–37.

Wadge G and Wooden JL 1982. Late Cenozoic alkaline volcanism in the northwestern Caribbean: tectonic setting and Sr isotopic characteristics. Earth and Planetary Science Letters 57, 35–46.

Walcott RI 1987. Geodetic strain and the deformational history of the North Island of New Zealand during the late Cainozoic. Philosophical Transactions of the Royal Society of London. Series A, Mathematical and Physical Sciences 321(1557), 163–181.

Wanke M, Clynne MA, von Quadt A, Vennemann TW, Bachmann O 2019. Geochemical and petrological diversity of mafic magmas from Mount St. Helens. Contributions to Mineralogy and Petrology 174, 10.

Weaver SD, Smith IEM 1989. New Zealand intraplate volcanism. In: Johnson RW, Knutson J, Taylor SR. ed. Intraplate volcanism in eastern Australia and New Zealand. Cambridge, Cambridge University Press. Pp. 157–188.

Wilson CJN, Gravley DM, Leonard GS, Rowland JV 2009. Volcanism in the central Taupo Volcanic Zone, New Zealand: tempo, styles and controls. Studies in volcanology: the legacy of George Walker. Special Publications of IAVCEI 2, 225–247.

Wilson CJN, Houghton BF, McWilliams MO, Lanphere MA, Weaver SD, Briggs RM 1995. Volcanic and structural evolution of Taupo Volcanic Zone, New Zealand: a review. Journal of Volcanology and Geothermal Research 68, 1–28.

Wilson CJN, Rowland JV, Gravley DM 2008. The Taupo Volcanic Zone, New Zealand: A Geological and Geophysical Review with an Emphasis on its Central Segment. Institute of Earth Science and Engineering, University of Auckland, New Zealand Report 2-2008.06, pp. 1–134.

Wilson JT 1963. A possible origin of the Hawaiian Islands. Canadian Journal of Physics, 41(6), 863–870.

Wright IC 1997. Morphology and evolution of the remnant Colville and active Kermadec arc ridges south of 33 30' S. Marine Geophysical Researches 19(2), 177–193.

Wright IC, Parson, LM, Gamble, JA 1996. Evolution and interaction of migrating cross-arc volcanism and backarc rifting: An example from the southern Havre Trough (35 20'–37 S). Journal of Geophysical Research: Solid Earth, 101(B10), 22071–22086.

Wright IC, Worthington TJ, Gamble JA 2006. New multibeam mapping and geochemistry of the 30–35 S sector, and overview, of southern Kermadec arc volcanism. Journal of Volcanology and Geothermal Research 149(3–4), 263–296.

Wysoczanski RJ, Todd E, Wright IC, Leybourne MI, Hergt JM, Adam C, Mackay K 2010. Backarc rifting, constructional volcanism and nascent disorganised spreading in the southern Havre Trough backarc rifts (SW Pacific). Journal of Volcanology and Geothermal Research, 190(1–2), 39–57.

Zheng Y 2019. Subduction Zone Geochemistry. Geoscience Frontiers 10, 1223–1254

Zindler A, Staudigel H, Batiza R 1984. Isotope and trace element geochemistry of young Pacific seamounts: implications for the scale of upper mantle heterogeneity. Earth and Planetary Science Letters 70(2), 175–195.

Chapter 4

A channelised debris avalanche deposit from Pirongia basaltic stratovolcano, New Zealand

'The traveller will choose one road or the other according to his point of starting on Kawhia Harbour or his place of destination on the Waipa'

Hochstetter, 1867

O.E. McLeod

A. Pittari

A channelised debris avalanche deposit from Pirongia basaltic stratovolcano, New Zealand

Invited article for the Geological Society of London Special Issue: Volcanic processes and sedimentary responses

McLeod OE., Pittari A

Introduction

Stratovolcanoes are large volume, internally complex volcanic landforms formed by a cycle of aggradation (e.g. cone-building, lava flows) and destruction (e.g. sector collapse, fluvial-glacial erosion) over periods typically spanning 200 to 350 kyr. Following the collapse and resurgent volcanism of Mt. St. Helens forty years ago (Voight et al. 1981), formative studies (e.g. Ui, 1983; Siebert, 1984; Crandell et al. 1984; Glicken, 1996) linked debris avalanche deposits with sector collapse events, and similar deposits were subsequently identified at numerous other volcanoes (e.g. Blong, 1986; Stoopes and Sheridan, 1992; Beget and Kienle, 1992; Belousov et al. 1999; Clavero et al. 2002; Shea et al. 2008; Delcamp et al. 2017). Sector collapse is an intrinsic, cyclical process affecting the growth dynamics of most stratovolcanoes (Zernack et al. 2009). Detailed studies of the ring plain thus reveal the style and tempo of volcanic collapses (Beget and Kienle, 1992, Zernack et al. 2011), which has crucial implications for understanding volcanic hazards associated with debris avalanches (e.g. Alloway et al. 2005).

At least twenty-three volcanic debris avalanches of Quaternary age are recognised in New Zealand, all associated with active andesitic stratovolcanoes. The two main centres of volcanic sector collapse, mounts Ruapehu and Taranaki, display contrasting deposition styles (spreading or channelised) that relate to their surrounding topography. Spreading (unconfined) debris avalanches with classical hummock-mound terrain occur at Taranaki (Neall, 1979), where deposits have flowed almost unimpeded across the ring plain for 25–40 km and further out to sea (Zernack et al. 2011). In contrast, many debris avalanches from Ruapehu have crossed over the ring plain into deep gorges, where channelisation resulted in extremely long runout distances (60–80 km) relative to deposit volume (Tost et al. 2014).

In this study we describe a previously unidentified, newly mapped debris avalanche deposit from the Pirongia basaltic stratovolcano in North Island, New Zealand (Fig. 1). The deposit, herein the Oparau breccia, is a prime example of a *completely* channelised, long runout (>20 km) debris avalanche that is traceable almost continuously from the source zone to its distal area.

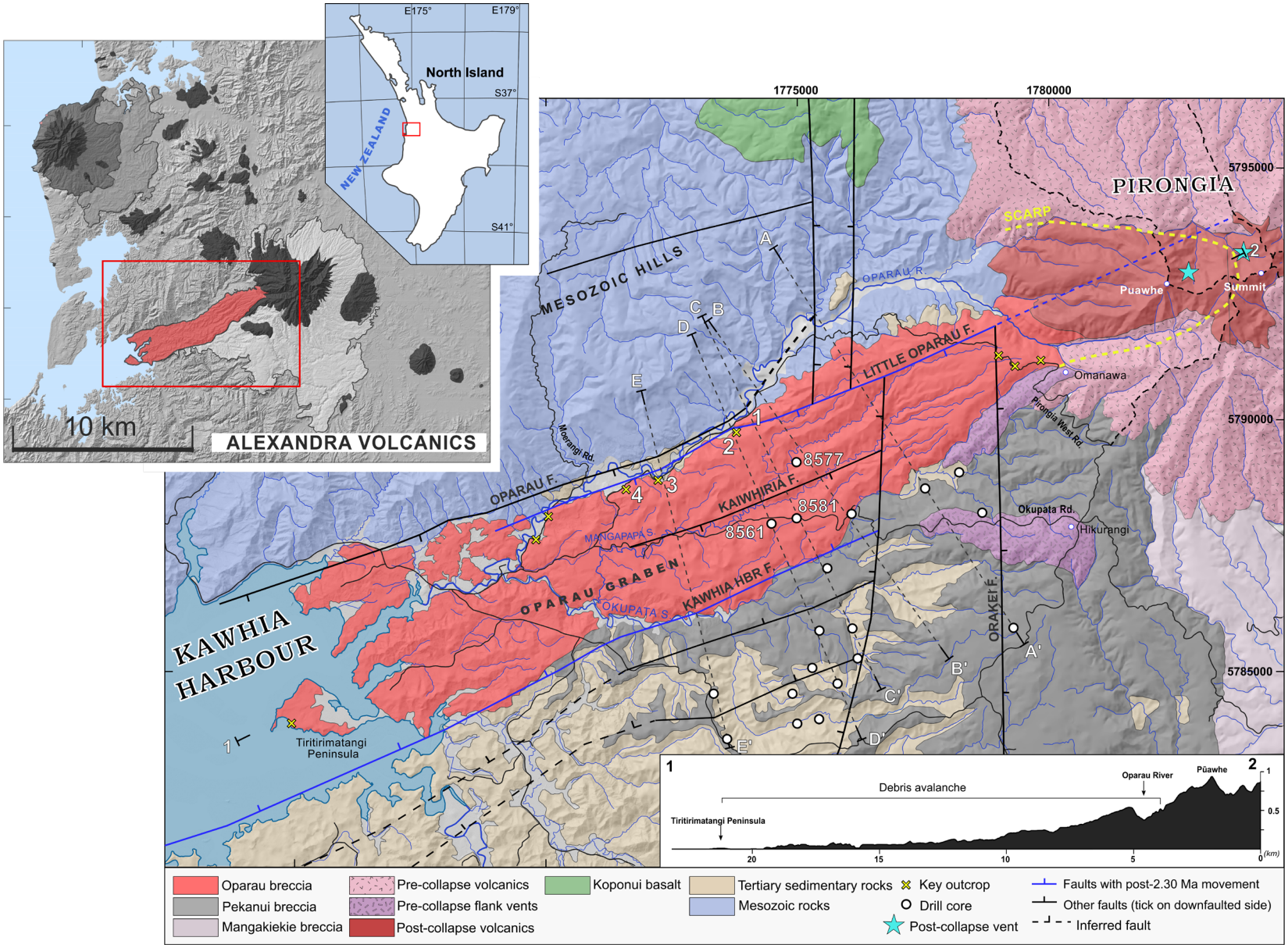
E175°
E179°
North Island
S37°
S41°
NEW ZEALAND
10 km
ALEXANDRA VOLCANICS
1775000
1780000
5795000
5790000
5785000
PIRONGIA
SCARP
Puawhe
Summit
OPARAU R.
MESOZOIC HILLS
LITTLE OPARAU F.
Omanawa
Pirongia West Rd.
Okupata Rd.
Hikurangi
Moerangi Rd.
OPARAU F.
KAIWHIRIA F.
8577
8581
8561
MANGAPAPA S.
OPARAU GRABEN
OKUPATA S.
KAWHIA HBR F.
ORAKEI F.
KAWHIA HARBOUR
Tiritirimatangi Peninsula
A
A'
B
B'
C
C'
D
D'
E
E'
1
2
3
4
Debris avalanche
Oparau River
Pūawhe
0.5
20
15
10
5
0
(km)
Oparau breccia
Pekanui breccia
Mangakiekie breccia
Pre-collapse volcanics
Pre-collapse flank vents
Post-collapse volcanics
Koponui basalt
Tertiary sedimentary rocks
Mesozoic rocks
Key outcrop
Drill core
Post-collapse vent
Faults with post-2.30 Ma movement
Other faults (tick on downfaulted side)
Inferred fault

Figure 1. (Previous page). Centre: simplified geological map of Pirongia and its southwestern ring plain (adapted from McLeod et al. 2020), showing the distribution of the Oparau Breccia debris avalanche deposit between Pirongia and Kawhia Harbour. The slope profile of the deposit is shown on the lower right. Inset: location map of Pirongia Volcano and the Alexandra Volcanic Group in North Island, New Zealand.

Pirongia Volcano

Mt Pirongia is an extinct stratovolcano (2.6–1.6 Ma; Briggs et al. 1989) within the Alexandra Volcanic Group (Fig. 1). It is the largest basaltic volcano in North Island, New Zealand. The volcanic stratigraphy of Pirongia Formation was described in detail by McLeod et al. (2020). Early volcanism constructed an ankaramite shield structure that was surmounted later by basaltic to andesitic cones at several sites dispersed across the summit zone. Each edifice-building phase is separated by an erosional unconformity and associated with a distinct phase of ring plain deposition by debris avalanches and/or lahars.

Ring plain stratigraphy

The Pirongia ring plain forms an expansive surface to the south and southwest of the volcano (Fig. 1), consisting of laharic and debris avalanche deposits intercalated with Pirongia-derived tephras, stream gravels and colluvium (McLeod et al. 2020, reference therein). The northern sections of the ring plain, similarly extensive, are completely buried by Quaternary deposits within the Hamilton Basin. The ring plain is mantled by a thick (1–10 m) succession of tephra deposits from distal rhyolitic and andesitic volcanic centres. The oldest and most expansive debris avalanche deposit(s) occur in the southern part of the ring plain, collectively forming the Pekanui breccia (Fig. 1) which covers >60 km^2 and is ≤ 150 m thick. The Pekanui breccia is distributed across a highland plateau south of the Kawhia Harbour Fault and is stratigraphically older than the Hikurangi dome (2.30 ± 0.05 Ma; Briggs et al. 1989) that erupted through the unit (Fig. 1). The eastern side of the Pekanui breccia plateau is truncated by a sector collapse scarp associated with the Mangakiekie breccia (Fig. 1). This debris avalanche deposit is at least 100 m thick in proximal areas and forms low rolling hills extending >10 km south of Pirongia. The collapse scarp is infilled by younger lavas erupted about 2.1 Ma. The subject of this paper, the Oparau breccia, is the youngest and most well exposed debris avalanche deposit of the ring plain, extending from the western flank of Pirongia into Kawhia Harbour (Fig. 1).

Previous interpretations of the Oparau breccia

The earliest geological maps of the Oparau-Kawhia area describe a unit of 'trachytic' conglomerate and tuff 'extending from the trachyte stock of Pirongia as far as the Eastside of Kawhia Harbour' (von Hochstetter and Sauter, 1867, p.331), later referred to as 'trachyte tuffs and

lavas that go into the sea at Kawhia' (Park, 1892). Over 100 years later, Briggs (1983) described these same deposits as 'large volumes of thick, coarse, unstratified and unsorted alloclastic volcanic flow breccias' with heterolithologic accessory fragments. Because of their strong welding and apparently crystalline groundmass, Briggs (1986) speculated that these alloclastic 'flow breccias' formed by mobilisation of high-level magma chambers that flowed out of the volcano following structural collapse. While alloclastic breccias are widespread on the main edifice, detailed mapping by McLeod et al. (2020) showed that the Oparau breccia consists of heterolithologic rock clasts set within a fragmental matrix of loose crystal-and-lithic-ash and lapilli and is therefore of epiclastic rather than alloclastic origin. The extremely high phenocryst content of Pirongia lavas (i.e. ankaramites) has contributed abundant crystal detritus to the matrix of the breccia, which appears to have led to its interpretation as a crystalline igneous deposit.

In their 1:50,000 geological map, Waterhouse and White (1994) described the Oparau breccia as a 'tongue of volcaniclastic *lahar* material', up to 200 m thick, composed of angular to sub-rounded volcanic blocks in a matrix of grey ash and clay. The term 'lahar', which refers to a rapidly flowing, gravity driven mixture of rock-debris and water from a volcano (Smith and Lowe, 1991), was historically applied to many New Zealand volcanic ring plain deposits that have since been reinterpreted as volcanic debris avalanches (e.g. Zernack et al. 2009). The Oparau breccia lacks the defining characteristics of a lahar deposit (either a hyperconcentrated flow or debris flow), being extremely clast and megaclast rich, clay-poor, unstratified and very thick (50–200+ m), with no evidence for water saturation (e.g. fine matrix lamination). All of these deposit characteristics are instead consistent with 'dry' volcanic debris avalanches, formed by instantaneous edifice collapse rather than periodic aggradation by 'wet' laharic flows.

Methodology

This study is based on extensive field mapping conducted as part of a larger 1:30,000 scale geological mapping project on the Pirongia Volcano (McLeod et al. 2020). The map unit boundary of the Oparau breccia was determined with field surveys and morphometric interpretation of aerial photos (0.5 m resolution) and a hillshaded digital terrain model (8 m resolution). Higher resolution LiDAR (0.5 m resolution) was incorporated into the hillshade model in the lowland areas around Kawhia Harbour. Information on the thickness of the Oparau breccia and surrounding ring plain was obtained from archived logs of drill cores collected for the Coal Resources Survey by the New Zealand Geological Survey between 1979 and 1985.

Terminology

We adopt a simplified debris avalanche deposit terminology in this manuscript appropriate to the scale and detail of field observations. The deposit texture is defined by two endmembers:

block facies and matrix (or mixed) facies (Glicken, 1991). Block facies consists of debris avalanche blocks (up to tens of metres wide) that represent mostly intact, transported pieces of the Pirongia edifice. Matrix facies refers to completely mixed parts of the debris avalanche deposit, containing numerous rock types from the edifice, sub-edifice and flow path, in an ungraded, unsorted and unstratified mixture. Matrix facies contains clasts (<1 m) and megaclasts (>1 m) which have internal lithological homogeneity and defined outer surfaces (Palmer et al. 1991). Domains are deformed and disaggregated megaclasts that are lithologically homogeneous but partly dispersed in the matrix (Palmer et al. 1991). In the matrix facies, clasts are embedded in abundant finer-grained matrix.

Results

Mapped distribution of Oparau breccia

The mapped unit of Oparau breccia (McLeod et al. 2020) covers an area of 32.5 km^2, extending 17 km from the lower southwestern flank of Mt Pirongia to Kawhia Harbour (Fig. 2A) where the deposit crops out at Tiritirimatangi Peninsula. Deposit width varies from 1.5 to 3.1 km. Near the harbour, the breccia is covered by a thick cover sequence of Quaternary tephras, which if removed, indicate a total deposit area of least 48 km^2. It is likely that the breccia extends some distance further into the harbour – the maximum being 10 km southwest of Tiritirimatangi Peninsula, where the harbour is enclosed by Urawhitiki Point.

The deposit terrain consists of elongate ridges, oriented southwest, that vary from a few hundred metres to 2.6 km in length (see Fig. 1). Ridge tops form rolling hills mantled by reddish, non-Pirongia derived distal tephra deposits, 1–5 m thick, with scalloped slope edges. These cover beds increase in thickness towards Kawhia Harbour, where the topography is notably more subdued than in proximal areas. The Oparau River, on the northern edge of the deposit, cuts a deep valley into bedrock over ~12 km in length. The valley separates uplifted Mesozoic rocks of the Kapamahunga Range from Mesozoic–Tertiary strata of the Oparau Graben, with displacement mainly accommodated along the Oparau Fault (see Fig. 1; Waterhouse and White, 1994). The Oparau breccia was originally emplaced into the graben as lowland terrain and now forms topographically inversed, erosion-resistant ridges above the valley floor.

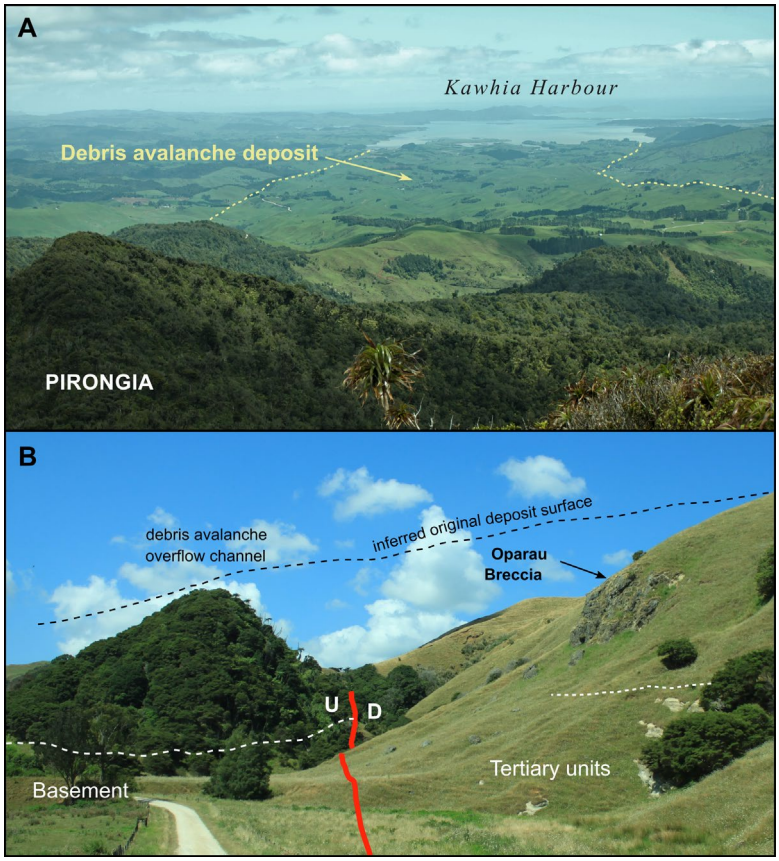

Figure 2. Debris avalanche morphology. (A) View southwest to Kawhia Harbour from Pirongia Volcano, showing the Oparau breccia in the middle ground. (B) Outcrop of Oparau breccia above the Oparau River valley. The breccia overlies a faulted surface of Mesozoic and Tertiary units (white dashed lines). The forested hill (left) marks a paleo-overflow channel where the debris avalanche flowed onto the uplifted Mesozoic block north of the Little Oparau Fault (red line).

Overview of textural facies of Oparau breccia

The Oparau breccia is composed of abundant matrix facies and subordinate block facies that outcrop discontinuously from the proximal to distal parts of the deposit.

Across the deposit, matrix facies consists of a completely mixed, massive, poorly sorted deposit comprising angular clasts (micron to metre size) embedded within a clay to sand-sized matrix. The fine matrix contains weathered volcanogenic clay and silt, fractured and/or rounded crystals (clinopyroxene, plagioclase, Fe-Ti oxides, hornblende) and non-volcanic minerals (glauconite) derived from pulverised Tertiary sandstone.

The block facies is recognised in proximal to medial parts of the deposit where large (2–30 m max. dimension), single-lithology blocks of lava, scoria or breccia crop out in cliff sections and within drill cores. Blocks are relatively cohesive and in medial areas form erosion-resistant outcrops above the Oparau River. In some sections, the block facies transitions into disaggregated domains that are intermingled with matrix material. Average clast size appears to decrease

significantly beyond ~11 km from the volcano, implying that most megaclasts and domains are disaggregated and completely mixed beyond this distance.

Deposit stratigraphy

Proximal Zone

The proximal deposit (≤ 200 m thick) is marked by boulder fields in farmland and sparse outcrops on the southwestern edifice flank dissected by the Oparau River. Boulders are 1–2 m wide and mainly of basalt to basaltic-andesitic composition, though at least one domain (~80 m wide) of finer-grained olivine basanite, probably part of a block facies, also occurs. A typical section of matrix facies exposed in a track cutting shows: (1) a clast-rich deposit (clasts ≤ 35 cm) overlain by (2) 1 m of lapilli-rich matrix with red scoria, overlain by (3) 2 m of clast-supported breccia with jigsaw fractured boulders of basalt and basaltic andesite (≤ 1.5 m wide). Weathering of plagioclase is evident in some boulders. Distinct multi-coloured breccias also crop out on Pirongia West Road (~500 asl), where the deposit consists of lapilli and small blocks (<30 cm) set within a matrix of reddish-brown clay and loose clinopyroxene crystals.

Medial Zone

The deposit forms prominent bluffs along the southern edge of the Oparau River, 7–11 km from source (site 1, Fig. 1). The basal contact is exposed on Pirongia West Road (~70 m asl), where the Oparau breccia overlies silty Mesozoic breccia along an undulating erosion surface (Fig. 3B) associated with a paleo-overflow channel of the debris avalanche. The deposit consists of pale-cream matrix facies with abundant heterolithologic clasts of coarse gravel to boulder-size. The matrix is interspersed with block facies ankaramite domains (1–2+ m wide) that display complex internal fracturing. In some areas, the clasts are oriented vertically to the basal contact surface.

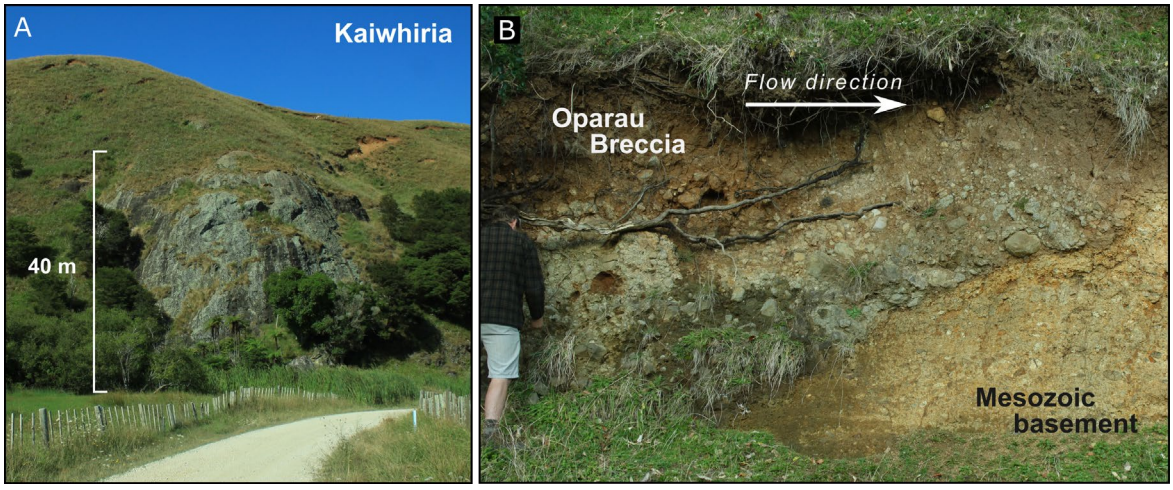

Figure 3. Medial debris avalanche deposit outcrops on Pirongia West Road. (A) Oparau breccia, >40 m thick, at Kaiwhiria Bluff (site 3, see Fig. 1). (B) Contact between Oparau breccia and Mesozoic siltstone breccia.

About 300 m southwest site 1, the Oparau Breccia overlies Tertiary sandstone that is downfaulted against the Little Oparau Fault (site 2, Fig. 1; 2B). The deposit (>12 m thick) consists of indurated block and matrix facies, equivalent to site 1. The matrix facies is pale-cream coloured with 10-25% lithics that average 2–4 mm in size. Clasts are mainly volcanic though abraded siltstone clasts (<10 cm) are also common. Rounded, alluvial-derived clasts are rare. The block facies consist of metre-scale domains of cohesive to disaggregated basalt with jigsaw fractures common. Ankaramite megaclasts are up to 2.5 m wide and can be sub-rounded. Highly deformed Tertiary sandstone domains (≤ 2 m wide) of similar lithology to the underlying Tertiary strata occur near the base of the breccia (Fig. 4). These domains are associated with fine-grained, clast-poor volcaniclastic matrix that shows complex interfingering relationships with the sandstone. The soft sandstone and fine-matrix are surrounded by a clast-rich matrix containing megaclasts.

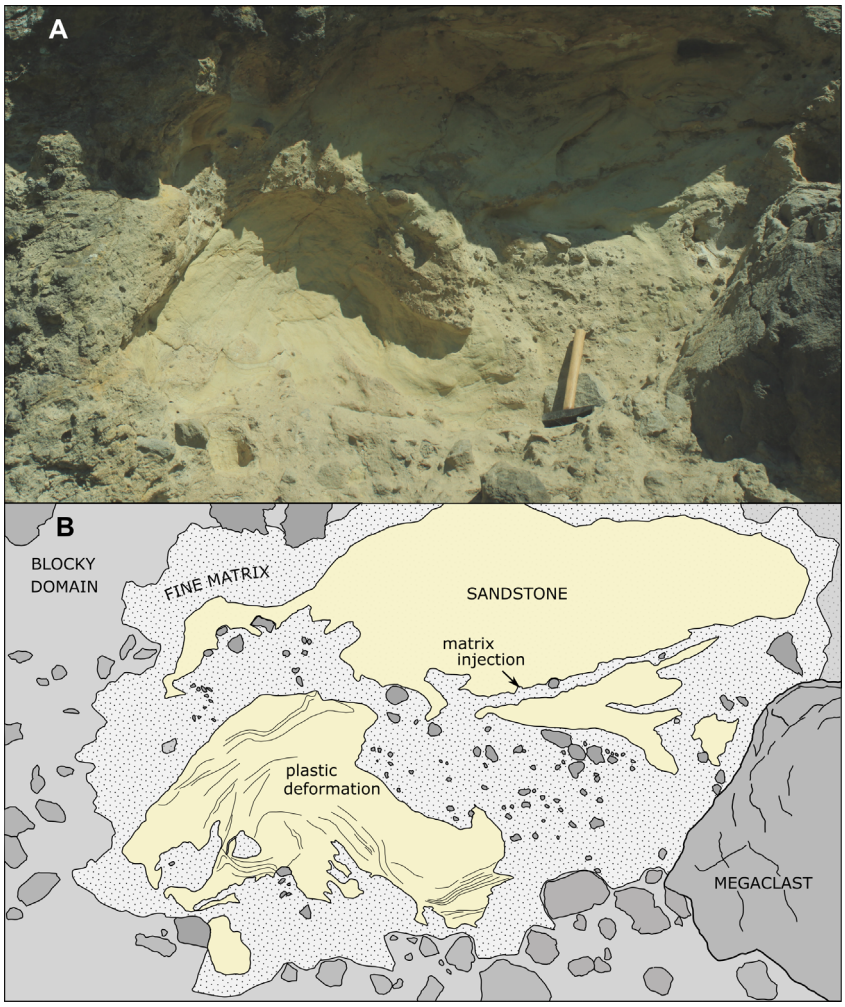

Figure 4. Fluidal deformation within Tertiary sandstone megaclasts of Oparau breccia, shown in field photo (top) and interpretive sketch (bottom). The sandstone is interfingered with fine volcaniclastic matrix and surrounded by blocky domain material.

At Kawhiria bluff (site 3, Fig. 1) a 40 m vertical section of the deposit is exposed above the Oparau River (Fig. 3A). The main deposit consists of strongly indurated block facies (a 30×20 m sized-block) composed of megacrystalline ankaramite breccia interspersed with clinopyroxene-rich lapilli-tuff. The large block and surrounding matrix facies both outcrop sporadically up to the ridgeline (~95 m asl). Matrix facies consist of 60–70 % fine-grained material. Of the clastic component, 1–20% are cobble to boulder sized (24–85 cm) and the remainder are angular lapilli (2–8 mm), which become finer (2–4 mm) towards the centre of the deposit. Jigsaw fracturing occurs in some larger clasts.

Matrix facies is exposed in a 5 m cliff section (site 3, Fig. 1) and in a large fallen block nearby. The deposit is very poorly sorted with angular clasts, grading from lapilli to metre scale blocks, embedded within a fine matrix of pale-brown fine sand with lapilli (2–5 mm), and abundant loose crystals of clinopyroxene (≤0.5 cm) and subordinate hornblende (max. 1 cm). Most clasts are ankaramites and finer-grained basalts of diverse texture, with small quantities of andesite (16–122 mm) and Tertiary sandstone (65–220 mm), and sparse Mesozoic siltstone (55–90 mm). Megaclasts (1-2 m) of basalt and basaltic-andesite are common, with the latter generally more angular and preserving columnar jointing or curvilinear fractures that are infilled by fine matrix material (Fig. 5C). Elongate columnar blocks often show sub-vertical orientation and lean in the direction of flow. Megaclasts (~1 m) and domains (~0.2–0.5 m) of scoriaceous agglomerate occur throughout the deposit, consisting of angular lapilli and blocks, some scoriaceous, surrounded by dark red, iron-stained matrix material. The blocks are infiltrated by pale-brown, clast-poor matrix and sheared slivers of pale-yellow sandstone that is squeezed between domains and complexly deformed within the matrix (Fig. 5A).

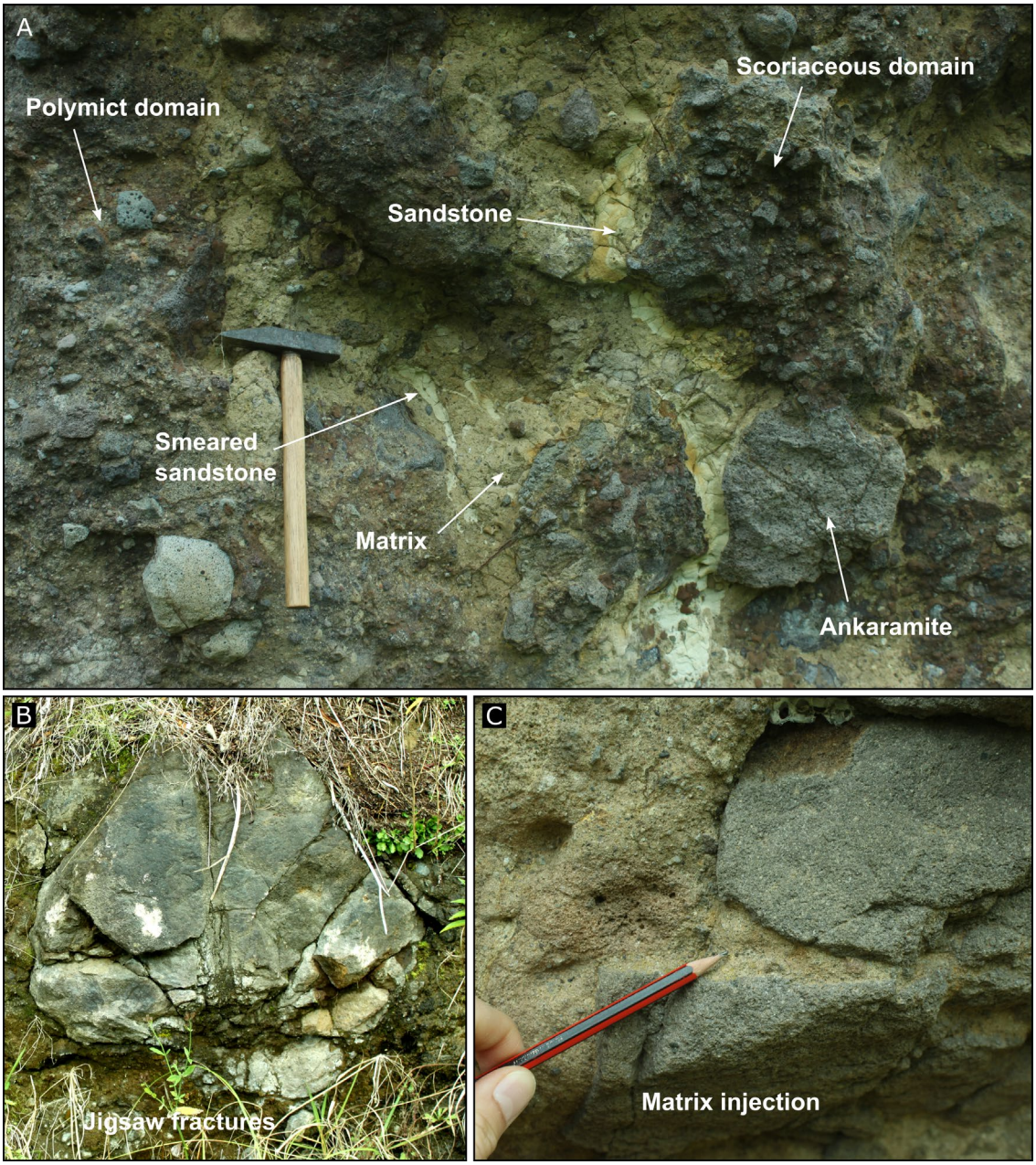

Figure 5. Textural characteristics of the Oparau breccia debris avalanche deposit. (A) Block and matrix texture, showing fine beige matrix material squeezed between clastic domains. The domains range from individual blocks to scoriaceous agglomerates to polymict breccia blocks. Tertiary sandstone embedded within the matrix shows complex smearing textures. (B) Jigsaw fracture pattern within columnar jointed clast. (C) Matrix injection into jigsaw fractured clast.

Distal Zone

The Oparau breccia is poorly exposed in the distal zone, forming subdued hill country mantled by a thick cover sequence of rhyolitic tephras. Sporadic outcrops above the Oparau River, on Moerangi Road (Fig. 1), show an indurated, clast-rich deposit like the medial zone, but lacking any large domains, megaclasts or sandstone blocks. Clast sizes range from fine lapilli to small

blocks (~85 mm). Rare larger blocks, 30–40 cm wide, show jigsaw fracturing/shattering (Fig. 5B) and some preserve columnar joints.

The top of the breccia outcrops beneath a thick tephra sequence in road cuttings along Okupata Road (20 m and 59 m a.s.l.) and at Tiritirimatangi Peninsula (Fig. 1). In all places it is deeply weathered to red clay with multi-coloured volcanic clasts. At 59 m a.s.l., the weathering horizon is ~3 m thick and outcrops above fresh, strongly indurated breccia exposed within the Mangapapa Stream, 15 m below the roadway. The most distal outcrop at Tiritirimatangi Peninsula (~19 km from source) was described by Horrocks (2000). Here, the top ~2 m of Oparau breccia outcrops beneath a thick (~15 m) succession of pale-coloured tephras (the Kauroa Ash Sequence), where it grades from weathered breccia into bright yellowish sand and then a 20 cm thick paleosol (Horrocks, 2000). Clasts are generally angular, ranging up to 10–20 cm in maximum width.

Drill cores

Archived drill core stratigraphic data (NZ Geological Survey) through the medial part of the Oparau breccia from sites at 7.5 km, 8.0 km and 8.5 km from source (see Fig. 1 for locations) were revised and re-interpreted here. The deposit varies in thickness from 107–175 m (Fig. 6). At all sites, the deposit is dominated by matrix facies with fine pebble to cobble sized clasts set within finer silt or sand. In the cores, the deposit consists of *matrix facies* basaltic gravels (moderately to strongly indurated, fine-pebble to cobble size clasts set within silt or silt), interspersed with clasts of Tertiary sandstone, siltstone and limestone and Mesozoic claystones and siltstones. Scoriaceous domains 2–25 m thick occur in cores 8577 and 8581 (Fig. 6) and probably represent intact blocks from the edifice, similar to that observed at Kaiwhiria bluff. Very indurated, monolithologic core sections are interpreted as megaclasts, including: ankaramite blocks ~2.5 m wide; a fine-grained olivine basalt (Okete-type) block 1.6 m wide; Mesozoic claystone and siltstone gravels, probably dissociated blocks, 1.8 m and 4.7 m wide; and clay zones ± calcareous siltstone clasts, 1–1.5 m wide. Mesozoic clasts are distributed in concentrated layers (± Tertiary clasts) mainly in the mid to top sections of the deposit. Tertiary clasts are restricted to the lowermost sections of cores 8577 and 8581, as observed in outcrop at site 2. In contrast, Tertiary clasts are widespread throughout core 8561. The top of the breccia consists of 12–14 m of yellowish clayey pebble-gravel with weathered basaltic clasts, in turn overlain by 6–10 m of undifferentiated Quaternary tephras.

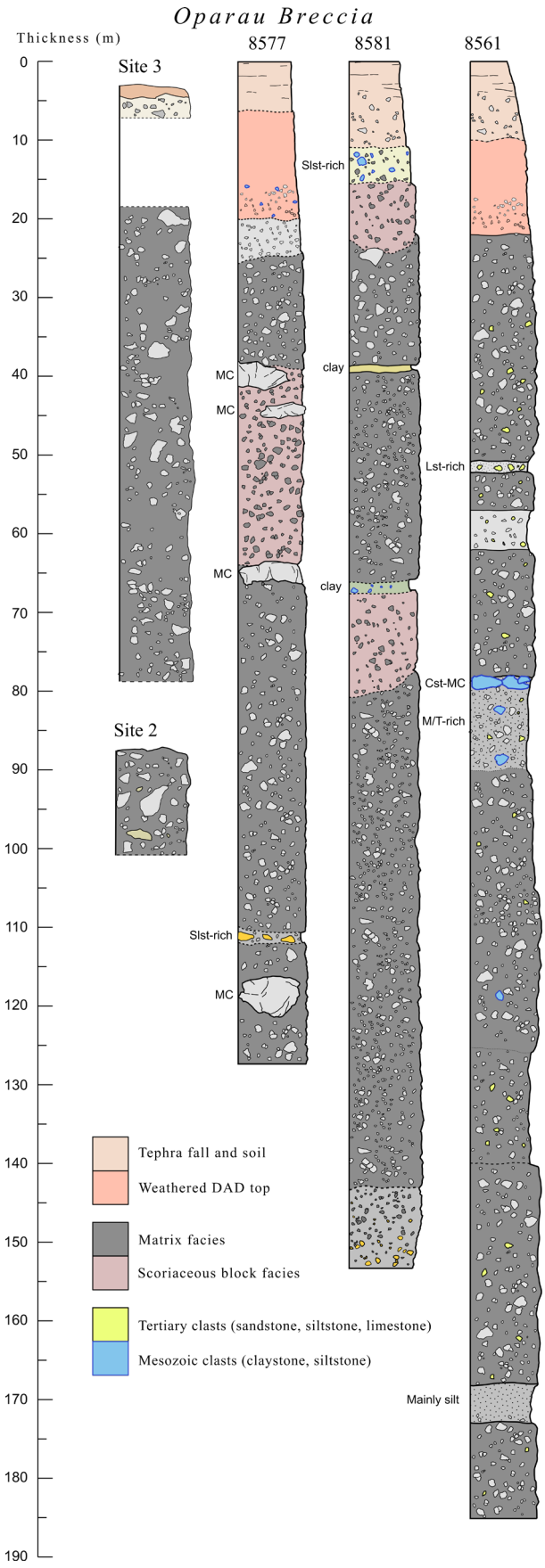

Figure 6. Stratigraphic logs for the medial portion of Oparau breccia based on outcrops (sites 2 and 3) and drill cores (ID numbers 8577, 8581 and 8561). The stratigraphy within the drill cores is based on re-interpretation of core logs from the Coal Resources Survey by the New Zealand Geological Survey. Original core logs are available in the New Zealand Petroleum and Minerals online exploration database. Abbreviations: MC=megaclast, M=Mesozoic clast, T=Tertiary clast, Lst=limestone, Slst=siltstone, Cst=claystone.

Cross sections

Deposit thickness in relation to the channel paleo-topography is shown in Fig. 7 (see Fig. 1 for cross section locations). The breccia overlies a faulted surface of Mesozoic basement and Tertiary rocks that transitions from a subdued, highland plateau below the southwest flank (Section 1), into the step-faulted Oparau Graben (sections 2–5). The cross sections show that the debris avalanche was channelised throughout its length, initially abutting the Little Oparau Fault and then entering the Oparau Graben, where the flow concentrated in the central channel between the Kaiwhiria and Kawhia Harbour faults. The downwards stepping faulted surfaces between the Oparau and Little Oparau faults, and Little Oparau and Kaiwhiria faults have acted as overflow surfaces for the debris avalanche as it flowed down the central channel into lowland areas. The Kawhia Harbour Fault separates Oparau breccia from older (pre-2.30 Ma) ring plain deposits (Pekanui Breccia) that outcrop along higher elevation, faulted terraces to the south of the graben.

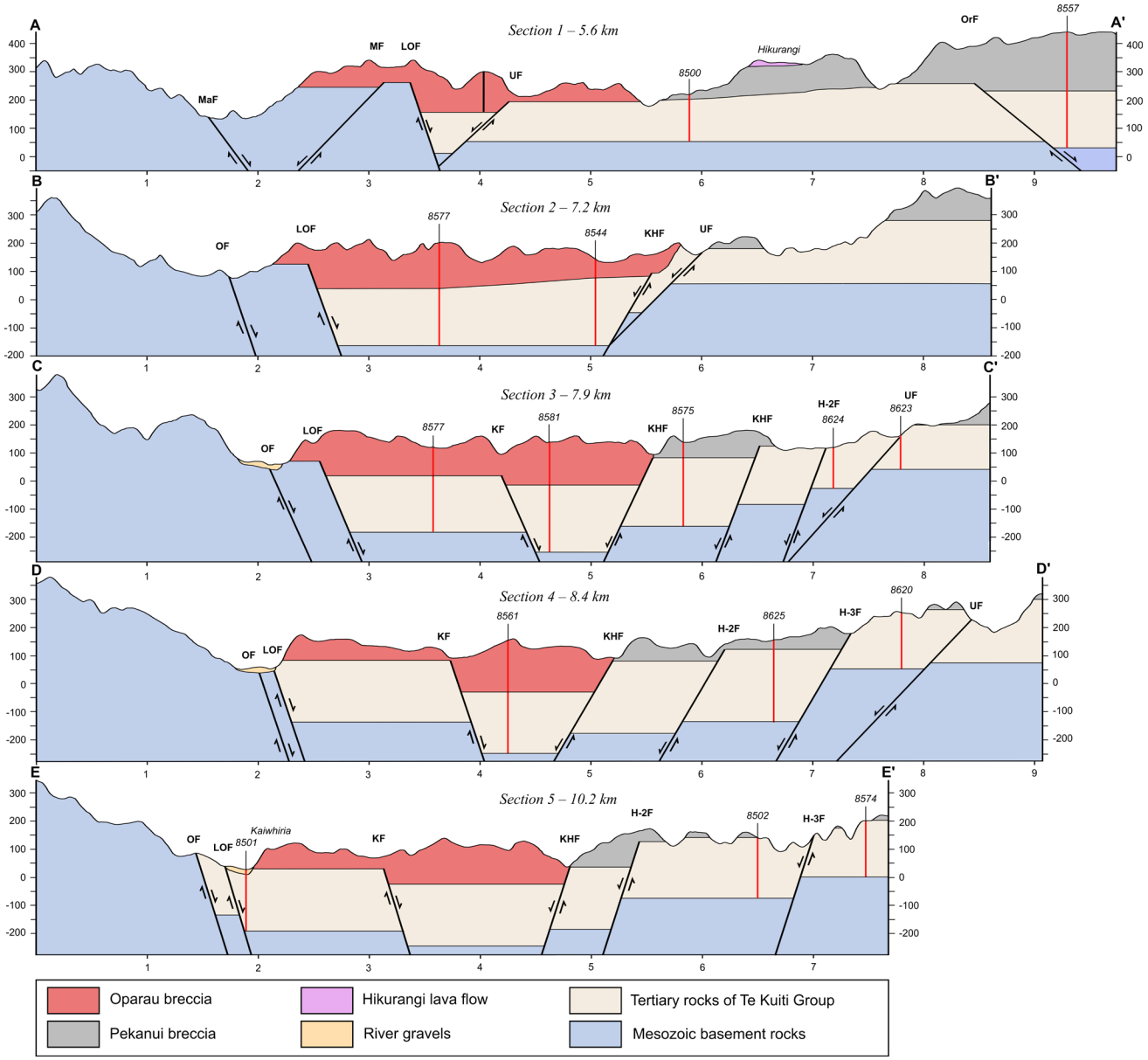

Figure 7. Cross sections showing the Oparau breccia in relation to underlying geological structures. Thicknesses of units were interpreted from drill cores (red lines) and field mapping. Fault abbreviations: OF=Oparau Fault, LOF=Little Oparau Fault; KF=Kaiwhiria Fault; KHF=Kawhia Harbour Fault; H–2F=Harbour Fault #2, H–3F=Harbour Fault #3, OrF=Orakei Fault; MF=Mangakino Fault, MaF=Mangawhero Fault; UF=unnamed Fault. Cross section locations are shown in Figure 1.

The progressive increase in channel depth into the Oparau Graben corresponds to relatively uniform deposit thickness of 150–190 m in medial-distal zones (sections 2–5 and Fig. 8). In distal areas (12–17 km), the deposit appears to thin abruptly from 90 to 50 m thick (based on additional cross sections). Beyond ~8 km from source, the breccia was emplaced below present sea level (sections 3–5).

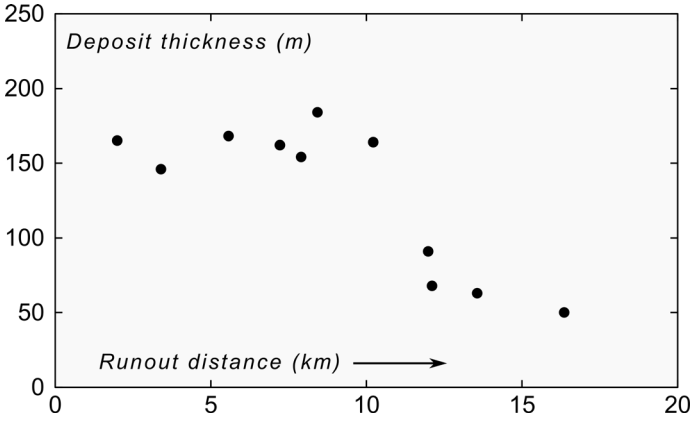

Figure 8. Relationship between runout distance and deposit thickness for the Oparau breccia. Distance is relative to fixed point within the sector collapse scarp.

Clast lithology

In order of abundance, the volcaniclastic component consists of ankaramites, fine-grained to scoriaceous basalts, purplish basaltic andesites, pale-grey andesites and rare diorites (Table 1 and Fig. 9). Non-volcanic clasts are Tertiary calcareous sandstones and indurated, Mesozoic siltstones and claystones. Hydrothermal alteration is evident in some clasts, e.g. zeolite amygales in ankaramite (Fig. 9F) and pervasive yellowish sulphur lining of vesicles in basaltic andesites.

Table 1: Clast lithology for Oparau breccia.

Clast type	Description
Basalt	Dark grey, relatively fine-grained, holocrystalline. Assemblage cpx + plag + ol + mgt. Minor fine-grained olivine basalt.
Ankaramite	Extremely porphyritic, clinopyroxene-rich basalt. Assemblage cpx + plag + mgt ± ol
Basaltic andesite	Fine-grained, medium grey. Assemblage: plag + cpx + mgt. Curviplanar jointing in larger blocks. Yellowish sulphurous lining in vesicles (hydrothermal alteration) common.
Andesite	Pale-grey to white, dense to pumiceous lapilli with pervasive alteration. Assemblage: plag + hbl ± altered glass. Some speckled black-white diorite. Assemblage plag + hbl.
Tertiary rocks	Dark greenish grey to yellowish, moderately indurated, very calcareous sandstones, fine-sandy siltstones and limestones. Moderately to very glauconitic. Some shells present.
Mesozoic rocks	Yellowish brown to olive grey, weakly to moderately indurated siltstones and claystones.

Ankaramites in the Oparau breccia (Fig. 9B, D) are among the most mega-crystalline basalts observed within Pirongia Volcanic Formation. Clinopyroxene forms equant, single crystals or glomerocrysts ranging in size from 1.5 mm to >1 cm. Many crystals show chemical zonation with greenish-black cores and darker black ~1 mm wide rims. Plagioclase is extremely abundant as microlites (<1 mm), whereas olivine forms only rare grains within glomerocrysts. These crystals are set within holocrystalline, fine-grained groundmass composed of the same minerals.

Whole-rock elemental data for a representative subset of clasts (see Appendix 1 for dataset) yield SiO_2 contents of 45.6–54.7 wt% and MgO 3.7–11.5 wt%. Alkali basalt clasts (exemplified by sample PW8) have distinctly higher TiO_2 (2.3 wt%) compared to the rest of the suite (0.8–1 wt%). Sample PY2 is a strongly altered hornblende-andesite with low SiO_2 (46.2 wt%) and K_2O (0.4 wt%), elevated Al_2O_3 and high LOI (3.6 wt%). All clasts (except for PW8) have trace element patterns typical of Pirongia Group-1 lavas (i.e. pronounced Nb-Ta anomalies), which represent the arc-type (IAB) endmember of the volcano (McLeod et al. in prep; see Chapter 3). Conversely, the alkali basalt clasts (i.e. PW8) are typical of Pirongia Group-3 OIB (i.e. intraplate), which have high Nb-Ta abundances relative to Group-1 rocks.

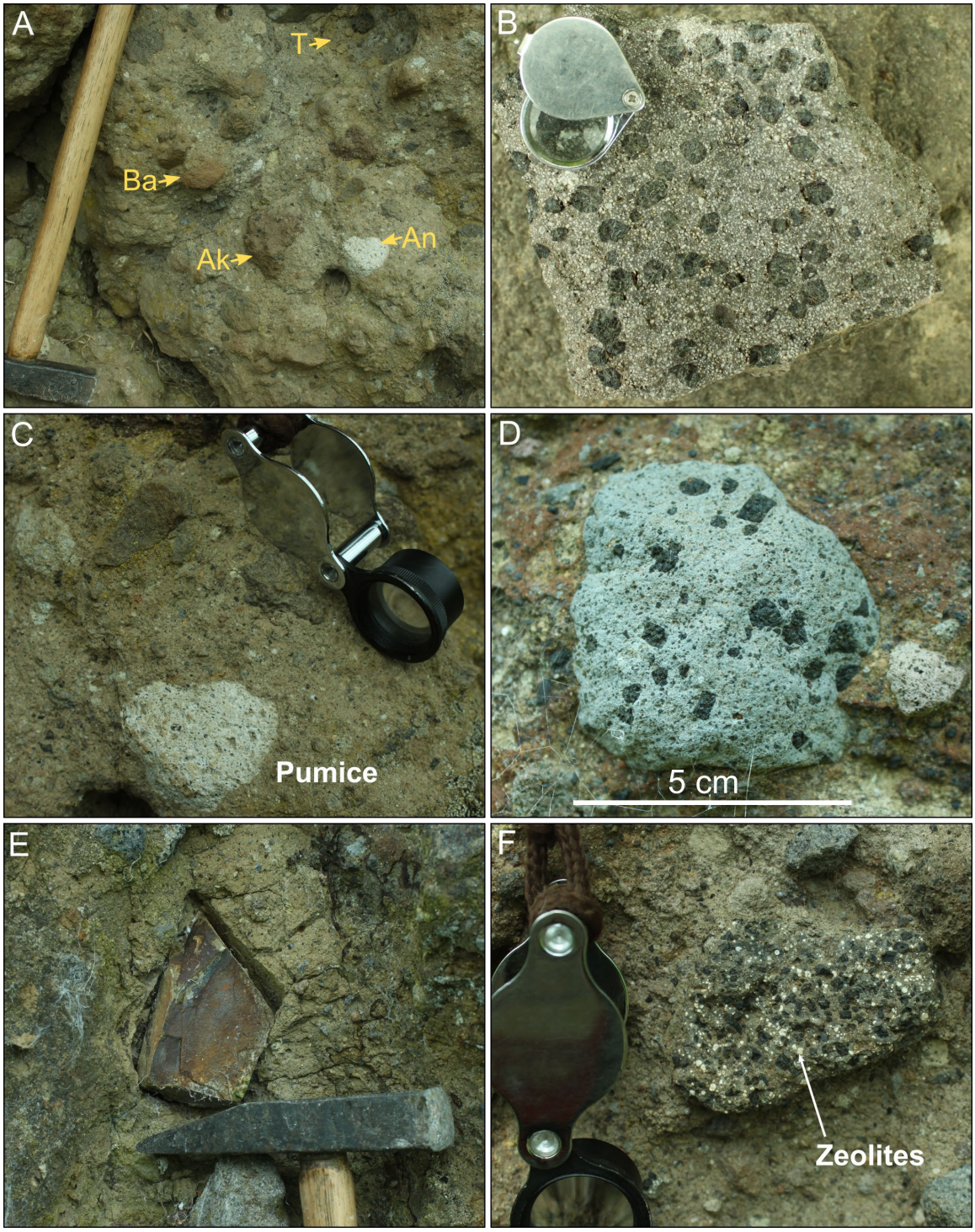

Figure 9. Clastic lithology of the Oparau breccia. A: lapilli-sized fragments of ankaramite, basaltic andesite (Ba), andesite (An) and Tertiary sandstone (T). B: ankaramite with large clinopyroxene phenocrysts. C: hornblende-phyric andesite pumice. (D) ankaramite with altered groundmass. (E) angular Mesozoic siltstone. F: ankaramite with 'salt and pepper' texture formed by zeolite amygdales.

Source zone for debris avalanche deposit

Geologic mapping by McLeod et al. (2020) identified a prominent horse-shoe shaped unconformity (see Fig. 1) on the southwest flank of Pirongia, separating older volcanic shield lavas (Paewhenua Member; 2.6–2.42 Ma) from younger infilling volcanics of the Pirongia Summit Member. The unconformity is 3.8 km long and its width narrows upslope from 2.60 km to 1.64 km wide at the scarp head. The scarp axis is oriented 262º (E-W), oblique to the debris avalanche flow direction (242º, NE-SW). The Oparau breccia forms a thick deposit at the southwestern toe of the unconformity where it underlies post-collapse lavas. A large, planar-surfaced block (1.2×1.1 km) of the Mesozoic basement, dipping 5.9º SSE, is also exposed at the foot of the slope, just north of Oparau River, partially overlain by post-collapse lavas. The block appears to have been rotated from the sub-strata of the volcano during the collapse. The flank location, areal magnitude, stratigraphic relations, and orientation of the unconformity are strong evidence that it was formed by sector collapse of the southwestern flank, and thus marks the source zone of the debris avalanche deposit.

The oblique orientation of the scarp relative to the debris avalanche deposit likely reflects strong channelization of the flow into the Oparau Graben. The distribution of the Oparau breccia mainly to the east of the Little Oparau Fault strongly supports channelization. Subsequent valley erosion in the headwaters of the Oparau River has removed most of the deposit west of the fault and exposed Mesozoic basement rocks.

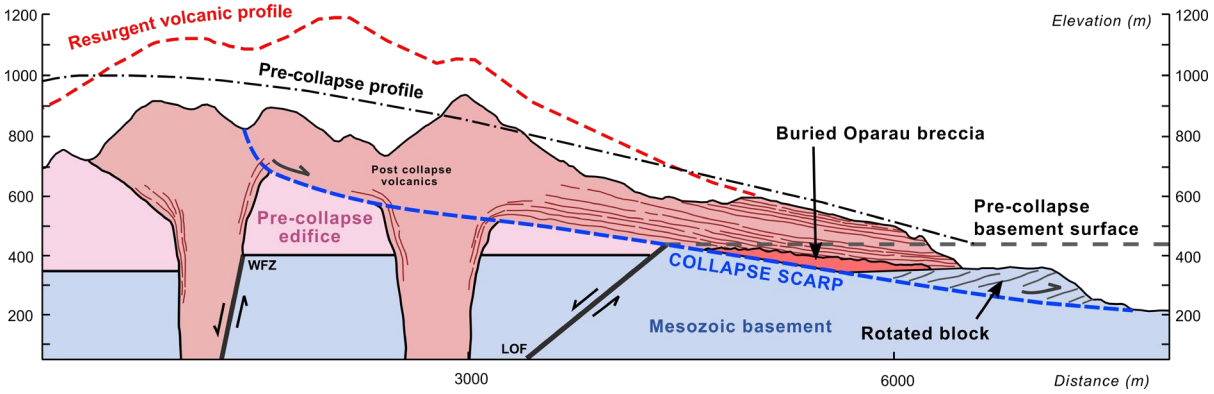

Figure 10. Cross section of the sector collapse scarp in relation to pre-collapse and post-collapse volcanic stratigraphy and faults (WFZ=Waipa Fault Zone; LOF=Little Oparau Fault). The pre-collapse basement surface and the overlying low-angle volcanic shield (pre-collapse profile) were partially destroyed by the collapse event, which may have been triggered by displacement on the LOF. Post-collapse volcanism infills the collapse scarp, forming the resurgent volcanic profile which has since been substantially eroded to its present slope profile. Mapping indicates that post-collapse lavas overlie the bottom edge of the Oparau breccia.

Deposit and scarp volume

The minimum (post-erosional) volume of the Oparau breccia debris avalanche deposit is 3.3 ± 0.1 km^3 based on the averaged area in the cross sections in Fig. 6 (and additional cross sections not published here) multiplied by a deposit length of 18 km. This corresponds to an average thickness of ~100 m over the mapped deposit area (32.5 km^2) or ~70 m thickness over the proposed original area of the deposit (48 km^2, as discussed earlier). The volume calculation does not exclude the cover of younger tephras (≤10 m thick) mantling the deposit, which may add 0.1–0.3 km^3 on to the volume of the Oparau breccia.

There is close correspondence between the deposit volume and the calculated volume of material displaced from the sector collapse scarp (3 ± 0.3 km^3). The displaced volume was calculated by measuring the pre-collapse flank area in cross section (Fig. 10) and multiplying by the average scarp width (2.2 km, see Fig. 1).

Age of the Oparau Breccia

The sector collapse scarp truncates the Paewhenua Member (2.50–2.42 Ma) and Hihikiwi Member (2.3–2.2 Ma) cones, thus providing a maximum stratigraphic age of ~2.2 Ma for the collapse event. This is supported by K-Ar dates from two clasts in the debris avalanche (correlated to Hihikiwi flank cone) that yield ages of 2.13 ± 0.10 Ma and 2.25 ± 0.10 Ma (Robertson, 1976).

The minimum deposition age is given by Kauroa Ash bed K3, which overlies Oparau breccia at Tiritirimatangi Peninsula (Fig. 11). The K3 bed is directly dated by zircon fission-track (ZFT) dating at 1.68 ± 0.12 Ma (Lowe et al. 2001) and was correlated via melt inclusion major-element chemistry, and magnetostratigraphy (Horrocks, 2000) to the Vinegar Hill Tephra (1.75 Ma; Naish et al. 1996 and Pillans et al. 2005). Vinegar Hill tephra was dated at 1.73 ± 0.08 Ma by Seward and Kohn (1997) (ZFT) and 1.75 ± 0.13 Ma by Naish et al. (1996) and 1.75 Ma ± 0.20 Ma by Pillans et al. (2005) (both via glass isothermal plateau fission-track dating, ITPFT). Pillans et al. (2005) also reported an astronomically tuned age of 1.75 Ma, consistent with correlation with Cycle 19 of Marine Oxygen Isotope Stage (MOIS) 61 for Vinegar Hil Tephra. Hence, we assign an age of 1.75 Ma to K3.

The degree of weathering suggests a moderate time break between deposition of the breccia and the overlying K3 tephra. The K3 tephra was deposited in warm conditions of marine oxygen isotope stage 61 but the period before this (MOIS 62) was colder, and slower weathering rates are probable. There is thus uncertainty over the time interval represented by the weathering and pedogenesis.

The stratigraphically older Kauroa K1 and K2 Ash beds are not present in the Tiritirimatangi section, but probably lie buried beneath the Oparau breccia. The K1 bed was dated

directly by ZFT at 2.24 ± 0.29 Ma (Lowe et al. 2001) and stratigraphically between 2.25 ± 0.10 Ma and 2.26 ± 0.08 Ma (Briggs et al. 1989). The age of the overlying K2 bed is within the Olduvai Subchron (Horrocks, 2000), spanning the period 1.925 to 1.780 Ma (Cohen and Gibbard 2019).

The sector collapse scarp is infilled by lavas and volcaniclastics of Pirongia Summit Member (McLeod et al. 2020) with a minimum K-Ar eruption age of 1.60 ± 0.04 Ma (Briggs et al. 1989). Post-collapse volcanism evidently began sometime between 1.75 and 1.60 Ma, following deposition of the Oparau breccia between ~2.2 and 1.75 Ma. If it is assumed that the K1 and K2 tephras underlie Oparau breccia, then its emplacement age can be constrained to the period 1.925–1.75 Ma. Future radiometric dating of the scarp-filling lavas may further constrain the minimum age of sector collapse.

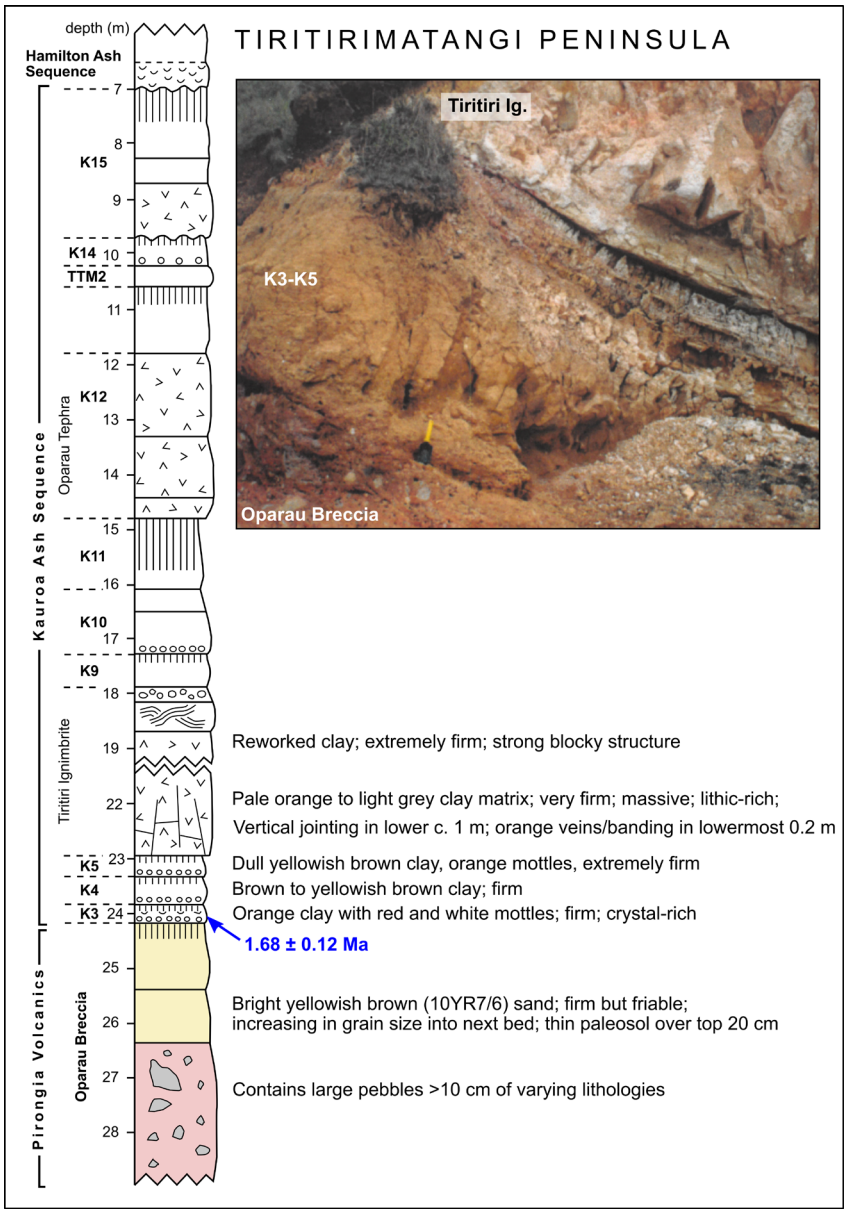

Figure 11. Stratigraphy of Tiritirimatangi Peninsula (adapted from Horrocks, 2000) used to constrain the age of emplacement of the Oparau breccia.

Discussion

Effects of debris avalanche channelization

The relationship between drop height (H) and run out distance (L) for volcanic debris avalanches is commonly expressed by the Heim coefficient (F=H/L), equivalent to the apparent coefficient of friction for volcanic dry avalanche deposits (Hsü, 1975). Slope reconstructions of the pre-collapse Pirongia Volcano (McLeod et al. 2020) suggest a conservative maximum edifice height (based on the Paewhenua shield and Hihikiwi cone) of H = 1.1 ± 0.1 km. Total runout distance for the debris avalanche is in the range 19–27 km, thus we adopt L = 23 ± 4 km. This gives an H/L range of 0.04–0.06 (Fig. 12A). H/L ratios for dry volcanic debris avalanche deposits are 0.05–0.18, thus the Oparau deposit is at the lower end of this range.

Channelised debris avalanche deposits can extend to 2.5 times the length of their unconfined counterparts (Tost et al. 2014), with the resultant H/L ratios being lower at a given volume in confined deposits than non-volcanic and unconfined volcanic landslides (Fig. 12B). The very low H/L ratio of the Oparau deposit is the direct result of channelization of the debris avalanche into the Oparau Graben. For this deposit, under unconfined conditions the flow out distance would be 8–12 km. Global examples of channelised debris avalanche deposits are sparse. Debris avalanches with low H/L were produced by Ruapehu (L=56–80 km, H/L= 0.03–0.04; Tost, 2014), Tashirodake (L=12.4 km), Ontake (46 km, H/L=0.05) (Takarada et al. 1999) and Nevado de Colima (L=100 km, H/L=0.04) (Stoopes and Sheridan, 1992). Confined debris avalanches may have longer run out because of limited dissipation of total mechanical energy during runout, related to the lower basal contact area to volume ratio within channelised flows, in comparison to spread flows that form broad deposit fans (Nicoletti and Sorriso-Valvo, 1991).

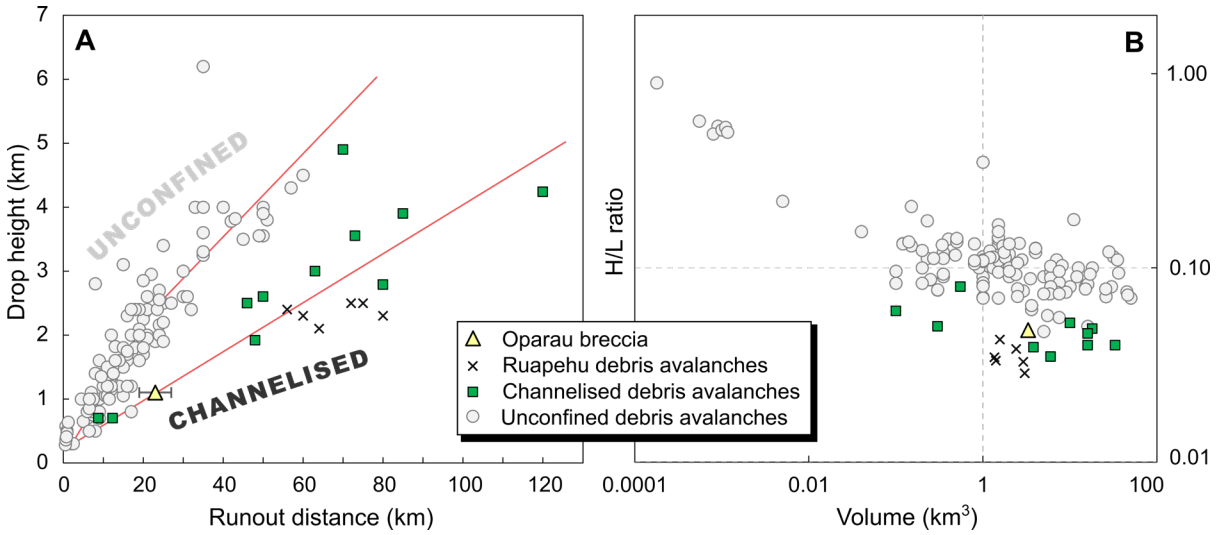

Figure 12. Volcanic debris avalanche physical parameters. A: relationship between drop height (H) and run out distance (L). B: relationship between H/L ratio and deposit volume. All data except for Oparau breccia compiled from the database presented in electronic supplementary material of Tost et al. 2014.

Clast provenance

Ankaramites

Ankaramite is the most abundant rock-type in the debris avalanche deposit, forming megaclasts, domains, and being the most abundant component of the clastic matrix in the form of ankaramite lithics and ankaramite-derived crystals. Stratigraphic relationships of the collapse scarp indicate that most, or all, of these ankaramites originate from the Paewhenua Member, the oldest basaltic shield structure of Pirongia. Ankaramites within the Oparau breccia are distinctly coarser-grained than most ankaramites observed on the ridges surrounding the scarp zone, but they are comparable to lavas exposed within deep stream valleys elsewhere in the Paewhenua shield (McLeod et al. 2020). These extremely coarse-grained basalts thus appear to represent a widespread basal formation of Pirongia. The occurrence of ankaramites at the base of the stratovolcanic succession is also observed at Mt Karioi, 30 km northwest of Pirongia (see Fig. 1).

Mesozoic and tertiary clasts

Deformed, partially disaggregated Tertiary clasts are concentrated at the base of the Oparau breccia, as evident in outcrop and in all three medial drill cores (see Fig. 6). Their origin is consistent with localised rip-up and entrainment as the debris avalanche flowed over the graben floor, which mapping and drill core data show is composed almost entirely of Tertiary units (see Fig. 7). In contrast, Mesozoic (mega-)clasts are concentrated mainly within the mid to upper parts

of the deposit. These clasts originate from the sub-edifice Mesozoic stratigraphy of the scarp, which was rotated and excavated during the collapse event (see Fig. 12).

Debris avalanche deposits with similar volumes, size distributions and deformation textures of Mesozoic/Tertiary clasts to the Oparau breccia occur at Ruapehu (Oreore, Lower Whangaehu and Murimotu Fms; Tost et al. 2014) and Taranaki (Okawa Fm; Alloway et al. 2005; and Waihi Fm; Zernack et al. 2011) stratovolcanoes. In these deposits, the sedimentary component (5–15% Tertiary, ≤2% Mesozoic) occurs mainly in the basal portion of the flow and originates from the erosion/entrainment of soft sedimentary strata in valley-confined parts of the avalanche (Tost et al. 2014). Much higher proportions of sedimentary clasts occur in debris avalanche deposits that involve sub-edifice collapse, such as the Maitahi Formation of Pouakai Volcano (part of the Taranaki Volcanics, New Zealand) (Gaylord and Neall, 2012). This deposit contains ~24 vol% megaclasts (some > 10 m wide) and 20 vol% clasts (>4 mm) derived from sub-edifice mudstone-rich bedrock. The Oparau breccia thus shares characteristics of both the channelised, scouring debris avalanches of Ruapehu and Taranaki, and the bedrock-rich sub-edifice collapse derived deposit of Maitahi Formation, Pouakai volcano.

Post-2.30 Ma fault movements

The lowland terrain west of Mt Pirongia is a graben structure bound by major (≥18 km long) normal faults (the OF and KHF) that extend into the Kawhia Harbour. New mapping and cross section stratigraphy indicate that the Oparau Fault is composed of two parallel fault strands, which are closely aligned in the graben and diverge at >10 km from the harbour. The inner fault strand, the Little Oparau Fault (new), is traceable over at least 7 km in the lowlands (see Figs. 1; 7) and projects directly into the sector collapse scarp area.

No normal fault movements younger than Mid to Late Miocene age are presently recognised in the Oparau/Kawhia area (Kear and Schofield, 1978). However, we infer graben fault movements as young as Pleistocene age because:

(1) At 3–7 km from source, the Oparau breccia is channelised against the Little Oparau Fault, indicating that this fault was a sharp (and possibly young) morphological feature in the landscape at the time of debris avalanche.

(2) At 8–11 km from source, the breccia directly overlies Tertiary bedrock with no basal ring plain unit present. This stratigraphic relationship indicates that either the graben formed after the main period of ring plain deposition, or that the debris avalanche completely scoured the existing ring plain. The general absence of alluvial clasts and the abundance of Tertiary rip-up clasts in the breccia suggests the latter is unlikely.

(3) Pre-2.30 Ma (Pekanui) ring plain deposits are extensive to the south and southwest of Pirongia, but do not appear to infill the graben. The Kawhia Harbour Fault separates Oparau breccia from older Pekanui ring plain that outcrops at higher elevations to the south of the graben. Downfaulting of Pekanui breccia on the KHF suggests that the graben was not the main flow path for ring plain deposition prior to 2.3 Ma and probably did not exist as a tectonomorphic structure during this early period.

Pleistocene-age (post-Hautawan) fault movements of the Kawhia depression (Oparau Graben) were also proposed by Chappell (1970), based on the altitudes of the Ohuka Carbonaceous Sandstone and Pumice silt P1 unit, which are at least 20 m lower around Kawhia Harbour than in coastal sections to the north. Based on the above evidence, we propose that movements along the LOF and KHF have occurred post-2.30 Ma, and pre-sector collapse (1.925–1.75 Ma), forming or at least substantially deepening the Oparau Graben.

Sector collapse trigger

Volcanic sector collapse is the result of major destabilising events (e.g. magmatic intrusions, eruption, volcanic or tectonic seismicity, or heavy rainfall) (Siebert, 1984) pre-conditioned by general edifice weakening factors such as gravitational spreading, unstable volcanic or sub-edifice stratigraphy (Francis and Wells, 1988, Vallance et al. 1995), or hydrothermal alteration (Ellsworth and Voight, 1995). In the case of the Oparau breccia, sector collapse occurred within the low-angle (11–13º), low elevation (~1000 m asl) basaltic shield underlain by faulted and fractured Mesozoic bedrock consisting of weathered siltstone and claystone (see Fig. 10). Field evidence suggests that the main preconditioning factor for collapse was edifice loading onto the basement rocks.

The Pirongia edifice is underlain by normal faults associated with the Hamilton Basin and Oparau Graben (McLeod et al. 2020), two major tectonomorphic features associated with back-arc extension in the Pliocene and early Pleistocene. Sector collapse may have been triggered by movement of sub-edifice basement on the meridional Waipa Fault Zone (WFZ), which underlies the central mass of the volcano, or the NE-SW trending Little Oparau Fault (LOF), which projects into the sector collapse scarp and terminates at the WFZ (see Fig. 1).

In analogue sand models (Wooler et al. 2009), normal faulting of the sub-edifice basement typically forms a collapse scarp in the downfaulted block with its axial trend perpendicular to the fault. By contrast, strike slip fault motion in the basement may produce fault-parallel scarp axes, commonly with paired scarps on either side of the edifice. The Oparau scarp axis strikes perpendicular to the WFZ but occurs on the up-faulted western block, which precludes this fault

on morphological ground as the most likely trigger of collapse. The absence of any vertical displacements on the edifice related to the WFZ corroborates this (McLeod et al. 2020).

A more likely trigger is the LOF, which has had normal fault movement post-2.30 Ma (see above), and which strikes sub-parallel (062) to the scarp axis (082) and projects directly into the scarp zone. Unlike other natural examples of fault-parallel collapse axes (e.g. Mt Iriga, Paguican et al. 2012), the LOF is graben related and contains no apparent strike slip component. The LOF is thus unlikely to have produced the observed fault-scarp geometry directly. We therefore suggest that post-2.30 Ma normal faulting on the LOF acted to destabilise the buttress of Mesozoic bedrock at the base of the southwestern flank (see Fig. 10), and this triggered the sector collapse. The oblique scarp to fault angle thus reflects a preferential zone of weakness in the sub-edifice basement. We consider gravitational spreading of the edifice was also a priming factor, and that spreading intensified as the Oparau Graben developed prior to sector collapse.

An eruption trigger for the collapse remains a possibility, given the clear stratigraphic evidence for *post-collapse* volcanism infilling the head scarp zone (see section below). However, the lack of any field evidence for a post-collapse blast deposit (as observed at Mt Helens, Glicken 1996) overlying the Oparau breccia near Pirongia means this hypothesis cannot be proven with any certainty.

Resurgent volcanism

The sector collapse scarp is infilled by ~5 km^3 of basaltic to andesitic lavas, volcaniclastics and dykes of the Pirongia Summit Member (≤1.60 Ma). Following the collapse, the main eruptive centres migrated 1.5–2.8 km north into the head scarp (at Pirongia Summit and Pūawhe; see Fig. 1), with prominent andesitic to basaltic cones constructed along strike of the LOF (Figs. 1 and 10) indicating strong fault control. In addition, most andesite dykes of the summit vent are oriented perpendicular to the scarp axis.

Deposit preservation

The remarkable thickness and preservation of the Oparau breccia is the direct result of channelisation into the Oparau Graben, a low-relief, low energy depositional environ that extends to (present) sea level. Similar preservation is observed in the Quaternary cover sequence around Kawhia Harbour, which includes numerous tephras and several rhyolitic ignimbrites (i.e. Tiritiri Ignimbrite, Fergusson, 1986; Oparau Tephra, Pain, 1975) that are substantially thicker than at other North Island localities (Horrocks, 2000). These ignimbrites, derived from vents >80 km from Pirongia, attest to efficient channelisation of directional volcanic-flow deposits at distances both proximal and distal to the channel itself.

Conclusions

In this study, we describe a previously unidentified long runout (>20 km), 3.3 km^3 channelised debris avalanche deposit from Pirongia Volcano. The Oparau breccia was emplaced following large-scale sector collapse of a low-angle basaltic shield dominated by ankaramite lavas. Channelisation of this deposit resulted in substantial thickening of the flow (≤200 m) in proximal to medial areas. The deposit consists of block and matrix facies, including jigsaw fractured clasts and megaclasts/domains up to 30 m wide. Tertiary rip up clasts are concentrated at the base of the deposit. Mesozoic clasts occur towards the centre of the deposit and originate from the sub-edifice bedrock. The sector collapse scarp is marked by a prominent unconformity on the volcanic edifice. Edifice stratigraphy and tephrochronology indicate an emplacement age between 2.2 and 1.75 Ma. Graben related normal faults separate the Oparau breccia from pre-2.30 Ma ring plain terraces. We infer that Pleistocene-age fault movements occurred within the graben and likely triggered the collapse event. In the post-collapse period, the scarp was infilled by 5 km^3 of volcanic material from vents aligned parallel to the scarp axis.

Acknowledgements

This paper benefited from in depth discussions over several years with Roger Briggs, David Lowe and Peter Kamp, and fieldtrips with Marco Brenna, Shane Cronin, Nick Mortimer, Szabolcs Kósik, George McQuillan and Geoff Lerner. Cam Nelson is thanked for information on the Te Kuiti Group in the Oparau area. Jo Horrocks is thanked for allowing us to use data from her thesis. Drill core data was sourced from the New Zealand Geological Survey – Coal Resources Survey conducted between 1979 and 1985. OEM was supported by a University of Waikato Doctoral Scholarship.

References

Alloway B, McComb P, Neall V, Vucetich C, Gibb J, Sherburn S, Stirling M 2005. Stratigraphy, age, and correlation of voluminous debris-avalanche events from an ancestral Egmont Volcano: Implications for coastal plain construction and regional hazard assessment. Journal of the Royal Society of New Zealand 35: 229–267.

Beget JE and Kienle H 1992. Cyclic formation of debris avalanches at Mount St Augustine volcano. Nature 356: 701–704.

Belousov A, Belousova M, Voight B. Multiple edifice failures, debris avalanches and associated eruptions in the Holocene history of Shiveluch volcano, Kamchatka, Russia. Bulletin of Volcanology 61: 324–342.

Blong RJ 1986. Pleistocene volcanic debris avalanche from Mount Hagen, Papua New Guinea. Australian Journal of Earth Sciences 33: 287–294.

Briggs RM 1983. Distribution, form and structural control of the Alexandra Volcanic Group, North Island, New Zealand. New Zealand journal of geology and geophysics 26, 47–55.

Briggs RM 1986. Volcanic rocks of the Waikato Region, western North Island, and some possible petrologic and tectonic constraints on their origin. In: Smith IEM Late Cenozoic volcanism in New Zealand: a collection of papers dealing with the nature and distribution of Late Cenozoic volcanic activity in New Zealand. 76–91.

Briggs RM, Itaya T, Lowe DJ, Keane AJ 1989. Ages of the Pliocene-Pleistocene Alexandra and Ngatutura Volcanics, western North Island, New Zealand, and some geological implications. New Zealand Journal of Geology and Geophysics 32: 417–427.

Chappell JMA 1970. Quaternary geology of the south-west Auckland coastal region. Transactions of the Royal Society of New Zealand (Earth Science) 8(10): 133–153.

Clavero JE, Sparks RSJ, Huppert HE, Dade WB 2002. Geological constraints on the emplacement mechanism of the Parinacota debris avalanche, northern Chile. Bulletin of Volcanology 64: 40–54.

Cohen KM, Gibbard PL 2019. Global chronostratigraphical correlation table for the last 2.7 million years. Quaternary International vol. 500. Fig. 1.

Crandell DR, Miller CD, Glicken HX, Christiansen RL, Newhall CG. Catastrophic debris avalanche from ancestral Mount Shasta volcano, California. Geology 12: 143–146.

Delcamp A, Kervyn M, Benbakkar M, Kwelwa S, Peter D 2017. Large volcanic landslide and debris avalanche deposit at Meru, Tanzania. Landslides 14: 833-847.

Ellsworth D and Voight B 1995. Dike intrusion as a trigger for large earthquakes and the failure of volcano flanks. Journal of Geophysical Research 100, 6005–6024.

Francis PW and Wells GL 1988. Landsat Thematic Mapper observations of debris avalanche deposits in the Central Andes. Bulletin of Volcanology 50: 258–278.

Gaylord DR and Neall VE 2012. Subedifice collapse of an andesitic stratovolcano: The Maitahi Formation, Taranaki Peninsula, New Zealand 124: 181–199.

Glicken HX 1991. Sedimentary architecture of large volcanic-debris avalanches. In Fisher RV and Smith GA (eds) Sedimentation in volcanic settings, vol 45. SEPM Special Publication, pp 99–106.

Glicken HX 1996. Rockslide-debris Avalanche of May 18, 1980, Mount St. Helens Volcano, Washington: U.S. Geological Survey Open-File Report 96-677, 90 p., 5 plates.

Horrocks JL 2000. Stratigraphy, chronology, and correlation of the Plio-Pleistocene (c. 2.2-0.8 Ma) Kauroa Ash sequence, western central North Island, New Zealand. Unpublished Ph.D. thesis, University of Waikato, Hamilton.

Hsü KJ 1975. Catastrophic debris streams (Sturzstroms) generated by rock falls. Geological Society of America Bulletin 86: 129–140.

Lowe DJ, Tippett JM, Kamp PJJ, Liddell IJ, Briggs RM, Horrocks JL 2001. Ages on weathered Plio-Pleistocene tephra sequences, western North Island, New Zealand. In: Juvigne ET, Raynal JP (eds). Tephras: Chronology, Archaeology, CDERAD editeur, Goudet. Les Dossiers de l'Archeo-Logis 1, 45–60.

McLeod OE, Pittari A, Brenna M, Briggs, RM 2020. Geology of the Pirongia Volcano, Waikato : 1 :30,000 Geological Map. Wellington, New Zealand, Miscellaneous Publicatoin v. 156, 60 p. Text + A0 fold out map.

Naish T, Kamp PJJ, Alloway BV, Pillans B, Wilson GS, Westgate JA 1996. Integrated tephrochronology and magnetostratigraphy for cyclothemic marine strata, Wanganui Basin: implications for the Pliocene-Pleistocene boundary in New Zealand. Quaternary International 34–36: 29–48.

Naish TR, Kamp PJJ, Alloway BV, Pillans BJ, Wilson GS, Westgate JA 1996. Integrated tephrochronology and magnetostratigraphy for cyclothemic marine strata, Wanganui Basin: implications for the Pliocene-Pleistocene boundary in New Zealand. Quaternary International, 34-36: 29–48.

Neall VE 1979. Sheets P19, P20 and P21 New Plymouth, Egmont and Manaia, Geological Map of New Zealand 1:50,000. 3 maps and notes. New Zealand Department of Science and Industrial Research, Wellington, p 36.

New Zealand Geological Survey – Coal Resources Survey. Drill core data available in the online in the New Zealand Mineral and Petroleum database: data.nzpam.govt.nz.

Nicoletti PG and Sorriso-Valvo M 1991. Geomorphic control of the shape and mobility of rock avalanches. Geological Society of America Bulletin 103: 1365–1373.

Paguican EMR, van Wyk de Vries B, Lagmay AMF 2012. Volcanic-tectonic controls and emplacement kinematics of the Iriga debris avalanches (Phillipines). Bulletin of Volcanology 74, 2067–2081.

Palmer BA, Alloway BV and Neall VE 1991. Volcanic-debris avalanche deposits in New Zealand–lithofacies organization in unconfined, wet-avalanche flows. In Fisher RV, Smith GA (eds) Sedimentation in volcanic settings, vol 45. SEPM Special Publication, pp 89–98.

Pillans B, Alloway BV, Naish T, Westgate JA, Abbot S, Palmer AS 2005. Silicic tephras in Pleistocene shallow marine sediments of Wanganui Basin, New Zealand. Journal of the Royal Society of New Zealand 35: 43–90.

Robertson DJ 1976. A paleomagnetic study of volcanic rocks in the South Auckland area. Unpublished MSc thesis, lodged in the Library, University of Auckland, Auckland.

Seward D, Kohn BP 1997. New zircon fission-track ages from New Zealand Quaternary tephra: an interlaboratory experiment and recommendations for the determination of young ages. Chemical Geology 141: 127–140.

Shea T, van Wyke de Vries B, Pilato M 2008. Emplacement mechanisms of contrasting debris avalanches at Volcán Mombacho (Nicaragua), provided by structural and facies analysis.

Siebert L 1984. Large volcanic debris avalanches: characteristics of source areas, deposits, and associated eruptions. Journal of Volcanology and Geothermal Research 22: 163–197.

Smith GA and Lowe DR 1991. Lahars: volcano-hydrologic events and deposition in the debris flow – hyperconcentrated flow continuum. In Fisher RV, Smith GA (eds) Sedimentaiton in volcanic settings, vol 45. SEPM Special Publication, pp 59–70

Stoopes GR and Sheridan MF 1992. Giant debris avalanches from the Colima volcanic complex, Mexico: implication for long-run-out landslides (>100 km). Geology 20: 299–302.

Takarada S, Ui T, Yamamoto Y 1999. Depositional features and transportation mechanism of valley-filling Iwasegawa and Kaida debris avalanches, Japan. Bulletin of Volcanology 60: 508–522.

Tost M, Cronin SJ, Procter JN 2014. Transport and emplacement mechanisms of channelised long-runout debris avalanches, Ruapehu volcano, New Zealand. Bulletin of Volcanology 76: 881.

Ui T 1983. Volcanic dry avalanche deposits – identification and comparison with nonvolcanic debris stream deposits. Journal of Volcanology and Geothermal Research 18: 135–150.

Vallance JW, Siebert L, Rose WI, Giron JR, Banks NG 1995. Edifice collapse and related hazards in Guatemala. *In* Ida Y and Voight B (eds): Models of magmatic processes and volcanic eruptions. Journal of Volcanology and Geothermal Research 66: 337–355.

Voight B, Glicken H, Janda RJ, Douglass PM 1981. Catastrophic rockslide avalanche of May 18. In Lipman PW and Mullineaux DR (eds). The 1980 eruptions of Mount St. Helens, Washington: U.S. Geological Survey Professional Paper 1250, p.347–377.

Von Hochstetter F and Sauter E 1867. New Zealand, Its Physical Geography, Geology and Natural History: With Special Reference to the Results of Government Expeditions in the Provinces of Auckland and Nelson.

Waterhouse BC and White PJ 1994. Geology of the Raglan-Kawhia area. Lower Hutt: Institute of Geological and Nuclear Sciences. Institute of Geological and Nuclear Sciences geological map 13, 48 p.

Wooler L, van Wyk de Vries B, Cecchi E, Rymer H 2009. Analogue models of the effect of long-term basement fault movement on volcanic edifices. Bulletin of Volcanology 71, 1111–1131.

Zernack AV, Procter JN, Cronin SJ 2009. Sedimentary signatures of cyclic growth and destruction of stratovolcanoes: A case study from Mt. Taranaki, New Zealand. Sedimentary Geology 220: 288–305.

Zernack AV, Cronin SJ, Neall VE, Procter JN 2011. A medial to distal volcaniclastic record of an andesite stratovolcano: detailed stratigraphy of the ring-plain succession of south-west Taranaki, New Zealand. International Journal of Earth Sciences 100: 1937–1966.

Appendices

Appendix 1

Major and trace element data for representative clasts from the Oparau breccia. Rock types: A-bas=alkalic basalt, And=andesite, Bas=basalt, T-bas= trachybasalt, Ank=ankaramite, Bas-an=basaltic andesite, Bas-T=basaltic trachyandesite.

Sample	PK3-B	PW8	PY2	PAD3-A	PPO1	PK3-A	PPO2-A	PK2-B	PW10	PAD3-B	PK2-A	PAD-1	PAD-3C
	Diorite	A-bas	And	Bas	Bas	Bas	Bas	T-bas	Ank	Bas-an	Bas-an	Bas-T	Bas-T
SiO_2	45.59	46.01	46.21	47.63	48.76	50.30	51.33	51.35	51.46	51.86	52.06	52.33	54.66
Al_2O_3	17.09	12.42	21.88	15.21	18.59	16.12	16.49	17.44	16.31	17.84	17.07	17.93	17.47
TiO_2	1.10	2.33	0.98	0.81	0.97	0.90	0.92	0.98	0.91	0.76	0.87	0.76	0.75
MnO	0.24	0.19	0.24	0.19	0.19	0.18	0.16	0.18	0.16	0.20	0.16	0.20	0.15
Fe_2O_3	12.48	12.69	11.34	11.04	11.54	11.04	9.95	10.63	10.08	9.25	10.21	8.81	8.61
MgO	6.88	11.54	4.11	5.87	4.91	5.83	5.24	4.82	5.81	4.21	5.11	3.72	3.76
CaO	12.69	10.32	8.67	11.88	10.38	10.82	10.96	9.25	10.69	9.54	10.17	9.49	8.53
Na_2O	2.42	2.98	2.93	3.59	2.88	2.90	2.88	3.28	3.02	3.31	3.13	3.76	3.71
K_2O	0.51	1.18	0.37	0.40	1.38	1.58	1.50	1.83	1.47	1.91	1.12	2.18	1.95
P_2O_5	0.36	0.54	0.29	0.52	0.29	0.31	0.29	0.34	0.21	0.37	0.24	0.43	0.29
LOI	1.28	0.09	3.55	2.88	0.62	0.26	0.60	0.28	0.04	1.24	0.32	0.66	0.37
Total	100.79	100.41	100.72	100.20	100.65	100.38	100.48	100.53	100.30	100.67	100.65	100.53	100.43
Sc	39	27	26	31	32	33	34	27	37	21	36	17	22
V	365	246	260	299	315	285	278	287	306	223	288	221	225
Cr	140	546	54	124	43	92	138	38	132	59	155	43	43
Co	51	74	38	41	45	52	44	47	49	39	51	34	28
Ni	76	266	51	135	24	50	116	27	42	24	49	33	20
Cu	47	69	35	87	82	88	43	99	76	27	26	40	94
Zn	76	92	78	63	91	74	74	78	73	77	66	72	69
Ga	18	18	23	15	18	16	16	18	17	17	18	18	17
Rb	14	19	3	46	22	44	39	48	41	53	24	72	62
Sr	632	559	568	829	540	456	450	545	445	626	386	755	533
Y	26	19	23	29	21	20	22	22	20	22	20	25	20
Zr	54	166	128	177	88	89	95	100	96	115	82	149	105
Nb	3.19	32.78	5.35	4.53	2.94	3.34	4.15	4.14	3.82	4.69	3.88	5.64	3.76
Rh	0.64	0.36	0.53	0.30	0.64	0.45	0.37	0.38	0.30	0.49	0.50	0.42	0.43
Pd	0.59	0.46	0.54	0.41	0.62	0.54	0.42	0.50	0.34	0.57	0.54	0.51	0.47
Cs	0.82	0.48	0.29	18.20	0.80	1.93	1.93	1.68	0.68	2.32	0.37	3.56	1.12
Ba	229	294	536	654	556	466	652	526	594	690	417	848	774
La	15.6	26.1	22.0	44.6	17.8	17.9	24.6	21.8	21.6	28.1	13.6	38.0	26.2
Ce	38.2	52.3	52.0	106.1	39.2	36.5	43.2	44.0	42.2	55.9	28.8	75.4	48.6
Pr	5.62	6.33	5.88	13.26	4.87	4.73	5.33	5.56	5.08	6.79	3.64	9.06	5.72
Nd	26.01	27.24	24.58	56.50	21.64	20.32	22.38	23.53	20.85	27.22	15.18	36.20	22.87
Sm	6.11	6.16	5.25	11.65	4.82	4.37	4.53	5.14	4.39	5.59	3.38	7.10	4.35
Eu	1.74	1.88	1.50	2.92	1.40	1.23	1.20	1.43	1.28	1.48	1.10	1.91	1.23
Gd	5.84	5.34	4.81	9.32	4.54	4.22	4.15	4.72	4.11	4.79	3.54	6.04	4.05
Tb	0.85	0.73	0.70	1.22	0.66	0.60	0.62	0.66	0.62	0.66	0.56	0.82	0.60
Dy	4.95	4.04	4.31	5.93	3.98	3.64	3.68	4.04	3.71	3.89	3.62	4.79	3.49
Ho	0.94	0.68	0.85	1.00	0.82	0.74	0.73	0.80	0.75	0.75	0.70	0.90	0.69
Er	2.67	1.87	2.35	2.70	2.42	2.07	2.13	2.29	2.10	2.31	2.11	2.39	1.96

Tm	0.35	0.22	0.33	0.32	0.30	0.29	0.27	0.31	0.29	0.32	0.31	0.35	0.28
Yb	2.30	1.47	2.29	2.04	2.23	1.85	1.87	2.15	1.92	2.11	2.08	2.39	1.92
Lu	0.33	0.19	0.32	0.29	0.31	0.30	0.27	0.32	0.28	0.33	0.31	0.35	0.29
Hr	1.85	3.88	3.46	4.24	2.52	2.56	2.57	2.74	2.68	2.91	2.32	3.57	2.78
Ta	0.39	2.11	0.54	0.39	0.40	0.46	0.44	0.47	0.51	0.45	0.47	0.52	0.43
Tl	0.04		0.10	0.13	0.06				0.04	0.07		0.14	0.12
Pb	1.59	2.18	5.81	5.00	4.43	3.98	6.41	4.69	4.16	4.97	2.68	6.12	3.80
Th	1.94	3.69	8.41	14.38	5.09	5.90	7.72	6.08	7.37	8.93	4.14	12.41	8.91
U	0.42	1.04	0.34	1.74	0.81	1.28	1.61	1.29	1.60	1.81	0.88	2.69	1.95
$^{87}Sr/^{86}Sr$									0.705047				
$^{143}Nd/^{144}Nd$									0.512736				

Chapter 5

Conclusions

5.1 Preamble

The work presented in this thesis firmly establishes the Pirongia Volcano and the Alexandra Volcanic Group as the type-site of basaltic volcanism within the Late Cenozoic history of North Island, New Zealand. Through the detailed geological mapping, geochemistry and ring plain analyses presented in chapters 2–4, this thesis fulfils the aims and objectives laid out in Section 1.3.

In the following sections, an overview of the main findings of chapters 2–4 is presented in the context of the research objectives. These findings are then evaluated in terms of their wider implications for the discipline of volcanology. Finally, some recommendations for the direction of future geological research are made, along with a final remark on the importance of detailed mapping illustrated by this study.

5.2 Review of chapter findings

5.2.1 Chapter 2 – a new volcano-stratigraphic map and its implications for volcanic history

The core output of Chapter 2 was a new 1:30,000 scale geological map of Mount Pirongia, which, along with the companion explanatory text comprises a stand-alone publication on the entire volcanic history of Pirongia Volcano.

The map subdivides the virgin territory and previously undifferentiated Pirongia Volcanic Formation into six new stratigraphic members and 36 new lithostratigraphic units. Collectively, the mapped deposits amount to ~30 km^3 of material that comprise the single largest basaltic volcano in the North Island, active between ~2.5 and 1.6 Ma.

Mapping indicates that the Pirongia edifice consists of a large-volume shield volcano overlain by three stratovolcanic cone-complexes and numerous minor vent centres. About 50 volcanic dykes crop out across the mountain, marking the sites of at least 18 volcanic vents. An exact location of the late-stage central vent at Pirongia Summit was proposed using the projected convergence zone of radial dykes on the surrounding ridgelines.

Erupted lavas show substantial variation in terms of composition, mineralogy and texture from clinopyroxene-rich ankaramite and alkali olivine basalt to finer-grained, hornblende-phyric basaltic andesites and andesites. These lithological variances played a fundamental role in the field and petrographic correlation of lithostratigraphic units.

The Pirongia ring plain is subdivided into four volcano-sedimentary packages on geomorphic, geographic and stratigraphic grounds. Two ring plain units demarcate extensive volcanic debris avalanche deposits, which correspond to major collapse-related unconformities on the edifice. The collapse scarps are infilled by younger edifice members, indicating that edifice 'healing' has occurred.

5.2.2 Chapter 3 – IAB-OIB systematics of back-arc volcanism

In Chapter 3, detailed stratigraphy, petrography, mineral chemistry, whole-rock geochemistry and isotope data were used to define the IAB-OIB systematics at play in the basaltic stratovolcanoes and their surrounding monogenetic fields. The new geochemical data represents the most complete geochemical 'portrait' of Pirongia, and the first geochemical dataset ever published for Karioi.

IAB-type lavas predominate in the AVG, forming large stratovolcanoes (Karioi and Pirongia) and smaller adjacent centres (Kakepuku and Te Kawa), while OIBs form low-volume, scattered monogenetic vents that increases in prevalence to the northwest. Minor intercalation of OIB with IAB occurs at Pirongia and Kakepuku, while OIB forms almost half of the rock mass of Karioi. The latter is most evident at Te Toto gorge, where extensive sampling provides unambiguous evidence of OIB-IAB intercalation in the lower stratigraphy of Karioi.

Elemental and Sr-Nd isotopic data show that all lavas of the Alexandra arc volcanoes have compositions falling on a spectrum between IAB and OIB endmembers. The compositional spectrum is most evident in the linear array of Sr-Nd compositions for the field, and in the substantial variations of the Nb-Ta anomaly among arc lavas. A two-component mixing model created for Pirongia was able to explain all Sr-Nd isotopic variation by mixing of between 5 and 81 % OIB with an IAB endmember composition.

Field-wide geochemical variation was examined in both a spatial and temporal context. There is a north-westward enrichment in $^{143}Nd/^{144}Nd$ and Nb/La from Te Kawa to Karioi that corresponds to a decrease in the 'arc' signature and increase in the 'intraplate-OIB' signature with increasing slab depth. Temporally, Karioi is defined by 'on/off' alternations of OIB-IAB volcanism, while Pirongia displays progressive and cyclical enrichment from IAB to transitional compositions. The latter is considered to represent contamination of the magma reservoir(s) by OIB magma injections.

An encompassing petrogenetic model was proposed to explain the geochemical systematics of the Alexandra Volcanic Group. The model defines slab-tearing and back-arc

extension as fundamental tectonic factors responsible for the formation of the volcanic lineament, and the juxtaposition of distinct mantle sources that give rise to IAB and OIB. Slab-rollback induces vertical and lateral flow of the asthenosphere into the metasomatized mantle wedge, forming OIB magmas through decompression melting, with secondary conductive melting of the wedge forming IAB magmas. Some OIB magmas ascend to the surface via crustal faults, while IABs (and some OIBs) underplate the crust, forming crystal mushes. Large-scale extension events in the back-arc lead to rapid depressurisation of the mushes and entrainment within fresh basaltic magmas. The subsequent eruptions of mega-crystalline (ankaramite) basalt occurred contemporaneously at multiple volcanoes across the field. At Pirongia, continued injection of OIB into the upper mantle/crustal IAB reservoirs led to eruptions with more transitional (OIB-like) compositions through time. A similar progression towards transitional compositions is also apparent in the late-stage summit cone of Karioi, though further stratigraphic work is required to confirm this.

5.2.3 Chapter 4 – origins of flank collapse and a major debris avalanche

In Chapter 4, the newly mapped Oparau breccia (the sole lithostratigraphic unit of Oparau Member) was identified as a large-volume (3.3 km^3) volcanic debris avalanche deposit from Pirongia Volcano. The deposit contains textural features characteristic of other debris avalanche deposits worldwide, i.e. block and matrix facies, jigsaw-fractured clasts and megaclasts up to 30 m wide. Using field stratigraphy and archived drill core data, the emplacement geometry and cross-sectional thickness of the deposit were defined. The debris avalanche was emplaced into a graben-valley (the Oparau graben), which resulted in rapid channelisation of the deposit. Channelisation led to a long run out distance (>20 km) and extraordinary thickness (~200 m) at medial distances (10 km) from Pirongia. Sector collapse occurred within the low-angle (11–13º), low elevation (1000 m) edifice underlain by faulted and fractured Mesozoic basement rocks. The source zone of the collapse is demarcated by a large unconformity on western Pirongia, separating old shield flanks (2.5 Ma) from younger lavas of Pirongia Summit Member (1.6 Ma). Stratigraphy and tephrochronology indicate that the debris avalanche deposit was emplaced between 2.2 and 1.75 Ma.

Sector collapse was pre-conditioned by gravitational spreading exacerbated by extension within the Oparau graben at the base of the mountain. The collapse may have been triggered by movement on the (newly mapped) Little Oparau Fault, which has moved after 2.30 Ma, based on offset in the ring plain stratigraphy within the graben. The fault projects under the collapse scarp

and is sub-parallel in strike to the scarp-axis. Following collapse, the scarp was infilled by 5 km^3 of material generated by late-stage resurgent volcanism at Pirongia Summit and Pūawhe/The Cone. These summit vents were aligned parallel to the Little Oparau Fault and are situated within its downfaulted block.

5.3 Wider implications

5.3.1 For North Island volcanism

The Alexandra Volcanic Group has remained an enigmatic and poorly defined volcanic feature in the North Island, and to date its integration into the literature has been either inconsistent or absent. In this thesis, the volcanic field has been firmly established as the epicentre of arc-related *basaltic* volcanism in North Island, and the point of inception for *intraplate (OIB)* volcanism of the Auckland Province. In the section below, some key implications of this study for North Island volcanism are listed.

Cross-arcs

The Alexandra Volcanic Lineament is a cross-arc feature associated with the Tonga-Kermadec-Hikurangi subduction system. Cross-arcs of similar orientation and length occur elsewhere on land in the western North Island (e.g. the Taranaki volcanics and Kiwitahi centres) and off-shore in the Kermadec Arc and older Colville Ridge. In the case of the AVG, formation of the cross-arc has been linked to tearing of the subducted slab (Chapter 3), which has caused linear focusing of melting, and which explains the bi-modal eruption of IAB and OIB. If the slab tear explanation is correct, this mechanism could explain the development of other cross-arcs in the North Island and offshore arc setting.

A window into the submarine arc

Continuing from the previous point, back-arc basaltic volcanism of the AVG is similar in composition, magnitude and cross-arc formation to back-arc basalts of the submarine Kermadec Arc and older Colville and Kermadec ridges. Recent bathymetric surveys have uncovered coarsely crystalline basalts from these volcanoes that are reminiscent of the AVG ankaramites (C. Timm, pers. comm. 2019). It is suggested that the AVG is a useful proxy site for studying back-arc, submarine basaltic volcanism in the region north of New Zealand.

Back-arc extension

The Hamilton Basin is a major (but largely unrecognised) tectonic depression associated with back-arc extension and volcanism in western North Island. Normal faults within the basin have controlled the position of arc-type volcanoes along the Alexandra Volcanic Lineament (i.e. Pirongia, Kakepuku and Te Kawa), while parallel faults west of the basin have controlled the location of Karioi. The Hamilton Basin is comparable to the active Hauraki Rift to its east (Hochstein and Ballance, 1993) in terms of dimension and orientation. Recognition of the Hamilton Basin as a back-arc extensional structure is crucial geomorphic evidence for slab-rollback, crustal extension and the generation of back-arc basaltic volcanism in the AVG.

Origin of intraplate volcanism

There is now a clear and indisputable stratigraphic link between arc-related (IAB) and intraplate-related (OIB) volcanism in the Alexandra Volcanic Group. This association, which occurs at only one volcanic field in the North Island and is rare globally, provides crucial information about the formation conditions of OIB magmas and their surface manifestation – monogenetic volcanic fields. In North Island, there is an ongoing discourse about the fundamental cause of intraplate volcanism (namely for the Auckland Volcanic Field) and why the fields of the Auckland Province show northward younging from Alexandra and Ngatutura to South Auckland and Auckland (Hodder, 1984; Briggs et al. 1994; Spörli and Eastwood 1997; Smith and Cronin, 2020).

New evidence presented in this study suggests that the Alexandra OIBs originate from vertical and lateral upwelling of asthenospheric mantle around the subducted slab. This process appears to be triggered by slab-rollback, which induces the asthenosphere to upwell and 'fill the gaps' in the mantle wedge as the slab retreats. Subsequent melting of this upwelled mantle forms OIB magmas within the wedge. It is argued here that the northward migration of OIB volcanism is likely associated with slab edge effects, with lateral flow of the asthenosphere induced in a propagating fashion as the slab migrated eastwards to its current position, which is subvertical ~100 km southeast of Auckland. This is in broad agreement with Smith and Cronin (2020) who describe the northward migration as the result of asthenospheric destabilisation associated with the subducted slab, which gives rise to discrete 'mini plumes' that erupt in an extensional setting. The rate of this propagation is ~5 cm/yr, based on the distance and age of OIB-volcanism from the AVG to Auckland Volcanic Field (Briggs et al. 1994).

In addition to the asthenospheric source processes, lithospheric controls (i.e. the north-south trending terrane boundaries, fractures and the regional fault network) have undoubtedly

played an additional (but secondary) role in defining the location of OIB-volcanism, as discussed by Spörli and Eastwood (1997).

An outstanding question is: *Why do arc-basalts not occur in the younger OIB-fields of the Auckland Province, if asthenospheric upwelling is capable of triggering IAB melting in the back-arc?* The answer to this question is likely related to the scale of OIB magma generation, which is markedly lower at Ngatutura (1 km^3), South Auckland (2.5 km^3) and Auckland (1.7 km^3) than the total OIB output of the AVG (8–10 km^3). The prolific generation of OIB-magma required to generate secondary melting of the metasomatized mantle wedge, as envisaged by the petrogenetic model in Chapter 3, has not occurred in the other monogenetic fields and thus these fields did not co-erupt IABs. However, on a smaller scale, the process of secondary melting of metasomatized mantle is documented in both the Auckland and South Auckland fields, giving rise to OIBs with some geochemical characteristics inherited from metasomatized mantle (Cook et al. 2005; McGee et al. 2013).

Future models attempting to the explain the development of Auckland Province volcanism must account for the *fundamental* inception process of slab tear and lateral flow that has occurred in the AVG.

5.3.2 Geoheritage

According to the definition of Brocx and Semeniuk (2007), geoheritage '*encompasses global, national, statewide, and local features of geology, at all scales that are intrinsically important sites or culturally important sites offering information or insights into the evolution of the Earth; or into the history of science, or that can be used for research, teaching, or reference*'.

In New Zealand, geological sites are indexed in the New Zealand Geopreservation Inventory, which provides an assessment of importance (A–C) and vulnerability to human damage (1–4).

A = of international scientific, aesthetic or educational value
B = of national scientific, aesthetic or educational value
C = of regional scientific, aesthetic or educational value

1 = vulnerable to complete destruction by human-related activities
2 = vulnerable to significant damage by human-related activities
3 = robust and not considered to be vulnerable to most human-related activities
4 = values (e.g. rock exposure) could be improved by targeted human-related activities

Currently, Pirongia and Karioi have an index of (B, 3), indicating that they are of national significance and not vulnerable to most human-related activities. A further six sites from the Alexandra Volcanic Group are specified in the index:

1. Ruapane ('bald spur') ridge on Pirongia (C, 3)
2. Te Toto Gorge on Karioi (C, 3)
3. Te Kawa quarry (C, 3)
4. Papanui Point, Okete Volcanics (C, 3)
5. Okete quarry, Okete Volcanics (C, 3)
6. Bridal Veil Falls, Okete Volcanics (C, 3)

Of these sites, it is argued that Te Toto Gorge is now of international significance, as it has the best exposed and most complete IAB-OIB stratigraphic succession globally. A new proposed index for Te Toto Gorge is (A, 3)

The current geopreservation index for Pirongia (B, 3) remains appropriate in light of this research. The national scientific and educational value of Mt Pirongia is reinforced with the following findings:

1. Pirongia is North Island's largest basaltic volcano;
2. the volcano is composed predominantly of ankaramite, the most crystal-rich basaltic lava type on Earth, which does not occur elsewhere in New Zealand (beyond the Alexandra Volcanic Group), and along with Karioi, Pirongia is essentially an onshore equivalent of the basaltic volcanoes that lie submerged along the volcanic arc to the north of New Zealand; and
3. globally rare karst-weathered basalt occurs at two localities on Pirongia.

This research has drawn significant and sustained interest from the people of the Waikato Region. This is exemplified in the following ways:

1. the Pirongia geological map has received significant interest from the public and, at the time of writing, is in press as a hard copy map and illustrated map bulletin (200 copies in the initial print);
2. over 250 people have attended three public lectures on the volcanic history of Pirongia – this is the highest attendance of any lectures related to the Earth Sciences department of University of Waikato in the last two decades – and invitations for further talks are ongoing, with at least two more large lectures planned in 2020;

3. new geological information signage and display of the geological map on Mt Pirongia is being organised through an invited collaboration with Maori stakeholders of Pirongia and Oparau, the Department of Conservation and the Pirongia Restoration Society;
4. new archaeological work on the provenance of stone adzes from the Pirongia Volcanic Formation is in the early stages of development, an idea that has arisen from discussion based on this research; and
5. consistent interest from journalists has yielded four newspaper articles in the New Zealand Herald, Te Awamutu Courier and Waitomo News, and several smaller articles have appeared in the Pirongia Heritage Centre monthly newsletter.

In conclusion, the new 1:30,000 geological map and publications of this thesis have brought the geoheritage value of Pirongia to the attention of a wider public audience. Recognition of the geoheritage value of Pirongia and all other volcanic landforms in the Alexandra Volcanic Group will assist in their preservation from both a geological and biological (i.e. conservation) perspective.

5.3.3 Global implications

The points below summarise the key scientific implications of this work that are relevant beyond the New Zealand setting and apply to other volcanic fields globally.

- **The Plio-Pleistocene 'sweet spot':** Stratovolcanoes formed between 2.5 and 1.0 Ma are ideal subjects for volcanic mapping because they have undergone enough erosion (100–300+ m vertically) to expose their shallow dyke structures. These volcanoes, which are within the 'planeze stage' of erosion (Kear, 1957) are crucial sites for investigating the magmatic plumbing system of central and flank vents that is not observable (i.e. is buried) in most Holocene volcanoes.

- **The intimate link between IAB and OIB volcanism:** The Alexandra Volcanic Group contains two of the best examples globally of intercalated IAB-OIB within the Karioi and Pirongia volcanic successions. In this study, the juxtaposition of these two magma types was explained by the flow of un-metasomatised asthenospheric mantle into the mantle wedge via a tear in the subducted slab, accompanied by lateral flow around the slab edge. While slab tear and lateral flow have been proposed at other OIB-bearing arcs globally (Ferrari et al. 2001; Hildreth, 2007), the AVG is the first field to display both tectono-magmatic controls together. Slab-rollback appears to be a key process in inducing the lateral (and vertical) flow of fresh asthenosphere into the wedge. In the back-arc, rollback

also induces extension in the overlying crust, which allows OIBs to rise and erupt within the typical 'arc' setting associated with the slab and metasomatized mantle wedge.

- **Ankaramites:** Megacrystalline basalts, such as the ankaramites of the AVG, are typical products of many ocean islands (e.g. Tahiti, the Cook Islands, Samoa, Hawaii and Tenerife) and some arc settings (e.g. Indonesia and Vanuatu). In the AVG, ankaramite formation has been linked to crustal underplating and crystal-mush formation followed by rapid release of crystals and melt during major back-arc extension events. Ankaramites in arc and intraplate settings worldwide may be important tectonic markers of back-arc extension, rifting or rapid collapse events. Radiometric dates and stratigraphic controls on ankaramite lavas/edifice packages may thus provide the timing of major tectonic extension/collapse events at individual stratovolcanoes and volcanic shields.

5.4 Directions for future work

- Pliocene and Early Pleistocene stratovolcanoes worldwide are excellent subjects for geological mapping because of their pronounced erosional state. Future mapping, using the mapping methodology of Chapter 2, should now be undertaken on similar extinct stratovolcanoes in other countries, particularly the volcanic arcs of Latin America (e.g. the Trans Mexican Volcanic Belt and the Andes) where hundreds of such volcanoes (both forested and unforested) remain unstudied. Mapping should be augmented where possible by newly established LiDAR drone surveys to produce high-resolution DEM base maps that 'see through' the forest cover.

- The most primitive AVG arc-basalts should be examined in the wider context of the Taupo Volcano Zone to determine whether they have any petrogenetic connection to the parental magmas feeding the rhyolitic and andesitic systems of central North Island.

- Ankaramites in the South Pacific islands (Tahiti, Cook Islands, Samoa, Tonga, Fiji) and the Kermadec Arc should be studied and compared to the Alexandra ankaramites. A detailed stratigraphic and petrological study should be undertaken to better understand the tectonic-magmatic significance of mega-crystalline basalt and what its formation implies about the mantle to crust migration of basaltic magmas in arc and intraplate settings.

5.5 Closing remarks

The study of volcanic systems reveals important details about the nature and cyclicity of magma generation, which in turn is linked to mantle fluxes associated with subduction, mantle plumes and spreading margins. In all these settings, accurate and detailed stratigraphic mapping of the volcanic terrain is the crucial and indispensable foundation upon which all other petrologic interpretations can be drawn. Stratigraphy is the single strongest evidence for the temporal expression of magmatism, which fundamentally constrains the geological meaning of other data such as radiometric dating and elemental and isotopic geochemistry. Indeed, the quality of geological investigation is directly related to the quality of outcrops, the extent of mapping and the depth of understanding of the stratigraphic relationships between volcanic units within any given volcanic succession.

The challenge for future generations of geologists is to maintain a pre-requisite focus on stratigraphy *before* applying existent and rapidly emerging geochemical techniques to questions of petrogenesis in the discipline of volcanology.

Finally, the author considers it of great importance that geologists continue to seek out, explore and map the 'unknown' volcanic terrain of New Zealand and further afield. Although the world may seem largely explored, there are still innumerable geological discoveries to be made.

References

The following references are those cited in the introduction (Chapter 1) and conclusions (Chapter 5). Reference lists for chapters 2-4 are contained at the end of those chapters.

Bacon CR 2008. Geologic map of Mount Mazama and Crater Lake caldera, Oregon. US Geological Survey Scientific Investigations Map 2832 (4).

Branca S, Coltelli M, Groppelli G, Lentini F 2011. Geological map of Etna volcano, 1: 50,000 scale. Italian Journal of Geosciences 130(3), 265–291.

Briggs RM 1983. Distribution, form and structural control of the Alexandra Volcanic Group, North Island, New Zealand. New Zealand Journal of Geology and Geophysics 26, 47–55.

Briggs RM and Goles GG 1984. Petrological and trace element geochemical features of the Okete Volcanics, western North Island, New Zealand. Contributions to Mineralogy and Petrology 86, 77–88.

Briggs RM, Itaya T, Lowe DJ, Keane AJ 1989. Ages of the Pliocene-Pleistocene Alexandra and Ngatutura Volcanics, western North Island, New Zealand, and some geological implications. New Zealand Journal of Geology and Geophysics 32, 417–427.

Briggs RM, McDonough WF 1990. Contemporaneous convergent margin and intraplate magmatism, North Island, New Zealand. Journal of Petrology 31(4), 813–851.

Briggs RM, Okada T, Itaya T, Shibuya H, Smith IEM 1994. K-Ar ages, paleomagnetism, and geochemistry of the South Auckland Volcanic Field, North Island, New Zealand. New Zealand Journal of Geology and Geophysics 37, 143–153.

Brocx M, Semeniuk V 2007. Geoheritage and geoconservation-history, definition, scope and scale. Journal of the Royal Society of Western Australia 90(2), 53–87.

Cole RP 2019. Andesitic glaciovolcanic interactions at Tongariro and Ruapehu volcanoes, New Zealand. Unpublished PhD thesis, lodged in the Library, University of Otago.

Conway CE 2016. Studies on the glaciovolcanic and magmatic evolution of Ruapehu Volcano, New Zealand. Unpublished PhD thesis, lodged in the Library, Victoria University of Wellington.

Cook C, Briggs RM, Smith IEM, Maas R 2005. Petrology and geochemistry of intraplate basalts in the South Auckland Volcanic field, New Zealand: evidence for two coeval magma suites from distinct sources. Journal of Petrology 46(3), 473–503.

Cotton C 1944. Volcanoes as landscape forms. Christchurch. New Zealand, Whitcombe and Tombs Limited.

Cox SH 1876. Report of the Raglan and Waikato Districts. New Zealand Geological Survey, Reports of Geological Explorations 9: 9-16.

Ferrari L, Petrone CM, Francalanci L 2001. Generation of oceanic-island basalt–type volcanism in the western Trans-Mexican volcanic belt by slab rollback, asthenosphere infiltration, and variable flux melting. Geology 29(6), 507–510.

Goles GG, Briggs RM, Rosenberg MD 1996. Late Pliocene stratigraphic succession and volcanic evolution of Karioi volcano, western North Island, New Zealand. New Zealand Journal of Geology and Geophysics 39, 283-294.

Hackett WR 1985. Geology and petrology of Ruapehu volcano and related vents. Doctoral dissertation, Victoria University

Hatherton T 1968. Mio-geosynclinal andesites. Earth and Planetary Science Letters 4: 441–447.

Hatherton T 1969. The geophysical significance of calc-alkaline andesites in New Zealand. New Zealand Journal of Geology and Geophysics 12: 436–459.

Hatherton T and Dickinson WR 1968. Andesite volcanism and seismicity in New Zealand. Journal of Geophysical Research 73: 4615–4620.

Hayward BW 1975. Lower Miocene geology of the Waitakere Hills, West Auckland, with emphasis on the palaeontology. Doctoral dissertation, University of Auckland.

Henderson J, Grange LI 1926. The geology of the Huntly-Kawhia Subdivision. New Zealand Geological Survey bulletin 28, 112.

Hildreth W 2007. Quaternary magmatism in the Cascades: Geologic perspectives (No. 1744). US Geological Survey.

Hildreth W, Fierstein J 1995. Geologic map of the Mount Adams volcanic field, Cascade Range of southern Washington. US Department of the Interior, US Geological Survey.

Hochstein MP, Balance PF 1993. Hauraki Rift: a young, active, intra-continental rift in a back-arc setting. South Pacific sedimentary basins, sedimentary basins of the world 2, 295–305.

Hodder APW 1984. Late Cenozoic rift development and intra-plate volcanism in northern New Zealand inferred from geochemical discrimination diagrams. Tectonophysics 101(3–4), 293–318.

Hutton FW 1867. Geological report on the lower Waikato district. New Zealand Geological Survey, Reports of Geological Explorations 2: 1–8.

Holm RF 1988. Geologic map of San Francisco Mountain, Elden Mountain, and Dry Lake Hills, Coconino County, Arizona. US Geological Survey, Miscellaneous Investigations Series Map 1:24000.

Keane AJ 1985. The age, form and volcanic mechanisms of the Okete Volcanics near Raglan. Unpublished M.Sc. thesis. Lodged in the Library, University of Waikato.

Kear D 1957. Erosional stages of volcanic cones as indicators of age. New Zealand Science Technology, 671–682.

Kear D 1959. Stratigraphy of New Zealand's Cenozoic volcanism north-west of the volcanic belt. New Zealand Journal of Geology and Geophysics 3, 578-589.

Kear D 1964. Volcanic alignments north and west of New Zealand's Central Volcanic Region. New Zealand Journal of Geology and Geophysics 7, 24-44.

Kear D and Schofield JC 1978. Geology of the Ngaruawahia Subdivision. New Zealand Geological Survey Bulletin 88, 167 p.

Marshall P 1907. Geology of the centre and north of North Island. Read before the Otago Institute, 10th September, 1907.

Martí J, Groppelli G, da Silveira AB 2018. Volcanic stratigraphy: A review. Journal of Volcanology and Geothermal Research 357, 68–91.

Matheson SG 1981. The volcanic geology of the Mt Karioi region. Unpublished M.Sc. thesis. Lodged in the Library, University of Waikato, Hamilton.

McGee LE, Smith IEM, Millet MA, Handley HK, Lindsay JM 2013. Asthenospheric control of melting processes in a monogenetic basaltic system: a case study of the Auckland Volcanic Field, New Zealand. Journal of Petrology 54(10), 2125–2153.

Mortimer N, Scott JM 2020. Volcanoes of Zealandia and the Southwest Pacific. New Zealand Journal of Geology and Geophysics, 1-7.

Neall VE and Alloway BV 2004. Quaternary Geological Map of Taranaki, 1: 100 000. Institute of Natural Resources, Massey University.

Park J 1885. Geology of the Auckland Provincial District. New Zealand Geological Survey, Reports of Geological Explorations 17: 141–147.

Player RA 1958. The Geology of North Kawhia. Unpublished thesis lodged in the Library, University of Auckland.

Pure L 2020. The volcanic and magmatic evolution of Tongariro volcano, New Zealand. Unpublished PhD thesis, lodged in the Library, Victoria University of Wellington.

Ritchie C and Brideau MA 2012. Controls on slope failure at the Te Toto amphitheatre. Conference report January 2012.

Robertson DJ 1976. A paleomagnetic study of volcanic rocks in the South Auckland area. Unpublished MSc thesis, lodged in the Library, University of Auckland, Auckland.

Sameshima T 1975. Silica indices of volcanoes in and around New Zealand, with special reference to volcanic zones in the North Island. New Zealand Journal of Geology and Geophysics 18: 523–559.

Sanders RJ 1994. Ultramafic and mafic xenoliths from the Okete, Ngatutura and South Auckland Volcanics. Unpublished M.Sc. thesis, lodges in the Library, University of Waikato, New Zealand.

Schofield JC 1967. Sheet 3 Auckland. Geological Map of New Zealand 1:250000. N.Z. Department of Scientific and Industrial Research, Wellington.

Sewell 1985. The volcanic geology and geochemistry of central Banks Peninsula and relationships to Lyttleton and Akaroa volcanoes. Unpublished PhD thesis, Lodged at the Library, University of Canterbury.

Smith IEM and Cronin SJ 2020. Geochemical patterns of late Cenozoic intraplate basaltic volcanism in northern New Zealand and their relationship to the behaviour of the mantle. New Zealand Journal of Geology and Geophysics, DOI: 10.1080/00288306.2020.1757470.

Spörli KB, Eastwood VR 1997. Elliptical boundary of an intraplate volcanic field, Auckland, New Zealand. Journal of Volcanology and Geothermal Research 79(3–4), 169–179.

Townsend DB, Leonard GS, Conway CE, Eaves SR, Wilson CJN 2017. Geology of the Tongariro National Park Area. GNS Science geological map, 4(1).

Von Hochstetter F 1867. New Zealand, its physical geography, geology and natural history: with special reference to the results of government expeditions in the provinces of Auckland and Nelson. Stuttgart: Cotta JG.

Hochstetter F and Petermann 1864. Geological and topographic atlas of New Zealand: six maps of the provinces of Auckland and Nelson. Auckland: Delattre T.

Hochstetter F 1864. Geology of New Zealand: contributions to the geology of the provinces of Auckland and Nelson. Translated and edited by CA Fleming. Government Printer, Wellington, 320 p.

Waterhouse BC and White PJ 1994. Geology of the Raglan-Kawhia area. Lower Hutt: Institute of Geological and Nuclear Sciences geological map 13, 48 p.

Zernack AV 2008. A sedimentological and geochemical approach to understanding cycles of stratovolcano growth and collapse at Mt Taranaki, New Zealand. Unpublished PhD thesis, lodges in the Library, Massey University.

Nairn IA 2002. Geology of the Okataina Volcanic Centre, scale 1:50 000. Institute of Geological and Nuclear Sciences geological map 25. 1 sheet + 156 p. Lower Hutt, New Zealand, Institute of Geological and Nuclear Sciences Limited.

Santacroce R and Sbrana A 2003. Geological map of Vesuvius: 1:15,000 scale. CARG project, National Geological Service, CNR.

Kear D 1960. Sheet 4 Hamilton. Geological Map of New Zealand 1:250 000. N.Z. Department of Scientific and Industrial Research, Wellington.

Benson WN 1968. Dunedin District. 1:50,000. NZ Geological Survey Miscellaneous Series Map 1. Wellington, New Zealand Department of Scientific and Industrial Research.